論文 / 著書情報
Article / Book Information

題目(和文)	
Title(English)	GaInAsP/InP Organo-Metallic Vapor Phase Epitaxy (OMVPE) for Quantum Box Lasers
著者(和文)	宮本恭幸
Author(English)	YASUYUKI MIYAMOTO
出典(和文)	学位:工学博士, 学位授与機関:東京工業大学, 報告番号:甲第1930号, 授与年月日:1988年3月26日, 学位の種別:課程博士, 審査員:
Citation(English)	Degree:Doctor of Engineering, Conferring organization: , Report number:甲第1930号, Conferred date:1988/3/26, Degree Type:Course doctor, Examiner:
学位種別(和文)	博士論文
Type(English)	Doctoral Thesis

GaInAsP/InP Organo-Metallic Vapor Phase Epitaxy (OMVPE) for Quantum Box Lasers

Directed by

Professor Yasuharu SUEMATSU

Associate Professor Kazuhito FURUYA

Presented by

Yasuyuki MIYAMOTO

Department of Physical Electronics,
Doctoral Course in
Graduate School in Science and
Engineering,
Tokyo Institute of Technology

Contents

Chapter 1. Introduction

1-1. Introduction

The present human community is characterized by a large volume of information. Various kinds of information are collected, stored, processed, selected and transmitted with the help of communication systems and computer systems. Our life is believed to be enjoyable by utilizing wide variety of information. This is driving us to look for more convenient tools handling information and hence the development of new communication systems and new computer systems providing higher speed, larger capacity and cost effectiveness becomes indispensable. The communication system using optical fibers[1] is attractive because of its advantageous characteristics such as very low loss, wide transmission bandwidth and inexpensive system cost in comparison with conventional coaxial cable systems.

The capability of the computer system is governed by three factors. The first is the speed of transistor. The second is how dense these transistor can be integrated. The third factor is softwafes. These three factors are closely related with each other and the most basic factor is the speed of transistor.

The ability of optical communication systems is also decided by the following three factors. The first factor is the speed of electronic circuits and this is very similar to the limitation of computer systems. The second one is opto-

electronic devices i.e., light emitting diodes, laser diodes or photodiodes. The third one is optical fiber cables. Among these factors, the opto-electronic device looks to have much room for improvement in comparison with the established fiber characteristics at present stage.

From the point of view of the aforementioned factors, the improvement of opto-electronic devices and transistor toward higher speed, higher efficiency and lower cost are very important.

1-2. Opto-electronic devices

One of major devices in opto-electronic is the semiconductor device[1] due to its attractive characteristics, i.e., compactness, low power consumption, low cost.

A fundamental requirement for optical devices is realizable materials giving expected optical properties. Semiconductor materials are separated into many groups. Silicon and germanium are elemental semiconductors and they have quite a long history of research. However, these semiconductors are not so usable for light emitting devices because of indirect transition[2] property. On the other hand, compound semiconductors[3] are quite attractive for optical devices due to the wide region of bandgap wavelength. Particularly, III-V compound material are good candidates because of a direct transition properties and suitable bandgap wavelength for optical

communications.

On the other hand, devices can be classified into two groups based on structure. Group 1 is devices with homogeneous semiconductor material. Group 2 devices have structures with hetero-interfaces of different materials such as GaAs-GaAlAs or GaInAsP-InP. III-V compounds can be used for heterostructure devices because of the possibility of many different composition with good lattice match as shown in Fig. 1-1 [4].

Heterostructures formed by III-V compound semiconductors are very important to obtain CW operations of a laser diode [5], which was basically high power, high efficiency, and high speed modulation capability. For the operation of the laser diodes, double heterostructure provides two important confinement effects as shown in Fig. 1-2. One is confinement of carriers within the active region with potential barrier of hetero interface. The other is optical confinement effect in the active region using difference of refractive index in each materials. Without these effects, CW operation at room temperature could not be obtained. First CW operation in room temperature was reported with double heterostructure formed by GaAs/GaAlAs systems in 1970 [6-7] and which was a milestone in the progress for opto-electronics devices.

Another merit of heterostructure for optical devices is quantum well structure [8] made of ultra thin film sandwiched by wider bandgap materials. The electron is confined in energy

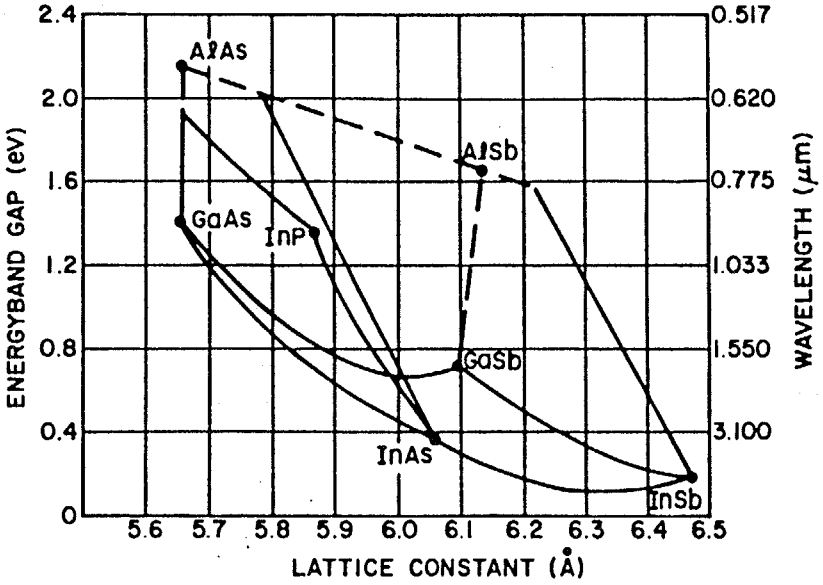

Fig. 1-1 Relation lattice constant and energy bandgap in III-V compounds semiconductor(4).

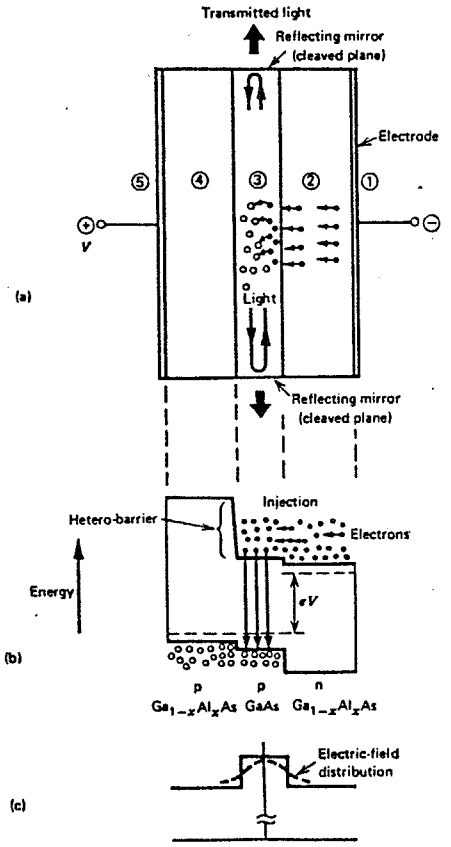

Fig. 1-2 Semiconductor laser with double heterostructure. (a) Layer structure, (b) Energy band, and (c) refractive-index and electric-field distributions(1).

potential well by this sandwiched structure and standing wave of electron is observed when well width is comparable to wavelength of electrons. By this effect, change in physical characteristics, such as, change of density of state and dipole moment with polarization, are obtained.

Improvement of lasing characteristics is expected by application of quantum well structure[9,10] to laser. Drastic improvement of characteristics such as decreasing of threshold current was achieved in GaAs/GaAlAs lasers. By single quantum well with graded index separate heterostructure as shown in Fig. 1-3[11], best confinement structure for carriers and photon were achieved separately and very low threshold current density[12-15] ($\sim$ 140A/cm^2) and extremely low threshold current (under 1mA)[15] were obtained. By the reduction of threshold current, problem of heating under CW operation is solved and bias of modulation[16] can be deleted. This facilitates integration of opto-electronic devices. Other improvements in lasing characteristics by quantum well structure, such as less dependence of temperature[17], narrow linewidth[18], high efficiency[19] and high modulation limit[20] were achieved in GaAs/GaAlAs quantum well systems.

As for modulator, enhancement of change in absorption coefficient[21] and refractive index[22] due to the electric field was expected in quantum well structure because overlap integral of wave functions of electron and hole, proportional to

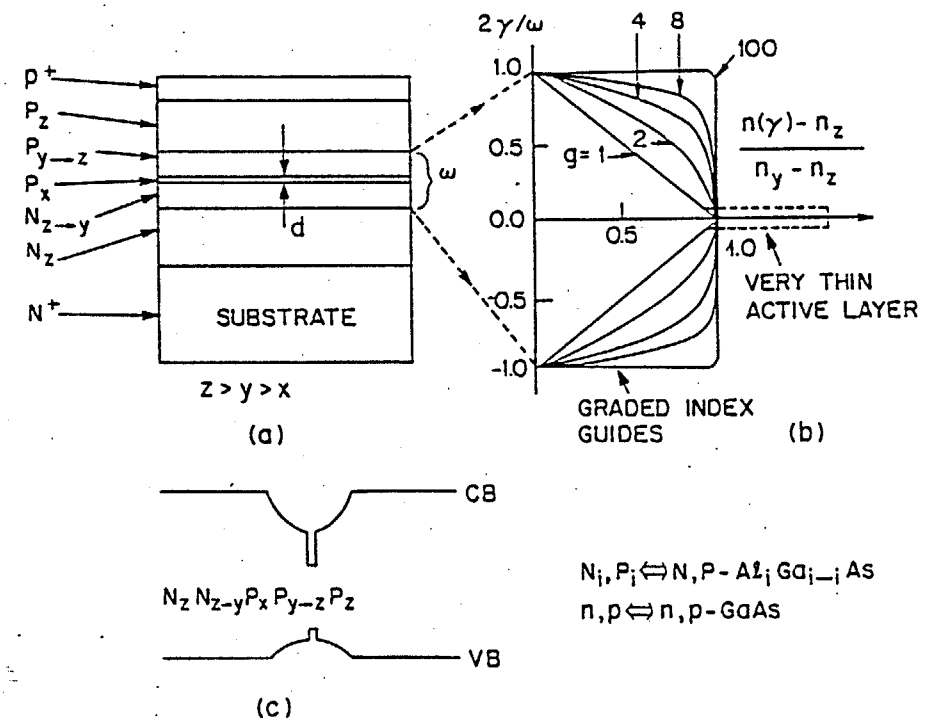

Fig. 1-3 (a) Shows schematically the layer structure of a graded-index waveguide separate confinement heterostructure laser with (b) power law refractive index profiles and (c) one of the corresponding energy band diagram (11).

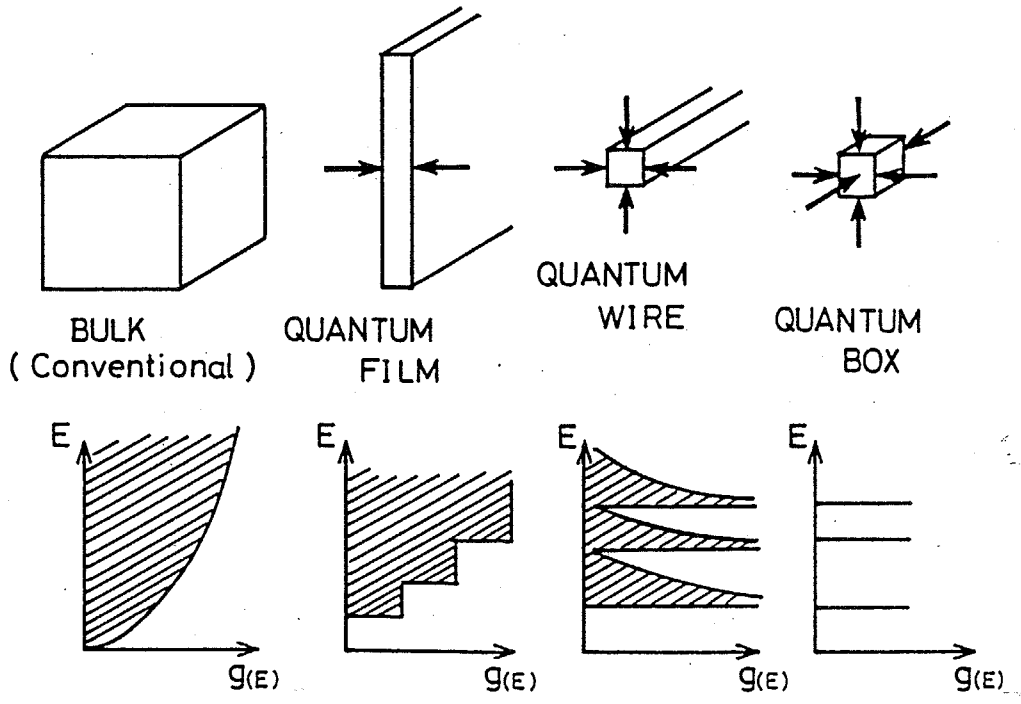

Fig. 1-4 Variation of density-of-states of electrons with the increase of the quantization dimension in quantum-well structures.

dipole moment, change appreciably by electric fields. Using large refractive index change, inter sectional optical switch[23] was proposed and high speed modulation can be achieved by reducing the capacitance which is possible due to small voltage applicable area.

Ultimate application of heterostructure to devices will be achieved by employing multidimensional quantum well effect[24]. By three dimensional quantum well (quantum box) structure, more superior lasing characteristics was analyzed[24, 25] because there is a big change in density of state as shown in Fig. 1-4. In quantum box structure, state density is simply composed of δ -function at each quantized levels and injected carriers are concentrated only in these levels. Hence, injected carriers are used effectively for lasing action compared to other structures where the state density gets distributed.

As mentioned above, the heterostructure by III-V compound semiconductor is very attractive structure for optical devices. The merits of heterostructure can be improved by quantum well structure and ultimate application of heterostructure will be higher dimensional quantum well structure.

1-3. Epitaxial growth technique

To obtain the heterostructure, thin film epitaxial growth technique is indispensable. First fabrication of laser diode was achieved by development of liquid phase epitaxy methods[6, 7].

After success of LPE, many epitaxial methods were developed for improvement of productivity and abrupt hetero interface. In case of liquid phase epitaxy, substrate is contacted with the melt and that method have a problem for uniformity, abrupt interface and cost for each growth. The second method is chloride vapor phase epitaxy[26, 27]. The epitaxy is performed in a gas phase where materials are transported as chloride-compounds. Hydride VPE[28, 29] and atomic layer epitaxy using chloride[30] use the same principle. The third is metal organic vapor phase epitaxy(OMVPE)[31, 32] where materials are transported as organic compounds. Flow modulation epitaxy[33], laser atomic layer epitaxy[34] and plasma assisted MOCVD[35] use the same principle. The fourth is molecular beam epitaxy(MBE)[36] in which materials are evaporated in high vacuum. Phase lock epitaxy[37] or migration enhanced epitaxy[38] use the same principle. The comparison of each epitaxial methods is shown in Table 1-1[39, 40].

To obtain productivity that is very important for development and cost economization, uniform growth is an important requirement in growth technique.

To obtain quantum well structure, growth must be limited by transportation of sources and etching after growth must be prevented. Thus, non-equilibrium growth mechanism is preferred to quasi-equilibrium growth mechanism. Hence, OMVPE and MBE are suitable for fabrication of quantum well structure. Observation

Table 1-1 The comparison of each epitaxial growth techniques(39.40).

Technique	Characteristics			
	Solid composition	Purity	Advantages	Disadvantages
LPE	Thermodynamics (phase diagram)	III melt,	Simple, Low cost apparatus	Volume limited, inflexible, morphology
VPE (hydride)	Thermodynamics	Gases, leaks, reactor materials	Flexible, Productivity, High purity	No AlGaAs or other Al alloys*
OMVPE	Kinetics, arrival at surface	OM sources, hydride, C contamination, leaks	Most versatile, Productivity, Abrupt	Toxic gas
MBE	Kinetics, flux, sticking coefficient	Vacuum, Sources, systems (wall)	Most abrupt, low temperature, In-situ observation	Expensive, Slow growth rate, Problems with phosphorus

of the quantum size effect and improvement of devices by quantum well structure have tight relation to development of those growth methods.

OMVPE was proposed by Reuhrwein in 1958[41] and developed by Manasevit, et al., in 1968[31]. In basic mechanism of OMVPE, organo-metallic compounds as III groups sources and hydride as V groups source are decomposed. As an example, trimethylgallium(TMG: $Ga(CH_3)_3$) and arsine(AsH_3) are used for growth of GaAs and basic reaction is as follows.

$$Ga(CH_3)_3 + AsH_3 \rightarrow GaAs + 4\ CH_4$$

Manasevit et al., applied OMVPE method for various III-V compounds, such as GaAs, GaP, GaAsP, GaSb, GaAsSb, AlAs, GaAlAs, AlN, GaN, InAs, InP, GaInAs, InSb and InAsSb[42-46] and feasibility of OMVPE for compound semiconductors growth was also indicated. However application was impossible at that stage because of poor crystal quality due to high impurity concentration of grown wafer because of impurity of sources. Expansion of OMVPE was stopped until improvement in purification of organo-metallic sources.

Present activity of OMVPE was restarted from report by Rockwell group(Dupius and Dapkas et al.)[32, 47-51]. They indicated high performance of OMVPE by fabrication of GaAs/GaAlAs double heterostructure lasers in 1977[47] by OMVPE with vertical

reactor as shown in Fig. 1-5. They reported fabrication of first quantum well laser in 1978 [50, 51]. After those reports, sufficiently high crystal quality and abrupt hetero interface for application to the devices were indicated and reports of GaAs/GaAlAs OMVPE increased year by year. At present stage, many excellent results were obtained by GaAs/GaAlAs OMVPE as follows.

1) High purity GaAs can be grown as shown by obtaining of high hall mobility at 77K ($139,000 cm^2/Vs$) [52].
2) Abrupt hetero interface can be grown by improvement of apparatus and growth condition [53]. Switching of different composition under one monolayer was confirmed with observation of lattice image by transmission electron microscope [54].
3) Fabrication of conventional double heterostructure laser with low threshold current [55], excellent uniformity [56] and high reliability [57] proved high performance of OMVPE.
4) The quantum well laser grown by OMVPE exhibited excellent lasing characteristics [58] as low threshold current density and high efficiency, and these are comparable to those fabricated by MBE.
5) Application to fine structure is also indicated by modulation doped field effect transistor [59] with high mobility and small fluctuation of threshold voltage and that have less surface defect as observed in MBE growth.

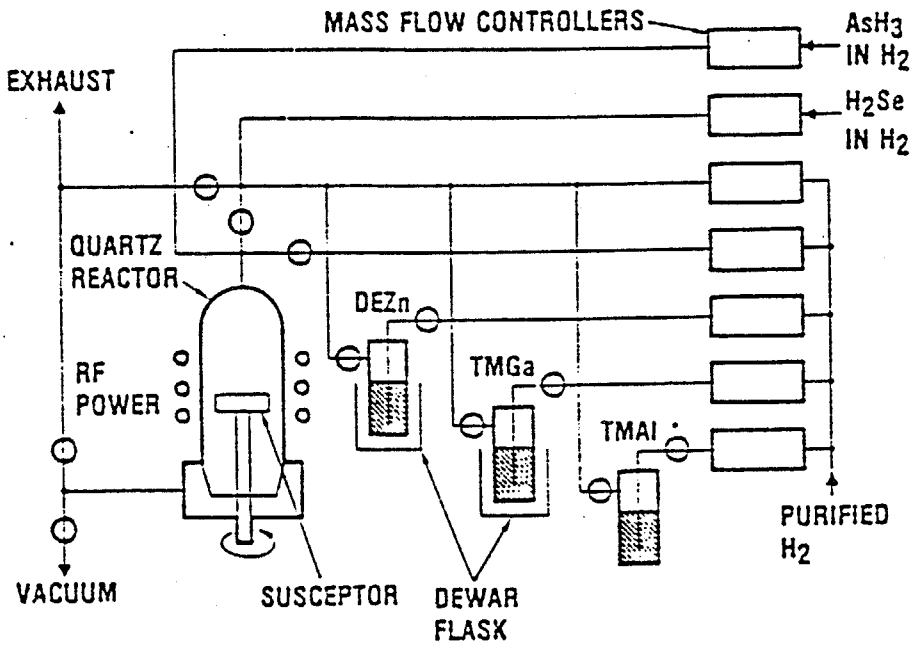

Fig. 1-5 Schematic diagram of typical vertical organo-metallic vapor phase epitaxy for the growth of GaAs-AlGaAs heterostructure (32).

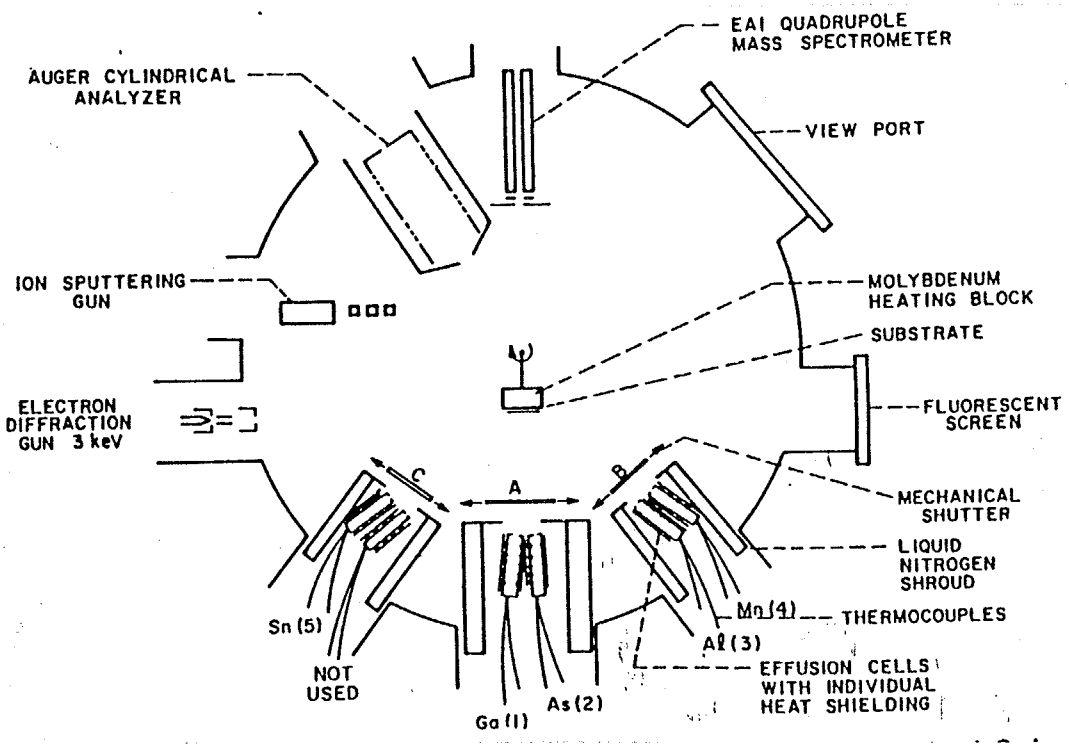

Fig. 1-6 Schematic views of typical molecular beam epitaxy for the growth of GaAs-AlGaAs heterostructure (3).

MBE was based on high vacuum evaporation and sources are supplied from effusion cell containing pure sources, to substrate by molecular beam as shown in Fig. 1-6. Purity of grown layer is decided by purity of sources and vacuum level. Gunter proposed the concept of MBE and fabrication of poly-crystal was reported in 1958[60]. First single domain of grown crystal was reported by Davey, et al., in 1968[61]. In 1974, first fabrication of laser was reported by T. P. Lee and A. Y. Cho[62]. Although, crystal quality was poor at this stage, lasing was made possible by annealing. Threshold current density comparable to other methods was reported by W. T. Tsang in 1979[63]. Low threshold current density by multi- quantum well laser was achieved by W. T. Tsang in 1981[64].

By comparison, MBE would be superior to OMVPE in abruptness of hetero interface. However, abruptness of hetero interface is limited by atomic layer and abruptness under one-atomic layer can be obtained by OMVPE[53]. Other demerits of OMVPE are complicate apparatus and many parameters for growth conditions, particularly, pattern of gas flow. However, these demerits can be solved experimentally. Demerit of MBE is mainly introduced from high vacuum chamber. Usually, chamber should be opened every time for the exchange of sources, hence maintenance of high vacuum is difficult for productivity.

To overcome this demerit, metal-organic molecular beam epitaxy (MOMBE) [65-68] was developed by combination of those two

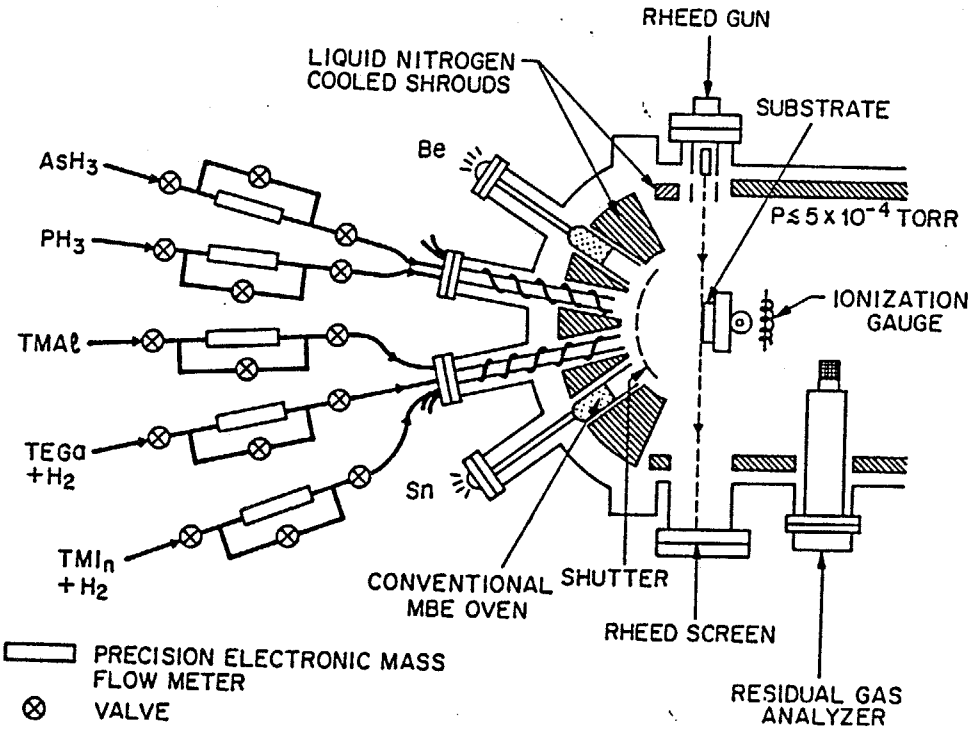

Fig. 1-7 Gas handling system and growth chamber with in-situ surface diagnostic capabilities incorporated in a metalorganic molecular beam epitaxy (MOMBE, or CBE) systems[68].

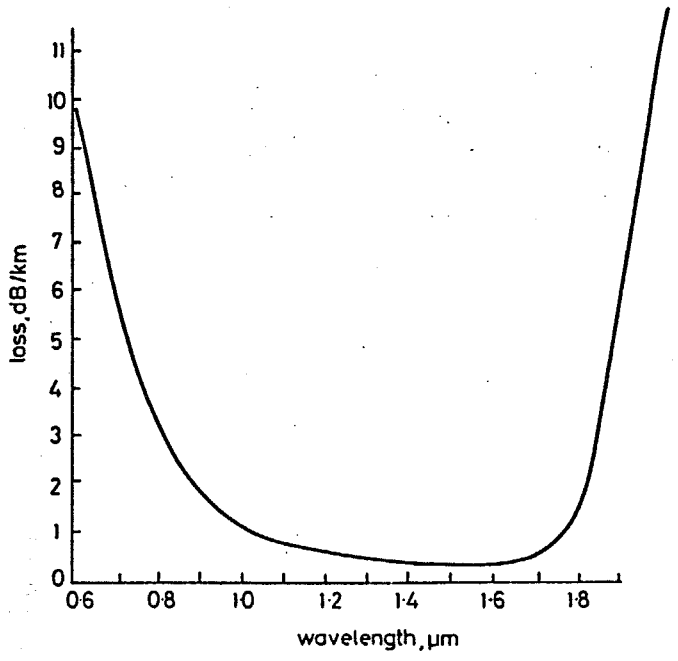

Fig. 1-8 Spectral attenuation curve of a single-mode fiber with germanosilicate core and silica cladding[70].

methods as shown in Fig. 1-7[68] and good result was reported. In this method, sources are supplied by gas phase from gas cylinder or metalorganic bubbler. Hence, opening of chamber is eliminated when source is exchanged. However, combination of two methods makes the apparatus expensive.

In conclusion, OMVPE is the most suitable growth method for fabrication of devices with quantum size effect from abrupt interface and productivity.

1-4. GaInAsP/InP OMVPE

As materials for research of III-V compounds, most popular and well known material is GaAs/GaAlAs systems. First CW operation of laser at room temperature was reported with double heterostructure of GaAs/GaAlAs systems. However, the emitting wavelength of this material is 0.78-0.87 μ m and this wavelength is not fit for lowest absorption region of silica optical fiber[69]. Long haul communication was improved by using lasers emitting in 1.3-1.5 μ m because absorption characteristic of silica optical fiber is extremely low, 0.2dB/km in this region as shown in Fig. 1-8[70]. For obtaining laser in this region, doble-hetero structure laser by GaInAsP/InP system was developed[69]. After fabrication of GaInAsP/InP conventional laser, research on GaInAsP/InP DSM laser emitting at single wavelength became more active[69, 71].

Hence, GaInAsP compound crystal lattice matched to InP is

very attractive material and development of new crystal growth method of GaInAsP/InP with high productivity and abrupt hetero interface is very important. As the new growth method of GaInAsP/InP, MBE is not suitable from following two reasons. First reason is that phosphorus is adsorbed to chamber wall after growth and high vapor pressure of phosphorus break high vacuum atmosphere. Trial to solve this problem was reported[72] by W. T. Tsang. However, the apparatus became more complicate and expensive. Second reason is that the controllability of V groups composition in the growth of quaternary is difficult due to instability of V groups elements because of high vapor pressure. Recently, MOMBE[65-68] or gas-source MBE[198] eliminated these demerits, although these growth methods were not developed when the author started this research. From these reasons, OMVPE was preferred in this research work.

For In-containing materials, i.e., GaInAsP/InP, it was difficult to get a good crystal quality by OMVPE due to the parasitic reaction of metalorganic sources at early stage. The organo-metallic sources of In were too reactive and undesirable reactions were occurred between organo-metallic sources and hydrides at room temperature[46, 73, 74]. Those reactions were confirmed by observation of non-volatile polymeric liquid or solid at upstream of reactor. As the results of this reaction, efficiency of growth and control of composition were poor. Hence, many methods were proposed to suppress those parasitic

reaction for growth of GaInAsP/InP.

First trial to prevent parasitic reaction is separation of metalorganic sources and hydride until just before the gas reaches the substrate[46, 75]. A demerit of this method is poor uniformity of grown wafer due to insufficient mixing of gas source.

The second method is using low pressure reactor and decomposition of hydride as shown in Fig. 1-9[73, 76, 77]. By low pressure, gas velocity increased and reaction time is reduced. Phosphine (PH_3) was decomposed through pyrolysis oven before introducing it to reactor to prevent extremely strong reaction between triethylindium (TEI) and PH_3. Decomposed P_4 has sufficient vapor pressure for transportation of source. Combining those two methods, first lasing[78] in GaInAsP/InP system was reported. The author's group also obtained lasing[79] by combination of sources gas separation, reduced pressure reactor and pyrolysis oven. Many results concerning quantum size effect in GaInAsP/InP were reported by this methods[81-84].

The third approach to prevent parasitic reaction is the method with adduct[85-87]. Stable metalorganic source is formed by reaction between metalorganic of III group and V group, as an example, trimethylindium (TMI) -trimethylarsenic (TMAs). This adduct can be used as III group source instead of conventional metalorganic source. This method is effective to prevent parasitic reaction. However, it is not so popular until now due

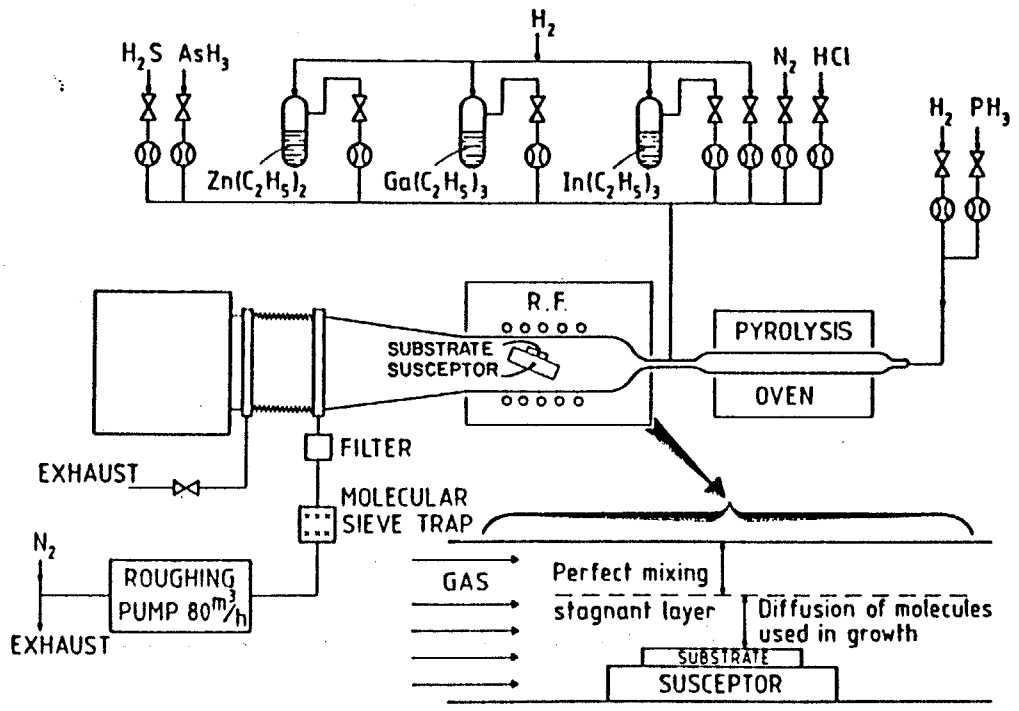

Fig. 1-9 Low pressure organo-metallic vapor phase epitaxy gas flow system for the growth of GaInAsP/InP heterostructure (77).

to the following reason:

1) Difficulty of treatment due to the low volatile characteristics of adduct.
2) Contamination of grown crystal due to the impurity from V groups organo-metallic sources.

Recently, C.C.Hsu, et al.[88], and Mircea et al.[89] found that parasitic reaction of TMI was not so strong. This phenomenon is strongly related with the purification of metalorganic source because Mircea et al.[89] reported that nitrogen mixing to carrier gas was effective to get a good crystal quality in their early stage, although they reported that the effect of nitrogen was disappeared after more purification[90]. By this development, GaInAsP/InP OMVPE research to devices was increased drastically[91-97] and OMVPE was applied to other materials containing In, as an example, AlGaInP[98-100], very attractive material for visible laser. TMI seems superior to TEI from stability of reaction. However, characteristics of TEI is also improved by purification. That was confirmed by elimination of pyrolysis oven without degradation of crystal[101]. When the author started research of this work, TMI seemed not suitable from high melting point and poor purity. Hence, TEI with reduced pressure was used in this research. More research of new growth conditions must be required if source material is to be changed.

1-5. Purpose and contents of this thesis

As mentioned until now, heterostructure is a good tool to obtain laser diodes with good characteristics and GaInAsP/InP are attractive materials for lasers. Moreover, enhancement of merits of heterostructure is expected by introduction of quantum well structure. To achieve quantum well structure devices, development of new growth technique is indispensable.

When the author started this research project, GaInAsP/InP OMVPE for fabrication of lasers was remained an unknown factor and there was no report at all about quantum well laser by GaInAsP/InP. For multi-dimensional structure, only a rough proposal was reported[24].

Hence, the first purpose of this work was improvement of GaInAsP/InP crystal quality grown by OMVPE and its application to optical devices such as laser diodes. Second purpose is formation of abrupt interface by OMVPE as a basic technique for fabrication of laser structure with three dimensional quantum well (quantum box) structure.

Summary of this thesis is given as follows.

In chapter 2, the growth apparatus and improvement of crystal quality in GaInAsP/InP OMVPE, particularly for growth of heterostructure, are discussed. Doping for InP is also discussed.

In chapter 3, the application of GaInAsP/InP OMVPE to conventional lasers is described. Threshold current density com-

parable to best value by other methods was obtained. CW operation by fabrication of buried heterostructure is also reported.

In chapter 4, fabrication of ultra thin films by OMVPE and single quantum well laser are described. Improvement of apparatus for ultra fine film and measurement of quantum well properties are also reported.

In chapter 5, quantum box laser is proposed theoretically. Optical gain in quantum box and estimation of threshold current density are described. Ideal materials for quantum box laser are also described.

In chapter 6, the fabrication of quantum box laser is described experimentally. The design of structure and processes are introduced from practical fabrication side. Development of fabrication process are also indicated. Measurement results of fabricated structure are described. The design of structure and processes are discussed again from experimental result.

In chapter 7, the conclusion of the thesis is given.

The flow chart of the thesis is as shown in Fig. 1-10.

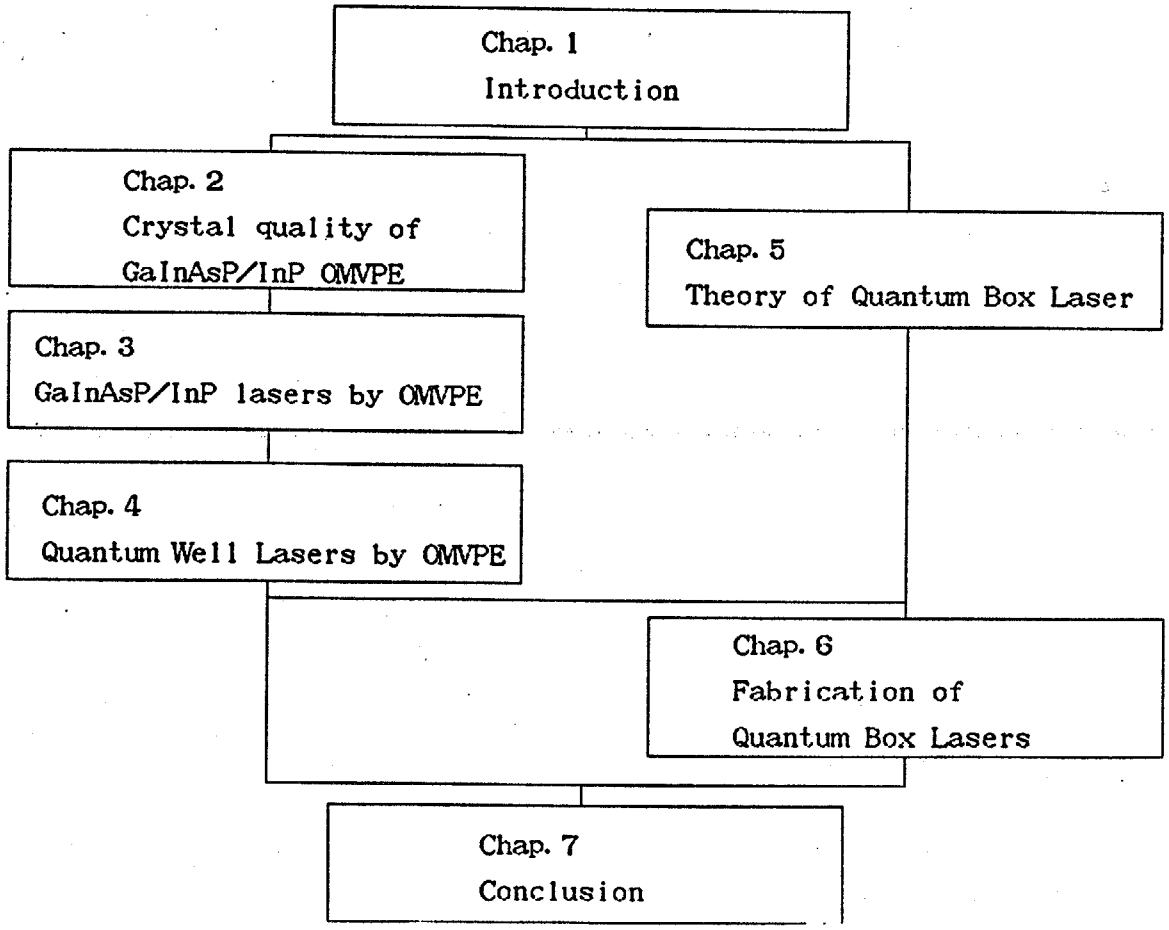

Fig. 1-10 The flow chart of this thesis

Chapter 2. Crystal quality of GaInAsP/InP OMVPE

2-1. Introduction

For fabrication of GaInAsP/InP opto-electronics devices with heterostructure, development of growth method is important. Particularly, for abrupt interface and mass-productivity, new epitaxy method must be developed. For abrupt interface, equilibrium in the growth mechanism must be weak. The available condition for epitaxial growth is expand to wide region when equilibrium in growth mechanism is weak. In fact, very thin film with abrupt interface(8, 54) or strained layer superlattice(102, 103) can be grown, although guarantee of crystal quality is reduced. On the other hand, growth with equilibrium, as an example, LPE, the crystal quality was not so difficult if layer was grown.

Hence, improvement of crystal quality is very important for OMVPE growth. Growth condition of quaternary materials and relation between gas flow and alloy composition were studied by the author's groups and it was reported in doctor thesis of S. Sugou. However, fabrication technique of heterostructure with good crystal quality is difficult in GaInAsP/InP and this technique was not so studied before this work. This difficulty is caused by two kinds of V group in quaternary composition. Each layer in heterostructure has different bandgap with different V group composition under lattice matching condition. Re-

vaporization of V group materials due to high vapor pressure is introduced degradation and that possibility is depend on fabrication technique of heterostructure.

In this chapter, improvement of crystal quality, particularly, for double heterostructure, is discussed. At first, growth mechanism of OMVPE is discussed while apparatus of OMVPE is described. Secondly, improvement of crystal quality of bulk growth is discussed. Thirdly, fabrication of hetero interface is studied. Lastly, doping condition of InP bulk is reported.

2-2. Growth mechanism and apparatus

In design of OMVPE apparatus, growth mechanism is important to get good crystal quality and abrupt interface.

The chemical reaction in OMVPE is supposed from supplied materials and grown crystal composition is as follows in the author's system:

For growth of InP

$$In(C_2H_5)_3 + PH_3 \rightarrow InP + 3C_2H_6$$

For growth of GaInAsP,

$$(1-x)\ In(C_2H_5)_3 + x\ Ga(C_2H_5)_3 + (1-y)\ PH_3 + y\ AsH_3 \rightarrow Ga_xIn_{1-x}As_yP_{1-y} + 3C_2H_6$$

The stagnant layer[104] above substrate is formed due to viscosity of gas and have gradient of temperature and velocity as shown in Fig. 2-1. Thermal decomposition is occurred in this stagnant layer or substrate surface. Growth is limited by supplement by diffusion of metalorganic source from gas flow to stagnant layers. Hence, the growth rate is proportional to concentration of metalorganic sources in gas flow and inversely proportional to height of stagnant layer. The height of stagnant layer is varied by reactor design, gas velocity and kinds of gas. Hence, the growth rate was changed by concentration of metal organic sources in gas flow, velocity of gas and kinds of gas. On the contrary, growth temperature is not so severe for the growth rate from growth principle of non-equilibrium.

Decomposition process from metalorganic sources to elemental metal is not well known. Some reports[105-107] showed that decomposition is finished in stagnant layer, and other reports[65, 66, 108, 109] showed the final bond between metal and organic had not decomposed until making of the bond between metal and substrate surface. From many reports, it may be concluded that both of two mechanisms exist and dominant mechanism is changed by growth condition, i.e. velocity of gas. When the final bond between metal and organic is cut after making a bond between metal and substrate surface, enhancement of migration -that is important for abrupt interface- was reported[110] as indicated in Fig. 2-2. To obtain those growth mechanism with

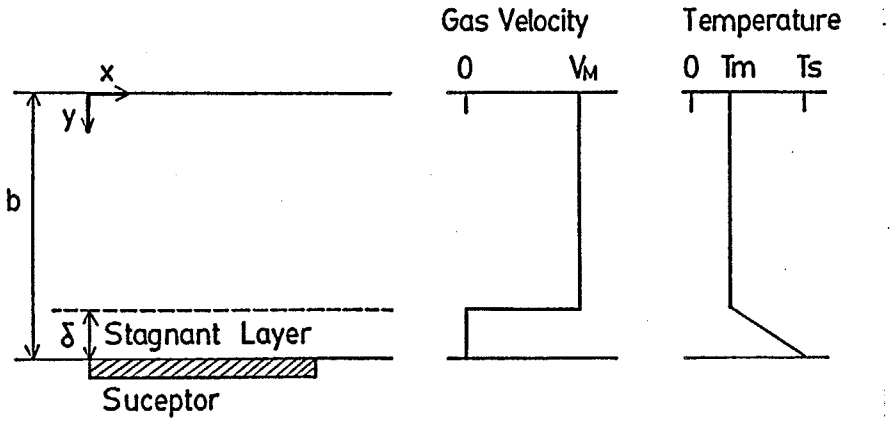

Fig. 2-1 The stagnant layer model in gas flow system. Gas flow velocity and temperature of gas in reactor tube have a distribution by the stagnant layer above the hot susceptor(104).

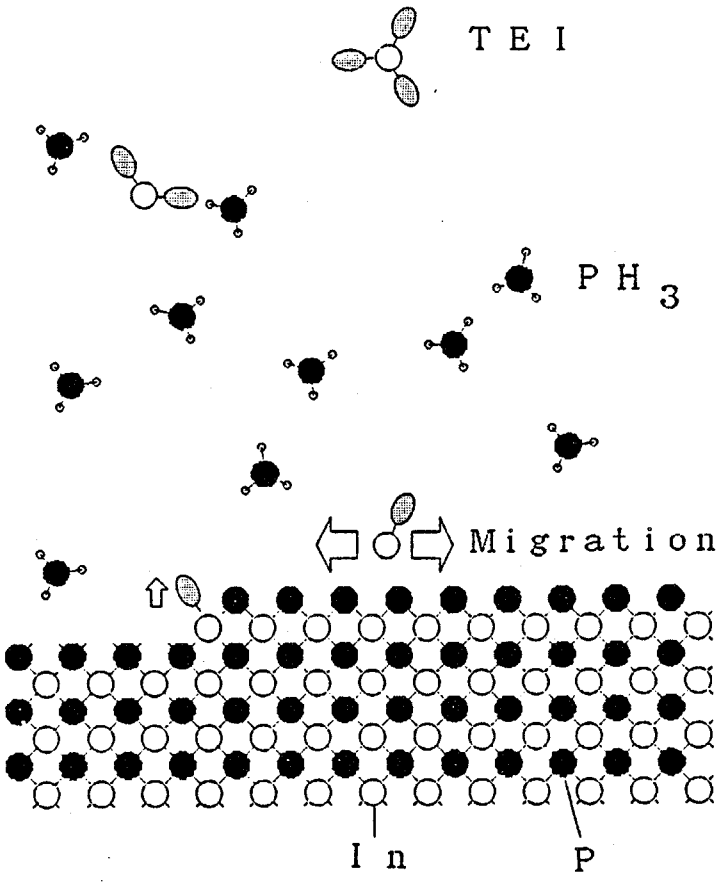

Fig. 2-2 Model of migration of III group atom on growth surface. Metalorganic source of III groups was decomposed by the temperature of stagnant later gradually. Migration would be enhanced by coupling between III groups atom and alkyl until surface. This coupling would be broken after making of bond between III groups atom and substrate. V groups atoms allows the low of equilibrium.

strong migration, it was reported(110) that high velocity of gas flow was important. Hence, thin stagnant layer may be important. Recently, OMVPE growth without hydrogen was reported by CNET(111) and possibility of another decomposition mechanism about metal organic source was indicated. However, main reaction with enhancement of migration may be same.

From above consideration of growth mechanism, high gas velocity is important for abrupt interface. Of course, high gas velocity introduces speedy change of atmosphere in reactor as other merit. Low pressure OMVPE(112) is attractive to obtain high gas velocity.

Other factor that must be taken into consideration in design of reactor are convection and entrance effect(113). Abruptness, purity and crystal quality are degraded when fabricated nuclees escape from stagnant layer and return to substrate after cooling. This phenomenon is occurred by a back flow. The The strong convection flow in vertical reactor introduces the back flow. Hence, horizontal reactor is prefer to vertical reactor. Entrance effect is recovery process from unstable flow by the change of gas flow condition (shape of tube, temperature, etc.,) to the stable flow. This recovery length is also changed by gas characteristics and long recovery length disturbs uniform growth.

Moreover, suppression of parasitic reaction must be considered in design of GaInAsP/InP OMVPE as described in section

1-4. For suppression of parasitic reaction, reduction of collision time between metalorganic sources and hydride is important and high speed gas velocity and suppression of back flow are also effective for this reduction. Hence, the authors use low pressure atmosphere and horizontal reactor for their OMVPE. Additionally, they use a separation of metalorganic sources and hydride just before substrate and pyrolysis oven of PH_3.

Other basic caution of OMVPE is suppression of leakage in apparatus. A contamination by the leakage introduces degradation of crystal quality while leakage of hydride is very dangerous for people due to toxic of hydride.

From above consideration, author's apparatus was designed. Diagram of apparatus is shown in Fig. 2-3. Photographs of apparatus are shown in Fig. 2-4. A reactor consists of horizontal quartz tube with water-cooling jackets. Substrate is fixed on SiC coated carbon susceptor and heated by RF induction. Susceptor temperature is measured by thermocouple inserted carbon susceptor and maintained by automatic-electrical controller of RF generator. The measured temperature is calibrated by an infrared thermometer because the thermocouple has a error due to quartz tube cover for protection from reactive atmosphere. Reduced pressure is used for reactor pressure. Pressure value is measured by diaflum type pressure gauge and maintained by orifice change of exhaust valve. Pressure in bubbler of metal organic source is equal to that in reactor for speedy exchange

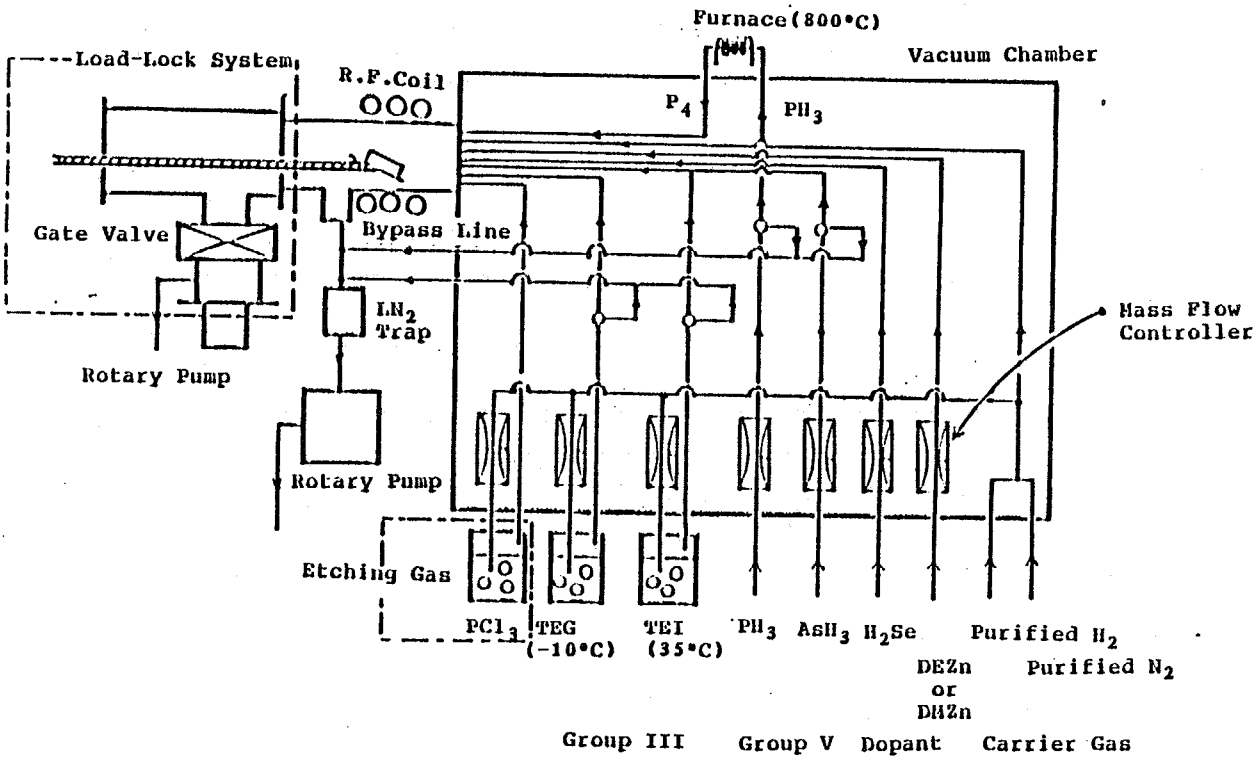

Fig. 2-3 Schematic diagram of low pressure OMVPE apparatus.

(a)

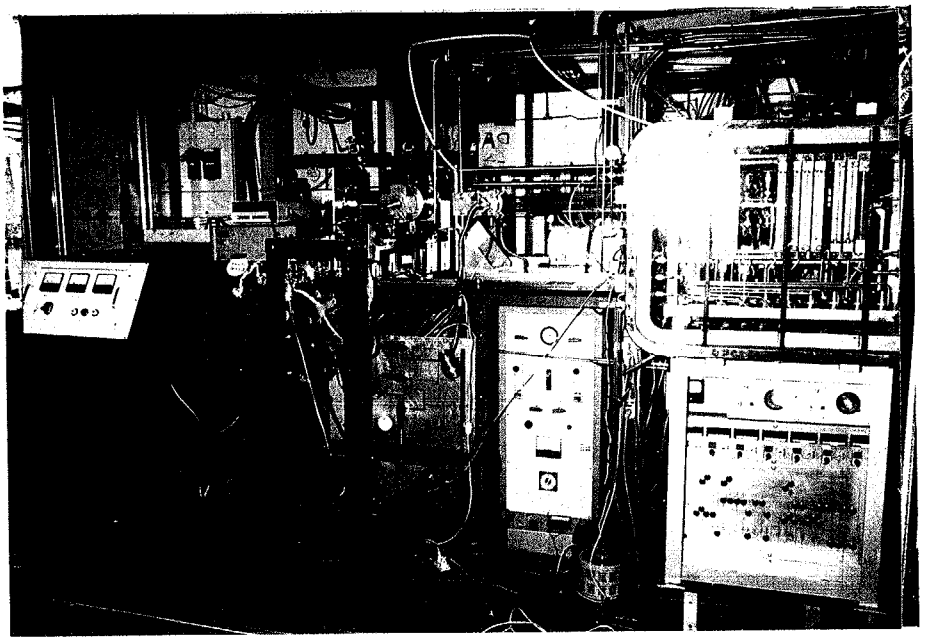

(b)

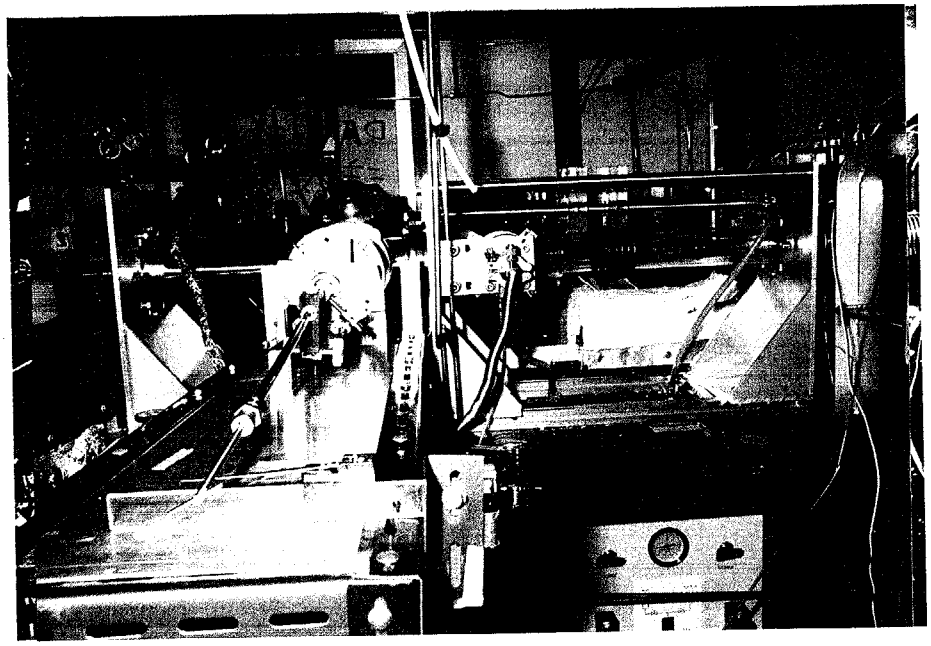

Fig. 2-4 Photographs of the apparatus. (a) Whole view of apparatus. This apparatus is placed in a small room for safety with air-duct. (b) Reactor tube, carbon susceptor and RF coil.

of atmosphere in bubbler and the bubbler has bypassing vent line for making of stable flow before switching to reactor. III group sources and V group sources are introduced through quartz tube just before susceptor and separated by coaxial structure of quartz tube. Separation length between the end of introducing tube and susceptor is 4-6cm.

To prevent contamination of air, the authors use load lock system for substrate transfer, welding piping and leak tight fitting(VCR fitting). Gas control systems(valve or mass flow controller) of upstream of reactor are fixed in vacuum box for purity of gas and safety of toxic gas. As carrier gas, H_2 and N_2 are used and impurity is eliminated by passing through purifier. These purity are monitored as less than 0.01ppm for oxygen and under -76℃ for dew point of water.

As sources, TEI, TEG, AsH_3 and PH_3 are used for III-V compounds and DMZn, DEZn and H_2Se are used for dopants. Metalorganic sources are supplied from Sumitomo Chemical Co.Ltd. and gas sources are supplied from Nippon Sanso Co.Ltd..

For reproductivity, reactor wall are cleaned by baking with flow of PCl_3 etching gas after growth every day. The temperature raised until 800℃ with resistance furnace around reactor and time of baking is about 2hours.

Basic growth conditions were determined from previous our work(114). Total flow rate of carrier gas was 2.4-2.8 slm. The pressure of growth was 76Torr. Crystals grew at the temperature

in the range from 560℃ to 680℃. Cracking furnace of PH_3 was kept at 800℃. Typical growth rate were 1-2 μm for InP and 2-4 μm for quaternary or ternary layer. Ratio of TEG/TEI was varied to obtain lattice matching condition while ratio of AsH_3/PH_3 was varied to obtain desirable bandgap energy.

2-3 Improvement of crystal quality of bulk growth

For the study of crystal quality, InP, GaInAsP or GaInAs layers in thickness of 1-4 μm were grown on S-doped n-type or Fe-doped semi-insulating (100) just InP substrate. Crystal quality of grown wafer was confirmed by observation of surface morphology and measurement of photoluminescence, X-ray diffraction and hall mobility.

At first, the author compared pure hydrogen and a mixture of hydrogen/nitrogen as the carrier gas to obtain good crystal quality. The use of the mixture gas (1:1 in mole ratio) [80, 89] improved X-ray diffraction characteristics of the crystal in comparison with those grown by using pure hydrogen carrier gas as shown in Fig. 2-5 (a), both sharpness and height of the diffraction peak were substantially improved. Of course, lattice mismatching of quaternary layer in Fig. 2-5 (a) was for an observation of carrier gases effect. X-ray diffraction pattern in lattice matching condition is shown in Fig. 2-5 (b). Furthermore, the mixture carrier suppressed pressure fluctuation observed in growth over 2 hours.

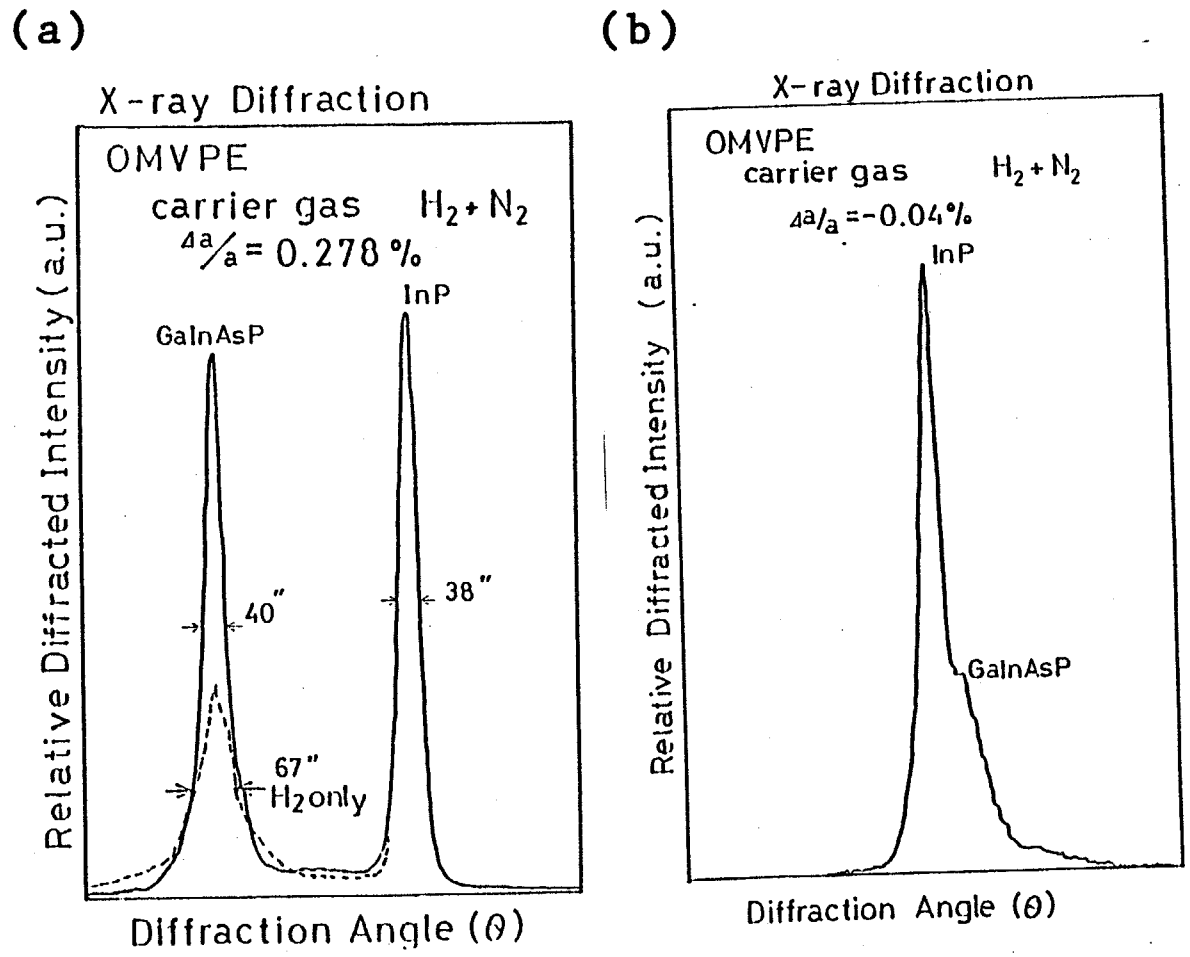

Fig. 2-5 Effect of selection of carrier gas by double crystal X-ray diffraction pattern. (a) Solid line was signal from quaternary layer grown by H_2+N_2 mixed carrier gas. Broken line was signal from quaternary layer grown by H_2 pure carrier gas. Lattice mismatching of quaternary layer was for observation of carrier gases effect. (b) X-ray diffraction pattern in lattice matching conditions.

Some reasons for the mechanism of the above improvement are given below. First, nitrogen reduces the thermal conductivity and the chemical activity of the carrier gas. Those change introduces reductions of the high temperature region above the susceptor. Hence, the deposition on the reactor wall was suppressed. Second, due to larger molecular weight, nitrogen effectively cleans wall surfaces of the reactor and the inside of the piping.

Change of the carrier gas from pure hydrogen to the mixture gas required readjustment of the flow rates. Growth rate for same flow rate of sources was increased by factor two. Fluctuation pattern of thickness after growth was changed and fluctuation along flow direction was reduced and fluctuation perpendicular to flow direction was enhanced as shown in Fig. 2-6. The fluctuation perpendicular to flow direction caused by entrance effect while the fluctuation along flow direction caused by change of stagnant layer thickness due to the changes of the diffusion constant and the viscosity of the carrier gas(115).

In range of conventional growth condition, surface of grown wafer had a mirror-like surface. Although, cross-hatching pattern was observed often when large lattice mismatching was occurred.

Photoluminescence measurement is powerful tool for optical property. Typical photoluminescence spectra are shown in Fig. 2-7. Intensity of photoluminescence was changed by growth condi-

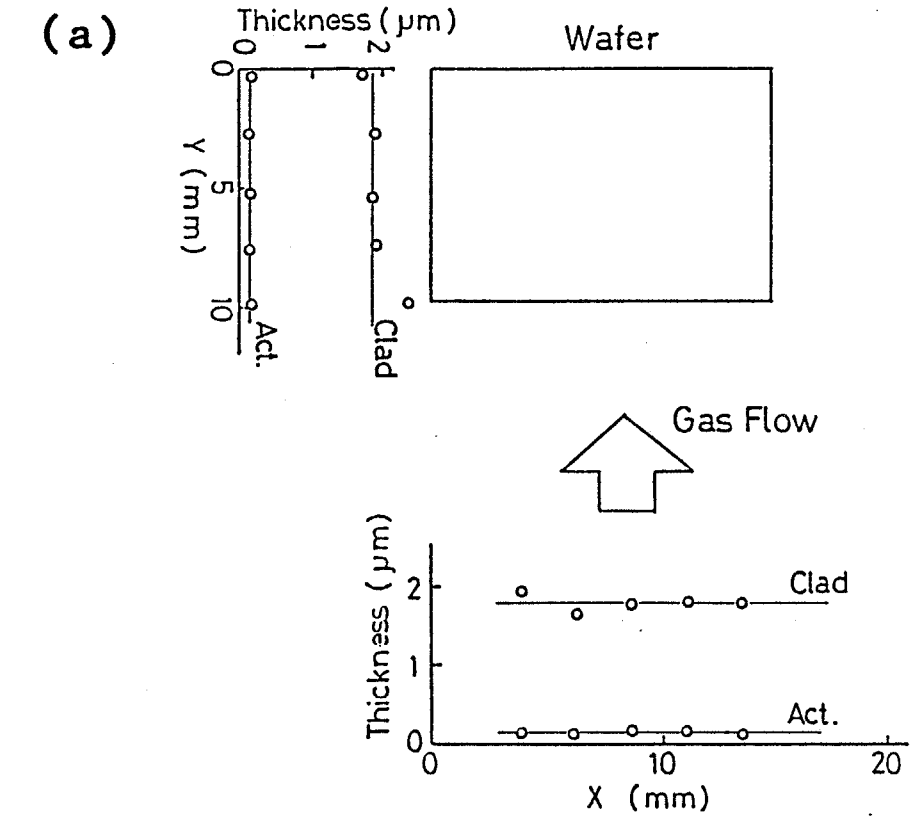

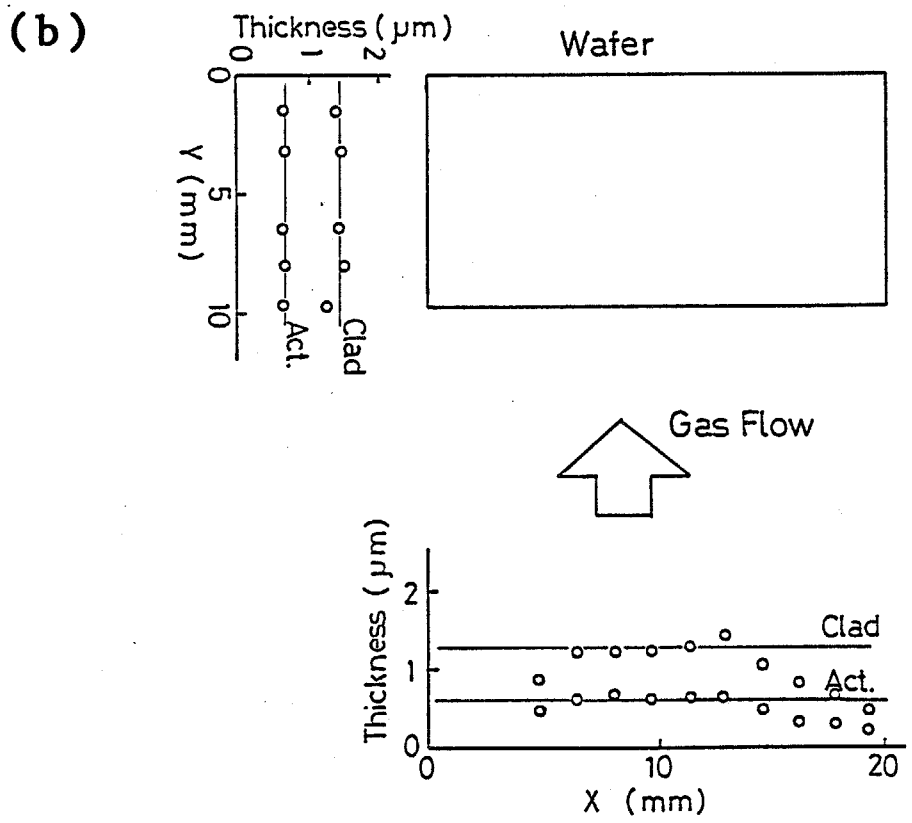

Fig. 2-6 The thickness fluctuation of grown layers by change of carrier gas. (a) Uniformity of DH wafer grown by pure H_2 carrier gas. (b) Uniformity of DH wafer grown by H_2+N_2 mixed carrier gas. Uniformity were improved by mixed carrier gas along gas flow direction, but degraded along the direction x lateral to the gas flow.

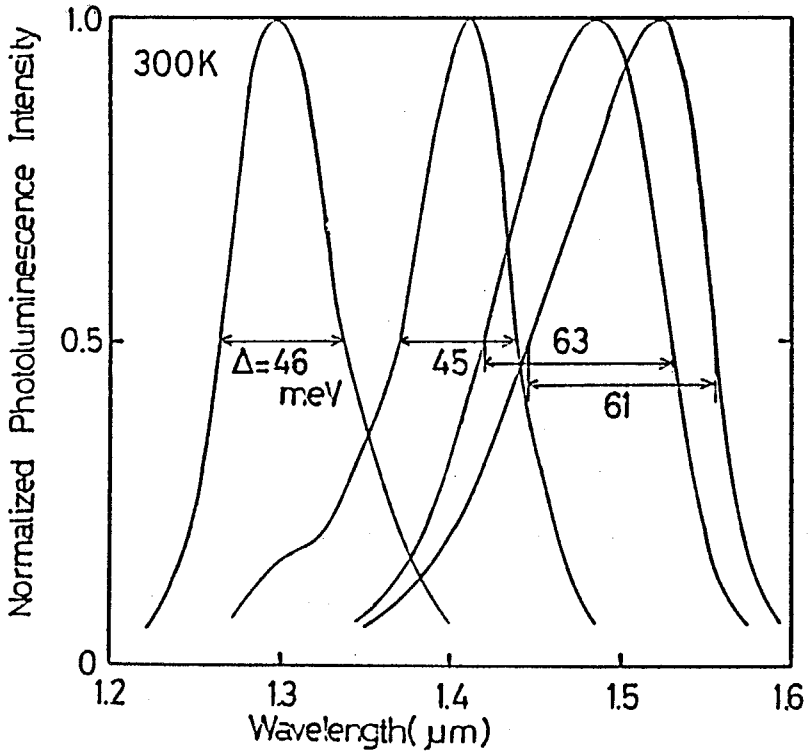

Fig. 2-7 Photoluminescence spectra of GaInAsP/InP grown by OMVPE with various bandgap wavelength at room temperature. Each intensity is normalized.

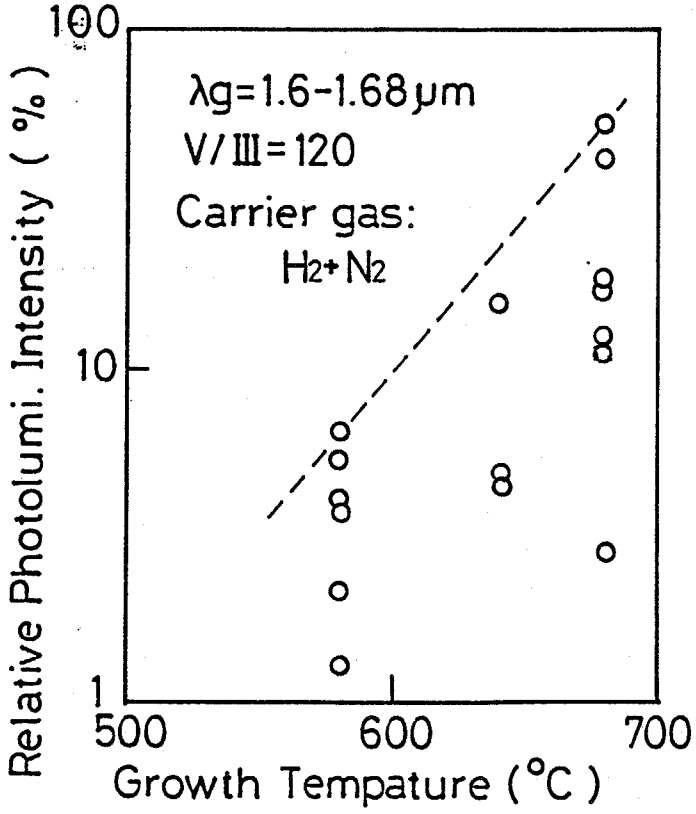

Fig. 2-8 Relation between growth temperature and intensity of photoluminescence of DH wafer. Growth conditions were that V/III ratio was 120 and the carrier gas was H_2+N_2 mixed carrier gas.

tions, particularly by lattice matching and growth temperature. the efficiency of light emission increased with raising of growth temperature in the range from 560℃ to 680℃ as shown in Fig. 2-8. However, the growth temperature was fixed at 640℃ for fabrication of laser diode because fluctuation of p-n junction was observed often in grown wafer at 680℃ by the dopant diffusion.

Back ground carrier concentration and mobility were measured by van der Pauw method in hall mobility measurement. Conduction type of undoped crystal was n-type constantly and back ground carrier concentrations was in the range of $8x10^{15}$-$5x10^{16}cm^{-3}$ at InP and $1x10^{16}$-$2x10^{17}cm^{-3}$ at GaInAs. Those value are still high from reported value[77, 116-118]. Although those value are enough for fabrication of laser because laser is injected by high carrier density and doping level for p-n junction is higher than this background carrier concentration.

Mobility of GaInAs had same tendency as photoluminescence intensity for growth temperature. Mobility increased with raising of temperatures in the range from 560℃ to 700℃ as shown in Fig. 2-9. Maximum value of mobility at room temperature are $3100cm^2/Vsec$ for InP ($n=4x10^{16}cm^{-3}$) and $5100cm^2/Vsec$ for GaInAs ($n=1.4x10^{17}cm^{-3}$). Maximum values of mobility at liquid nitrogen temperature are $13700cm^2/Vsec$ for InP ($n=1.3x10^{16}cm^{-3}$) and $7200cm^2/Vsec$ for GaInAs ($n=1.3x10^{17}cm^{-3}$). Recently, PH_3 pyrolysis oven was eliminated to reduce the contamination of Si.

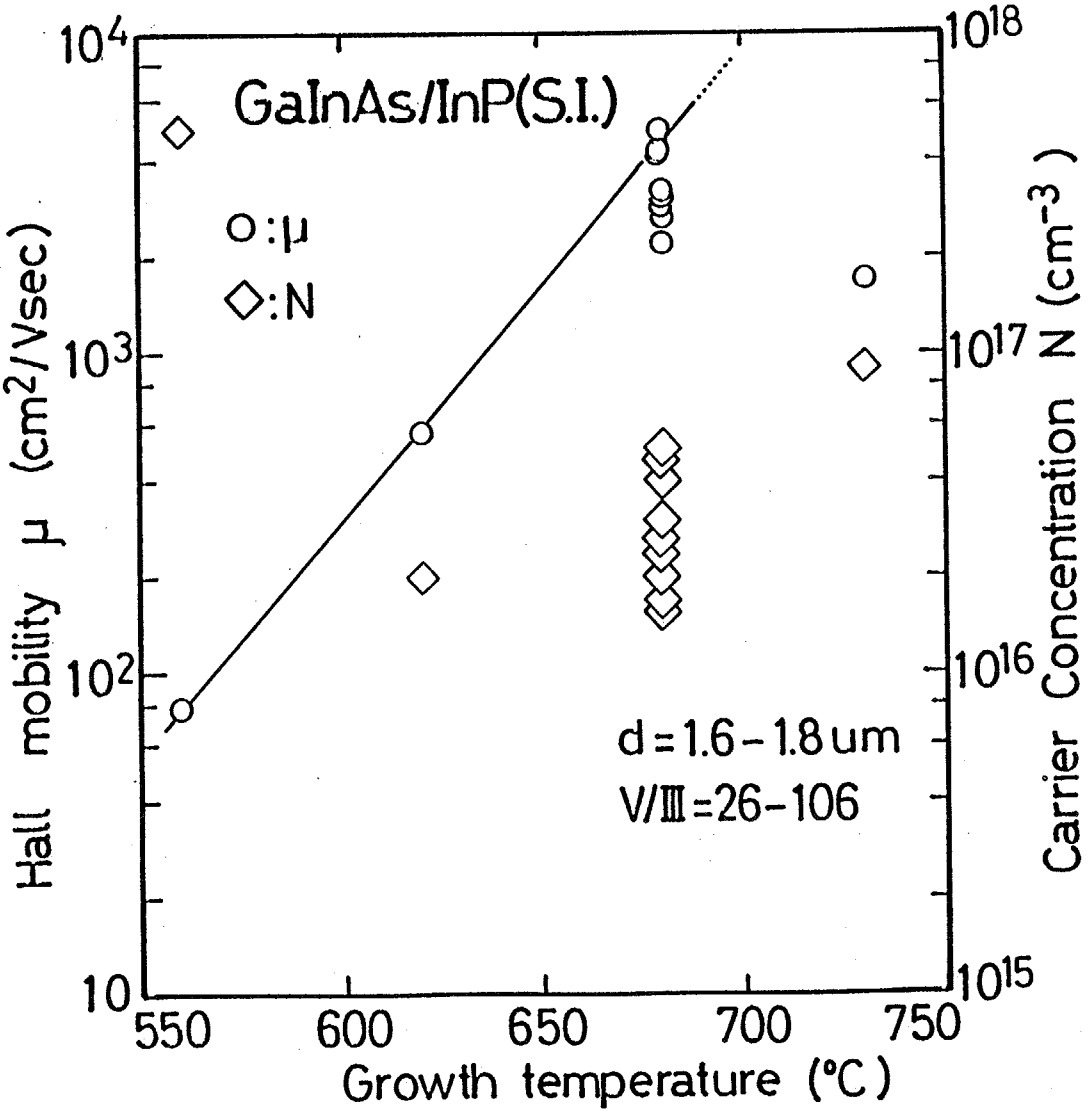

Fig. 2-9 Relation between growth temperature and hall mobility at room temperature. Van-der Pauw method was used for measurement method. The carrier concentration is also indicated in same figure.

and mobility of InP was increased from 2500cm^2/Vsec to 3100cm^2/Vsec while degradation of crystal quality by parasitic reaction was not observed. However, Maximum values of mobility are still poor from best reported value[117, 118] and mobility was not so increased by cooling until 77K, particularly at GaInAs. Thus, high compensation may be occurred and ionized impurity may be dominant for scattering mechanism[119].

2-4 Hetero-interface

The growth of GaInAsP crystal requires precise control of the ratios of Ga/In and As/P [114] for lattice matching with that of the preceding layer. Depending on the procedure of gas switching at the hetero-interface, lattice-mismatching and degraded layers are grown due to transient changes of the Ga/In and/or As/P ratios. Hence, it is very important to understand and optimize gas switching.

GaInAsP/InP and InP/GaInAsP hetero-interfaces were grown for study about the effects of gas switching. In the author's apparatus, source gases were switched into either the vent line or the reactor.

In the formation of a GaInAsP/InP hetero-interface, after growth of InP buffer layer by flowing TEI and PH_3 to reactor, growth was interrupted by switching only TEI flow to the vent line for three seconds to five minutes. After the interruption,

a quaternary layer growth was started by switching TEI, TEG, and AsH_3 flows from the vent line to the reactor.

On the other hand, the InP/GaInAsP interface was formed without the growth interruption. That is, after the growth of the quaternary layer, flows of TEG and AsH_3 were switched from the reactor to the vent line and growth of the InP layer was started. The gas switching program for DH lasers is shown in Fig. 2-10 including switching of dopant gases.

The necessity of the growth interruption at the GaInAsP/InP hetero-interface is explained below. At the switching of group III source from the vent to the reactor, the pressure in the bubbler was changed due to a slight difference in pressures of the vent line and the reactor causing the change in mole flow rate as shown in Fig. 2-11. The transient change of the pressure in the bubbler was detected by monitoring the sound of bubbling. The sounds of bubbling was stopped during 2-3 seconds after switching of valve. For the case that only Ga flow was switched from vent to reactor, i.e., without growth interruption, the Ga/In ratio changed in transient, causing degradation of the interface and subsequent growth. Hence the author could not attain lasing from the wafers grown without the growth interruption at the GaInAsP/InP interfaces. To solve this problem, after the growth interruption, TEI and TEG were simultaneously switched from the vent to the reactor. During the interruption, the surface of the InP layer was protected by a PH_3 atmosphere. Eventually, an im-

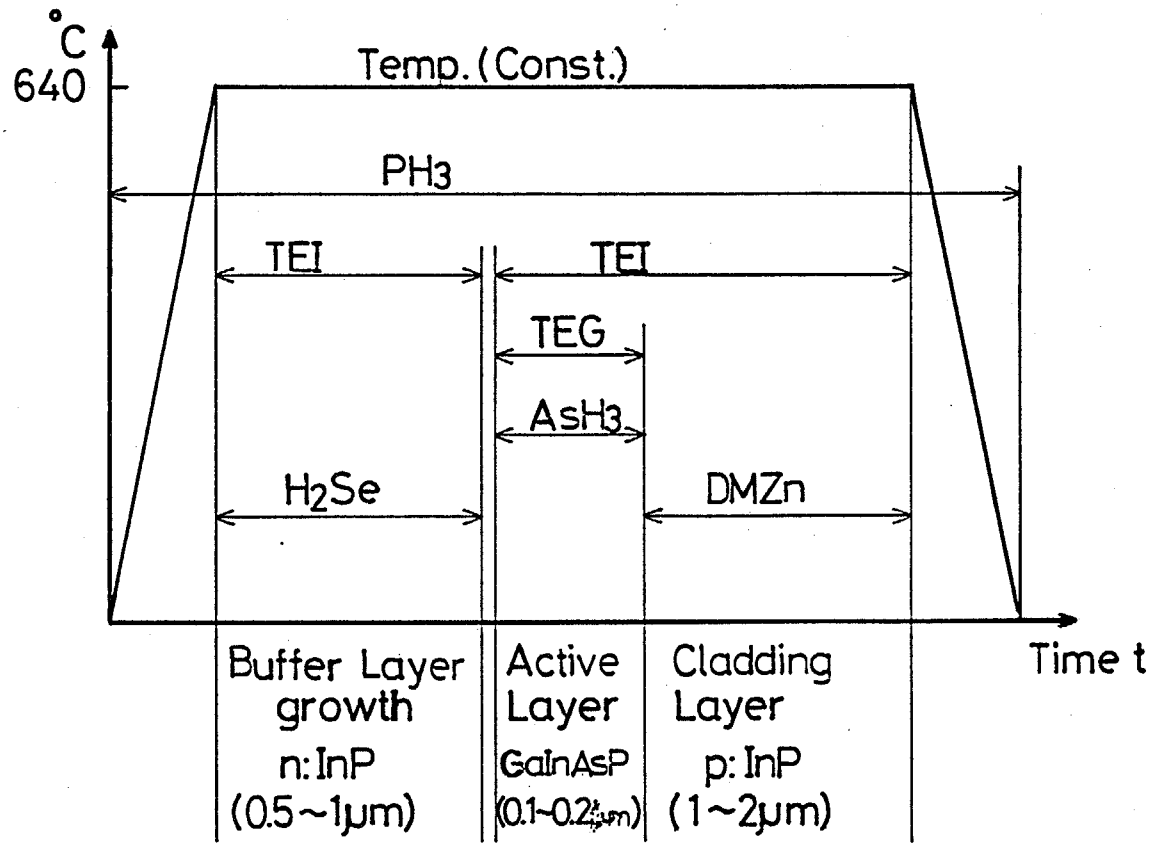

Fig. 2-10 Gas switching program of growth for DH lasers

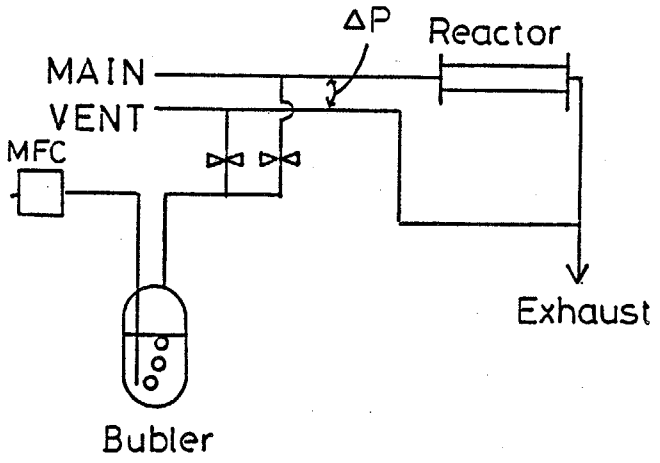

Fig. 2-11 Schematic view of pressure difference between reactor line and vent line for switching of III groups source.

provement in the apparatus so that the pressures are precisely balanced between the vent line and the reactor may make the interruption unnecessary.

On the other hand, growth interruption degraded severely the InP/GaInAsP hetero-interface when the atmosphere above the surface of the quaternary crystal was not controlled very carefully. That is, to prevent the surface degradation during the interruption, the atmosphere consisting of two group V sources should be adjusted to equilibrium with the quaternary crystal surface. The following are descriptions of the results of various manners of the crystal growth at the InP/GaInAsP interface.

For the case that, during the interruption, only PH_3 was flown at 640℃ intending cleanup of the arsenic atoms in the reactor, laser oscillation was not obtained at all. As seen from X-ray diffraction pattern in Fig. 2-12 (a) corresponding to the InP grown on the hetero-surface, the interruption reduced the diffraction intensity and broadened the width of the peak in comparison with the crystal grown without interruption (Fig. 2-12 (b)).

Furthermore, photoluminescence properties also indicated the degradation of InP grown on the interface as follows. Photoluminescence intensity from the quaternary layer was weak by a factor of 3-10 in comparison with that measured after stripping off the InP layer using selective etching. The

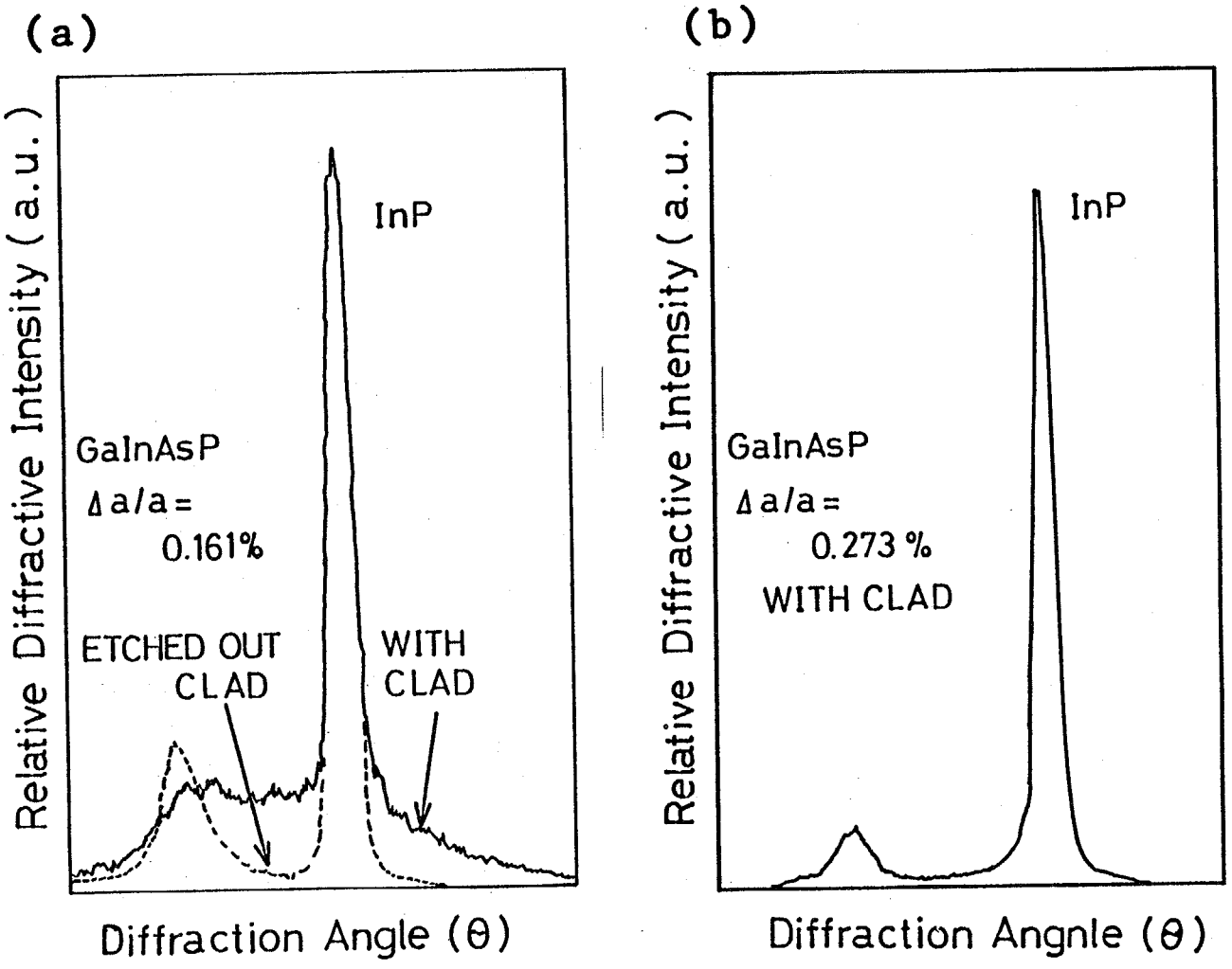

Fig. 2-12 Double crystal X-ray diffraction observation of DH wafer for effect of existence of interruption at InP/GaInAsP interface. (a) With interruption by PH_3 atmosphere. Broken line indicates the signal from wafer in which InP cladding layer was eliminated by etching. (b) Without interruption.

reduction of photoluminescence intensity may be attributed to the absorption of the pumping light and/or photoluminescence light due to the degraded InP layer. It was also observed that photoluminescence intensity from the wafer grown without interruption was three times that measured after stripping off the InP layer. Thus, properly grown InP cladding layer enhanced the photoluminescence intensity.

Moreover, the growth with interruption in InP/GaInAsP interface was introduced rough surface at InP surface on quaternary layer with 1.5 μ m bandgap wavelength when the thickness of InP was more than 1 μ m and pure H_2 gas was used as carrier gas. This phenomenon also indicated poor crystal quality grown by this procedure.

Degradation of the crystal due to the growth interruption was made less severe by lowering temperature down to 560℃. This tendency agreed with the report by J.P.Hirtz, et al.(77). However, photoluminescence intensity by this procedure was poor in comparison with that by above mentioned procedure in this experiment.

In order to study the effect of the atmosphere in the reactor during the interruption, AsH_3 and PH_3 flow were kept at the same rates as in the growth of quaternary layer causing a fairly good wafer. This result indicates that the surface of the quaternary layer and subsequent growth of InP layer degraded due to the separation of arsenic atoms in the case of pure PH_3 at-

mosphere during interruption. In conclusion, for the case that the growth of the crystal including two group V atoms, such as arsenic and phosphorus, was interrupted, surface protection requires crucially precise adjustment of the atmosphere and, therefore, is difficult.

In the case of growth of GaInAs on InP, more attention to procedure was necessary. In the case of GaInAsP growth on InP, PH_3 flow rate is kept constant for all growth time in principle. On the contrary, PH_3 must be stopped in the growth of GaInAs to prevent incorporation of P. To prevent degradation of surface of InP, PH_3 was switched off simultaneous with start of GaInAs growth. However, starting time of growth was decided by introducing of III groups sources and that had delay from switching of valve by slight pressure difference. Hence, the author carried out gas switching as shown in Fig. 2-13 for growth of GaInAs. Flow of PH_3 was switched off with 5second delay after introducing of III groups sources and AsH_3. The author assumed that switching of PH_3 was occurred simultaneous with start of growth. It was not severe when assumption of delayed time had a small error, because only few strained atomic layer grow with good crystal quality, even if P was incorporated in crystal by miss of procedure. Crystal quality was confirmed by X-ray diffraction measurement, photoluminescence and hall mobility. X-ray diffraction pattern is shown in Fig. 2-14. Other programs similar

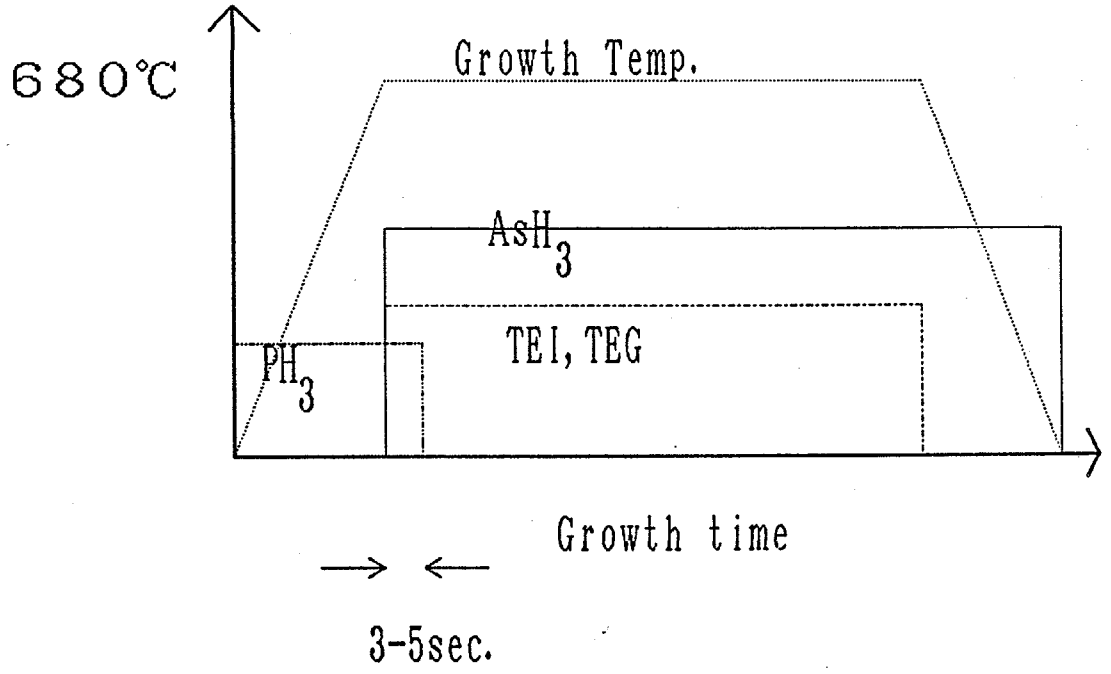

Fig. 2-13 Gas switching program for growth of GaInAs layer. PH_3 was used for protection of surface and switched off after introduction of sources of GaInAs with 3-5 second delay time.

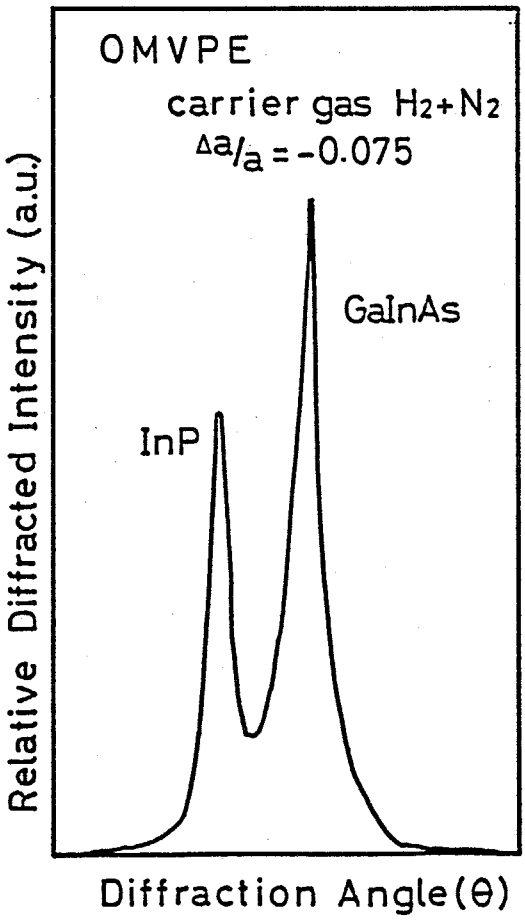

Fig. 2-14 X-ray diffraction pattern of GaInAs grown layer using the gas switching program as shown in Fig. 2-13.

to report from Kuo et al. [116] were also tried. At first, the growth temperature was changed from low temperature to high (usual) temperature and PH_3 was not introduced as shown in Fig. 2-15. In this case, the author couldn't obtain good crystal quality. By similar program without temperature change and with introduction of PH_3, crystal quality could not be compared with crystal that by program of Fig. 2-13, too.

2-5. Doping

Doping is important for fabrication of laser diodes. Diethylzinc (DEZn) and dimethylzinc (DMZn) for p-type and hydrogenselenide (H_2Se) for n-type were investigated as dopants. All dopants were supplied from gas cylinders where the dopants were diluted with hydrogen.

Carrier concentration was measured by the Van der Pauw method and C-V measurement [120]. For the former method, doped InP layers were grown on Fe-doped InP substrates at the thickness of 1 μm. For the latter measurement, wafers of DH structure for a laser diode were used where the carrier concentration of the adjacent layer is sufficiently large ($>10^{19}cm^{-3}$) and, hence the depletion layer extend to p-InP layer to be measured.

In case that DEZn and pure hydrogen were used as the dopant and the carrier gas, acceptor concentrations was in the range of $0.5-1.5\times10^{18}cm^{-3}$ under conditions that DEZn / TEI mole flow ratio was 10% , V/III ratio was 29, and growth temperature was

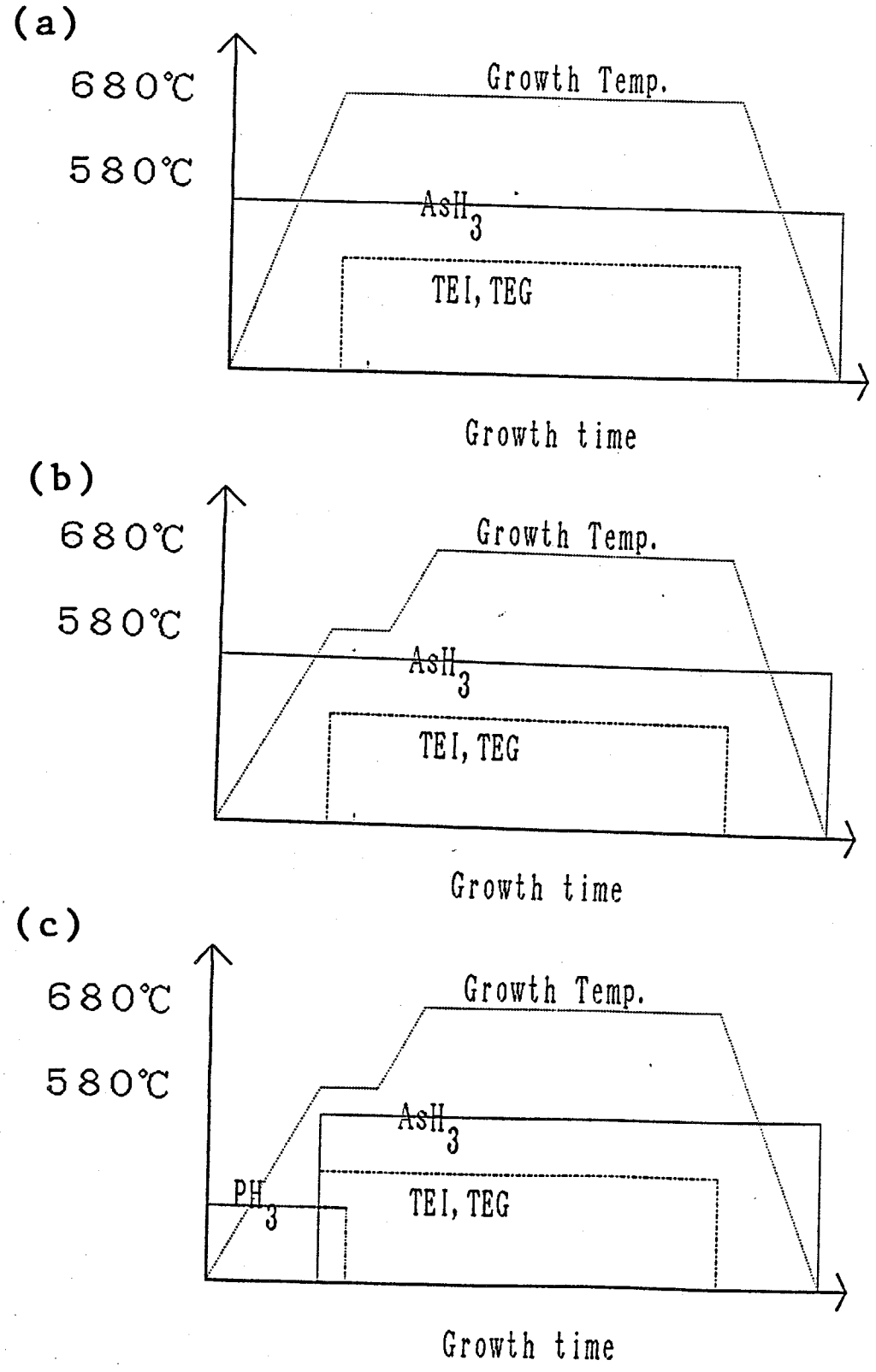

Fig. 2-15 Other gas switching program for growth of GaInAs layer. (a) PH_3 was not introduced to prevent the incorporation of P in the grown wafer. (b) The gas switching program was same as the program of (a) and the growth temperature was changed from 580℃ to 680℃ after the start of growth to prevent degradation of surface. (c) The gas switching program was same as the program of Fig. 2-13 and the growth temperature was changed from 580℃ to 680℃ after the start of growth.

565℃. However, in case that, when V/III ratio was increased up to 78 in order to get mirror surface, p-type InP layer could not be obtained. As the background carrier concentration of undoped InP was measured to be less than $1x10^{17}cm^{-3}$, this phenomenon may be explained not by compensation but by some parasitic reaction between DEZn and PH_3 or Zn and P. Furthermore, when DEZn /TEI mole flow ratio was not as high as 10%, p-type InP was not stably grown.

In order to solve the difficulties mentioned above, the dopant source and the carrier gas were changed to DMZn and the hydrogen-nitrogen mixture, respectively. DMZn is higher in decomposition temperature[121] than DEZn and, therefore, is more stable. In this case, p-type InP layer of acceptor concentrations in the range of $3x10^{16}$-$7x10^{17}cm^{-3}$ was obtained under growth conditions that V/III ratio was 169 and growth temperature was 580℃. In the above range of acceptor concentration, surfaces of the grown layers were mirror-like.

The relation between mole flow ratio of DMZn/TEI and acceptor concentration is shown in Fig. 2-16. In Fig. 2-16, the triangles were data from the C-V method while squares were from Van der Pauw measurements. Results of the two methods agreed well. As shown in Fig. 2-16, the acceptor concentration depended linearly on the flow rate of DMZn. Incorporation of Zn into the crystal was almost independent of the growth temperature up to 640℃.

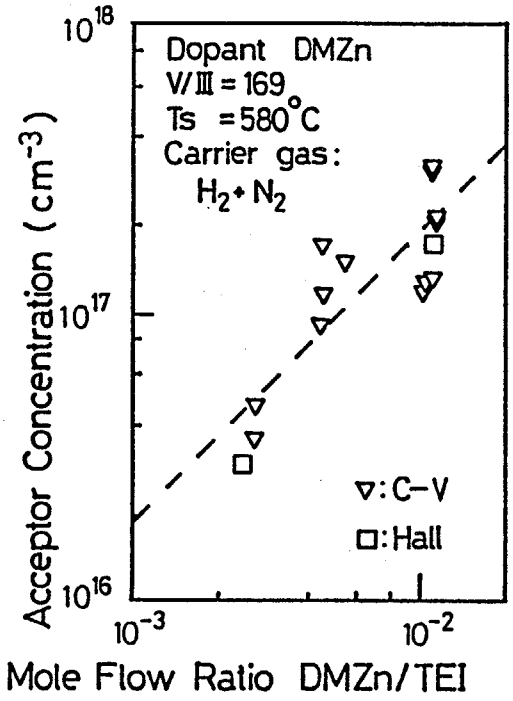

Fig. 2-16 The relation between mole flow ratio of DMZn/TEI and acceptor concentration. The triangles points were data measured by C-V method while squares points were from van der Pauw measurements. Growth conditions were that V/III ratio was 169 and growth temperature was 580℃.

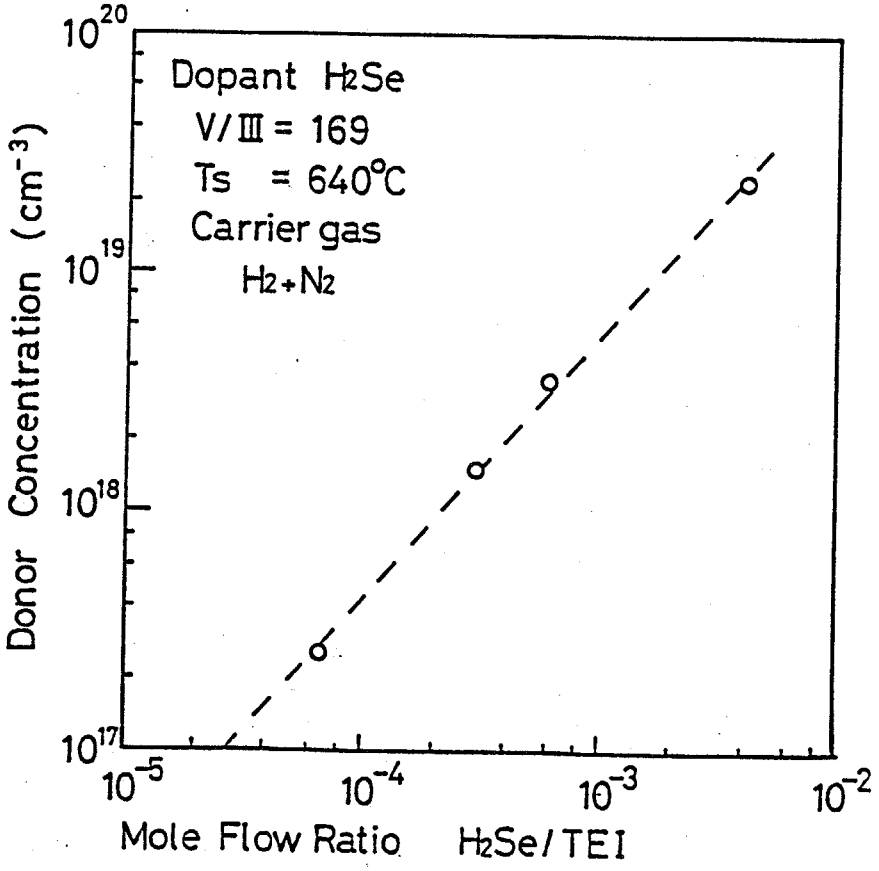

Fig. 2-17 The relation between mole flow ratio of H_2Se/TEI and carrier concentration. Growth conditions were that V/III was 169 and growth temperature was 640℃.

From these experimental results, the author concluded that DMZn is a more suitable dopant than DEZn with respect to controllability of the carrier concentration in case that the dopant source is fed from gas cylinder instead of the bubbler. Hydrogen-nitrogen mixture carrier gas also remarkably improved the doped InP growth.

N-type doping using H_2Se was studied. The relation between carrier concentration and dopant flow rate was linear as shown in Fig. 2-17 where V/III was 169 and growth temperature was 640℃.

Incorporation of selenium depended exponentially on the inverse of the growth temperature as shown in Fig. 2-18. This dependence is explained as follows; Incorporation efficiency of H_2Se was as high as that of TEI at lowest temperature, 560℃, suggesting that H_2Se decomposed well into a secondary form at the substrate surface in the range of the growth temperature. The incorporation of the secondary form of the selenium was determined by its concentration at the surface of the crystal which was decided by diffusion coefficient[80] depending on the temperature. In addition to the above, the following mechanism also explain the temperature dependence. That is, both selenium and phosphorus entered to V group site in competition[122]. The pyrolysis efficiency of PH_3 depended on the growth temperature even if PH_3 flow passed through the pyrolysis oven[114] and, therefore, incorporation of selenium depended on the tempera-

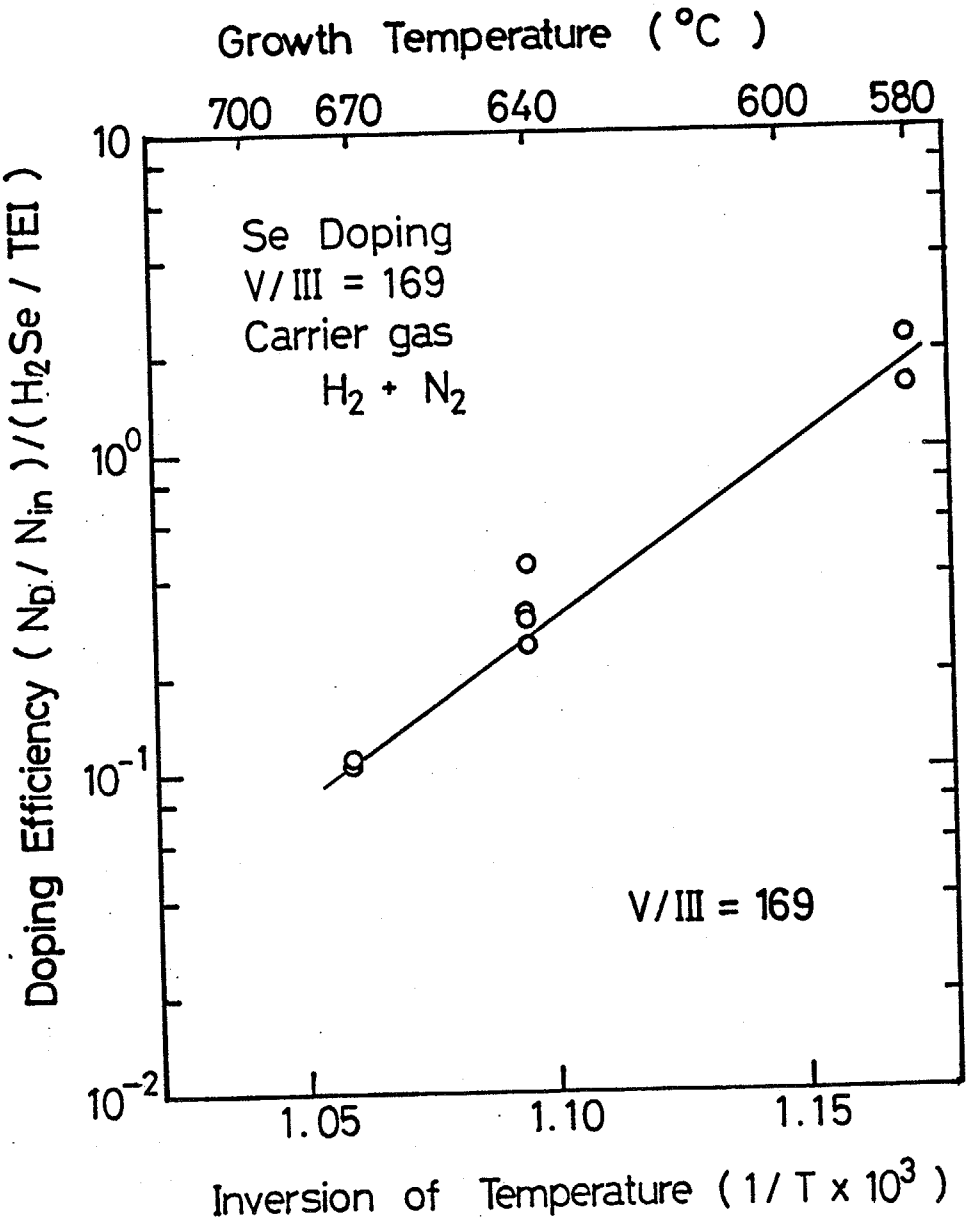

Fig. 2-18 The relation between ratio of incorporation (mole flow ratio H_2Se/TEI versus carrier concentration per In concentration) and growth temperature. V/III ratio was 169

ture.

2-6. Concluding remarks

Improvement of crystal quality grown by GaInAsP/InP OMVPE are described. At first, growth apparatus in consideration with growth mechanism and parasitic reaction are described. Secondly, the author reports that crystal quality was improved by using of nitrogen mixing carrier gas and higher growth temperature. Thirdly, the author reports that procedure of source gas switching was important for hetero interface without degradation. Finally, it is pointed out that DMZn and H_2Se were suitable for p- and n-type doping sources, respectively.

Chapter 3. Application of GaInAsP/InP OMVPE for lasers

3-1 Introduction

Many measurement methods were developed for evaluation of crystal quality. However, most important and most severe evaluation is practical application to devices. Of course, a part of purpose was achieved by operation of devices and characteristics of devices was powerful for evaluation. Particularly, the threshold current is a figure of merit in laser devices. In this chapter, it is reported that conventional laser was fabricated by OMVPE and crystal quality was evaluated by laser characteristics. The author achieved about 1kA/cm^2 for lowest threshold current density when cavity length is from 200 to 400 μ m and this value is comparable to the lowest threshold current density reported in conventional laser[123-125].

In section 3-2, broad contact laser on n-type substrate was evaluated. Since n-type conductivity is most popular as substrate. Effect of leakage could be eliminated by evaluation of broad contact lasers. Estimated value with change of parameter was compared with that obtained with LPE[126].

In section 3-3, laser on p-type substrate was described. As a merit of laser on p-substrate, ohmic contact on p-side becomes easy, as a results, quaternary cap layer and Zn-diffusion process can be eliminated. Moreover, high output power was desirable by high reverse voltage of current blocking

layer[127].

For practical application, laser is operated by CW condition and BH structure was important for achievement of CW operation. Hence, the author tried by two approach for CW operation. One is the hybrid method with LPE and the other is the method entirely by OMVPE. In section 3-4 and 3-5, those research are described. Aging test for reliability of fabricated laser by OMVPE is also reported.

Recently, many research groups[93-95, 128-130] reported buried heterostructure laser by OMVPE because OMVPE system is very attractive from productivity, and the author's study was one of the first trials to obtain buried heterostructure laser by OMVPE.

3-2. Threshold current density on n-type substrate

In order to evaluate the quality of the crystal from lasing characteristics, crystal wafers were grown in the following double heterostructure (DH) form. DH structures on n-InP substrates (S-doped, $N=2\times10^{18}cm^{-3}$) consisted of

(1) InP buffer layer ($1\mu m$, Se-doped $N_D=1\text{-}5\times10^{18}cm^{-3}$),

(2) quaternary active layer ($0.1\text{-}0.45\mu m$, undoped),

(3) InP cladding layer ($1\text{-}2\mu m$, Zn-doped, $N_A=5\times10^{16}\text{-}5\times10^{17}cm^{-}$), and

(4) InP or quaternary cap layer (Zn-doped).

Typical growth conditions are summarized in Table. 3-1.

Table 3-1 Typical growth condition for DH laser on n-type substrate.

Layer	Gas flow rate (sccm)						Growth time(min)
	TEI	TEG	AsH_3	PH_3	DMZn	H_2Se	
n-clad	0.11			19.3		1.9×10^{-4}	50
active	0.11	0.068	10.5	19.3			5
p-clad	0.11			19.3	4.7×10^{-3}		90
p^+-cap	0.11	0.043	2.4	19.3	9.4×10^{-3}		5

Total carrier gas (H_2:N_2=1:1) 2400 sccm

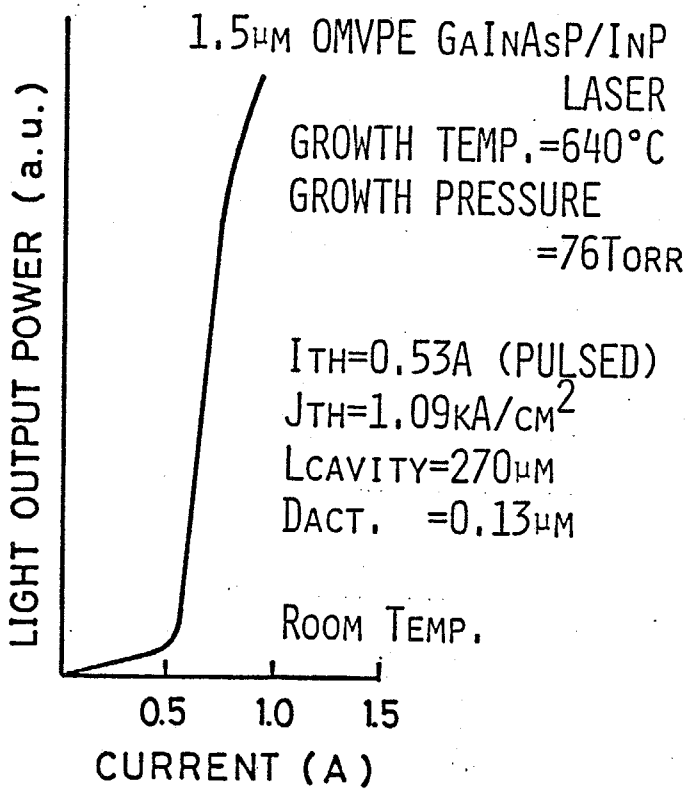

Fig. 3-1 Typical I-L characteristics in broad contact laser on n-type substrate.

This wafer was lapped from the substrate side down to 150-200 μ m thick, and then contact electrodes were formed. Au/Sn and Au/Zn alloys were deposited on n-side and p-side, respectively by vacuum evaporation. Annealing with 450℃ and 5min was performed to get low contact resistance. Then the wafer was cleaved into chips (80-200 μ m x 140-1000 μ m). Threshold current densities were measured from these broad-contact laser at room temperature under pulsed operation with a repetition of 3kHz and a width on 100-200ns. Near field patterns of the emission from the broad-contact lasers were observed by using an infrared TV camera to confirm that current flow and lasing were homogeneous over the whole width of the laser. Lasing wavelength was measured in the range from 1.53 μ m to 1.58 μ m. The lowest value of the threshold current density obtained was 0.9kA/cm^2 for the device with cavity length of 400 μ m. Typical I-L characteristics was shown in Fig. 3-1. These values of the threshold current density are comparable to those of LPE[125].

In early stage of this research[114], initiation of introduction of p-type dopant had 6-8 minutes delay after start of InP cladding layer growth to adjust the p-n junction. However, this delay introduced shift of p-n junction to upper side and it was not observed shift of junction by diffusion of acceptor when initiation of introduction of p-type dopant was simultaneous with start of InP growth. Hence, p-type dopant and TEI were introduced reactor simultaneously for growth of cladding layer.

The DH lasers were analyzed by means of experimental plotting on $\sqrt{}$ Jth vs. 1/L graph. With this experimental plotting being fitted on the theory described below, gain and loss coefficient can be determined and compared with those value obtained by LPE.

First, theoretical dependence of the threshold current density on parameters of lasers are outlined[131]. The material gain g depends on the carrier density n linearly as follows[132].

$$g = A_0 n - \alpha_{in} , \qquad (3-1)$$

where A_0 is the proportional constant and α_{in} is the biased absorption loss coefficient due to band-to-band transition[132]. Threshold gain g_{th} compensates the loss in the laser as follows.

$$\xi g_{th} = \alpha_{ac} \xi + \alpha_{ex}(1-\xi) + \ln(1/R)/L , \qquad (3-2)$$

where α_{ac} and α_{ex} are loss coefficients inside and outside the active layer, respectively, ξ is optical power confinement factor, L is cavity length and R is the reflectivity at the end facets. The loss coefficient inside active layer, α_{ac}, is the sum of the absorption $K_0 n$ due to the intervalence band absorption[131] and absorption α_2 due to transition from the split-off band to the acceptor level, given as

$$\alpha_{ac} = K_0 n + \alpha_2 \cdot \qquad (3\text{-}3)$$

Taking into account that the carrier lifetime is inversely proportional to the carrier density, the carrier density is related with injection current density J as follows[131].

$$n = B\sqrt{J/d}\ , \qquad (3\text{-}4)$$

where B is a proportional constant and d is the active layer thickness. Combining eqs. (3-1)-(3-4), threshold current density J_{th} is obtained as

$$\sqrt{J_{th}} = K\sqrt{d} + (\sqrt{d}/\xi\ /L)H\ , \qquad (3\text{-}5)$$

where

$$H = \ln(1/R)/((A_0-K_0)B)\ , \qquad (3\text{-}6)$$

$$K = ((\alpha_{in} + \alpha_2) + ((1-\xi)/\xi)\alpha_{ex})/((A_0-K_0)B)\ . \qquad (3\text{-}7)$$

Figures 3-2 (a) and (b) show experimental plots of the relations between square root of J_{th} and 1/L for two different active layer thicknesses, which are in agreement with the above theory. From Fig. 3-2, putting values of optical confinement fac-

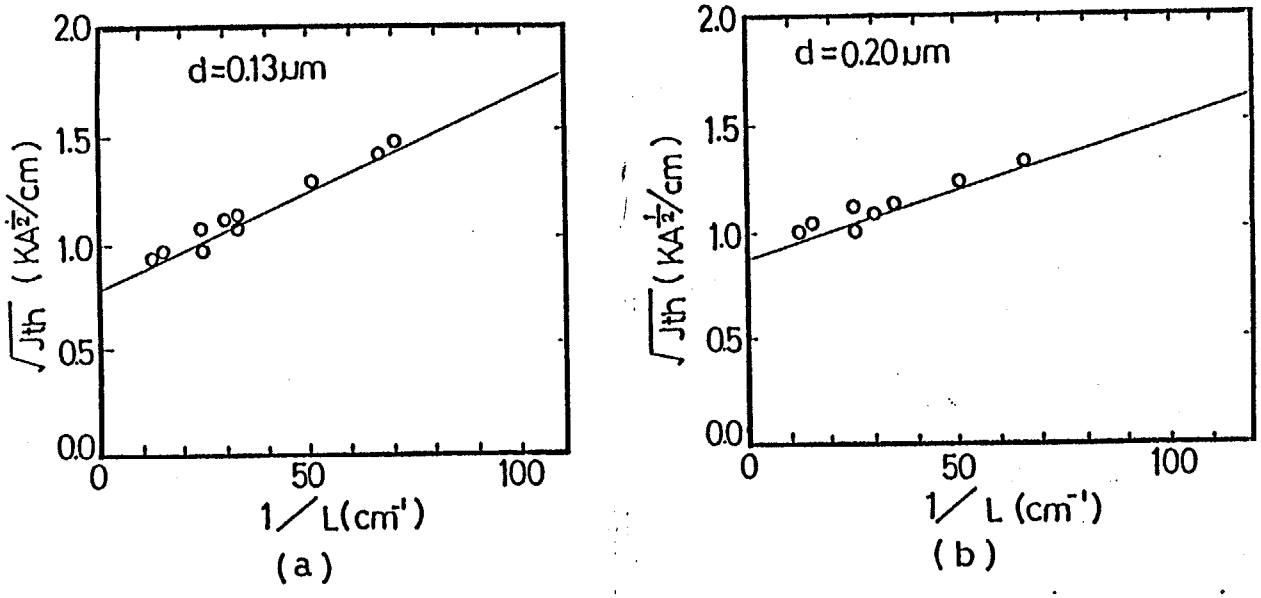

Fig. 3-2 Square root of threshold current density versus reciprocal cavity length. (a) Active layer thickness d=0.13 μ m. (b) d=0.20 μ m.

Table 3-2 Parameters obtained from the experiment.

d(μm)	ξ	R	H ($\sqrt{kA/cm}$)	K ($\sqrt{kA/cm^3}$)	$(A_0-K_0)B$ ($\sqrt{cm/A}$)
0.13	0.26	0.33	0.65±0.06	220±10	0.055±0.006
0.20	0.45	0.36	0.63±0.03	200±10	

tors ξ =0.26 for d=0.13μm and ξ =0.45 for d=0.20μm[133] into eq. (3-5), the values of K are obtained from the intersection of the line with the vertical axis, while the values of H are obtained from the gradient. Furthermore, the values of $(A_0-K_0)B$ are obtained using that R=0.33 for d=0.13μm and 0.36 for d=0.20 μm[134] where waveguide structure is taken into consideration. Obtained values are summarized in Table 3-2.

From values of K for the two different active layer thicknesses, using eq. (3-7), loss coefficients $\alpha_{in}+\alpha_2$ and α_{ex} are calculated to be $320cm^{-1}$ and $20cm^{-1}$, respectively, which are comparable to values $250cm^{-1}$ and $30cm^{-1}$ for 1.58μm-lasers grown by LPE[126]. Figure 3-3 shows experimental relation between the threshold current density and active layer thickness which agrees with theoretical curve given by eq. (3-5) and values in Table 3-2.

3-3 Threshold current density on p-type substrate

The following layers were grown on Zn-doped ($p=5\times10^{18}cm^{-3}$) InP substrate.

(i) 1μm p-type ($p=1-5\times10^{17}cm^{-3}$) InP buffer layer

(ii) 0.13-0.2μm undoped GaInAsP active layer

(iii) 1.5-2μm n-type ($n=5-10\times10^{18}cm^{-3}$) InP cladding layer.

Growth rates were 1-2μm/h for InP layer and 2-4μm/h for GaInAsP layer, on which the threshold current density is depen-

dent sensitively as mentioned later. After the growth, electrode was formed as conventional manner and broad contact laser was made for evaluation of DH wafer.

Fabricated laser was operated under pulsed condition at room temperature and threshold current density was measured. Near field pattern was observed to confirm the homogeneous. The lowest threshold current density was 1.2kA/cm^2 which was obtained by high growth rate, 2μ m/h for InP and 4μ m/h for GaInAsP, in contrast with the threshold current density of 2.1-4kA/cm^2 for low growth rate, 1μ m/h for InP and 2μ m/h for GaInAsP. Typical growth conditions for these two kinds of growths and the obtained lowest threshold current density are listed in Table. 3-3. The relation between threshold current density and thickness of active layer with high growth rate is shown in Fig. 3-3, too.

The dependence of the threshold current on growth rate is explained as follows: It was reported that the threshold current density was increased by Zn diffusion from the adjacent layer to the active layer and was sensitive to the Zn concentration in the adjacent layer in LPE grown wafers(133). In OMVPE, the growth time is much longer than LPE and Zn-diffusion may be more severe. Hence, the threshold current density was sensitive to the growth time. As an evidence of the relation between the threshold current density and the Zn concentration, the author experimentally compared wafers grown by OMVPE on lightly-

doped ($7x10^{17}cm^{-3}$) and heavily-doped ($5x10^{18}cm^{-3}$) substrates to reveal appreciable difference, factor more than two, in the threshold current density. The control of Zn diffusion from p-type is an important point in OMVPE. Lightly-doped substrate cannot be used for device with CW operation due to high resistivity of substrate. The reduction of the growth time was effective for decreasing the threshold current density. The optimization of the thickness and doping concentration of the buffer InP layer may be also effective.

The problem of growth on p-type substrate was observed in measurement of photoluminescence. In case of DH structure on p-type substrate, intensity of photoluminescence was weaker than same structure on n-type substrate. Difference of intensity was reduced by increasing of power density of excitation. Same tendency was observed by p-doped quaternary layer. From dependence of excitation levels, non-radiative center would be increased growth with p-type dopant (136). Hence, room of improvement of p-type dopant may be still remained.

3-4. BH lasers by hybrid growth

In the hybrid method, a mesa structure was formed on the DH structure prepared by OMVPE using conventional photolithography and etching process. Then, n- and p-blocking layer were grown by LPE. In the fabrication of BH lasers, DH wafers grown were etched into mesa-shape by Br-CH_3OH through SiO_2 stripe

masks. Width and direction of the stripe were 5 μ m and <01$\bar{1}$>, respectively. Then n- and p-InP current-blocking layers were successively grown by LPE method to form buried hetero-structure. Electrodes were formed with Zn/Au and Sn/Au for p- and n-sides, respectively. Laser facets were formed by cleaving.

BH lasers were operated under room temperature CW conditions. The threshold current of 62mA was obtained at the lasing wavelength of 1.54 μ m. The I-L curve and lasing spectrum are shown in Fig. 3-4. The active region width and length were 7 μ m and 220 μ m, respectively. Multiple transverse modes observed in the spectrum can be eliminated by narrowing the stripe width. The external differential quantum efficiency was 14% per facet. The output power of more than 7mW was obtained.

Threshold current density of this wafer was 3.7kA/cm^2 and it was not changed much after BH growth process (4kA/cm^2). Hence, it was confirmed that the current was effectively confined by the blocking layers.

The device had been operated at constant current mode, I/Ith=1.25, at room temperature. No degradation was observed after an aging test of 4000 hours.

3-5. BH lasers entirely by OMVPE

For realization of BH structure by OMVPE apparatus, the author proposed two different methods. One was mass transport

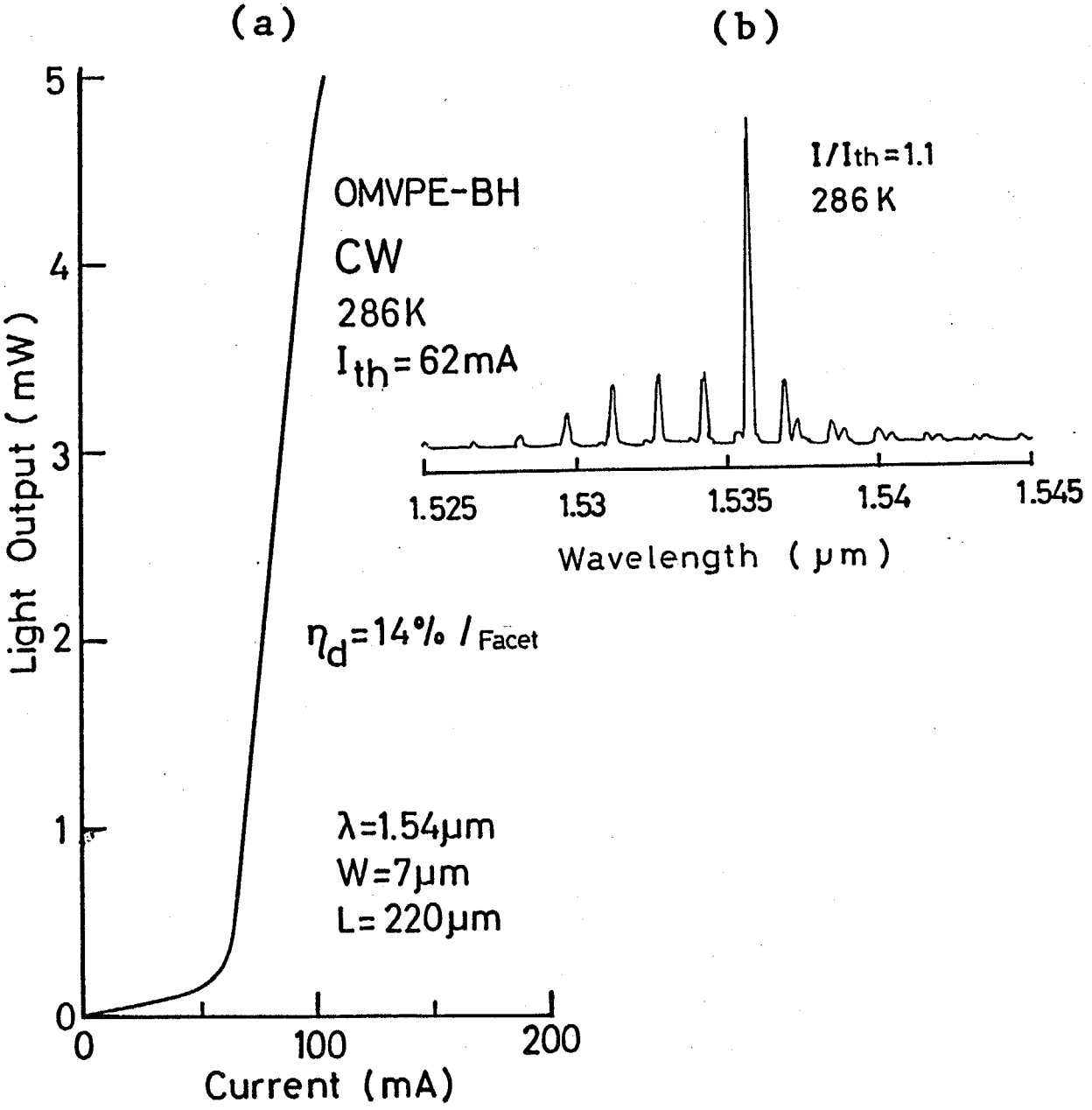

Fig. 3-4 CW lasing characteristics of OMVPE-LPE hybrid grown BH lasers with the stripe width of 7 μ m. (a) I-L curve. (b) Lasing spectrum.

methods[137, 138] and the other was selective regrowth by OMVPE[139]. At first, mass transport methods are described.

The mass transport process offered extremely narrow active layer less than 1 μ m without such a narrow mask and one of the attractive methods for fabrication of BH lasers. The mass transport technique was employed in the OMVPE system with adjustment of PH_3 flow rate.

All process of fabrication of mass transport laser is shown on Fig. 3-5.

The DH wafer grown by OMVPE on n-type substrate was processed into the shape illustrated in Fig. 3-5 (b). First, a SiO_2 stripe mask was formed with 5 μ m width and along <01$\bar{1}$> direction as a mask. Then the InP cladding layer in unprotected area was removed by $4HCl:H_2O$ solution and a trapezoidal InP cladding was formed. Finally, the quaternary region was etched down to 2 or 3 μ m wide by $3H_2SO_4:H_2O_2:H_2O$ solution. The SEM photograph in Fig. 3-6 (a) is shown this cross sectional view.

By the mass transport phenomenon, undercut portion was filled by InP in OMVPE apparatus. The total flow rate of H_2/N_2 was 2.4 slm. The pressure in the reactor was kept at 76Torr. These parameter were chosen because it was benefit for following successive InP over-growth by OMVPE. The phosphorus pressure was important as parameter of mass-transport conditions. In case that PH_3 pressure was too low, phosphorus of InP surface was

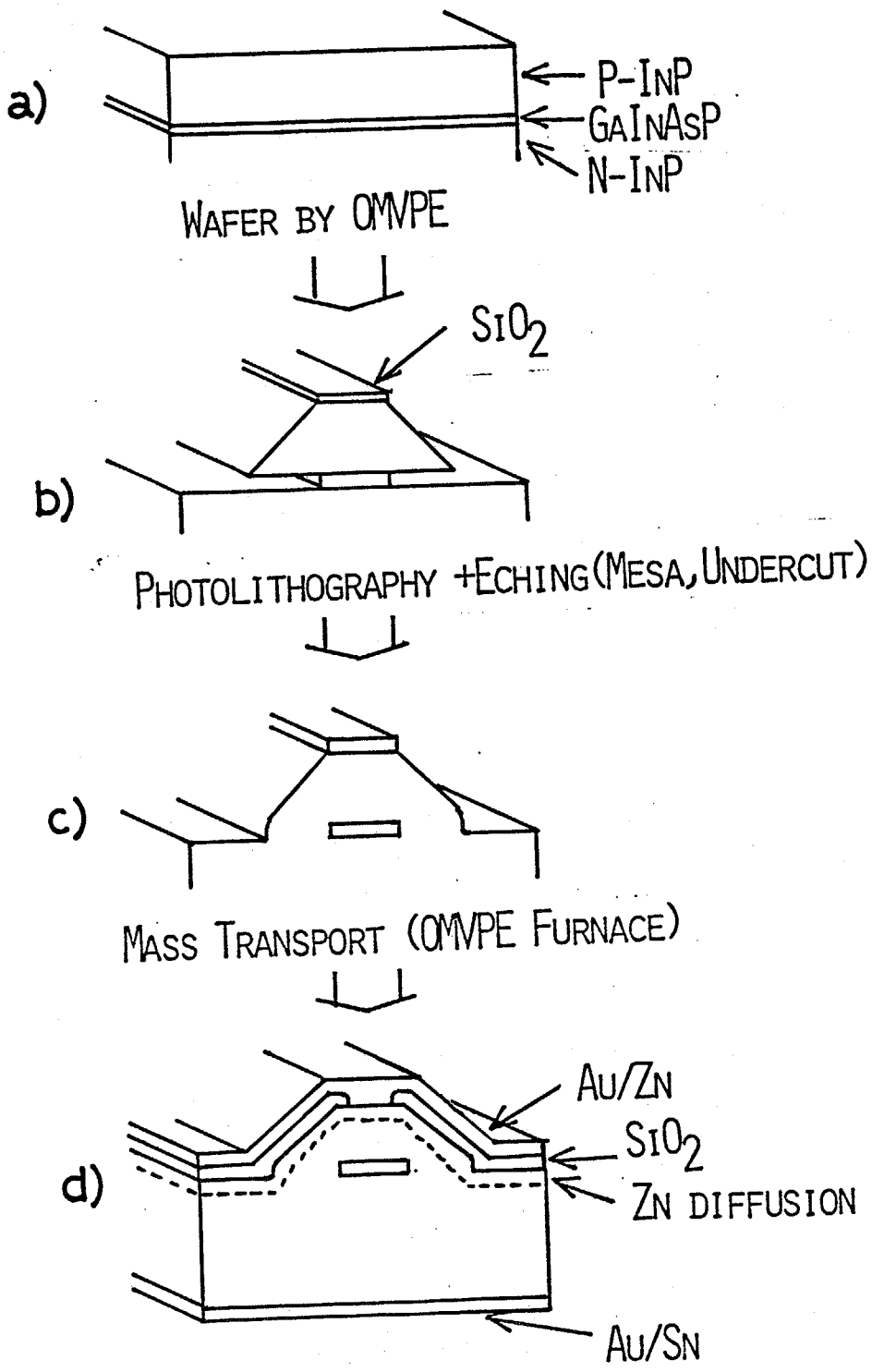

Fig. 3-5 All process for fabrication of mass transport laser.

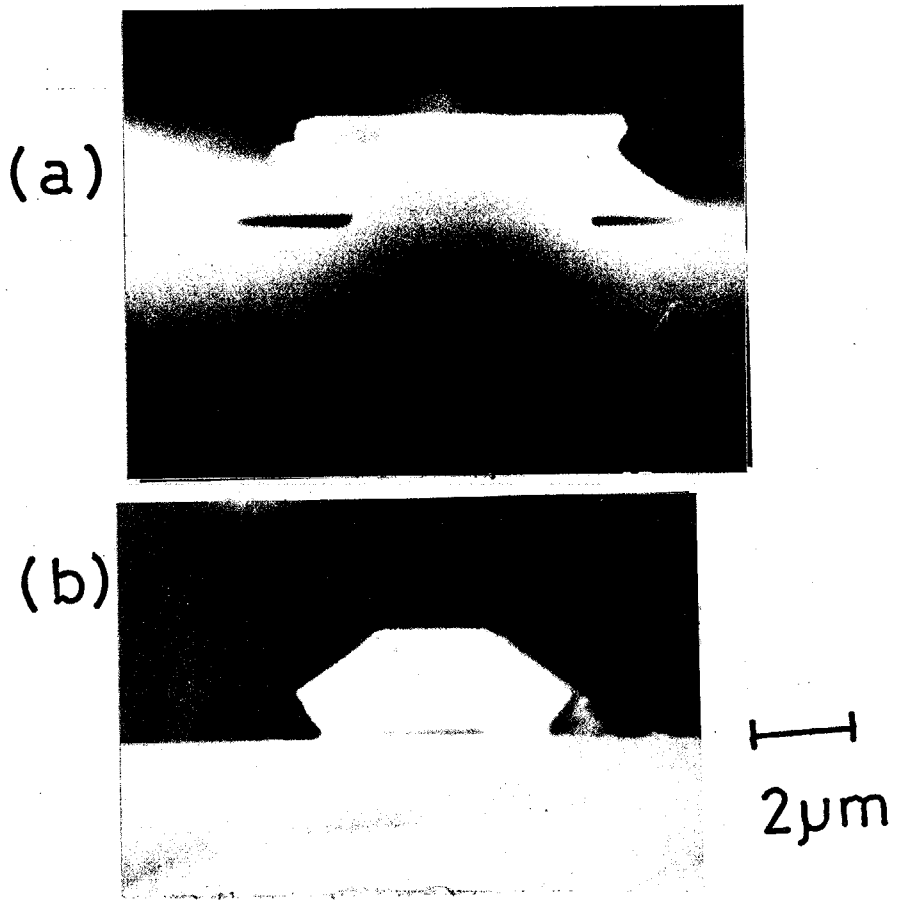

Fig. 3-6 Cross sectional view of (a) after etching and (b) after mass transport process.

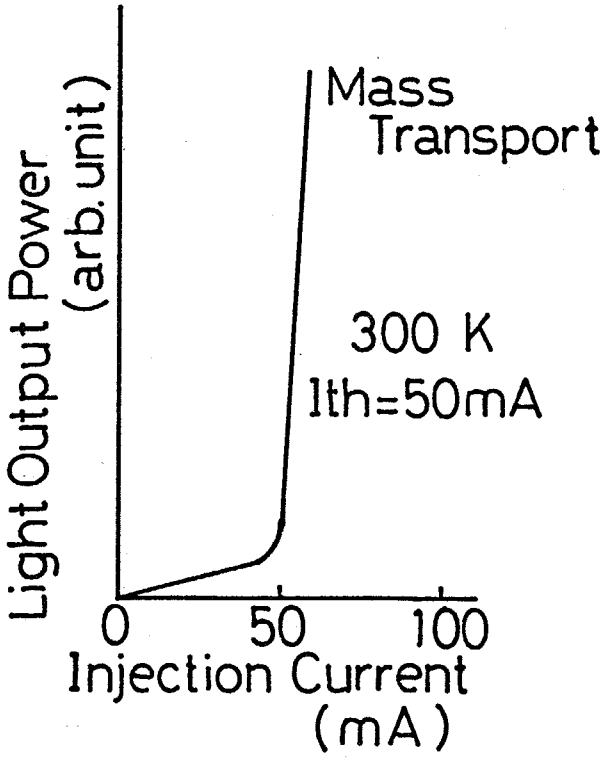

Fig. 3-7 The I-L characteristics of mass transport laser. The measurement was carrier out under pulsed operation.

evaporated and degradation was occurred. In case that PH_3 pressure was too high, mass transport occurred insufficiently compared with process under appropriate pressure and reproducibility was reduced by long time process under high temperature. To adjust the phosphor pressure, the flow rate of PH_3 was controlled by a mass flow controller in the OMVPE system. PH_3 diluted by H_2 in 5% was supplied through a cracking furnace at 800℃. The threshold value not to decompose of InP surface at 700℃ was 125sccm. Good mass transport was observed with this condition after 1hour as shown in Fig. 3-6 (b).

The sample buried in this manner were transferred to the next process. Figure 3-5 (d) shows the process, Zn-diffusion over epi-side, 5 μ m wide electrode contact windows made by an SiO_2 mask, and electrode with Zn/Au and Sn/Au for p- and n-side, respectively after lapping. The I-L property for this laser is shown in Fig. 3-7. The lowest threshold current was 50mA in pulsed operation at room temperature. The cavity width and length were 3 μ m and 350 μ m, respectively. This value is not so enough compared with expected value by the threshold current density (1-2kA/cm^2). The cause is some current leakage probably because the process was not optimized. In this sample, CW operation was not observed by high resistance of sample caused by n-type substrate.

As the next methods, regrowth process by OMVPE process was

described. The flat surface after buried process has advantage for electrode process and thermal radiation and that is obtained by selective growth. Current blocking was made by multiple p-n junction(140).

At first, conditions of selective growth are described. When the crystal surface is covered by a SiO_2 mask, crystal growth is not observed by LPE, by contrast the deposition of poly-crystal was observed by normal OMVPE. Although, when the stripe mask was narrow(139), crystal growth was not observed on the SiO_2 mask by OMVPE. When growth temperature was 640℃, poly-crystal was deposited when stripe width was over 8 μm, however deposition was not observed under 5 μm. Using this phenomenon, the buried structure of the mesa under narrow SiO_2 stripe was obtained by selective growth.

Next, the etched shape before buried growth is described. The ordinary OMVPE growth is limited by the transport of source gases. Growth in the portions shaded by the inclination of wall of the reverse mesa was suppressed due to the restriction in the flow of source gases. Hence, as the reverse mesa was buried, caves was remained after OMVPE growth. On the other hand, when the etched shape is an upright mesa, the stripe width of the active layer is broader than that of the SiO_2 mask and this is not suitable for low threshold current. Hence, the rectangular shape is suitable for the buried process.

Fabrication procedure of the buried structure is shown in

Fig. 3-8. After the growth of a DH wafer on p-type substrate, 5 μm SiO_2 stripes were along <011> crystal axis. The InP cladding layer was etched by $HCl-H_2O$(4:1) to leave a rectangular shape. Then the quaternary active layer was etched by $H_2SO_4-H_2O-H_2O_2$(3:1:1) to leave the mesa structure with undercut. The growth conditions of re-growth were V/III ratio of 170 and growth temperature of 640℃. The first blocking layer was lightly doped p-InP (0.3 μm). Then 10 pairs[140] of lightly doped p and n layers were grown up to 1.7 μm thick in total for current blocking. Figure 3-9 shows a typical cross-section view after re-growth.

The rectangular shape with undercut portion was perfectly buried by re-growth. From this results, the process with high temperature and long time for mass transport before the regrowth can be eliminated. However, it cannot be concluded that the end of the narrow and deep undercut was filled only by normal OMVPE process. The filling process was started from the end of the undercut channel as observed in mass transport[137, 138]. It was confirmed that time for filling of undercut was reduced by stopping of regrowth at early stage as shown in Fig. 3-10. Hence, it is probably because In atoms adsorbed on the InP surface migrated toward the undercut channels where the shape is concave and which has a lower surface energy[138] as shown in Fig. 3-11.

As current blocking layer, single pair of p-n junction was also tried and CW operation was not observed in this case due to

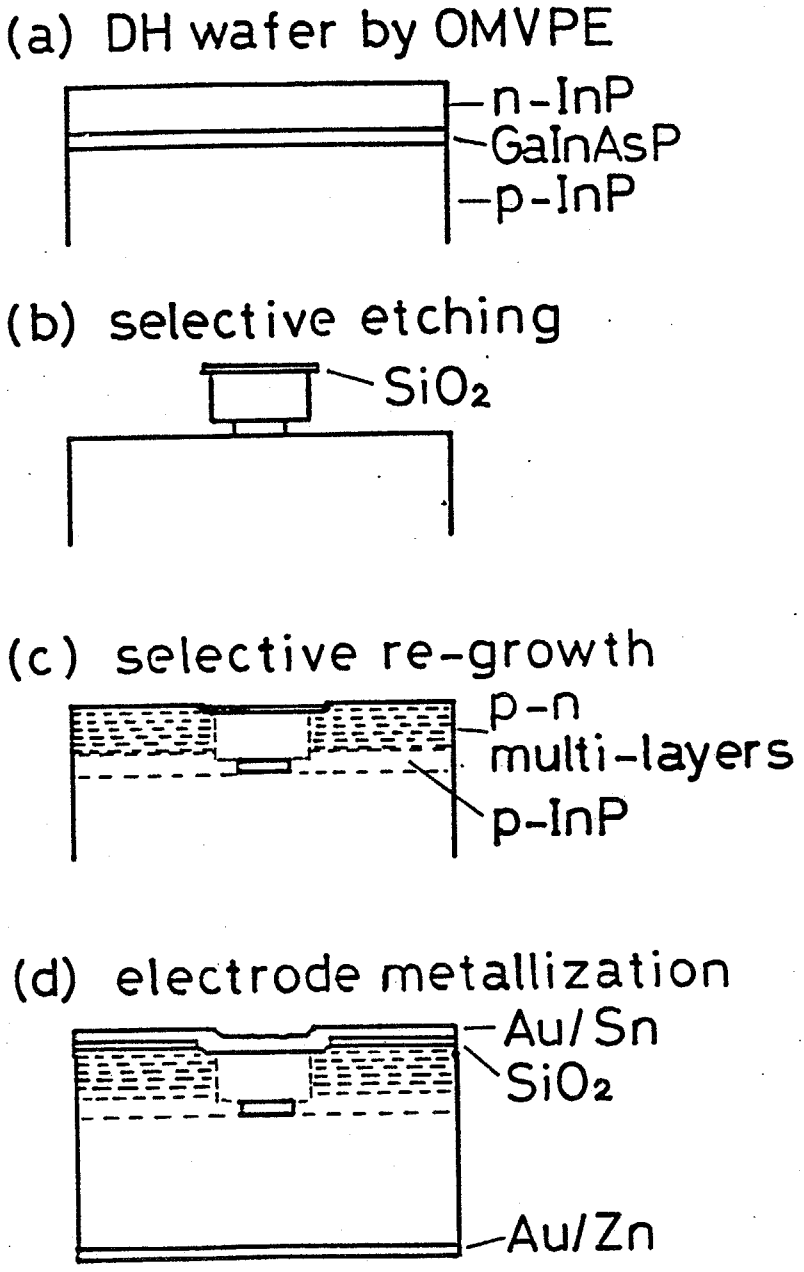

Fig. 3-8 Process of buried heterostructure fabrication by OMVPE.

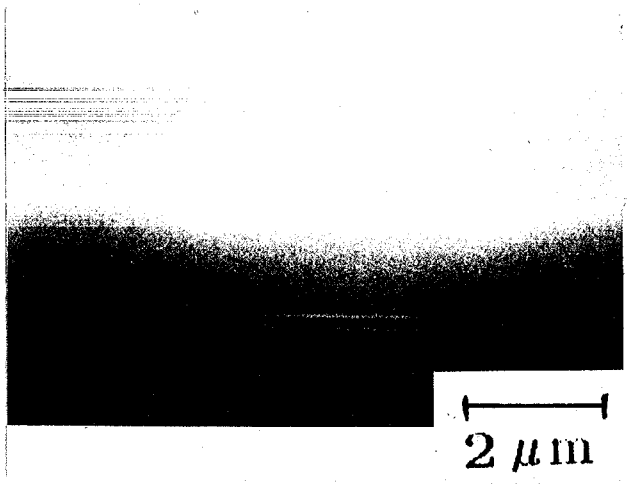

Fig. 3-9 A typical cross sectional view after OMVPE regrowth.

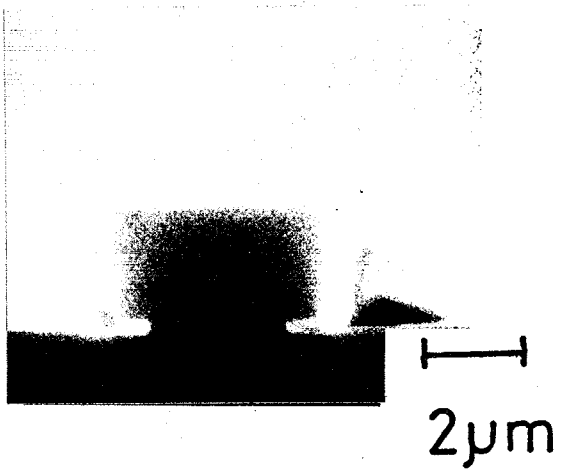

Fig. 3-10 Cross sectional view after interruption of regrowth at early stage. The growth time is about 5 minutes.

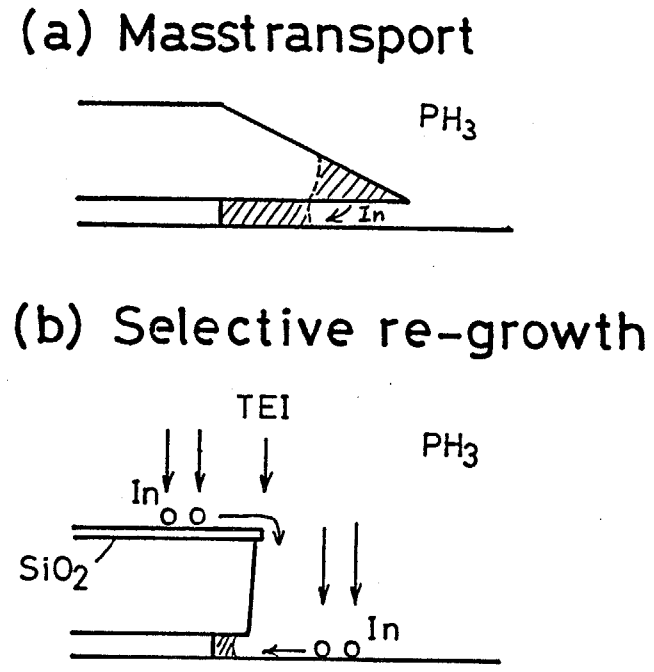

Fig. 3-11 Explanation of buried re-growth. The migration was enhanced by supply of metalorganic source.

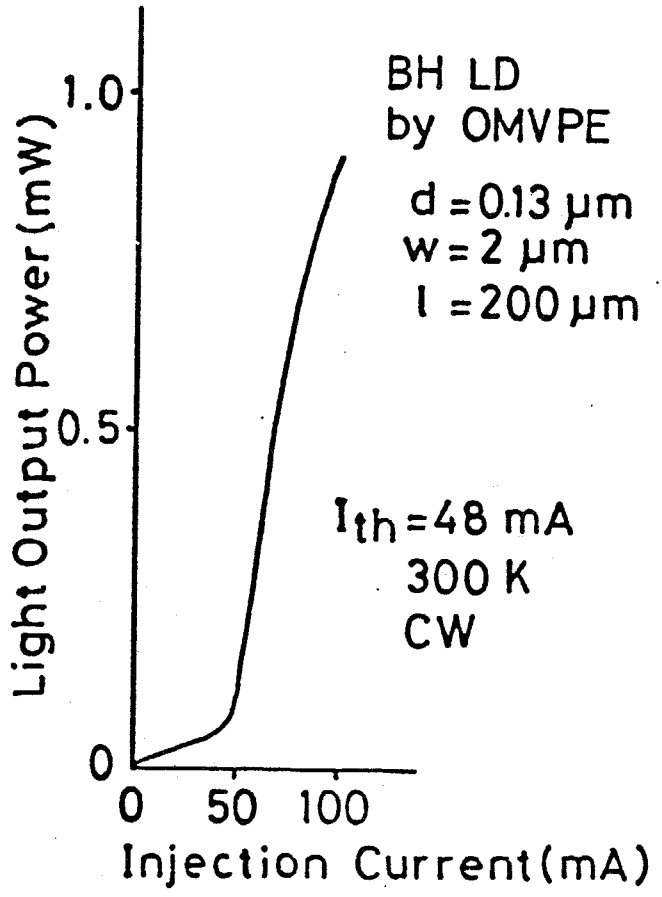

Fig. 3-12 CW I-L characteristics of BH laser by entirely with OMVPE.

the increase of leakage.

After the re-growth, electrode contact windows were formed and lasing characteristics was tested. The I-L curve is shown in Fig. 3-12. The lowest threshold current was 48mA under CW conditions at room temperature. The maximum output power was 2mW. The cavity width and length were 2μm and 200μm, respectively. However, there is room for improvement for current blocking and high power operation from its I-L characteristic. This device has also been operated at constant current mode, I/Ith=1.25, at room temperature. No degradation was observed after an aging test of 5500 hours.

3-6. Conclusion remarks

In this chapter, evaluation of crystal quality was confirmed by characteristics of fabricated lasers. Threshold current density by broad contact laser was pointed out that crystal quality was compared with that grown by LPE. BH laser was also fabricated by hybrid methods and entirely by OMVPE. CW operation was confirmed by both of them. Reliability of laser was confirmed by a several thousands hour's aging test of CW laser.

Chapter 4. Ultra fine structure and quantum well lasers by OMVPE

4-1. Introduction

To improve device characteristics, quantum well structure is very attractive. In GaAlAs/GaAs systems, very excellent results were obtained as described in section 1-2. However, it is not reported advantage in low threshold current of GaInAsP/InP quantum well laser, that is very important for optical communications, and more research for quantum well structure of this material is indispensable for improvement of devices.

To apply quantum well structure to devices, very thin double heterostructure with the thickness of the order of electron wavelength must be fabricated with good crystal quality and reproductivity. Hence, the author had to develop crystal growth method suitable for fabrication of those structure. OMVPE method is one of the suitable methods for fabrication of ultra fine structure and the author obtained good crystal quality about conventional DH structure mentioned above. However, more development of apparatus and procedure were indispensable for fine structure fabrication.

To develop growth method for fine structure, evaluation of those fine structure must be also developed. Bulk crystal was established by liquid phase epitaxy and evaluation of bulk crystal can be used established methods. Particularly, fabrication

of laser is practical evaluation of crystal quality. However, quantum well structure on GaInAsP/InP is not established for practical use and evaluation of quantum well structure is very difficult.

In this chapter, development of growth method and measurement of quantum well structure are discussed. Fabrication of single quantum well lasers based on those development is also reported.

4-2. Fabrication of quantum well structure by improved apparatus

For evaluation of quantum well structure, multi quantum well structure was grown on n-type InP substrate. The selection of n-type as conductive type of substrate was caused by weak photoluminescence intensity in grown crystal on p-type substrate as described in section 3-3. Switching of valves for growth of quantum well layers and barrier layers were controlled by a computer for uniform thickness of each layer.

As the first, multi quantum well structure was fabricated with same growth procedure reported in section 2-4. Growth sequence is shown in Fig. 4-1. A 150nm InP buffer layer, fifteen 12nm quaternary quantum well layers separated by fourteen 12nm InP barrier layers, and a 15nm InP cladding layer were successively grown on n-type InP substrate. Growth conditions of the quaternary layer were the same as conditions obtained for the 1.55 μm bandgap wavelength in conventional growth. Evaluation of

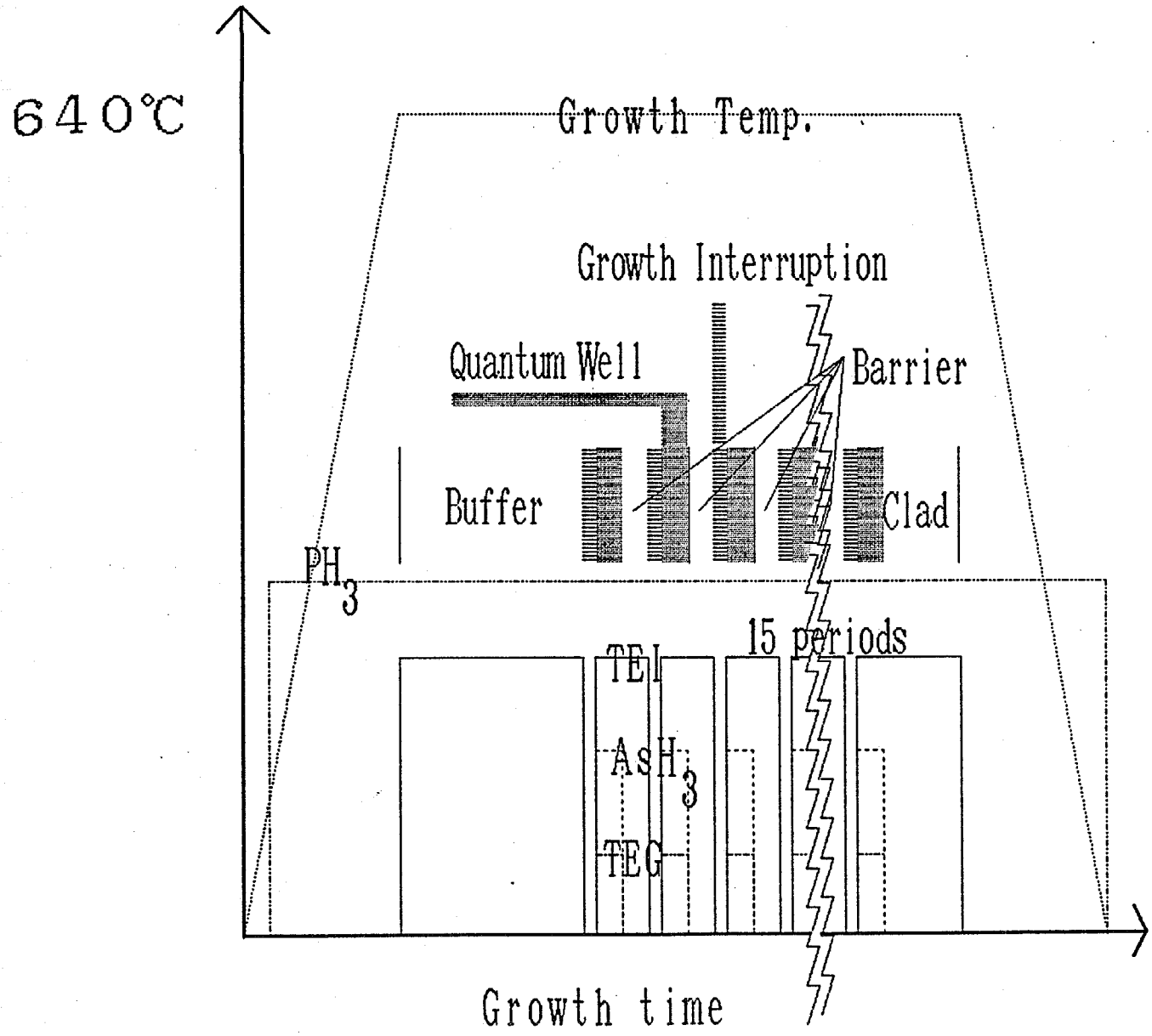

Fig. 4-1 Growth sequence for multi quantum well structure

this crystal is described in next section.

However, the switching of group III source had a delay of initiation for introduction of source after switching by a slight difference in pressures between the vent line and the reactor described in section 2-4. Hence, the author couldn't fabricate multi layer structure with very short periods of switching time and growth rate in very thin layer was reduced in comparison with growth of conventional thickness ($> 0.1\,\mu$ m). Thus, the author improved the apparatus for the precise pressures balance between the vent line and the reactor for controllability of ultra thin layer.

As improvement of apparatus, the author set a pressure control of vent line. Exhaust system was changed for pressure control of vent line as shown in Fig. 4-2. Vent line was connected to dummy reactor. This dummy chamber had a pressure gauge and a nitrogen flow line for set of chamber pressure. The dummy chamber was exhausted by rotary pump with auto pressure controller or by main pump with connection of valve. Another auto pressure controller was added to main exhaust line at the same time. Using two auto pressure controller was not stable for short period switching because those short period is too severe for the time constant in auto-pressure controller. Hence, vent line is connected to main pump, while total flow rate for auto pressure controller of main exhaust line is maintained at constant. Pressure of dummy chamber was valanced with needle valve (V_0 in

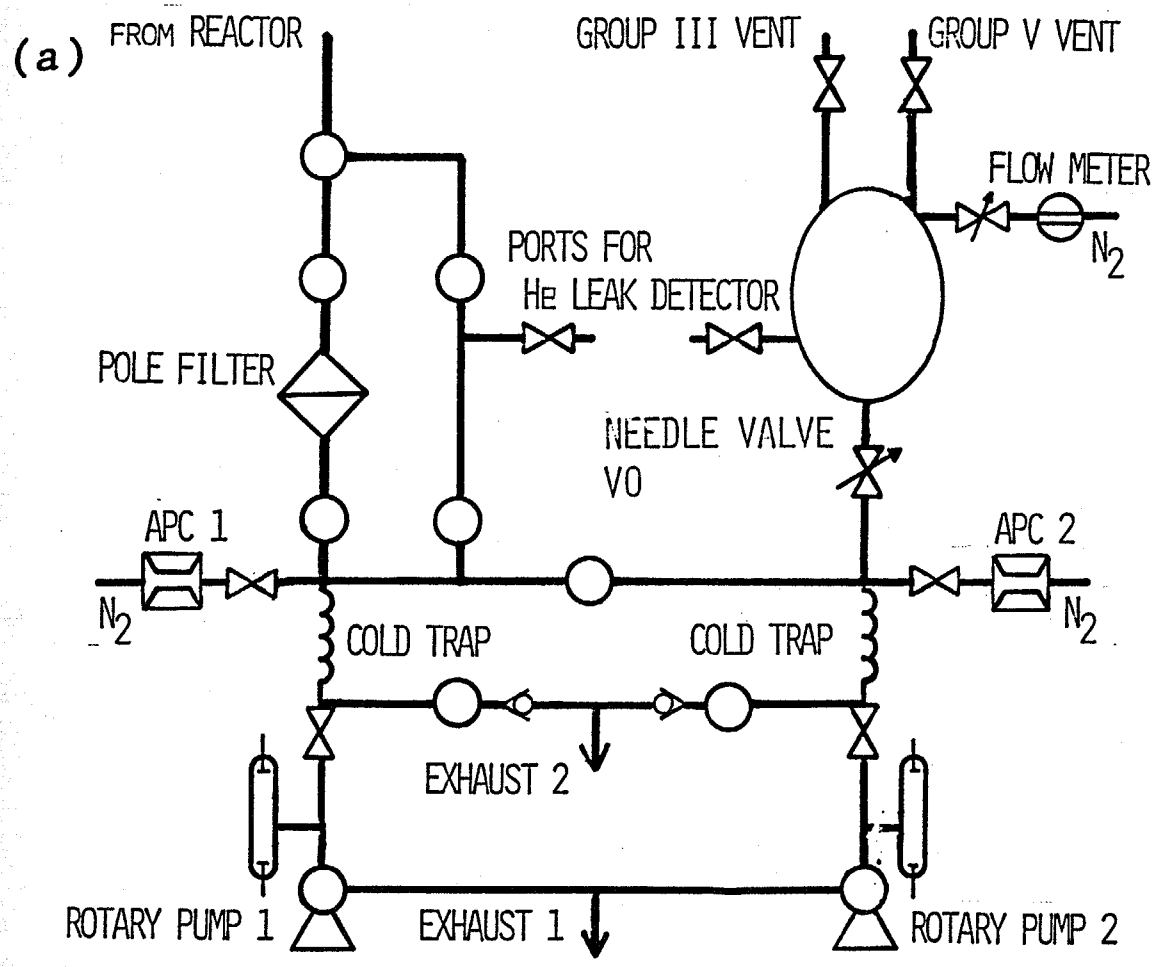

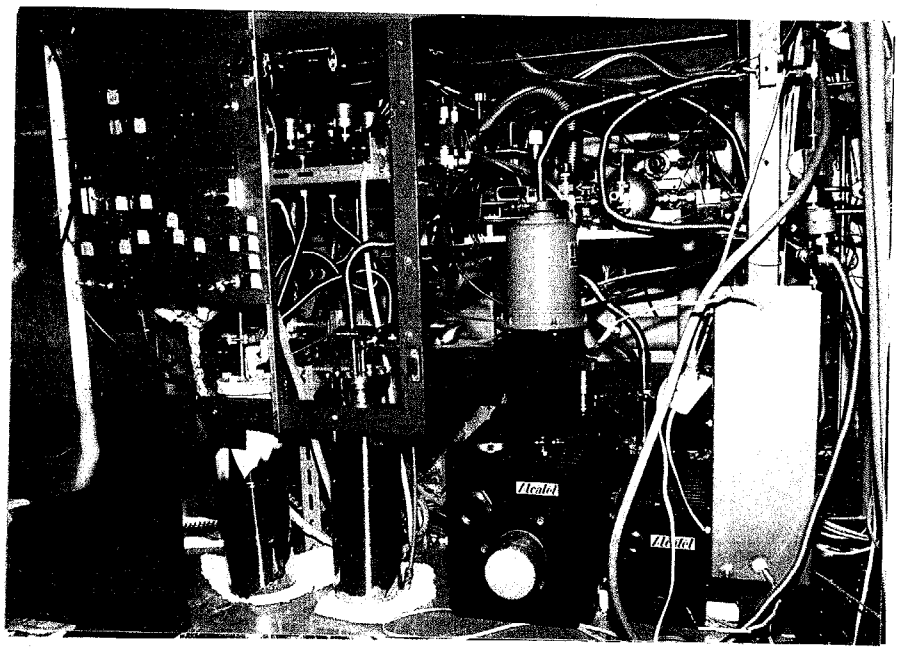

Fig. 4-2 Improvement of exhaust line for abrupt interface. (a) Schematic view of improved exhaust line. (b) Photograph of new exhaust system.

Fig. 4-2) and flow rate of nitrogen introduced to dummy chamber. By this improvement, stopping period of bubbling was reduced in switching of the valve and controllability was improved. Results after this improvement is also described in next section. However, fluctuation of bubbling sound couldn't be eliminated completely by this improvement and the reproductivity is also poor as mentioned later.

For design of apparatus with constant flow of metal organic sources, fluctuation of metal organic source bubbler was simulated. It was very difficult that adjustment of pressure difference between reactor line and vent line keep under 0.1-1Torr due to the accuracy of pressure sensor and controllability of pressure. Hence, flow rate fluctuation of sources must be suppressed by apparatus design even under a residual pressure difference. Supplying source quantity was decided by following equation:

Real flow rate of metalorganic source =
(Flow rate from bubbler) X (Vapor pressure of sources)
/ (Pressure of Bubbler) (4-1)

Thus, those two values, i.e., flow rate from bubbler and pressure of bubbler, must be calculated from simulation. Flow rate, pressure, volume and resistance of gas flow can be replaced to current, voltage, capacitance and resistance in electric cir-

cuits, respectively when dropped pressure is linearly with flow rate. Equivalent electric circuits is shown in Fig. 4-3. For simulation, switching to vent line in stable conditions was assumed at first. As the next, left circuits in Fig. 4-3 was switched to reactor line and response by slight difference of each lines was occurred.

Typical calculated result by assumed parameter from the author's apparatus is shown in Fig. 4-4. In author's apparatus, resistance from bubbler to switching point is too small and pressure consumed by this resistance is also small. When pressure fluctuation by switching was larger than pressure consumed by this resistance, large back current flow was occurred. As the results of back current flow, large volume of gas was transferred to bubbler and time until stable flow was changed to very long. From the simulation, it is pointed out that fluctuation by switching is proportional to ratio of pressure difference between bubbler and switching point to fluctuation pressure by switching. Hence, larger resistance[141] between bubbler and switching point is desirable. Recovery time is decided by fluctuation quantity and time constant that was similar to CR constant of electric circuits. If this CR time constant is longer than time constant of automatic pressure controller, fluctuation could be suppressed by electrical control. Larger resistance between bubbler and switching point is also desirable from this point.

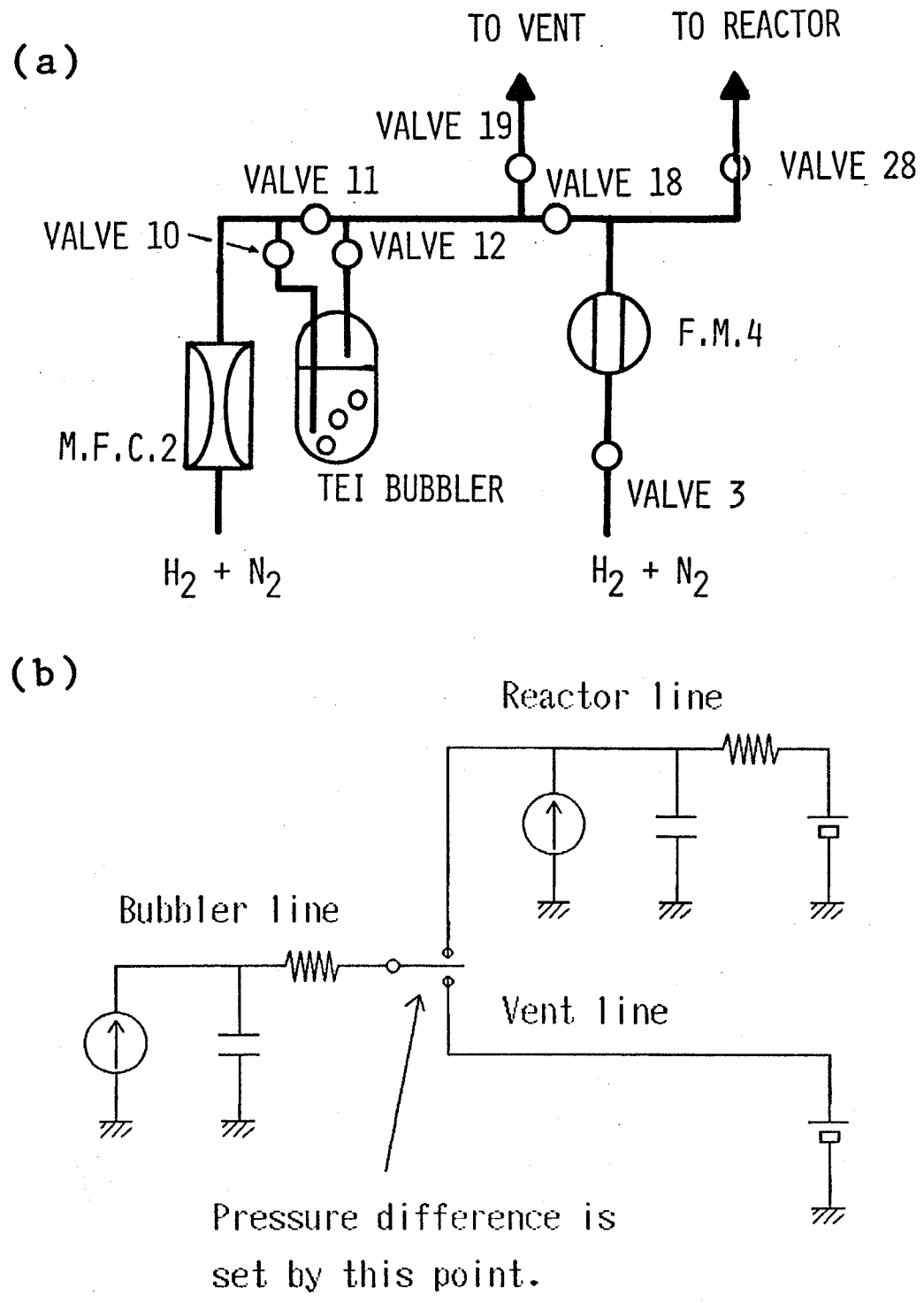

Fig. 4-3 Simulation model of fluctuation of source supply by gas switching. (a) Actual piping around TEI bubbler. (b) Electric circuits equivalent to actual piping. Resistance is equivalent from orifice of pipe and valve. Capacitance is equivalent for volume of pipe and bubbler. Current source is equivalent flow meter or mass flow controller. Pressure difference was set by value of switching point. We add dilution of source flow by back current in upper stream of switching point in actual simulation.

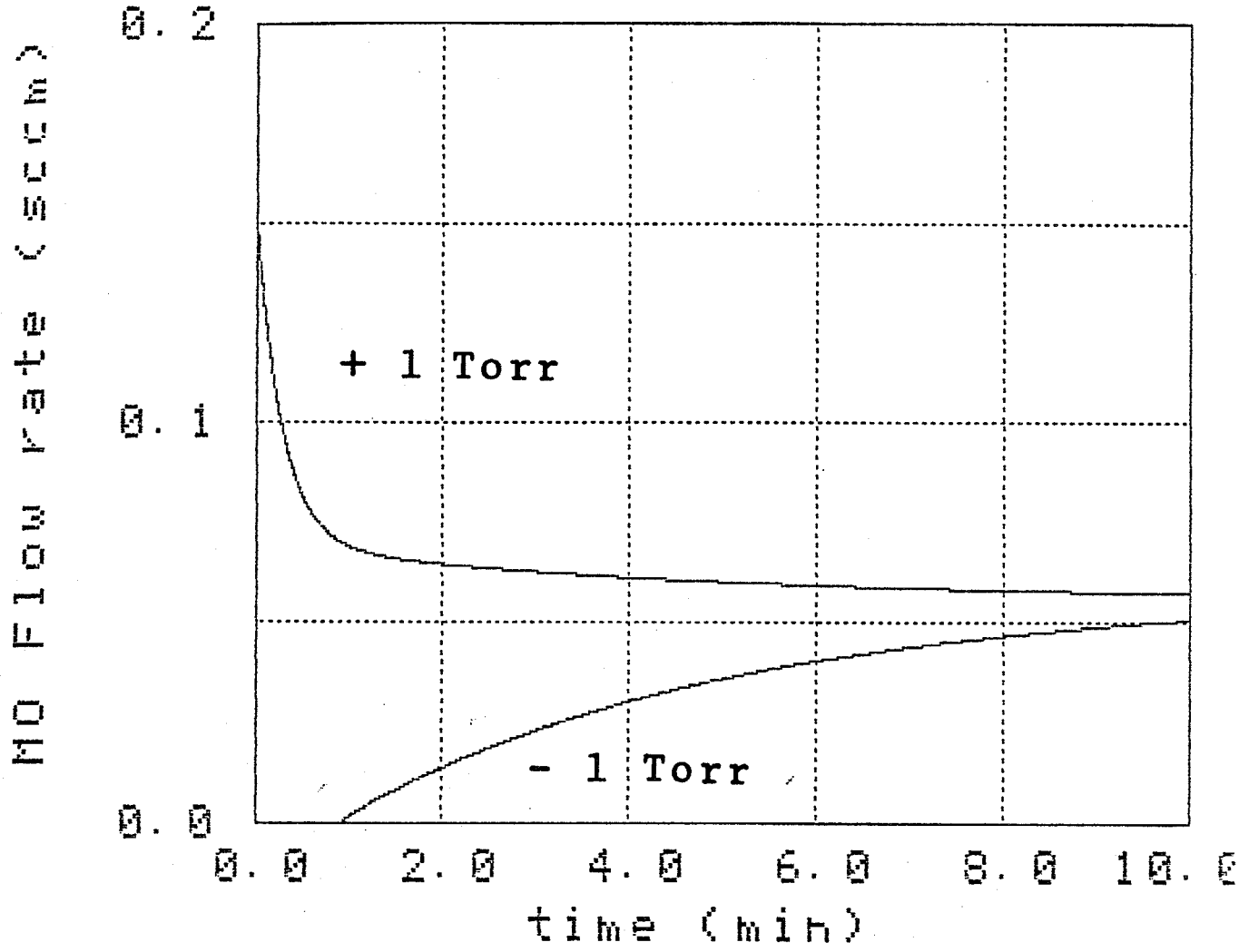

Fig. 4-4 Calculated result by simulation of fluctuation. The parameter was supposed from our apparatus. The capacitance was supposed from volume of bubbler. Effect to lattice mismatching of this fluctuation would be suppressed by switching procedure in practical experiment. The gas switching procedure contains growth interruption as mentioned in section 2-4 before quaternary layer growth and simultaneous opening of two valves that are connected to reactor line and to vent line with 1 seconds periods.

For more accurate analysis, relation of consumed pressure by resistance and flow rate must be studied(142). Although dropped pressure is linearly with flow rate in small dropped pressure, this linearlity was broken if consumed pressure was large. In this case, flow rate Q in straight pipe was represented by following equation:

$$Q = \pi d^4/(128 \eta l) \times (P_1+P_2)(P_1-P_2)/2 \qquad (4-2)$$

Where, P_1 is pressure of upstream, P_2 is pressure of downstream, d is diameter of pipe, η is viscosity and l is length of pipe.

Resistance of flow is changed by shape of piping. Equation for pressure dropping by narrow hole is represented by other equations. When the velocity of flow is lower than the speed of sound, flow rate is changed by more complicate equation. However, when the velocity of flow rate is equal to the speed of sound, only pressure of upstream determined flow rate and down stream pressure is not influenced by pressure of upstream. This situation is occurred when pressure relation is in following equation.

$$P_2/P_1 \leqq 0.52 \qquad (4-3)$$

Hence, pressure difference on switching point have no relation to fluctuation of supplied sources when concentrated resistance,

i.e. needle valve, is consumed sufficient pressure for saving eq. (4-3) between bubbler and switching point. Of course small effect of switching is still remained for volume between needle valve and switching point.

After switching point, flow from bubbler is diluted by main flow and introduced into reactor. Introduction of source gas to reactor introduce additional pressure difference between the switching point and reactor. Hence, this effects is also in consideration with switching of sources. This pressure fluctuation is increased with increasing of the ratio of bubbler flow rate to diluted flow rate. Of course reducing of resistance between switching point and reactor is also important. For reduction of fluctuation, reducing of ratio of bubbler flow rate to diluted flow rate is important. Hence, the author considers it can be reduced or not. Mole flow ratio of metalorganic sources in reactor atmosphere determines growth rate, while total flow rate is determined by reactor design and necessary flow speed for abrupt interface. Thus, real flow rate of metal organic sources is determined by those parameter. Hence, variable parameters are pressure of bubbler and vapor pressure of sources in eq. (4-1) for reduction of flow rate of bubbler. Vapor pressure of metalorganic sources is increased by rising of temperature. However, when flow is passed colder point after bubbler at high temperature, sources is adsorbed in the wall of piping and lattice matching condition have difficulty by this

adsorption and re-vaporization of wall. Reproductivity of lattice matching was not obtained at 40℃ as bubbler temperature with keeping warmth of piping at 60℃ experimentally. More heating of pipe has technical difficulty and introduce possibility of contamination. Hence, capable temperature of bubbler is also limited lower than 40℃.

Remained parameter is only pressure of bubbler. Pressure of bubbler must be decreased for reducing of bubbler flow rate.

As a result, best condition for switching is lowest resistance obeyed eq. (4-3) between bubbler and switching point and minimum resistance between switching point and reactor.

Of course, fluctuation by introduction of source gas can be reduced by dummy line with same flow rate that is switching at same time.

From consideration based on discussion above, new machine was fabricated. Design of piping is shown in Fig. 4-5. Photograph of new machine is shown in Fig. 4-6. Main improvement is having needle valve between bubbler and switching point. Pressure gauge for each bubbler is necessary to confirm a stable set pressure. Vent line was fabricated as similar conditions to diluted flow for reactor.

Other improvement points from old machine are follows:

(1) Full automatic system with computer control: opening of valve, loading of substrate, etc..

(2) High vacuum system with turbo molecular pump for reduction

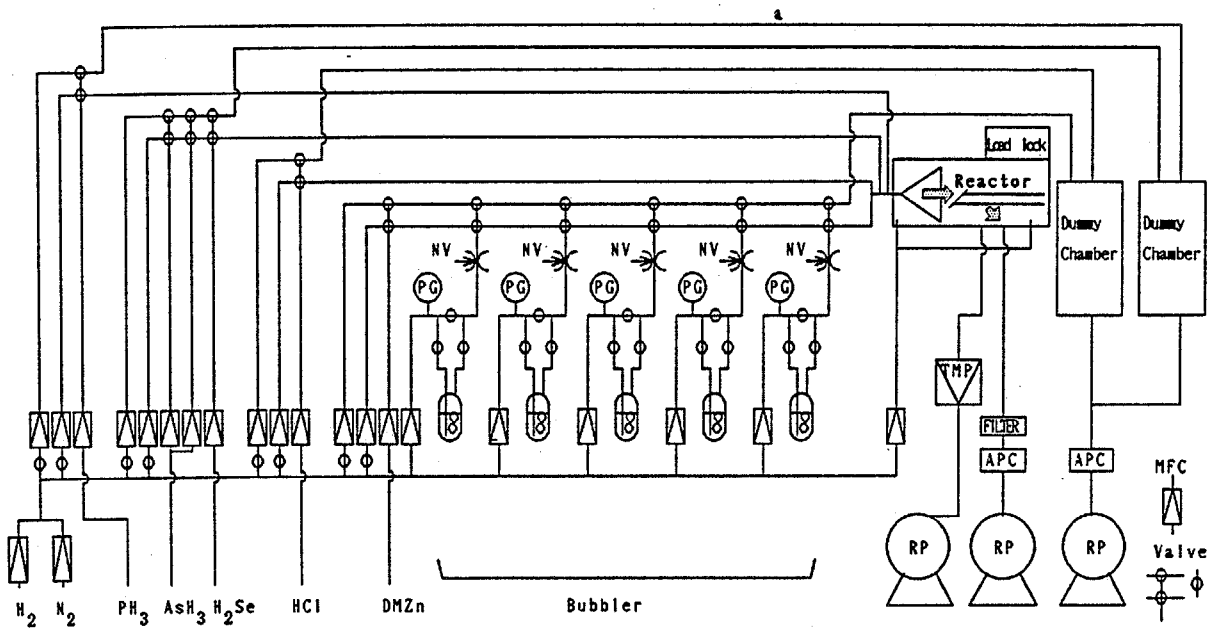

Fig. 4-5 Schematic gas line of new apparatus.

(a)

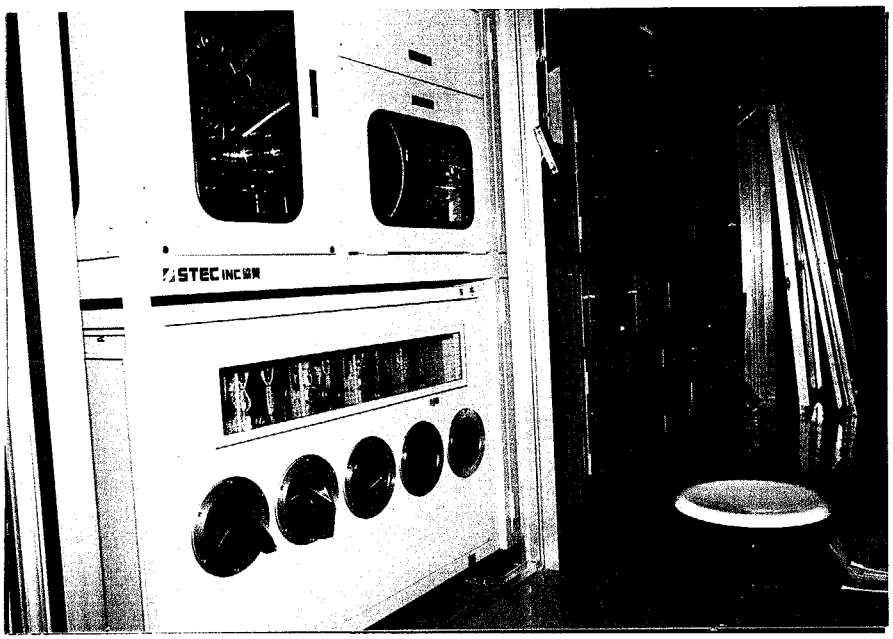

(b)

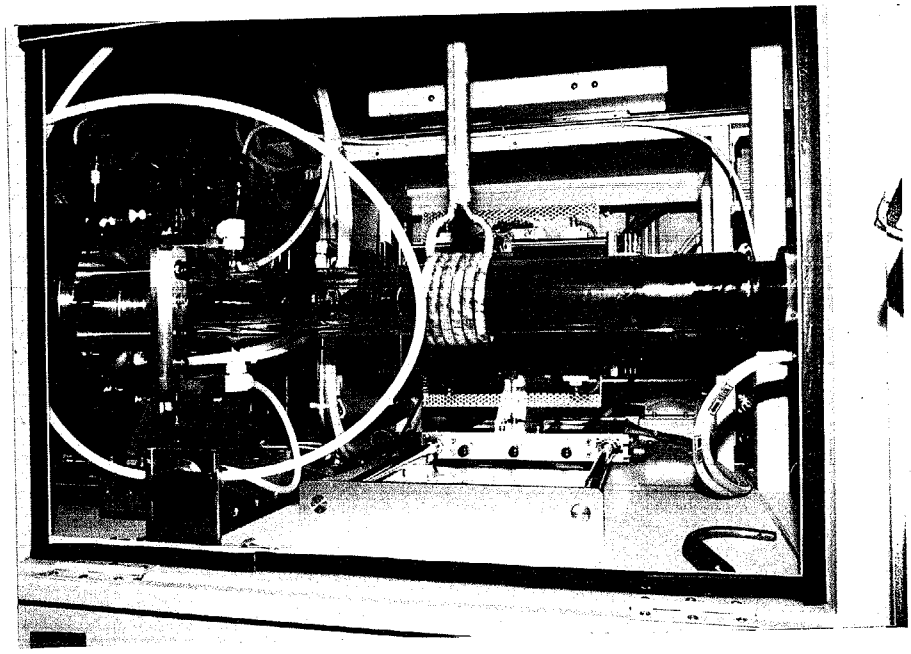

Fig. 4-6 Photographs of new apparatus. (a) Whole view of apparatus. This apparatus is also placed in a small room for safety with air-duct. (b) Reactor tube, carbon susceptor and RF coil.

of contamination.

(3) Taper shaped introducing tube after mixing of III groups and V groups sources for uniformity.

(4) Exchange of etching gas from PCl_3 to HCl to eliminate leaky teflon piping.

(5) Two AsH_3 lines for abrupt change between different composition's quaternary layers.

(6) Five metalorganic bubbler lines for future extension.

As actual use, flow rate for bubbling is fixed at 500sccm because setting of stable pressure is very difficult when flow rate is less than 500sccm. This situation will be changed by automatic control of needle valve. Adjustment of lattice matching was done by change of set pressure in bubbler as shown in Fig. 4-7. Photoluminescence intensity and diffraction signal of X-ray in bulk crystal are comparable to measurement result grown by old machine.

Results of multi quantum well structure grown by this machine is reported in next section.

4-3. Measurement of quantum well structure

At first, results with apparatus before exhaust improvement is reported.

Estimation of thickness of quantum well is a important technique because confined electron level is determined by thickness of well. Most reliable estimation of well thickness is

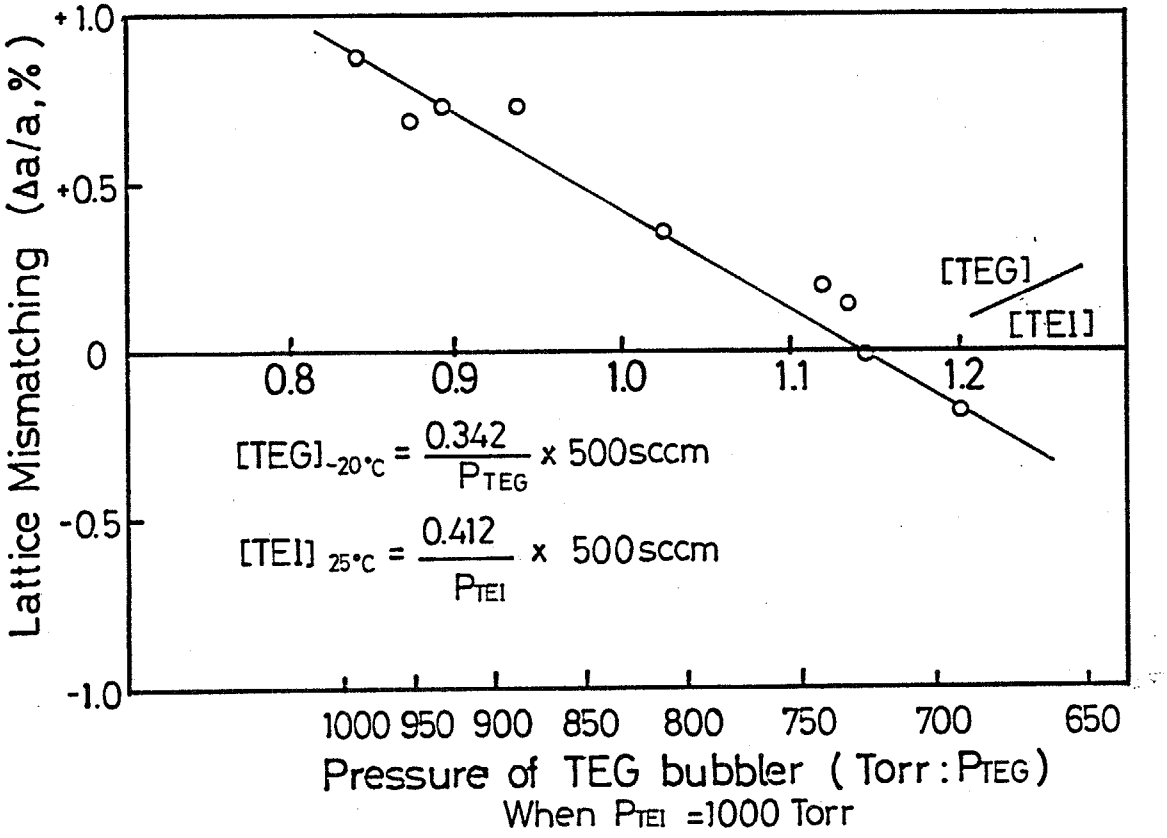

Fig. 4-7 Lattice matching condition by change of pressure of bubbler. The vertical axis indicates lattice mismatching. The middle horizontal axis indicates the ratio of mole flow ratio between TEI and TEG calculated by equation indicated in figure. The lower horizontal axis indicates the pressure of TEG bubbler when pressure of TEI bubbler is normalized at 1000Torr.

observation of lattice image by transparent electron microscope (TEM) (54, 144, 145) with high resolution. However, treatment of TEM with high resolution and making of sample for TEM are very difficult. Hence, the author gave up observation of lattice image by TEM. Reflection electron microscope (REM) (146, 147) is more convenience by easy sample fabrication. However, this method requires also difficult skillfulness for treatment of electron microscope and it is also difficult to apply conventional evaluation. Cross sectional view by REM is shown in Fig. 4-8.

Scanning electron microscope (SEM) was used for conventional observation of well thickness. Cross section view by SEM is shown in Fig. 4-9. Contrast for observation by SEM was obtained by KOH-$K_3Fe(CN)_6$-H_2O etchant. Observed thickness of well was changed by etching time and result with minimum etching time for contrast is fit to the result of photoluminescence and reflection electron microscope. The problem of this etching is that enough depth of contrast is larger than well thickness and barrier fell sometime as shown in Fig. 4-10. Same phenomenon was observed in structure fabricated by high aspect ratio etching (148).

In photoluminescence measurement, shift of peak wavelength was observed. Photoluminescence spectrum of multiple quantum well structure is shown in Fig. 4-11 and shifted by 70nm to shorter side from peak wavelength of photoluminescence from bulk

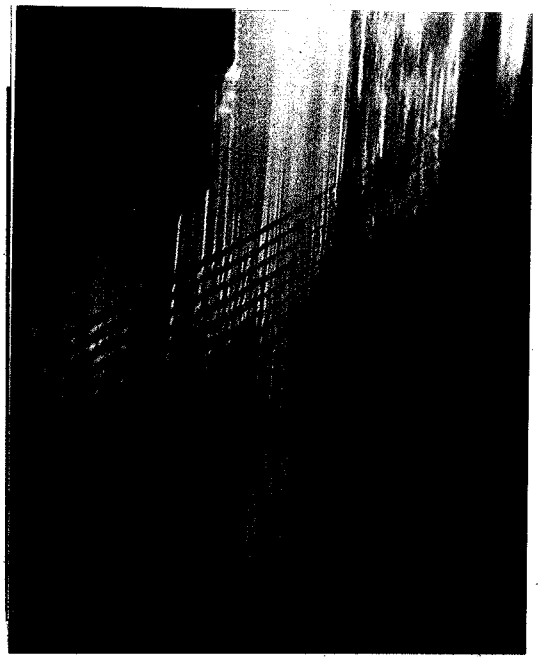

Fig. 4-8 Cross sectional view of multi quantum well structure by reflection electron microscope.

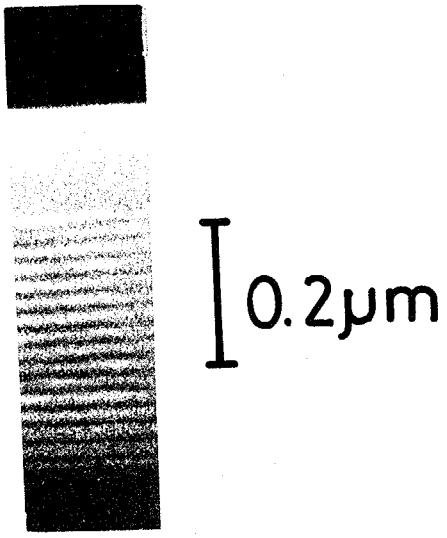

Fig. 4-9 Cross sectional view of multi quantum well structure by scanning electron microscope.

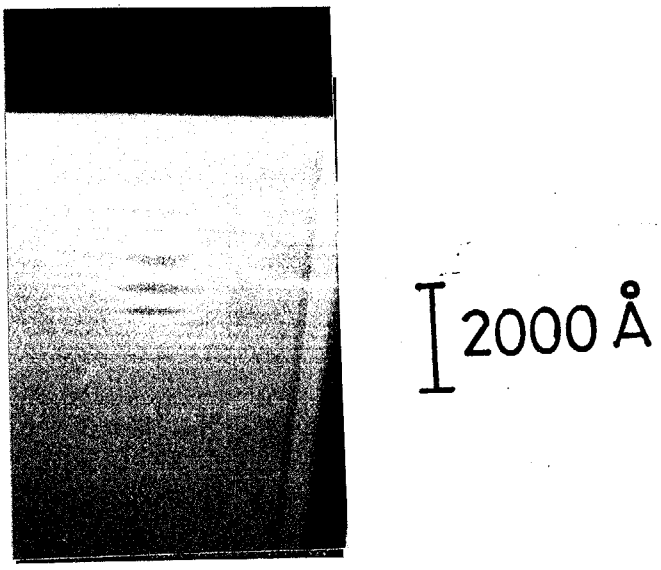

Fig. 4-10 Failed cross sectional view of multi quantum well structure by scanning electron microscope. Some wells fell by wet etching.

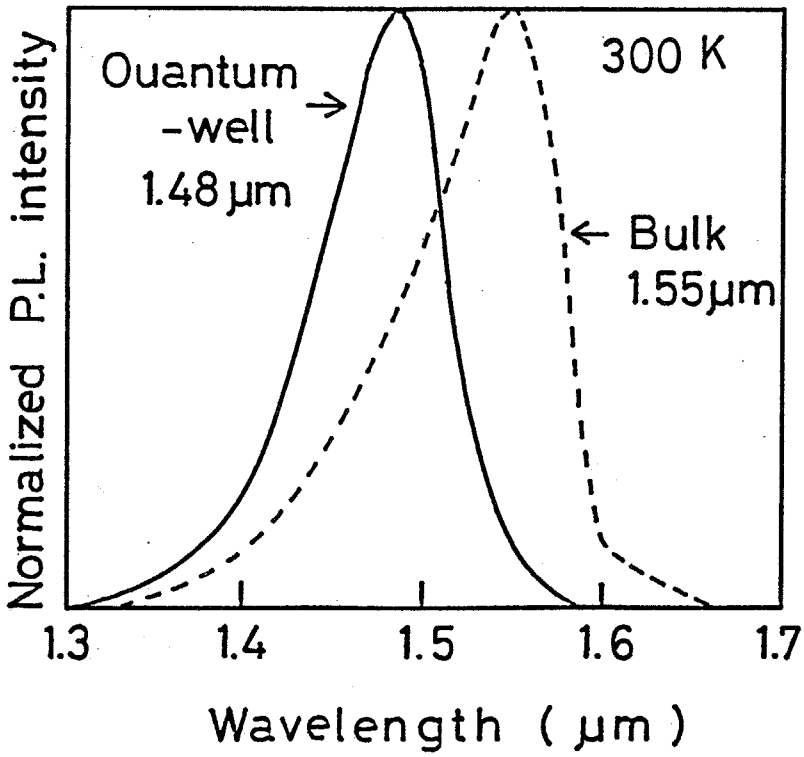

Fig. 4-11 Photoluminescence spectrum of multi quantum well structure at room temperature. Photoluminescence from bulk with same composition is also indicated.

crystal. This shift agreed with the result of calculation with observed well thickness[149]. Photoluminescence intensity from multi quantum well structure was weaker than conventional DH structure that had almost the same thickness about total quaternary layers. The multi quantum well structure should be sensitive about slight damage at hetero-interface because that has many interface and consisted by ultra thin layer, and it is pointed out that fabrication of hetero-interface left a room for improvement. When the number of well layers was changed from 15 to 3, intensity was changed almost linearly by the number of wells. Thus the author believes that damage of interfaces was remained in one well layer and was not accumulated to the next layer.

The change of peak shift quantity was not observed by the existence of growth interruption at InP/GaInAsP interface and change in time length of growth interruption. Hence, in the author's apparatus, the time for exchange of reactor atmosphere and dead space of piping did not affect the abruptness of hetero-interface.

Half width of photoluminescence was equal or larger than those of conventional bulk crystal. This phenomenon indicated fluctuation of thickness by pressure difference between reactor and vent line. In this case, half width of photoluminescence was not so reduced by low temperature measurement.

In multi quantum well structure after improvement for

pressure control of bubbler, reducing of half width was observed. Photoluminescence of GaInAs/InP multi quantum well structure is shown in Fig. 4-12 (a). Half width of signal was reduced until 36meV. Measurement result at liquid nitrogen temperature was also indicated narrow linewidth (18meV) as shown in Fig. 4-12 (b). However, productivity of multi quantum well structure with narrow linewidth by this apparatus was very low because required control of pressure was more severe than precision of pressure gauge.

For measurement of fluctuation in composition, Auger electron spectroscopy measurement (AES) (150, 151) was used conventionally. In early stage of this research, composition change of DH structure was measured by AES as shown in Fig. 4-13 with Ar sputtering. However, this methods was difficult for application to quantum well structure due to the large sputtering roughness (198) as shown in hetero interface of Fig. 4-13. For reduction of roughness effect, electron beam diameter was reduced with decreasing of beam current until that only strongest signal, i.e., signal of P, was remained in detection level of system. By this improvement, existence of quantum well structure was confirmed. Result by multi quantum well structure is shown in Fig. 4-14. However, abruptness was estimated larger than 15nm and abruptness from other measurement was lower than this measurement, For reduction of roughness, sputtering at low temperature was reported (152). Others report used etched surface

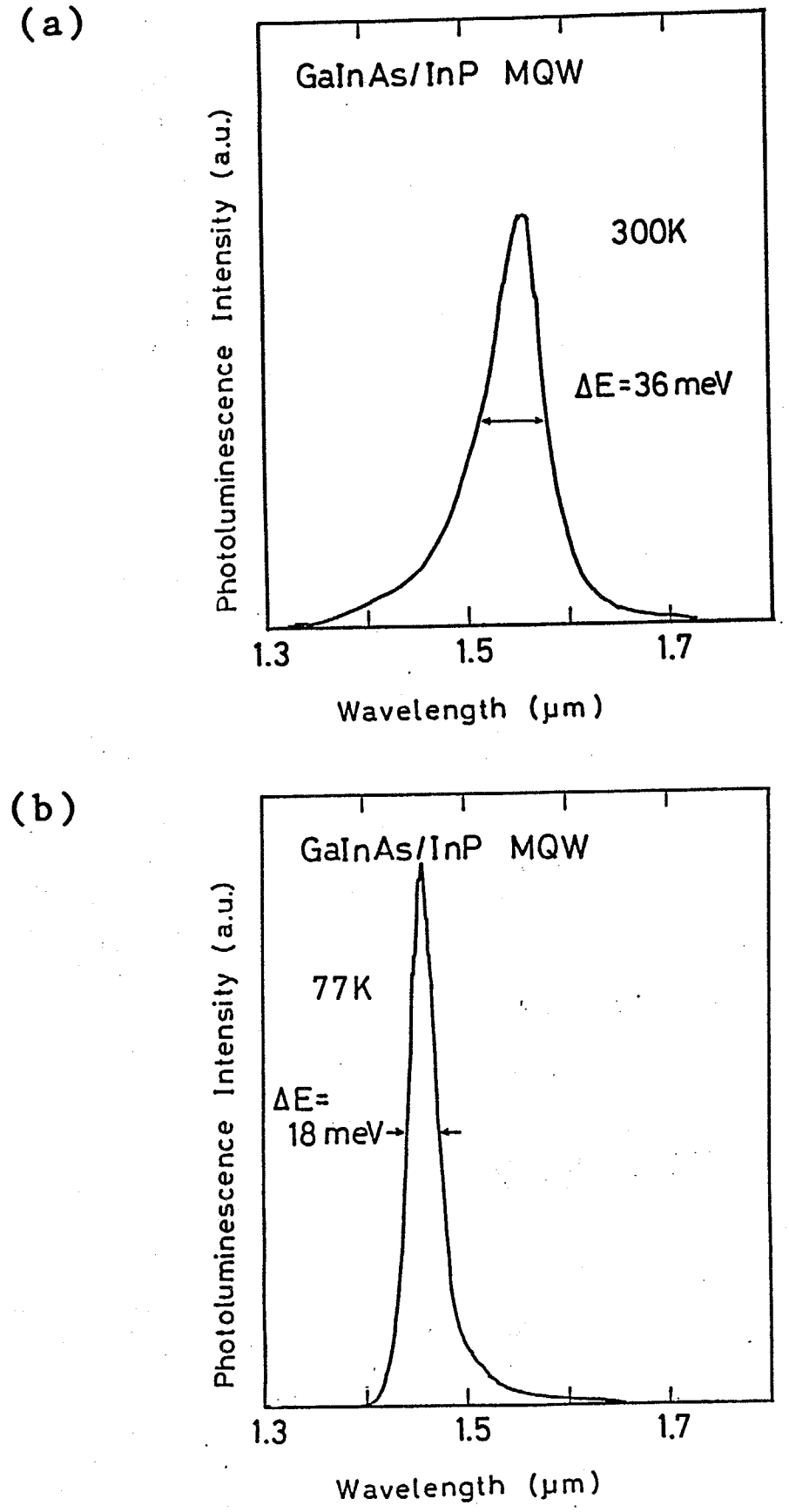

Fig. 4-12 Photoluminescence spectrum of multi quantum well structure grown by improved apparatus about exhaust line. (a) Spectrum at room temperature. (b) Spectrum at 77K.

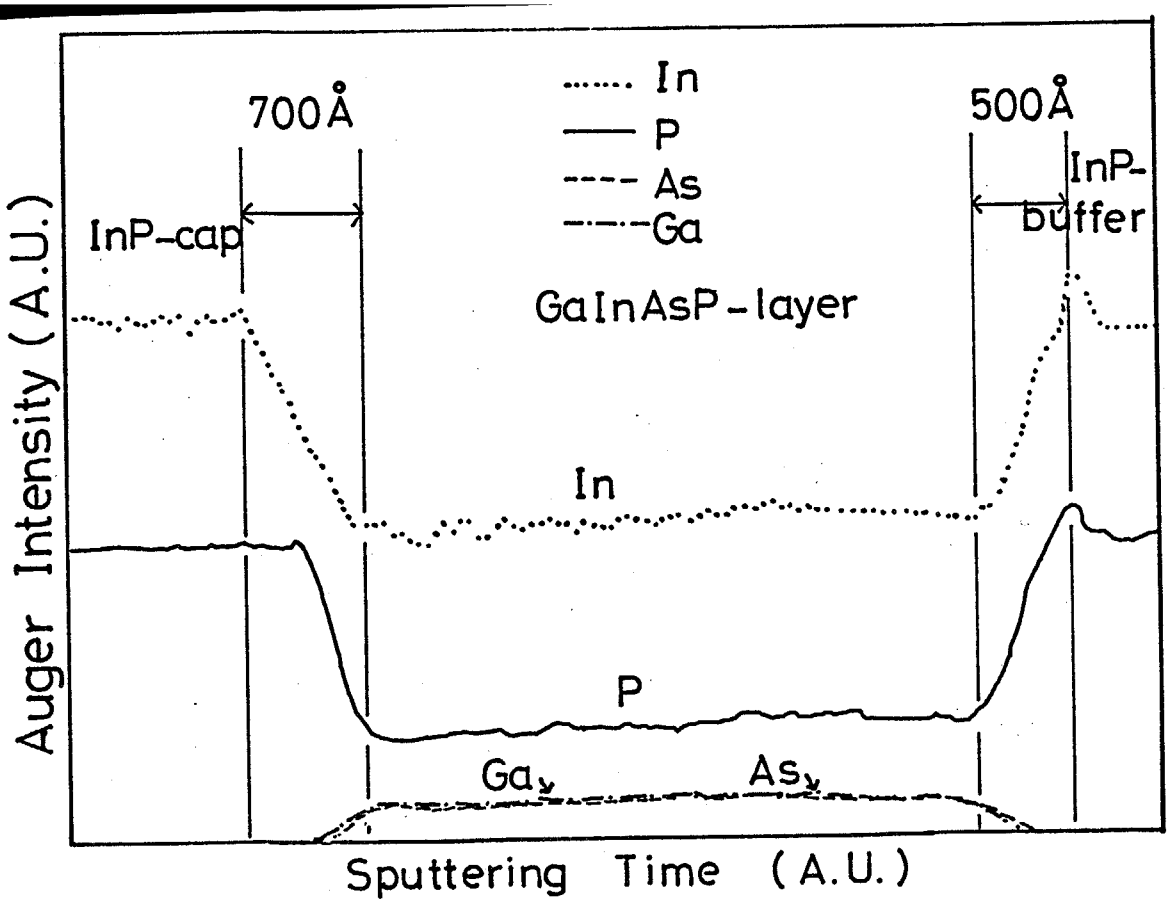

Fig. 4-13 Measurement result of composition change of DH laser structure by Auger electron spectroscopy.

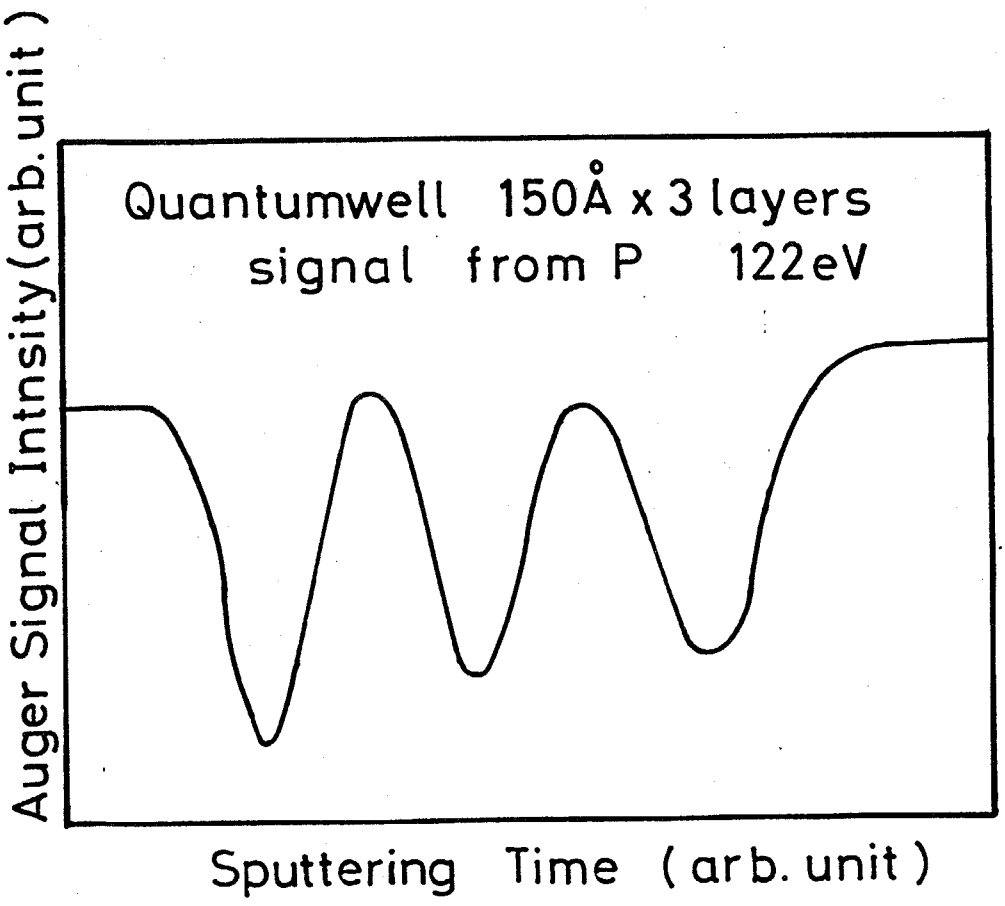

Fig. 4-14 Measurement result of composition change observed in P peak in multiquantum well structure by Auger electron spectroscopy.

with very shallow angle[153]. Development of those methods is desirable for estimation of composition abruptness.

Excellent result was obtained by new machine with large resistance between bubbler and switching point. Multi quantum well structure was fabricated by switching of TEG and V groups sources. Flow of TEI was constant and growth interruption before growth of ternary layer was eliminated to confirm elimination of fluctuation. At first, ten pairs of 12nm GaInAs quantum well layer and 10nm InP barrier layers were grown. Half width of photoluminescence measurement at 77K was reduced until 12meV as shown in Fig. 4-15. The accuracy of periods in multi quantum well structure was confirmed by X-ray satellite peak measurement. Measured sample have 50 periods of multi quantum well structure. Results with 22nm and 12nm periods are shown in Fig. 4-16 (a) and (b), respectively. Satellite peaks were confirmed in both sample. This measurements indicates improvement of reproductivity of multi layer. Change of state density by quantum size effect was confirmed by absorption measurement in same sample. Absorption loss have a step-like change as shown in Fig. 4-17.

However, fluctuation of composition was still observed in multi quantum well structure. When thickness was changed, lattice mismatching was changed as shown in Fig. 4-18. Relation between peak of photoluminescence and well width was also not allow to calculated value as shown in Fig. 4-19. These phenomenon

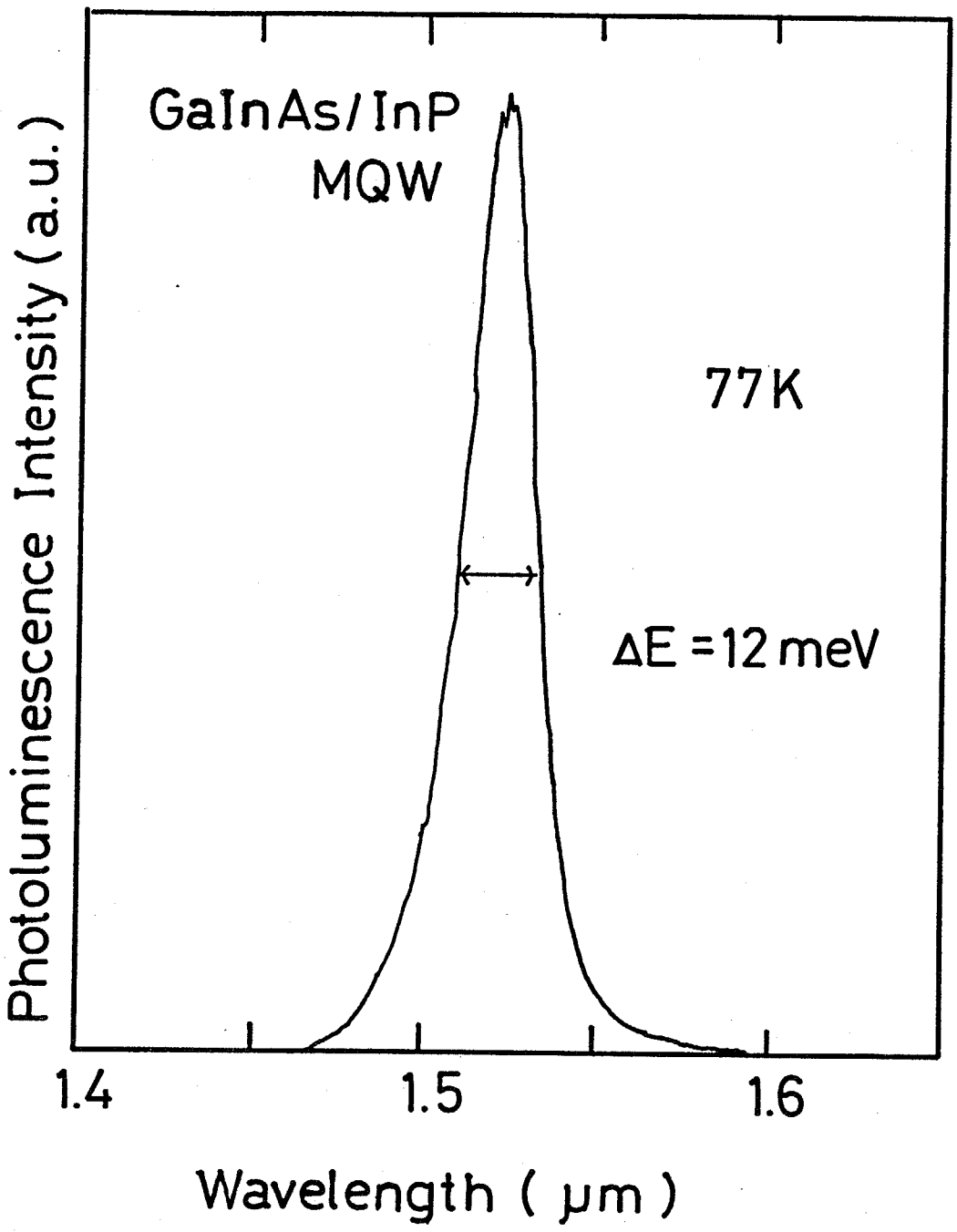

Fig. 4-15 Photoluminescence spectrum of multiquantum well grown by new apparatus at 77K

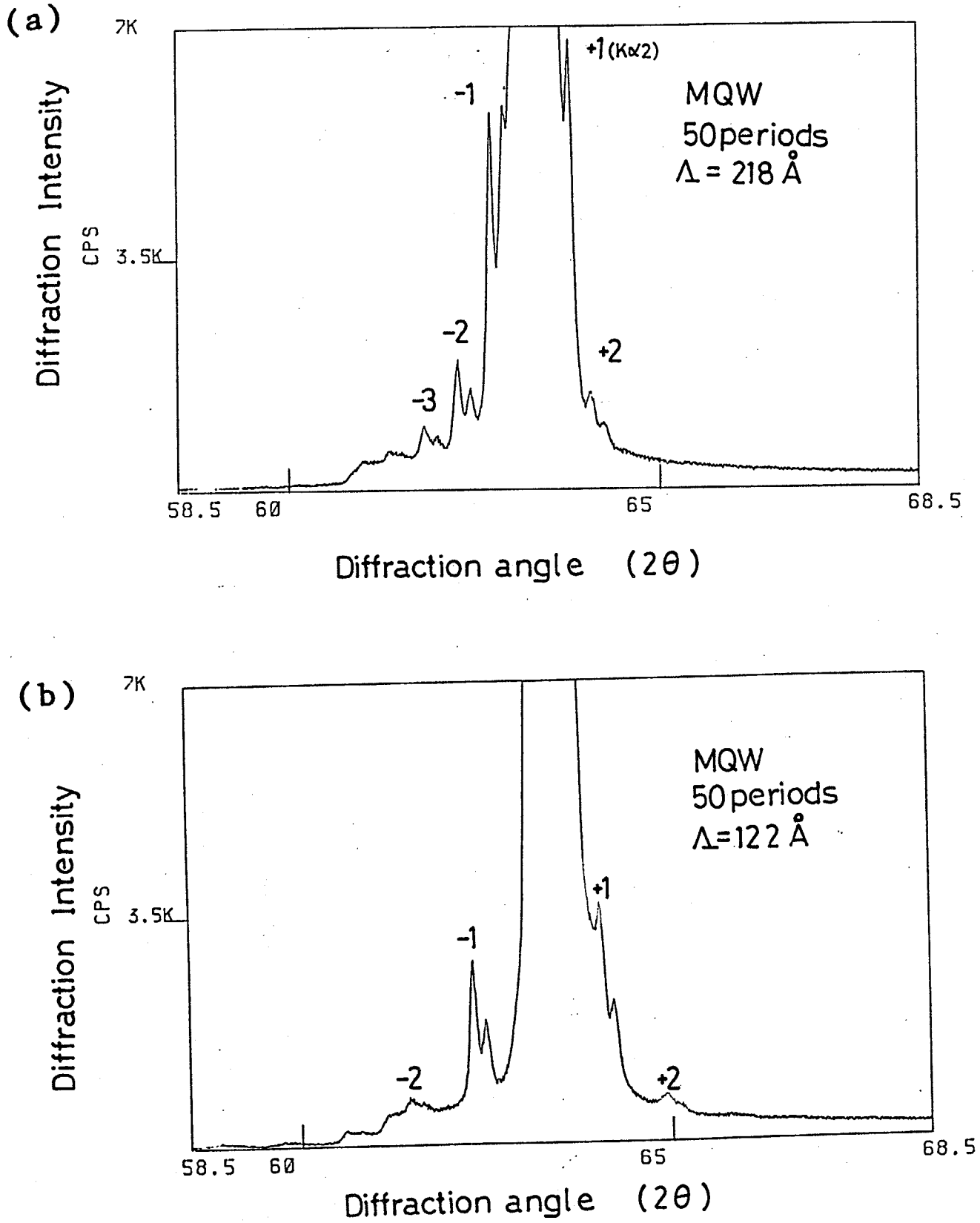

Fig. 4-16 X-ray satellite peak of multiquantum well. The number of periods is 50. (a) The period length is 22nm. (b) The period length is 12nm.

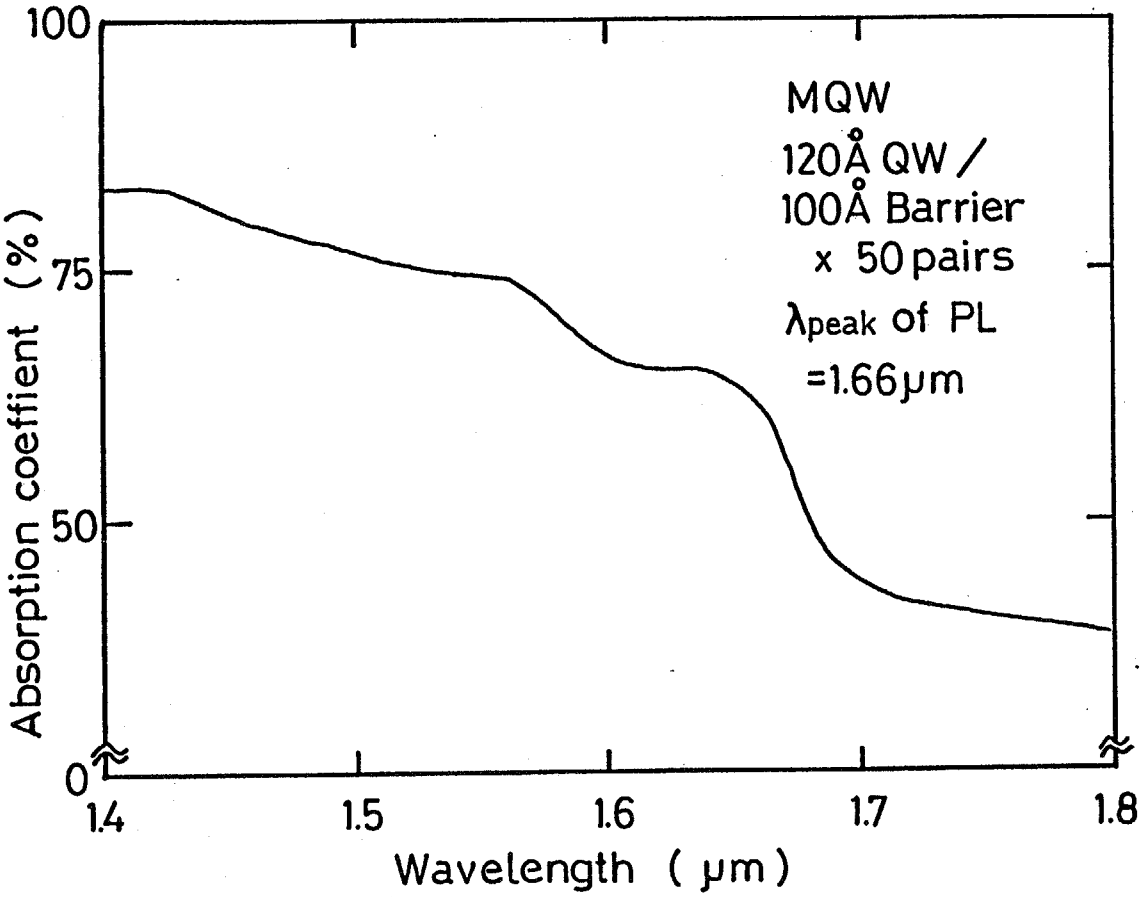

Fig. 4-17 Absorption loss of multiquantum well. The number of periods is 50. The period length is 22nm.

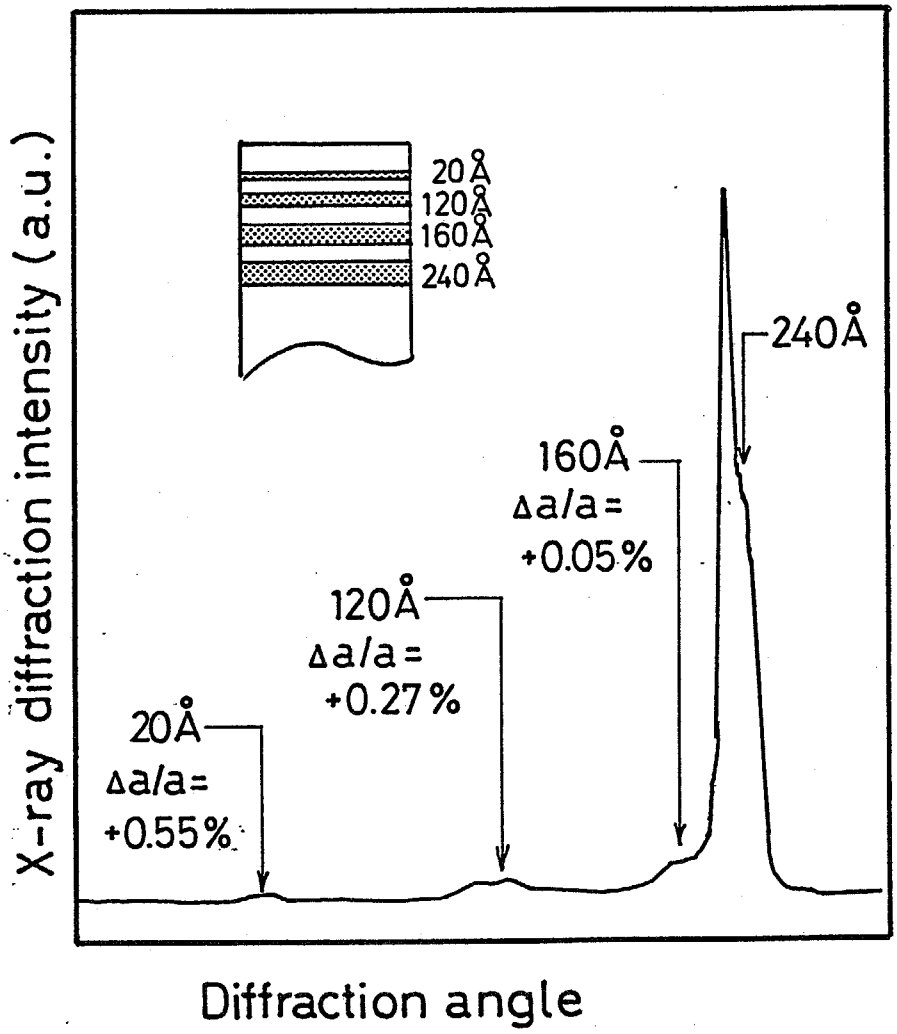

Fig. 4-18 X-ray diffraction measurement in multi-layer structure with different thickness. The growth of this structure have no growth interruption. The thickness of each layers is 2nm, 12nm, 16nm and 24nm, respectively. Each X-ray diffraction peak for each layer is confirmed. Hence, lattice constant was changed by each layer.

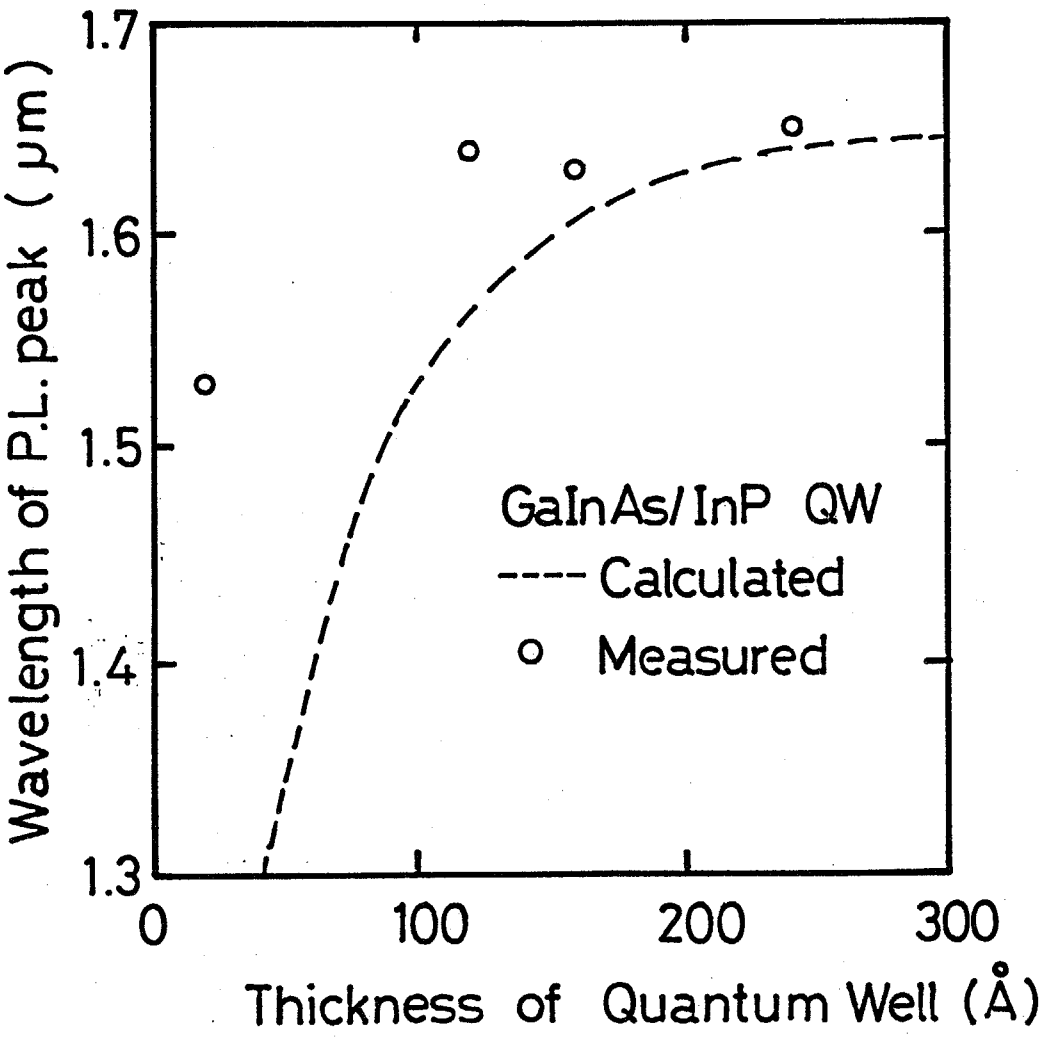

Fig. 4-19 Relation of photoluminescence peak and well width in multiquantum well grown by new apparatus without growth interruption. The measurement value is not allowed the calculated value that is indicated by broken lines. This phenomenon indicates lattice mismatching in thin layer.

indicated delay of introduction about TEG after switching. It is very difficult to explain this phenomenon, because supplying rate of metalorganic sources is constant theoretically when resistance between bubbler and switching point is sufficient large. One of the possibility was volume between needle valve and switching valve was effective for fluctuation of switching. Simulation results in consideration with volume between needle valve and switching point is shown on Fig. 4-20. Slow change of source flow rate is shown in simulation results. Eventually those problem will be reduced by interruption before growth of GaInAs as described in section 2-4.

4-4. Single quantum well laser

Evaluation of crystal quality in quantum well was estimated by laser fabrication. The quantum box structure is very attractive from expected characteristics as described in chapter 5. Quantum box structure was fabricated by a two dimensional patterning and embedding process based on a one-dimensional quantum-well structure as mentioned later. Hence, the study of one-dimensional quantum well laser is essential to confirm crystal quality until fabrication of quantum box structure. Single quantum well layer was used for the based structure of quantum box structure as described in chapter 6. Thus, single quantum well lasers are fabricated to confirm crystal quality.

On the other hands, single quantum well lasers with

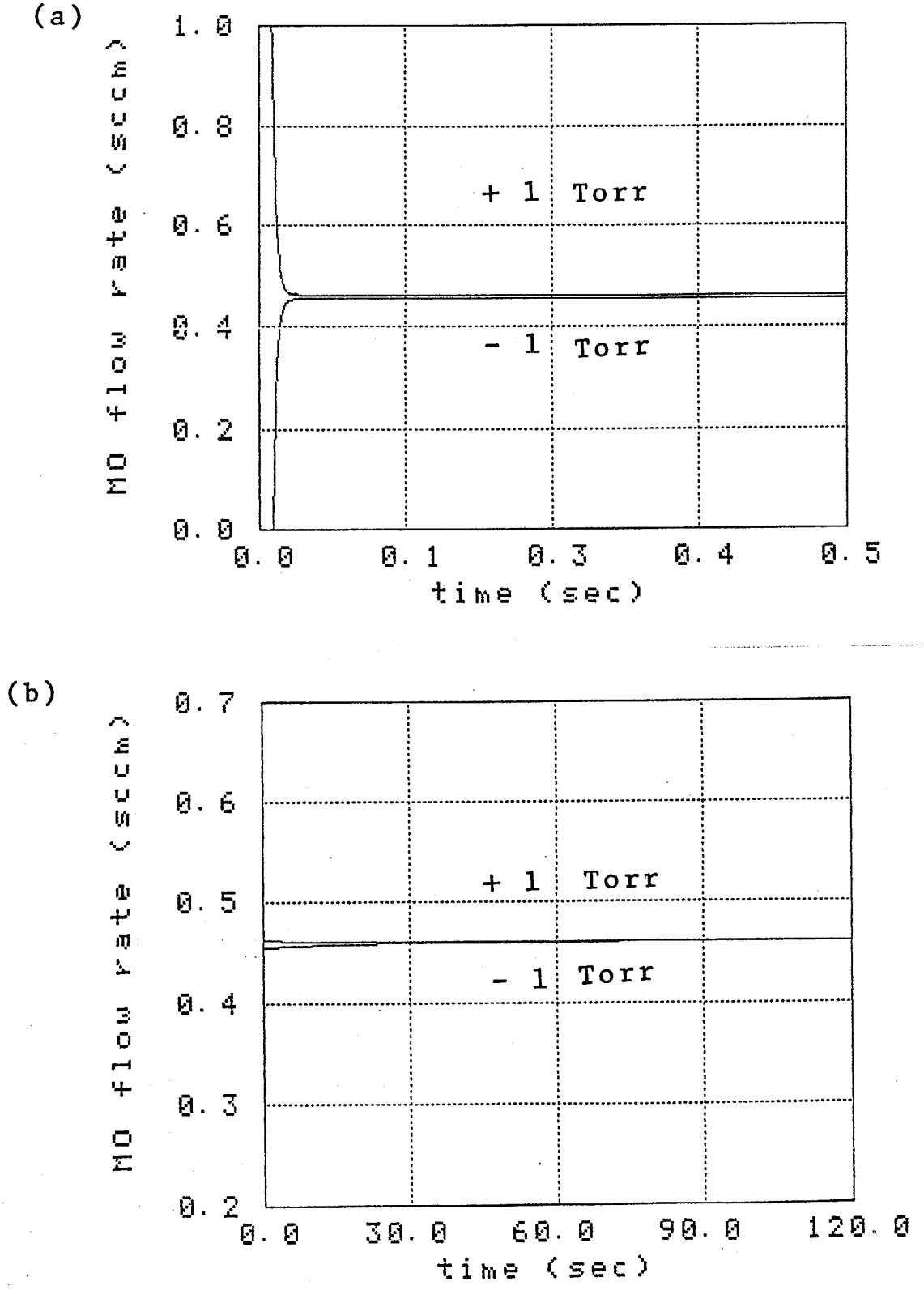

Fig. 4-20 Calculated fluctuation results. The simulation model is same as Fig. 4-3. Each parameter is set from new apparatus. The capacitance and resistance was decided from piping between needle valve and switching point. (a) Pressure fluctuation was suppressed under 0.03 seconds after switching and (b) dilution of sources is effective for fluctuation between 10-60 seconds.

separate-confinement heterostructure (SCH) [154] are also promising with respect to the low threshold current density [12-15]. However, in the GaInAsP/InP single-quantum-well laser, although lasing in the optical confinement layer of the SCH structure was reported [155], lasing in the quantum-well layer has not yet been attained, possibly because of difficulty in the carrier confinement within the quantum-well layer.

In this section, lasing in the quantum-well layer of GaInAsP/InP SCH single quantum-well laser is reported.

SCH single-quantum-well structures shown in Fig. 4-21 were grown on n-type substrates by the following sequence:

1) n-InP layer 1 μ m thick,
2) n-GaInAsP optical confinement layer with bandgap wavelength λ g of 1.26 μ m and thickness of 150nm,
3) InP barrier layer 2nm thick,
4) GaInAsP quantum-well layer with λ g of 1.66 μ m and thickness of 15nm,
5) InP barrier layer 2nm thick,
6) p-GaInAsP optical confinement layer with λ g of 1.26 μ m and thickness of 150nm,
7) p-InP clad layer 1 μ m thick, and
8) p-GaInAsP contact layer

In designing the above SCH single-quantum-well structure, the following points were considered. In order to confine carriers sufficiently within the quantum-well layer and avoid light

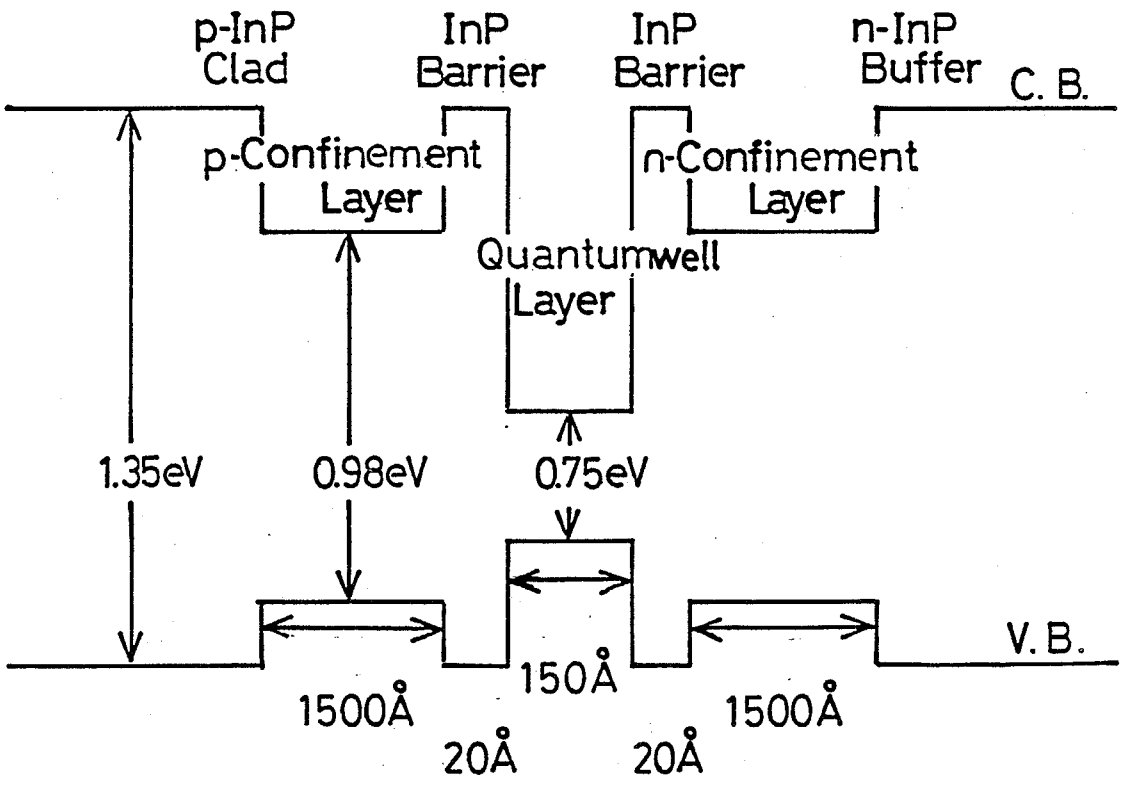

Fig. 4-21 Structure of single quantum well laser with separate confinement heterostructure.

absorption due to the optical confinement layers, bandgap energies of the optical confinement layer and the quantum-well layer selected were 0.98eV(1.26μm) and 0.75eV(1.66μm), respectively in consideration with source gas flow rates. It was important to make the bandgap energy difference between optical confinement layer and quantum-well layer sufficiently large.

When the bandgap energy difference was as small as 0.1eV, i.e., 0.7eV(1.38μm) and 0.8eV(1.55μm), luminescence from the optical confinement layer was stronger than that from the quantum-well layer under high excitation as shown in Fig. 4-22. In the laser without sufficient bandgap difference, lasing of quantum well was observed in only at low temperature (148K) and optical confinement layer lased after lasing of quantum well as shown in Fig. 4-23. Those results indicated that carriers were not confined sufficiently within the quantum-well layers. Energy difference of 0.17eV was tested and that difference was not sufficient also for lasing at room temperature.

Thickness of the optical confinement layer was theoretically designed so as to obtain maximum optical confinement within the quantum-well layer. When the thickness and bandgap energy of the quantum-well layer are 15nm and 0.75eV, respectively, and the bandgap energy of the optical confinement layer is 0.98eV, the ratio of the optical power in the quantum-well layer to the total optical power is maximized to 3% for the range of optical confinement layer thickness from 100nm to 200nm

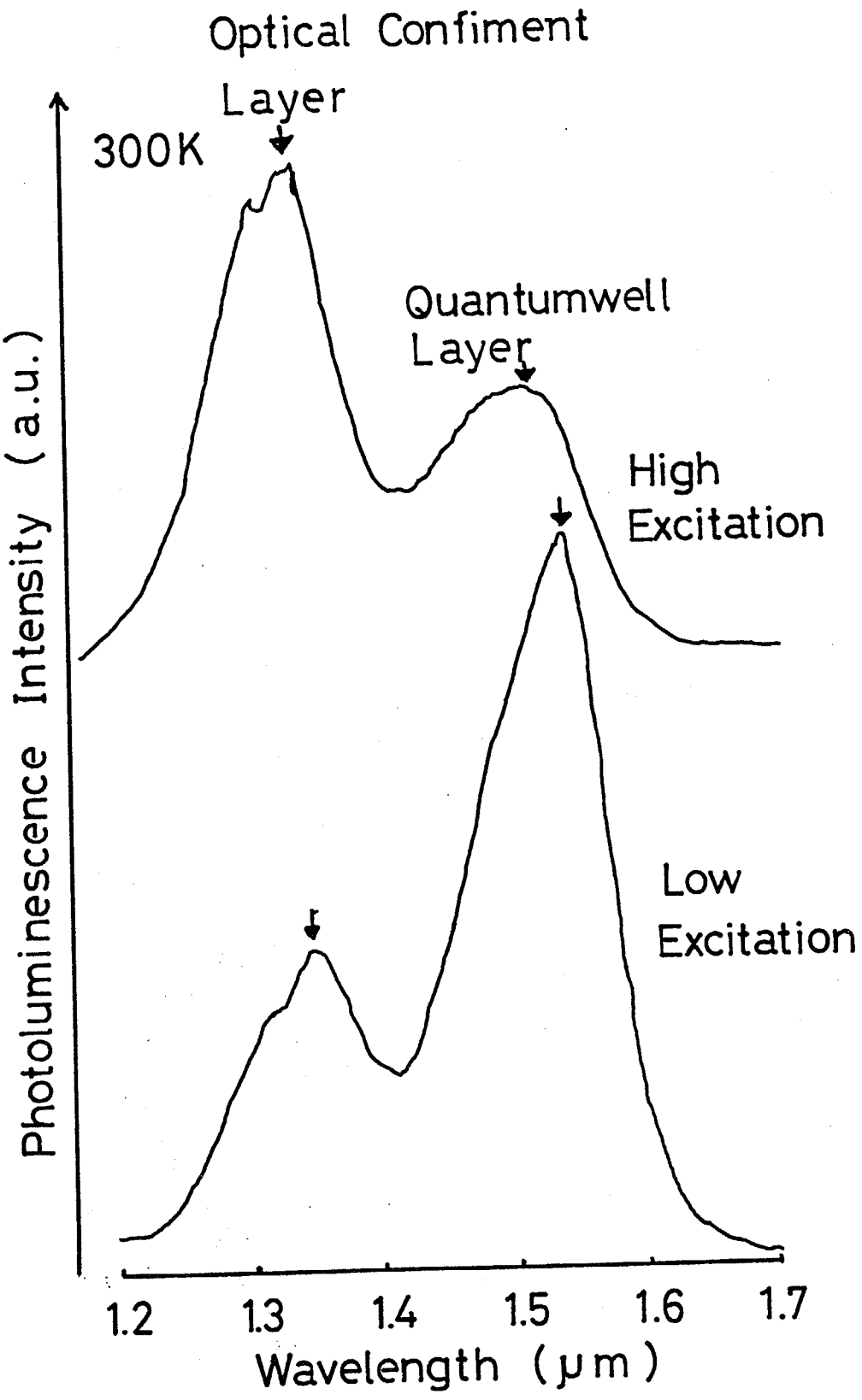

Fig. 4-22 The change of dominant peak by change of excitation intensity in SCH structure. Low excitation level was 40W/cm^2 while high excitation level was about 3kW/cm^2.

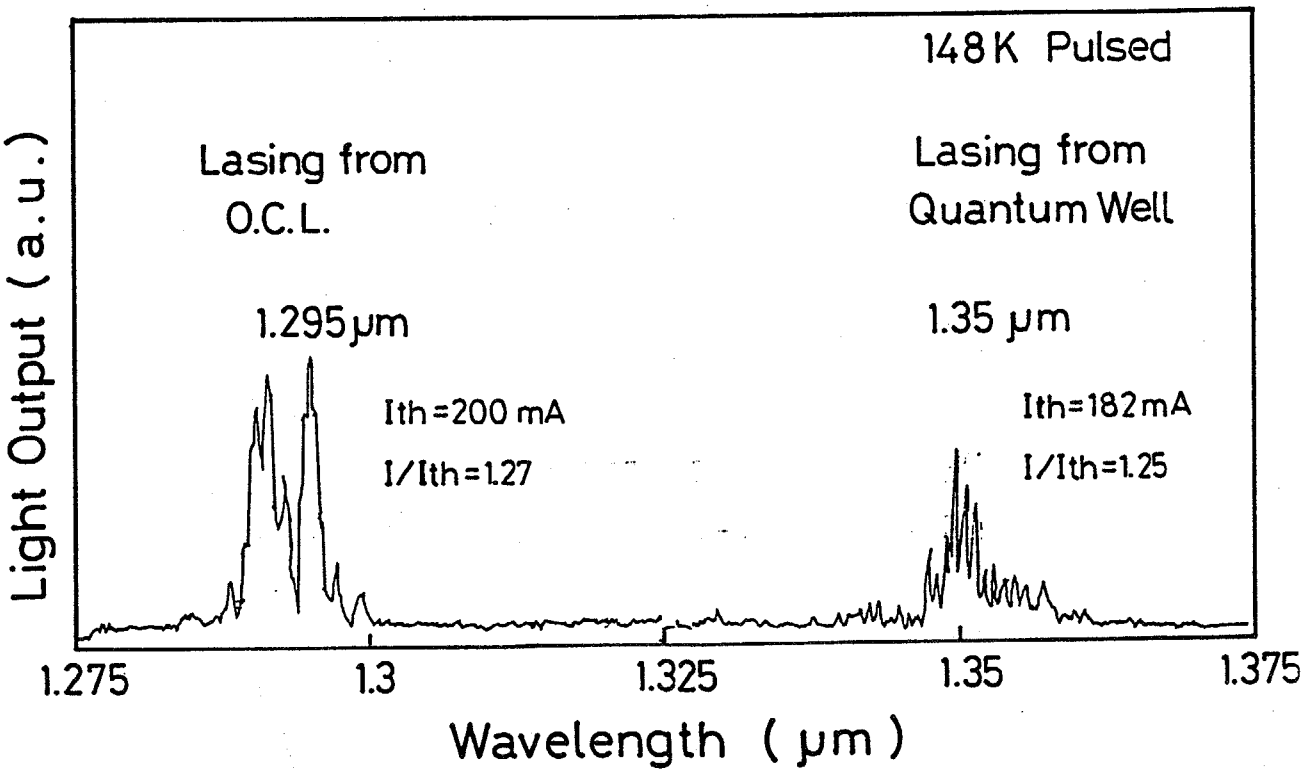

Fig. 4-23 Spectrum of lasing at low temperature(148K) without sufficient energy separation between quantum well layer and optical confinement layer. Measurement was carried out by pulsed operation. Lasing of optical confinement layer was occurred after lasing of quantum well layer.

as shown in Fig. 4-24.

The necessity of the InP barrier layer between the quantum-well layer and the optical confinement layer came from a functional limitation in the apparatus. As described in section 2-4, grown surface must be maintained same atmosphere with growth conditions about V groups in the interruption of growth. The old apparatus have only one line for each V groups gas and abrupt change of flow rate was limited by ability of mass flow controller. Hence, quaternary layer of difference composition could not grow after growth of quaternary layer continuously. Of course, reduction of the barrier thickness was very important for the carrier injection into the quantum-well layer. At first, this thickness was 12nm and interrupted smooth carrier injection. It was confirmed by photoluminescence with high excitation. As the next, the thickness of the barrier layer was reduced until 2nm, while the carrier can pass through the barriers via tunneling. This thin thickness was achieved by improvement for pressure control of vent line as described in section 4-2.

The formation of the quantum-well was confirmed by the photoluminescence measurement. Samples with a quantum-well thickness from 10nm to 50nm were prepared. Peak of photoluminescence was shifted by reduction of well thickness as shown in Fig. 4-25. Theoretical value is also indicated in Fig. 4-25 where broken lines (a) and (b) correspond to quantum-wells with bar-

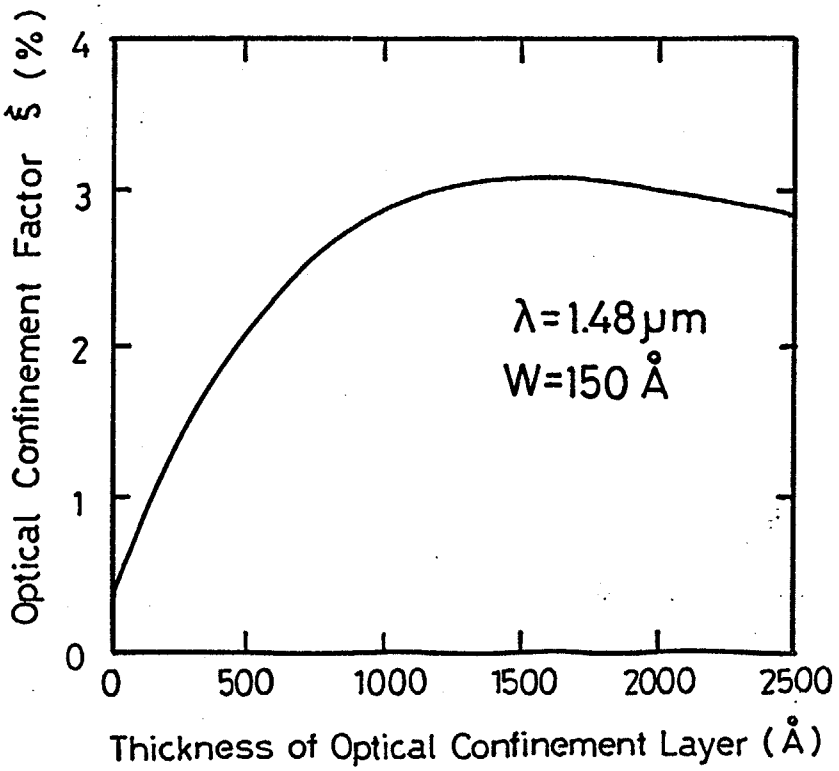

Fig. 4-24 Calculated result of optical confinement factor as a function of thickness of optical confinement layer.

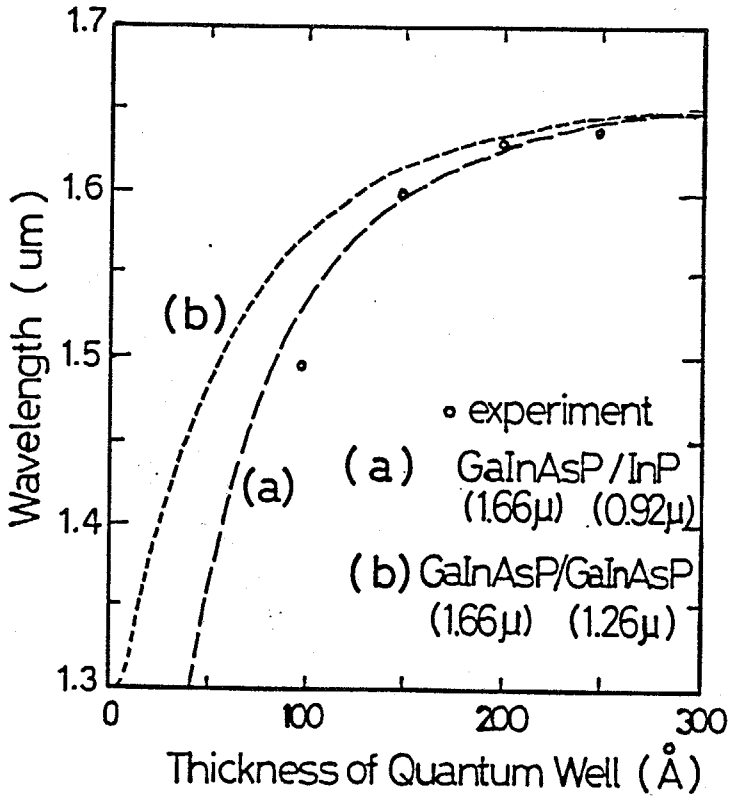

Fig. 4-25 Relation photoluminescence peak and well thickness in SCH structure. The broken line (a) indicates calculated value by GaInAs/InP quantum well, while the broken line (b) indicates calculated value by GaInAS/GaInAsP(1.26 μ m) quantum well.

riers of InP and GaInAsP(λ_g=1.26μm), respectively. Measured value was fitted to calculated value by InP barrier.

The stripe-contact lasers was fabricated with 15μm-width window in SiO_2 mask. CW operation at 77K was obtained as shown in Fig. 4-26. Threshold current was 29.3mA and lasing wavelength was 1.411μm. From the lasing wavelength, assuming the bandgap wavelength at 77K, it was confirmed that the lasing occurred in the quantum-well layer. Threshold current density was calculated as 230A/cm^2.

Pulsed operation at room temperature was obtained in the above device as shown in Fig. 4-27. Threshold current was 1.38A and lasing wavelength was 1.345μm. Threshold current density was 11kA/cm^2. Lasing was obtained up to 325K of temperature and the maximum output power was 9.2mW.

The lasing wavelength at room temperature was longer than the bandgap wavelength of the optical confinement layer by 80nm, and therefore was not explained by lasing in the optical confinement layer. On the other hand, the wavelength coincided with theoretical value corresponding to the transition between the second levels of the quantum-well as shown in Fig. 4-28. Hence, the lasing was occurred by the transition between second levels in the quantum-well layer at room temperature since the optical gain between seconds levels is higher than that between the ground quantum levels by high carrier injection.

Theoretical threshold current density at room temperature

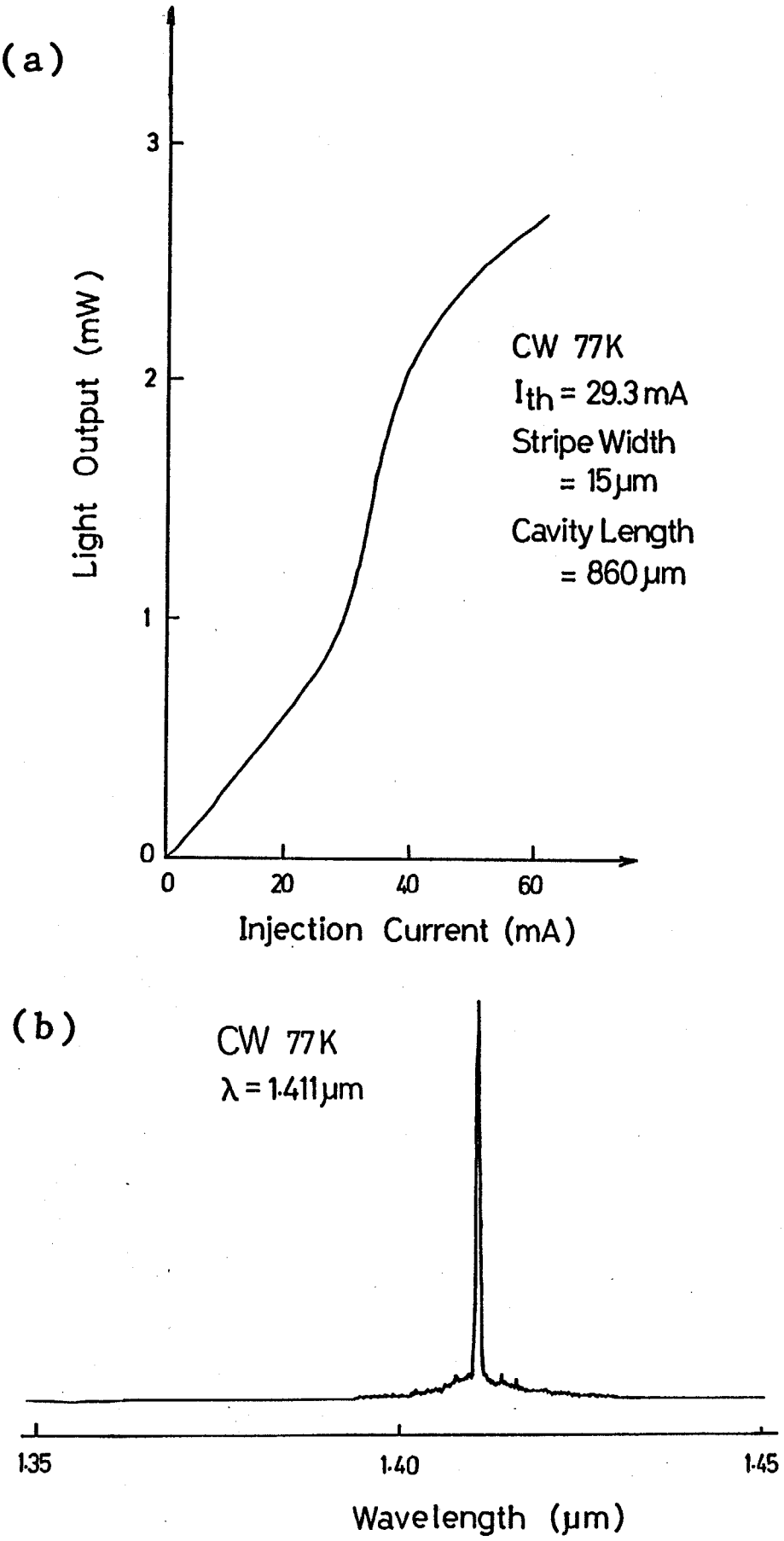

Fig. 4-26 Lasing characteristics under cw operation at 77K.
(a) I-L characteristics. (b) Lasing spectrum.

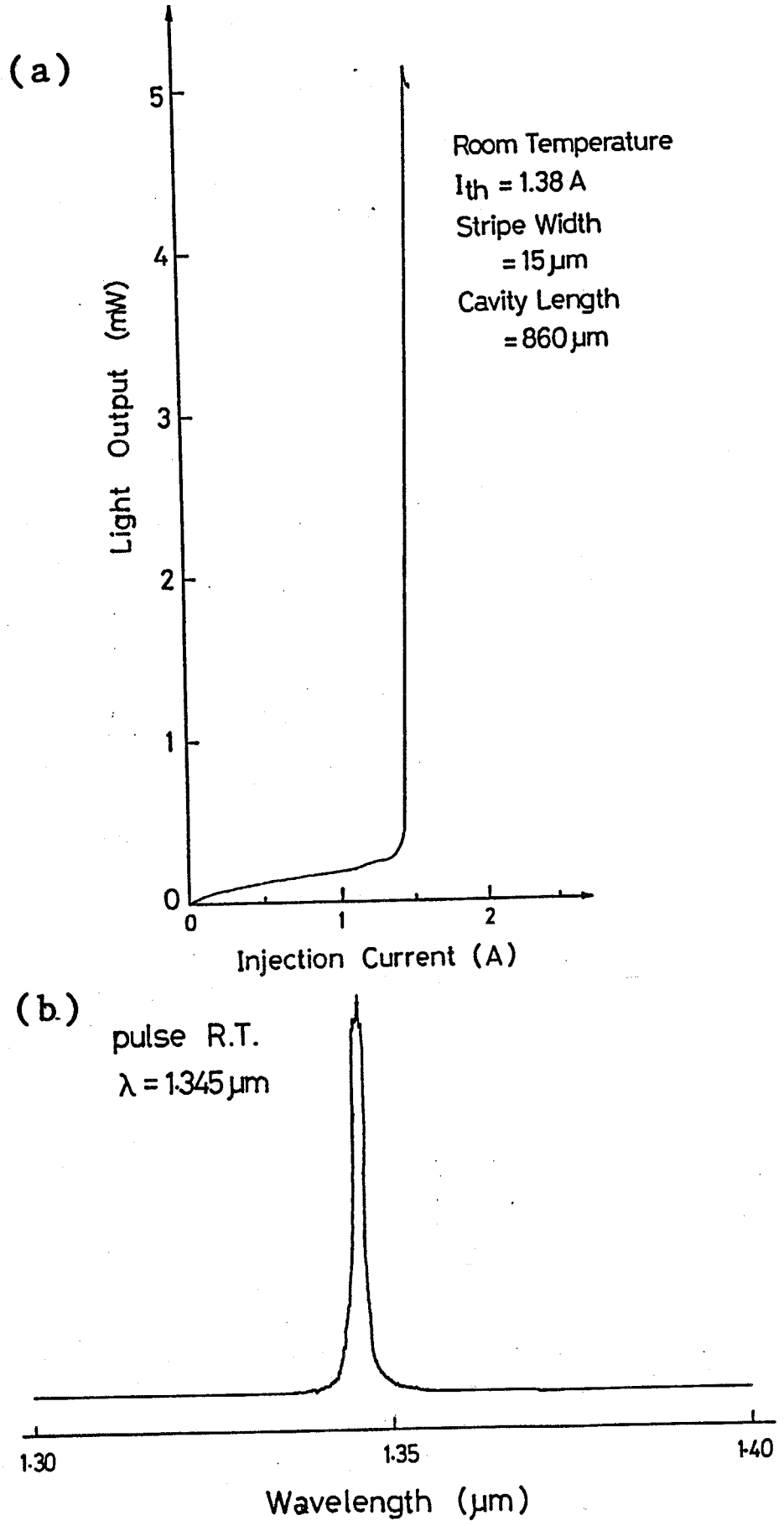

Fig. 4-27 Lasing characteristics under pulsed operation at room temperature. (a) I-L characteristics. (b) Lasing spectrum.

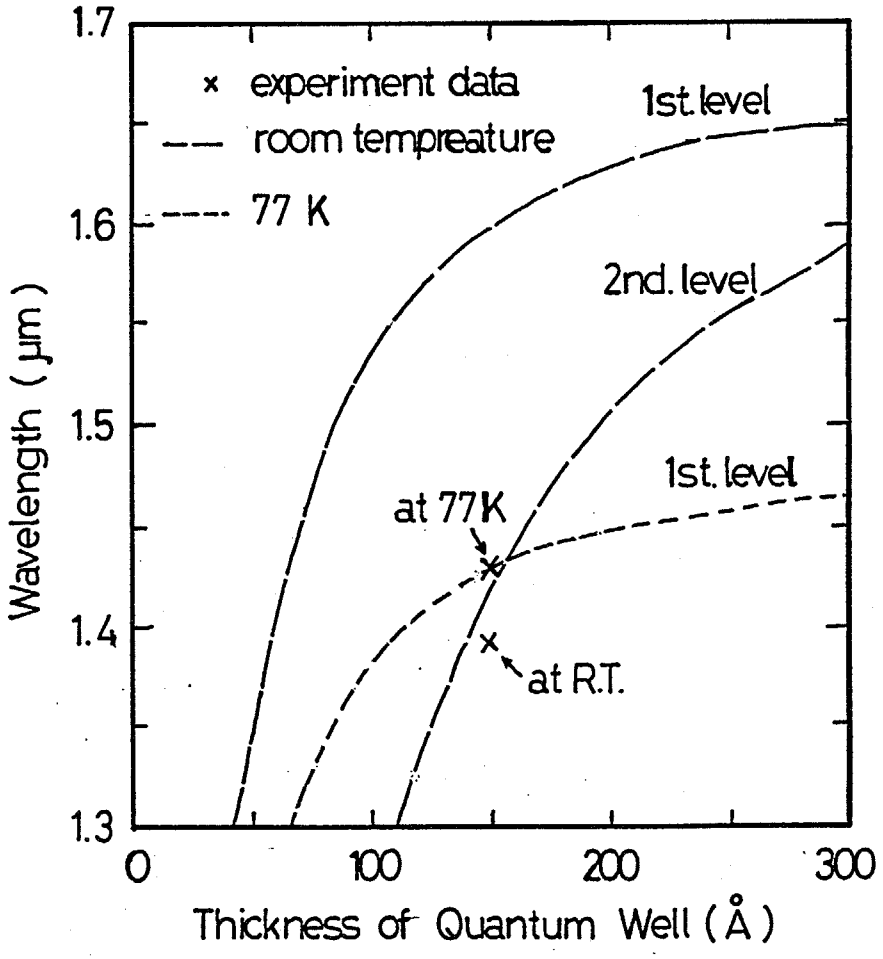

Fig. 4-28 Calculated wavelength transition of first levels and second levels at 77K and room temperature. The observed lasing wavelength at 77K and room temperature are also indicated. For calculation, GaInAs/InP quantum well was used.

in the GaInAsP/InP SCH single-quantum-well lasers is estimated[149] as about 3kA/cm^2 and, therefore, the above experimental result has a great deal of room for improvement. The main causes of the difference between the theoretical and experimental results are still the problem of carrier injection into the quantum-well-layer and its accompanying optical loss due to the excess number of carriers in the optical confinement layer. It was also pointed out that temperature dependence of threshold current density is poor than conventional laser from difference of threshold current density between 77K and room temperature. For more optimization of the SCH structure, graded-index structure[11] or some barrier structure for carrier confinement[156] is needed.

4-5. Concluding Remarks

In this chapter, technique for fabrication of multi quantum well structure and single quantum well lasers are reported. Abruptness and controllability of thin film thickness were strongly coupled characteristics of apparatus. Improvement for constant supply of metalorganic sources are reported. By these improvement, good quantum well structure was fabricated. Narrow linewidth of photoluminescence, step-like shape in absorption characteristics and X-ray satellite peak were observed. Based on these structure, operation of GaInAsP/InP single quantum well lasers was obtained for the first time. However, the low

threshold current was not observed. GaInAsP/InP system have tendency of severe for high carrier injection due to the non-radiative recombination. The estimation of non-radiative recombination is more important in next chapter.

Chapter 5 Theory of quantum box laser

5-1. Introduction

Considerable attention has been paid to the quantum-well lasers with ultra-thin active layers, since there have superior characteristics described in section 1-2[8-20]. These merits are expected to become more remarkable as the dimension of the quantization is increased. However, gain and the laser threshold in three-dimensional quantum-box structures[24, 25], where electrons are three-dimensionally confined, has not yet been discussed theoretically before this research. Optimization of laser structure for quantum box laser is also not reported.

In this chapter, the author indicated the low threshold current property of quantum box laser, based on the density-matrix theory of semiconductor lasers with relaxation broadening[25, 132, 158]. At first, gain and the laser threshold are analyzed. Next, the structure is optimized from calculation of threshold current density. Finally, ideal structure of quantum box laser is also discussed.

5-2 Threshold current of GaInAsP/InP quantum Box lasers

It is expected that drastic change in state density by quantum box structure will be provide more superior lasing characteristics. In quantum box structure, state density is simply composed by δ -function at each quantized levels as shown

in Fig. 5-1 and injected carriers are concentrated only in these levels. Hence, injected carriers are used effectively for lasing action compared to other structures with distribution of state density. Figure 5-2 shows the gain spectra calculated for 10nm x 10nm x 10nm cubic $Ga_{0.47}In_{0.53}As/InP$ quantum box[25] compared with 10nm x 10nm quantum wire[161], 10nm thick quantum film[149], and bulk crystal[158].

At first, the author explain the merit of quantum box laser by simple model. For simple modeling, the author assumed only one quantized level in each band. The optical gain α is given by following equation, generally:

$$\alpha = A (f_c - f_v) g \qquad (5-1)$$

where, A is a function for gain and includes dipole moment and intraband relaxation effect[132, 158], f_c, f_v are Fermi function in conduction band and valence band, respectively and g is density of state. From electrical neutral condition and the assumption about only one quantized level, function of f_c is equal to function of $1-f_v$ and a new function f is defined as follows:

$$f = f_c = 1-f_v \qquad (5-2)$$

The state density g is simply composed by δ -function, hence, the density state have infinite value at quantized levels.

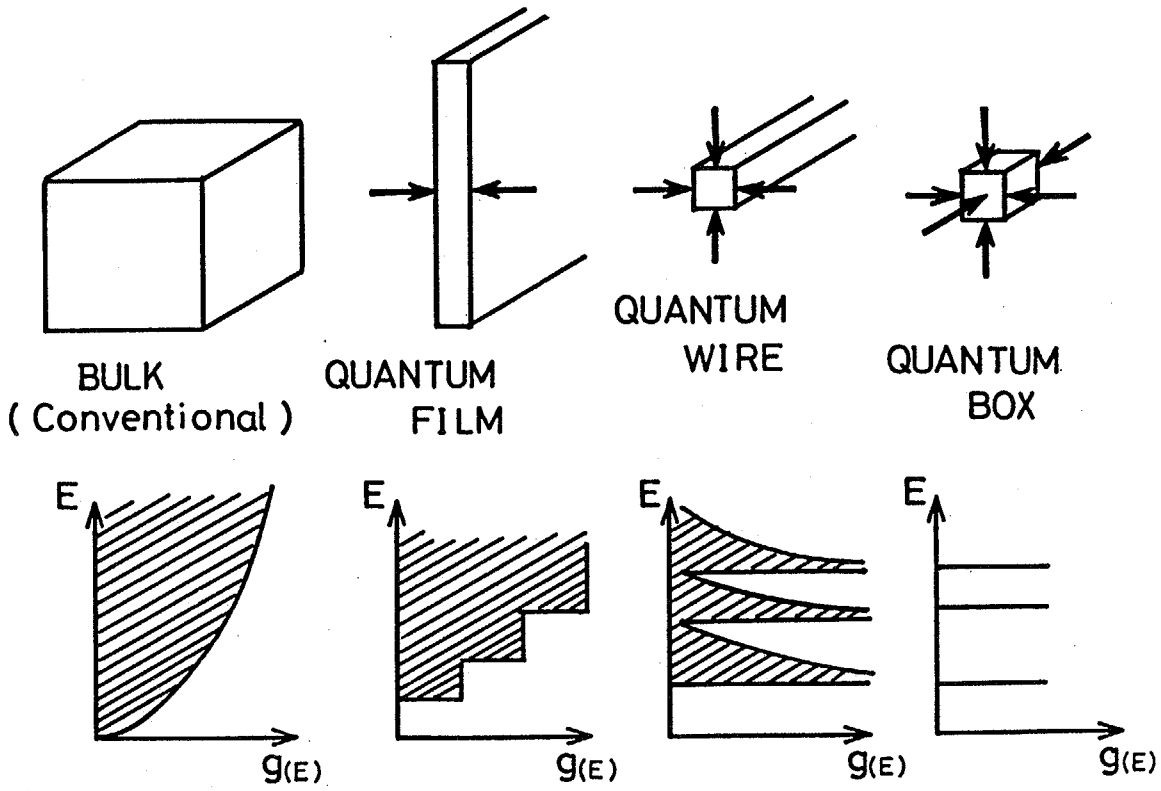

Fig. 5-1 Variation of density-of-states of electrons with the increase of the quantization dimension in quantum-well structures.

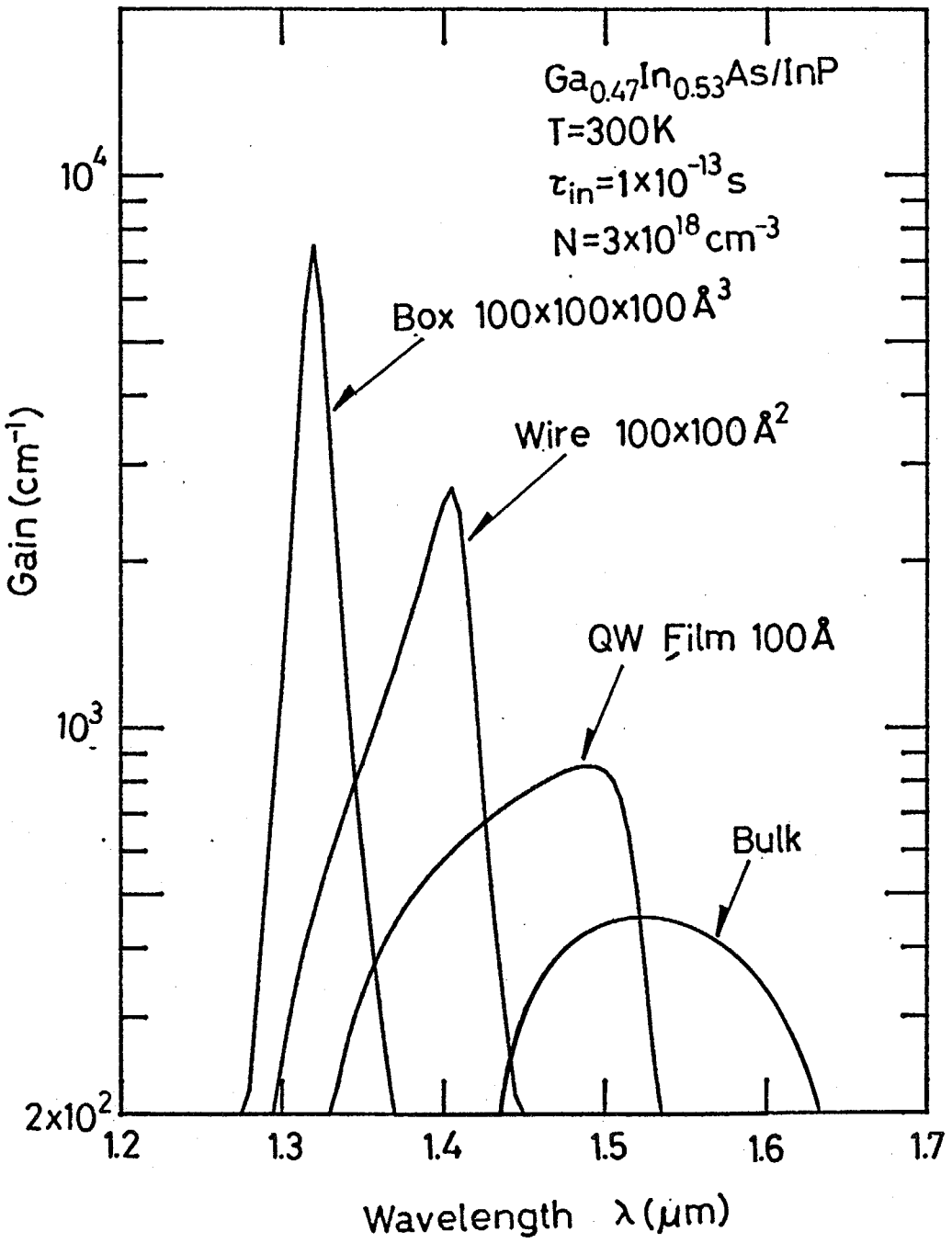

Fig. 5-2 Gain spectra calculated for $Ga_{0.47}In_{0.53}As/InP$ 10nm x 10nm x 10nm cubic quantum box, 10nm x 10nm quantum wire, 10nm thick quantum film, and bulk crystal at T=300K.

However, the optical gain have no infinite value from Lorentz function in function A by intraband relaxation. And the state density is inversely proportional to the volume of quantum box and represented as follows:

$$g(E) = \delta(E)/V \qquad (5\text{-}3)$$

where, V is the volume of quantum box.

The carrier density N in quantum box is given by a product between the maximum number of carrier in the quantized state and Fermi function and represented as follows from the Pauli theorem:

$$N = 2f/V \quad < \quad 2/V \qquad (5\text{-}4)$$

From above equations, eq. (5-1) can be rewritten as follows to indicate the relation between carrier density and optical gain.

$$\begin{aligned} \alpha &= A\,(\,2f - 1\,)\;\delta(E)\;/\;V \\ &= A\,(\,N - 1/V)\;\delta(E) \qquad (\,N < 2/V\,) \end{aligned} \qquad (5\text{-}5)$$

Hence, the relation between carrier density and optical gain is changed by volume of quantum box. As shown in Fig. 5-3, when the volume of quantum box is increased, maximum optical gain is decreased although injection carrier concentration for

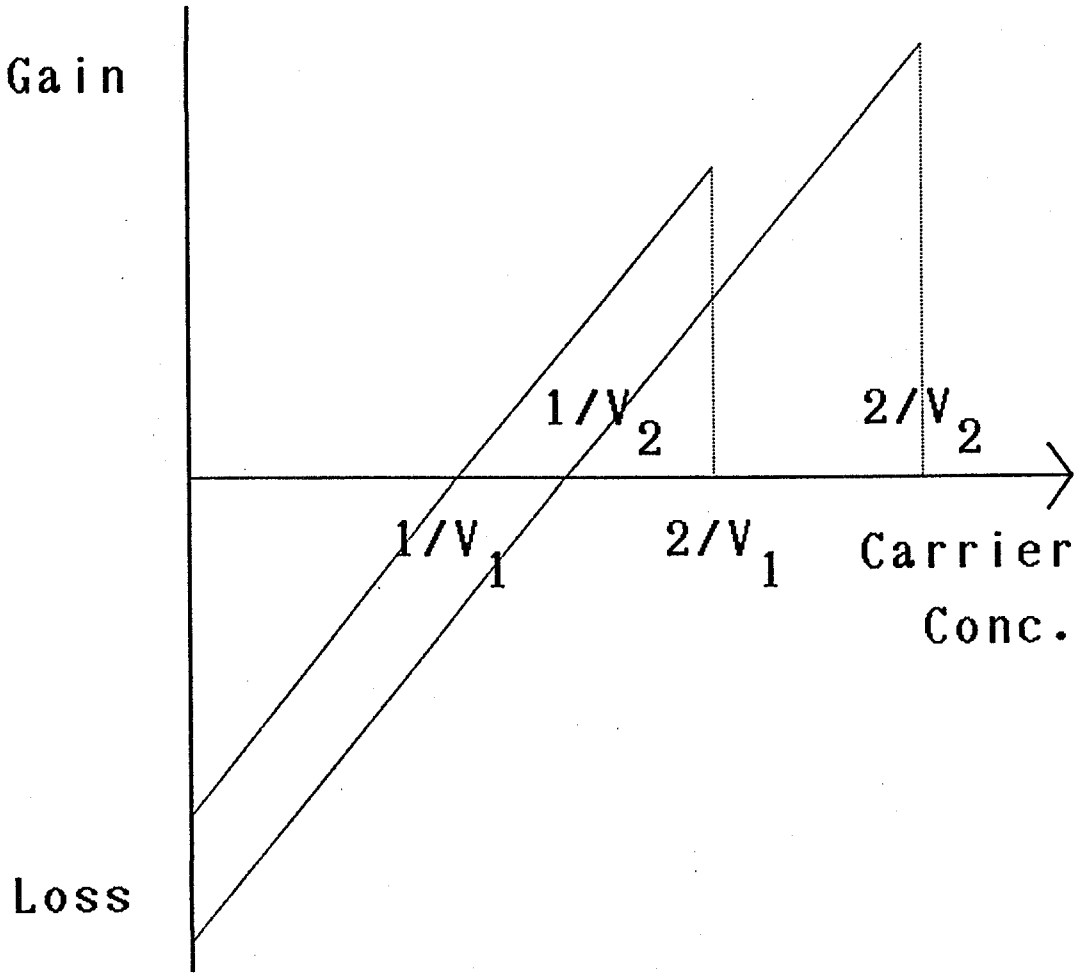

Fig. 5-3 Optical gain as a function of injected carrier with a simple assumption that each band has only one level. The change point from loss to gain and maximum point is inversely proportional to each quantum box volume. Permitted carrier density is limited by Pauli theorem.

elimination of loss is decreased. The other hand, when the volume of quantum box is decreased, maximum optical gain is increased although injection carrier concentration for elimination of loss is increased.

As the next step, threshold current density is calculated. For realization of quantum box structure, the author assumes the structure with optical waveguide and p-n junction as shown in Fig. 5-4. For simple calculation, dependency in carrier lifetime τ_s by carrier lifetime is neglected at first. For optical waveguide, separate optical confinement structure (SCH) is used and the total optical confinement factor of quantum box ξ is increased linearly with by total volume of quantum box as follows:

$$\xi = anV \qquad (5\text{-}6)$$

where, a is constant coefficient and n is number of quantum box per area in the plane perpendicular to the injection current as shown in Fig. 5-4.

From above equations, threshold gain g_{th} is expressed as follows:

$$g_{th} = \xi \alpha = anVA (N_{th} - 1/V) \delta (E) \quad (N_{th} < 2/V) \qquad (5\text{-}7)$$

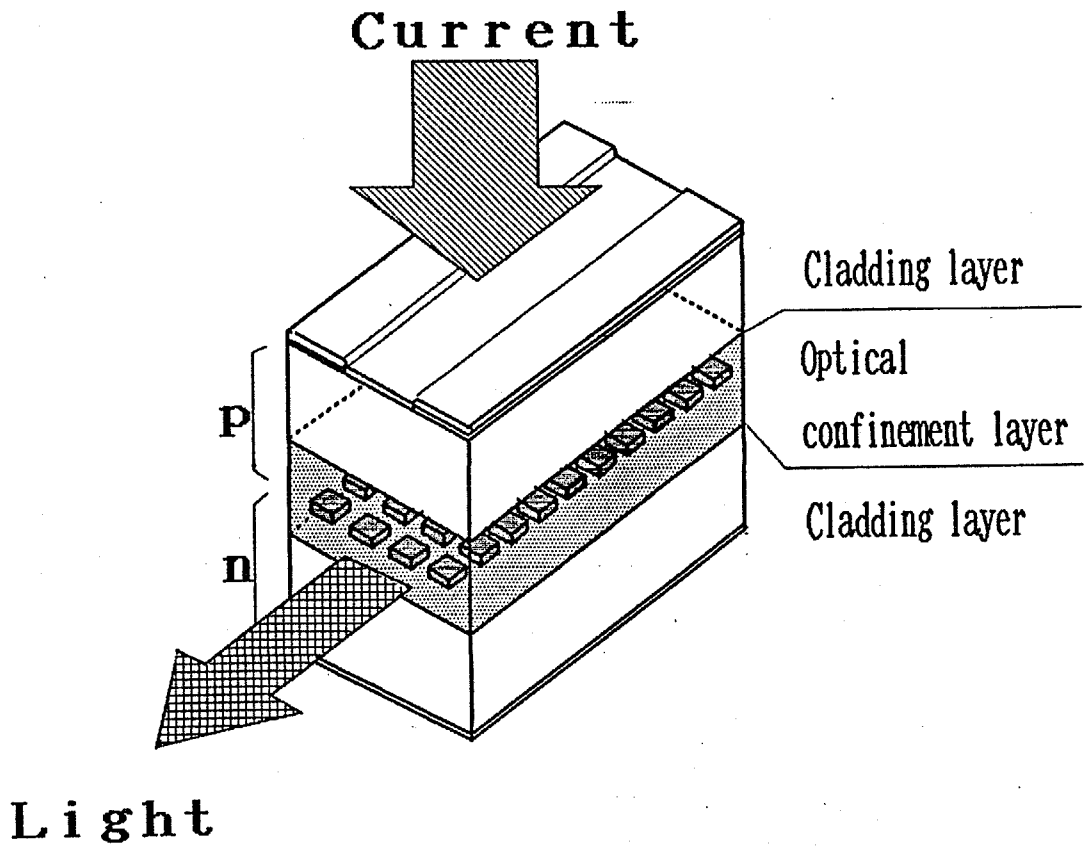

Fig. 5-4 The schematic view of quantum-box laser with p-n junction and optical waveguide by SCH structure.

And threshold current density J_{th} is obtained by following equation.

$$Jth = Nth\ enV/\tau_s$$
$$= e\ (\ gth/a/A/\delta\ (E)\ +\ n\ )/\tau_s \qquad (5\text{-}8)$$

where, e is the electron charge and τ_s is the carrier lifetime in quantum box. At first, τ_s is assumed as constant.

Threshold current density is decided by density of quantum box n, only. Term of n is corresponding to carrier injection for elimination of loss in quantum box and threshold current density is decreased with decreasing of density of quantum box. However, excessive decreasing of n interrupt lasing by limitation of maximum gain in quantum box by the Pauli theorem as shown in eq. (5-7). From eq. (5-8), volume of quantum box V has no relation with threshold current density J_{th}. Hence, this simple assumption is too simple to explain the merit of quantum box laser. As the next step, the motive force of advantageous of quantum box is revealed by change of assumption.

At first, calculated relation[25] between carrier density and optical gain as shown in Fig. 5-5 have different tendency in gradient from Fig. 5-3. Gradient is increased with decreasing of box size. This phenomenon can be explained by consideration of other levels. Actual carrier density on quantum box N_{QB} is represented by the summation of carrier in each levels as follows:

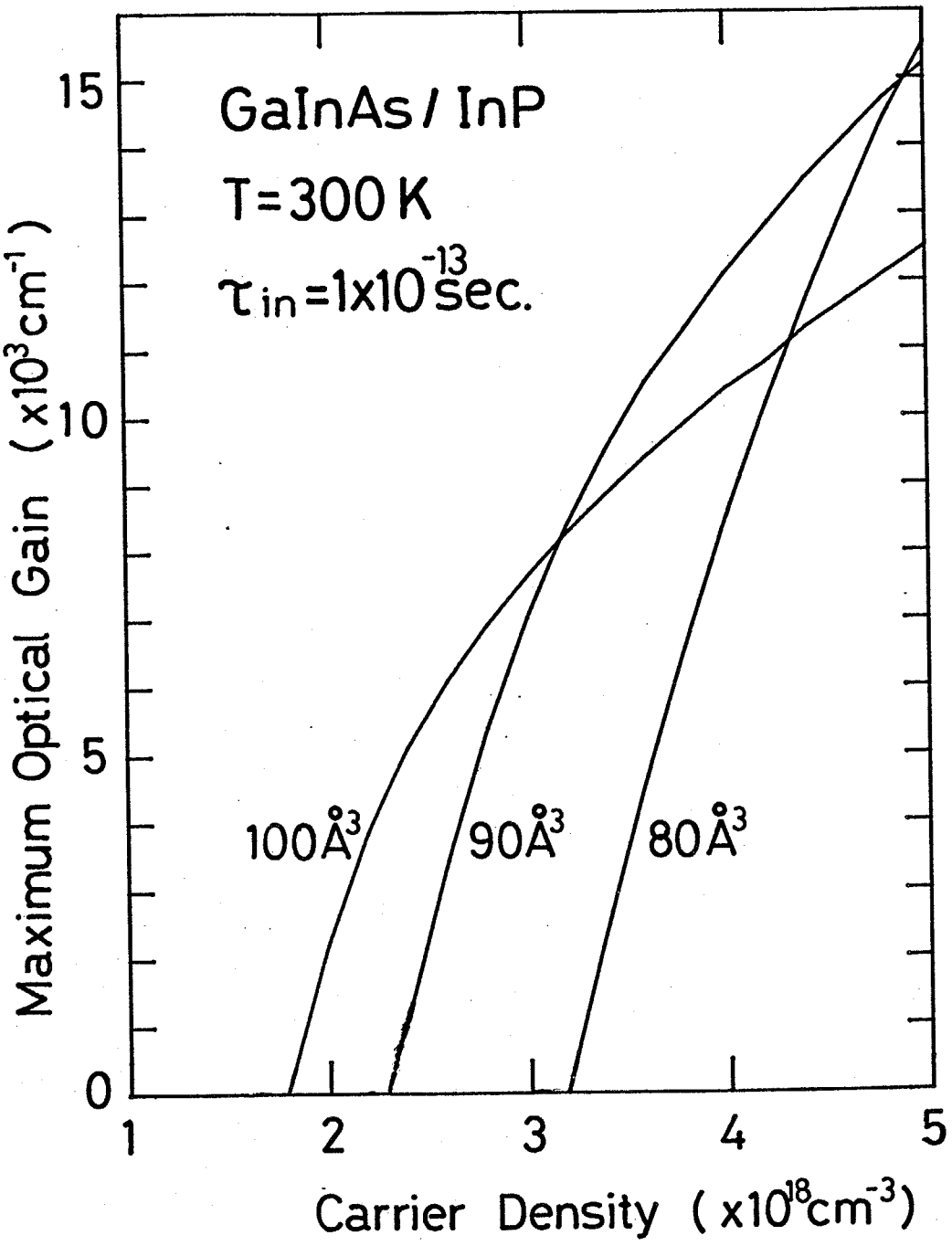

Fig. 5-5 Maximum gain as a function of carrier density calculated for $Ga_{0.47}In_{0.53}As/InP$ quantum box. The sizes of quantum boxes are 8, 9, and 10nm cubic, respectively.

$$N_{QB} = \sum_{n} 2f_n / V \qquad (5\text{-}9)$$

where, subscript n is indicated each level and f_n is indicated Fermi function in each level determined by energy separation and temperature. By reduction of size, energy separation between observed basic level and the other level is increased until cut off condition and, therefore, confinement ratio in observed basic level for whole carrier density, gradient between whole carrier density and optical gain are increased with reduction of size. Threshold current density can be reduced by reduction of quantum box volume and this phenomenon is motive force of reduction of threshold current density.

Actually, other structure, i.e., bulk or quantum well is correspond to quantum box with very large size. In that case, basic parameter is not changed as principle although function A in eq. (5-1) have a possibility of increasing by factor 1.5 due to the isotropic effect by directional bias of wave vector[149, 160, 161].

However, when additional consideration is only that of other levels, excessive reduction of size is introduced. As the next step, assumption of constant carrier life time is changed. Carrier life time is inverse proportional to carrier density in the range of conventional carrier density[131]. Hence, threshold current density is increased by excessive reduction of volume of

quantum box.

Another demerit of excessive reduction of quantum box structure is carrier overflow in optical confinement layer. The conventional analysis was neglected carrier lifetime in optical confinement layer and leakage current[166] from active layer is in account of non-radiative recombination time with dependence of carrier density. However, consideration of carrier lifetime in optical confinement layer is very important because large quantity of carrier was flow from active region to optical confinement layer by small carrier density and high carrier injection in quantum box structure. Moreover, leakage current from active layer of GaInAsP/InP system is larger than that of GaAlAs/GaAs systems. Hence, carrier lifetime in optical confinement layer must be in consideration.

The carrier density in optical confinement layer is calculated from quasi-Fermi level. Carrier overflow from quantum well to optical confinement layer is determined by barrier height for each band and state density. Hence, electron and hole have different overflow rates and electron has larger overflow by small state density due to the small effective mass of carrier. Hence, bending of band structure is occurred by the condition for charge neutrality. Figure 5-6 shows calculated result of this band bending in conventional quantum well laser structure reported by Yamada et al.[167] and this calculation needs self-consistent method with Poison's equation. To eliminate those

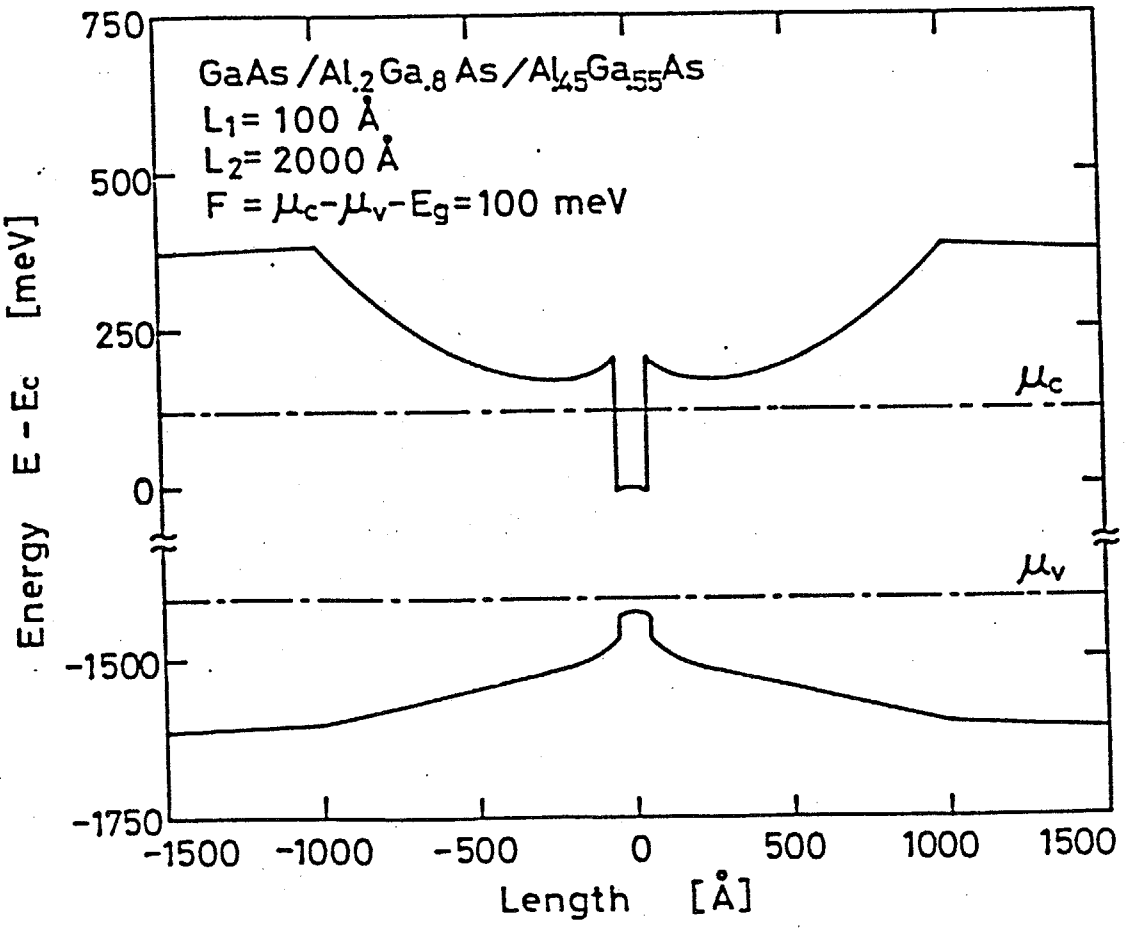

Fig. 5-6 Cálculated results of the bended band gap profiles due to the coulomb force between electrons in the conduction band and the holes in the valence band in GaAs/GaAlAs SCH structure(167).

complicate method, the author use approximate method with some assumption. Assumption are as follows. The charge neutrality is saved in quantum box region. Because carrier density of quantum box is higher than carrier density in optical confinement layer and Coulomb force must be strong in quantum box. The carrier density in optical confinement layer is assumed as average value of overflow between electron and hole. Because charge neutrality in whole system must be saved by loose band bending and carrier density in homogeneous optical confinement layer is almost equal to average of overflow of electron and hole around quantum box structure, which are most off from charge neutrality.

By consideration until now, the threshold current J_{th} in eq. (5-8) is rewritten as follows:

$$J_{th} = N_{QB}\, enV \,/\, \tau_{sQB} + (N_{overflow} + P_{overflow})\, eV_{OCL} \,/ 2\tau_{sOCL} \qquad (5\text{-}10)$$

where $N_{overflow}$ and $P_{overflow}$ express carrier density in optical confinement layer around quantum box determined by barrier height and quasi-Fermi level of quantum box, respectively. V_{OCL} is volume of optical confinement layer per area and τ_{sQB} and τ_{sOCL} are carrier lifetime in quantum box region and optical confinement layer, respectively.

5-3 Calculation result of threshold current

By equations above mentioned, the author can obtain the threshold current density of quantum box lasers. Hence, lowest threshold current density value and structure is determined by computer calculation. The author assumed SCH structure laser as shown in Fig. 5-4 and active material is limited to GaInAs. For simplicity of calculation, refractive index and loss in active region are neglected. The parameter for calculation is assumed as follows.

The loss in cavity is $40cm^{-1}$, from sum of conventional waveguide loss($10cm^{-1}$) and mirror loss in conventional cavity($30cm^{-1}$). The conventional carrier lifetime τ_s included term of carrier leakage in non radiative time and this term in τ_{sQB} must be eliminated when carrier leakage to optical confinement layer is considered. More detailed formula of τ_s is as follows(166):

$$1/\tau_s = 1/\tau_r + 1/\tau_{nr} \qquad (5\text{-}11a)$$

$$1/\tau_r = B_r N \qquad (5\text{-}11b)$$

$$1/\tau_{nr} = A + B_{nr} N + C_{nr} N^2 \qquad (5\text{-}11c)$$

where τ_r and τ_{nr} are radiative and non-radiative recombination times, respectively. B_r is coefficient of radiative recombination and value is 3.5×10^{-11} cm^3/s. A is coefficient for non-

radiative recombination by defect and this coefficient is neglected. B_{nr} is coefficient for carrier leakage and the value is $9.5\times10^{-11}cm^3/s$. C_{nr} is coefficient for Auger effect and the value is 4×10^{-29} cm^6/s. By account in leakage to optical confinement layer in eq. (5-10), B_{nr} in eq. (5-11c) must be neglected for τ_{sQB}. On the other hand, dependence of carrier lifetime in optical confinement layer is expressed as $1/\tau_s \sim B_{eff}N^{\gamma-1}$ with $B_{eff} \sim 1.5\times10^{-10}cm^3/s$ and $\gamma \sim 2$ (164-166). Effective mass and band discontinuity are determined from reports of R. J. Nicholas, et al., (159), Dutta (162) and Harrison (163).

In this calculation, density of quantum box is very important parameter. The author expressed density of quantum box by parameter η, that is a product of the number of layers of quantum boxes array and the rate of the surface area of quantum boxes included in the whole area. For calculation, η is assumed as 0.25 and 0.5 because increasing of this parameter introduces difficulty of fabrication and breaks a assumption of fine volume of total quantum box area. When each quantum box is separated by same length of a side of cubic box, 0.25 of η is equivalent to single layer and 0.5 is equivalent to double layers. Of course, value of 0.5 can be obtained by single layer when density of quantum box is twice.

From calculation, threshold current density in quantum box with InP barrier is lower that that with quaternary barrier because of larger energy separation between each levels. The

lowest threshold current in quantum box with InP barrier is $60A/cm^2$, although that with quaternary barrier is about $100A/cm^2$.

The threshold current density has large dependence with thickness and composition of optical confinement layer due to effects of optical confinement and carrier leakage. Dependence of thickness is shown in Fig. 5-7 and 5-8. When bandgap wavelength in optical confinement layer λ_{OCL} is 1.2 μ m, carrier leakage was not suppressed sufficiently. Hence, lowest point of threshold current density J_{th} is not fit to the maximum point of optical confinement factor ξ as shown in Fig. 5-7, although lowest point of consumed current in quantum box region J_{QW} is fit to the maximum point of ξ. On the other hand, when λ_{OCL} is 1.1 μ m, carrier leakage was suppressed and lowest point of J_{th} is fit to the maximum point of ξ as shown in Fig. 5-8. Moreover, lowest J_{th} when λ_{OCL} is 1.1 μ m is lower than that when λ_{OCL} is 1.2 μ m, although, relation of J_{QW} is inverse due to larger optical confinement factor. Figure 5-9 shows dependence of λ_{OCL}. By the effect of optical confinement and carrier leakage, best value is obtained at 1.1 μ m. Moreover, the author neglects change of optical loss by λ_{OCL} in this calculation and longer λ_{OCL} may have more disadvantageous in consideration of optical loss change.

Figure 5-10 shows dependence of size of quantum box. The best value is obtained by 10nm as a side of cubic box. Figure 5-

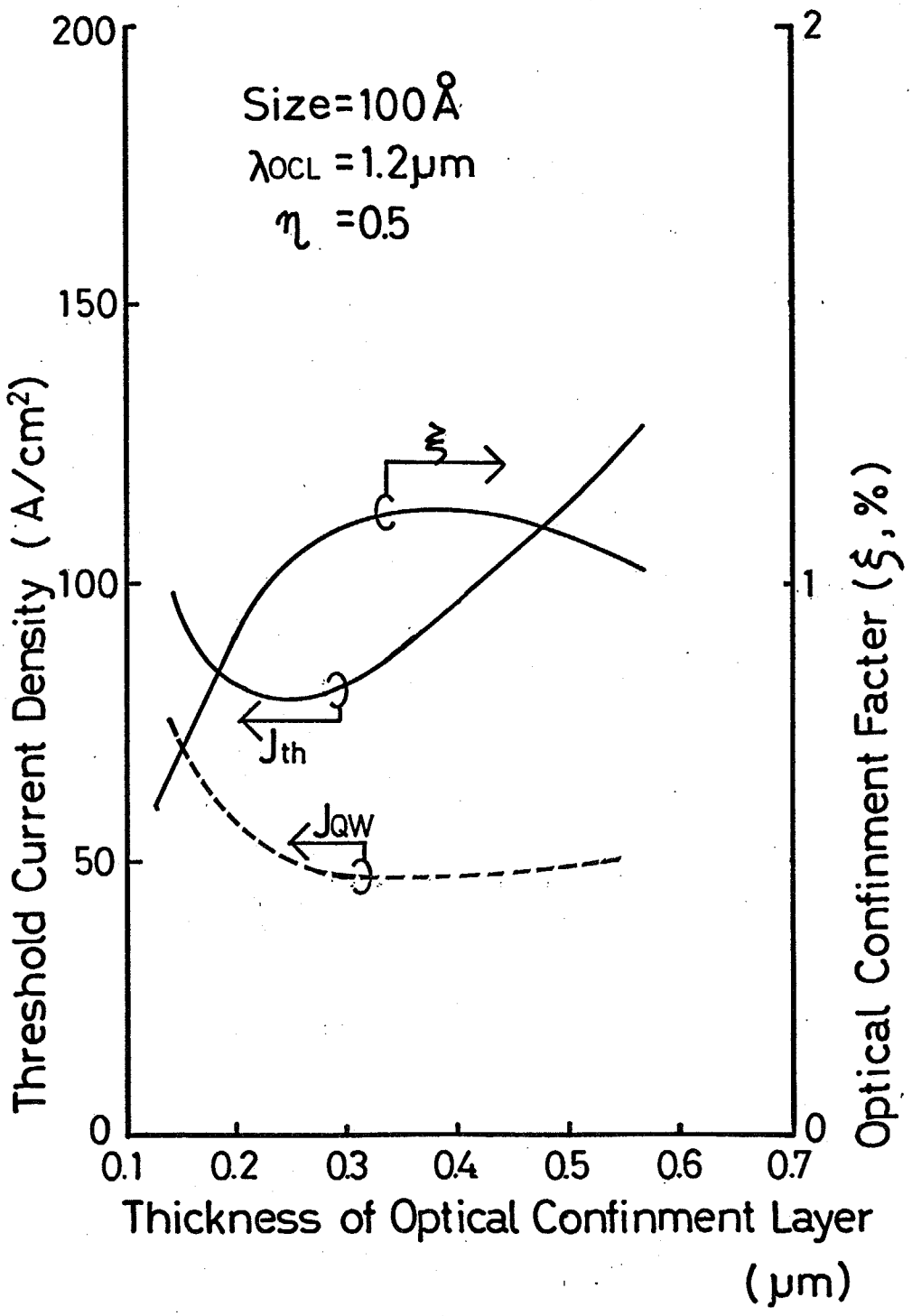

Fig. 5-7 Lowest threshold current density as a function of total thickness of optical confinement layer. λ_{OCL} is 1.2 μm. J_{th} and J_{QW} are indicated threshold current density and consumed carrier density at threshold point, respectively. ξ is indicated the optical confinement factor in quantum box region.

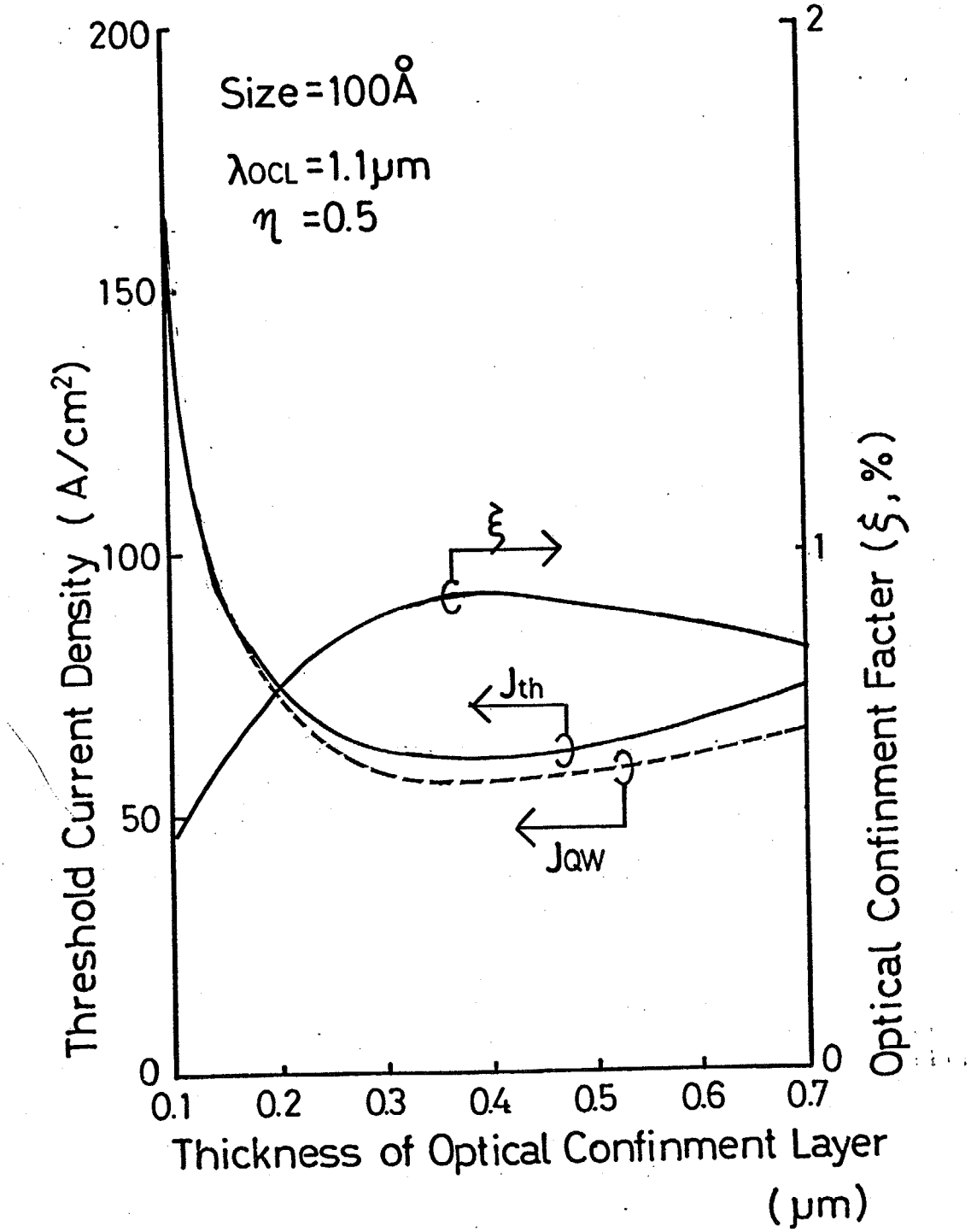

Fig. 5-8 Lowest threshold current density as a function of total thickness of optical confinement layer. λ_{OCL} is 1.1 μm. J_{th} and J_{QW} are indicated threshold current density and consumed carrier density at threshold point, respectively. ξ is indicated the optical confinement factor in quantum box region.

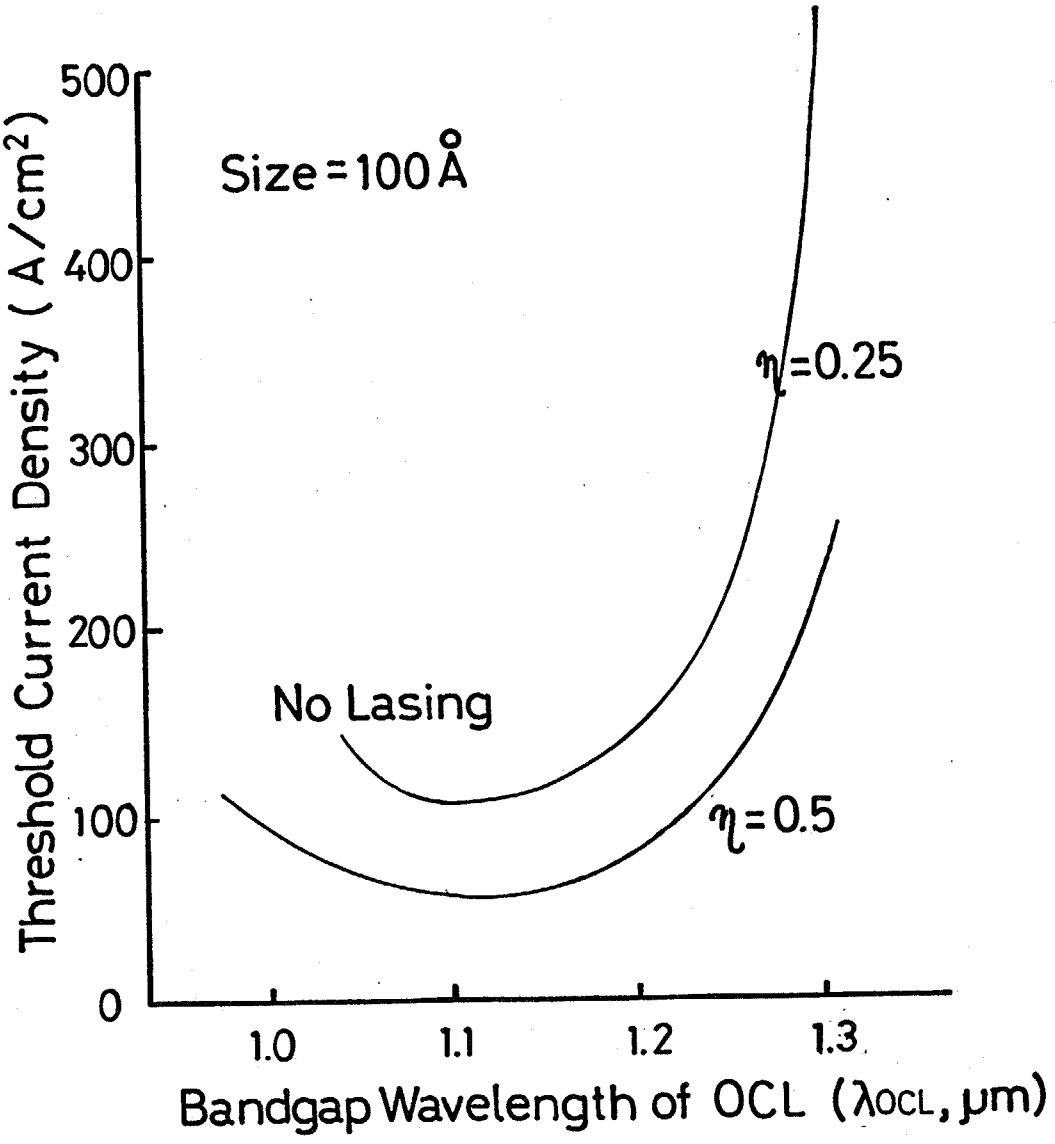

Fig. 5-9 Lowest threshold current density as a function of bandgap wavelength of optical confinement layer. Thickness of optical confinement layer is optimized in each point.

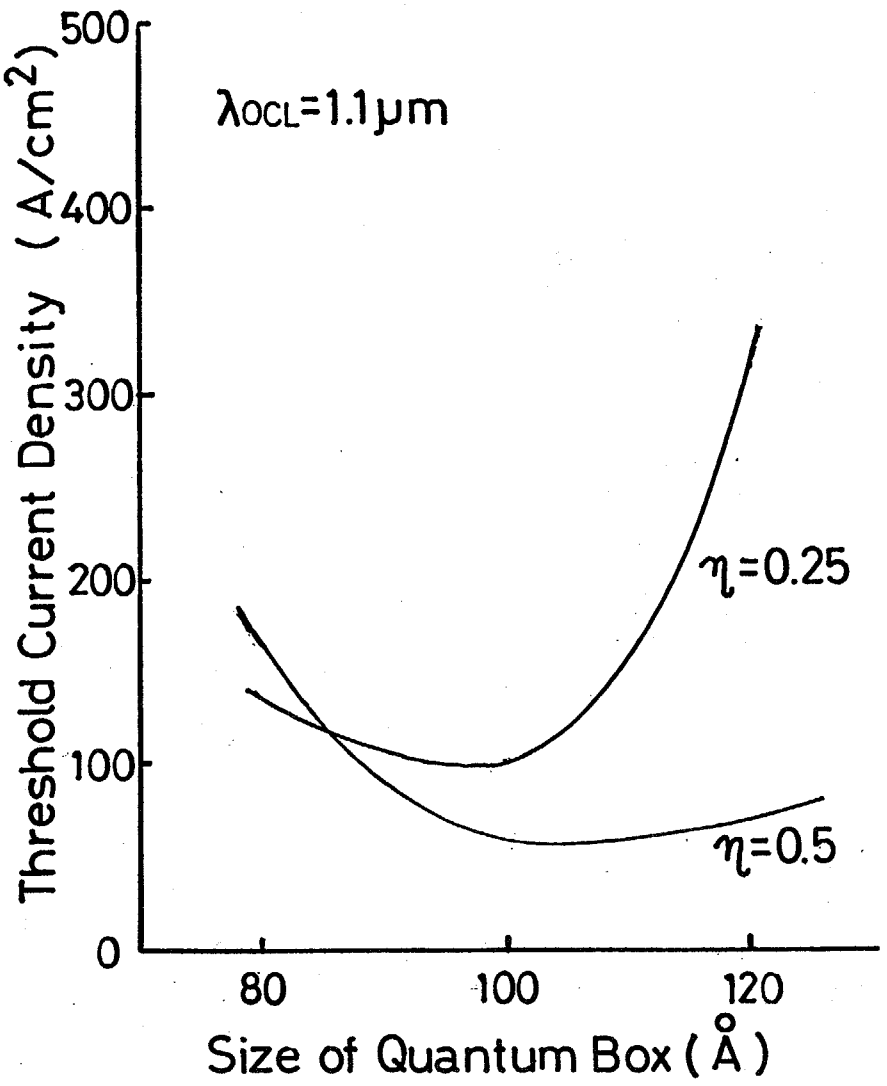

Fig. 5-10 Lowest threshold current density as a function of quantum box size. λ_{OCL} is 1.1 μ m. Thickness of optical confinement layer is optimized in each point.

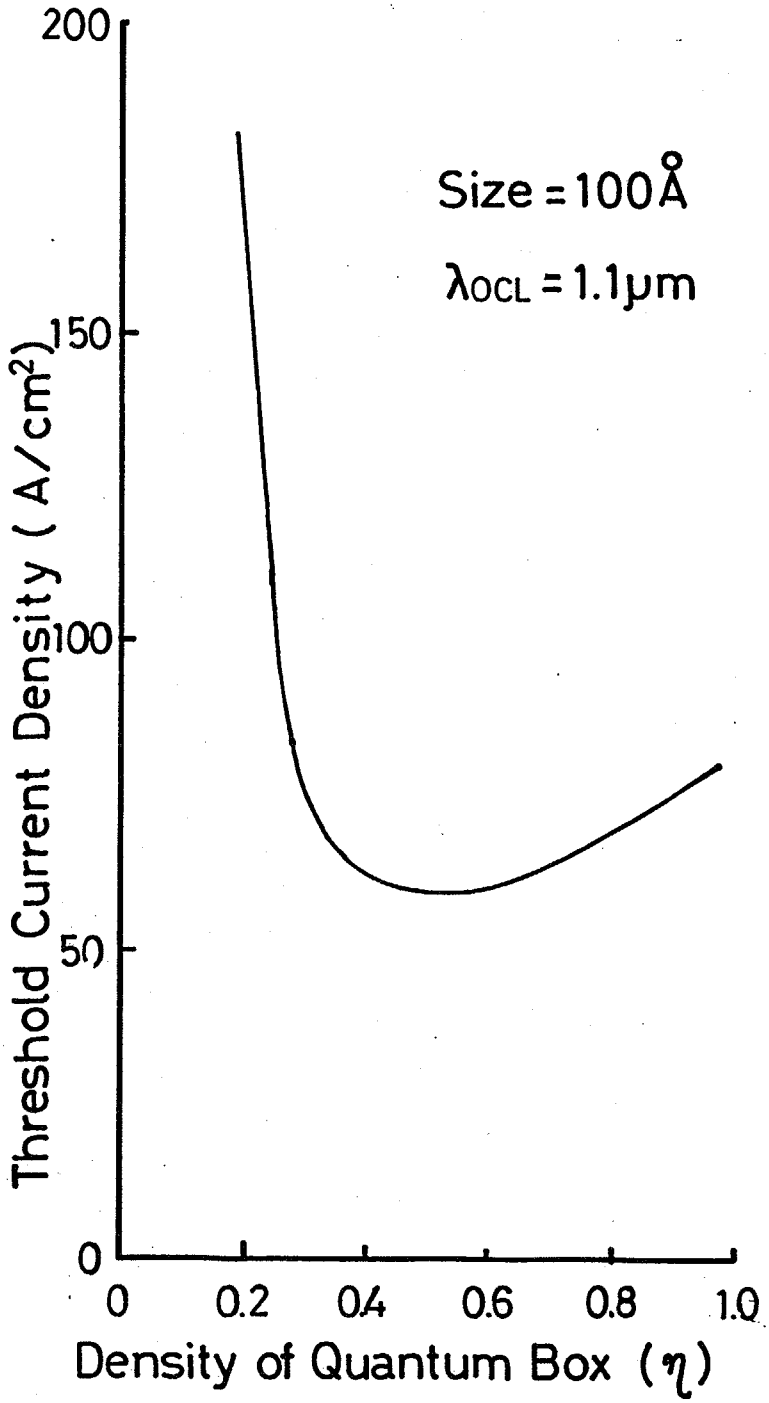

Fig. 5-11 Lowest threshold current density as a function of density of quantum box per area. λ_{OCL} is 1.1 μ m. Thickness of optical confinement layer is optimized in each point. When each quantum box is separated by same length of a side of cubic box, 0.25 and 0.5 of η are equivalent to single layer and double layers, respectively.

11 shows dependence of η. Selected values, 0.25 and 0.5 are in the range of lowest region for J_{th}. Consequently, lowest threshold current density is 60A/cm^2 when size of quantum box, thickness of optical confinement layer, λ_{OCL} and η are 10nm, 0.35μm, 1.1μm and 0.5, respectively.

On the other hand, quantum box lasers consisting to multi-layers of quantum box as shown in Fig. 5-12 is one of the expected structure for realization of quantum box laser and the author calculates threshold current in this structure. In this case, decreasing of total volume of quantum box in this structure introduces more severe decreasing of optical confinement factor than that in SCH structure because total optical confinement becomes also weak when total volume of quantum box is decreased. For calculation of optical confinement factor in quantum box, refractive index of quantum box region is necessary. The calculation is as follows. At first, the author assumes 10nm cubic quantum box in 3-dimensional 20nm period and InP as barrier material. In this case, refractive index of quantum box and InP are 3.52 and 3.21, respectively. Hence, average refractive index is 3.25 from summation of products between each volume and each refractive index(23). Optical confinement factor can be solved with 3-layers slab waveguide model with this average refractive index, while real optical confinement factor of quantum box is decreased by ratio of volume from calculated value. Optical loss in quantum box structure is also into con-

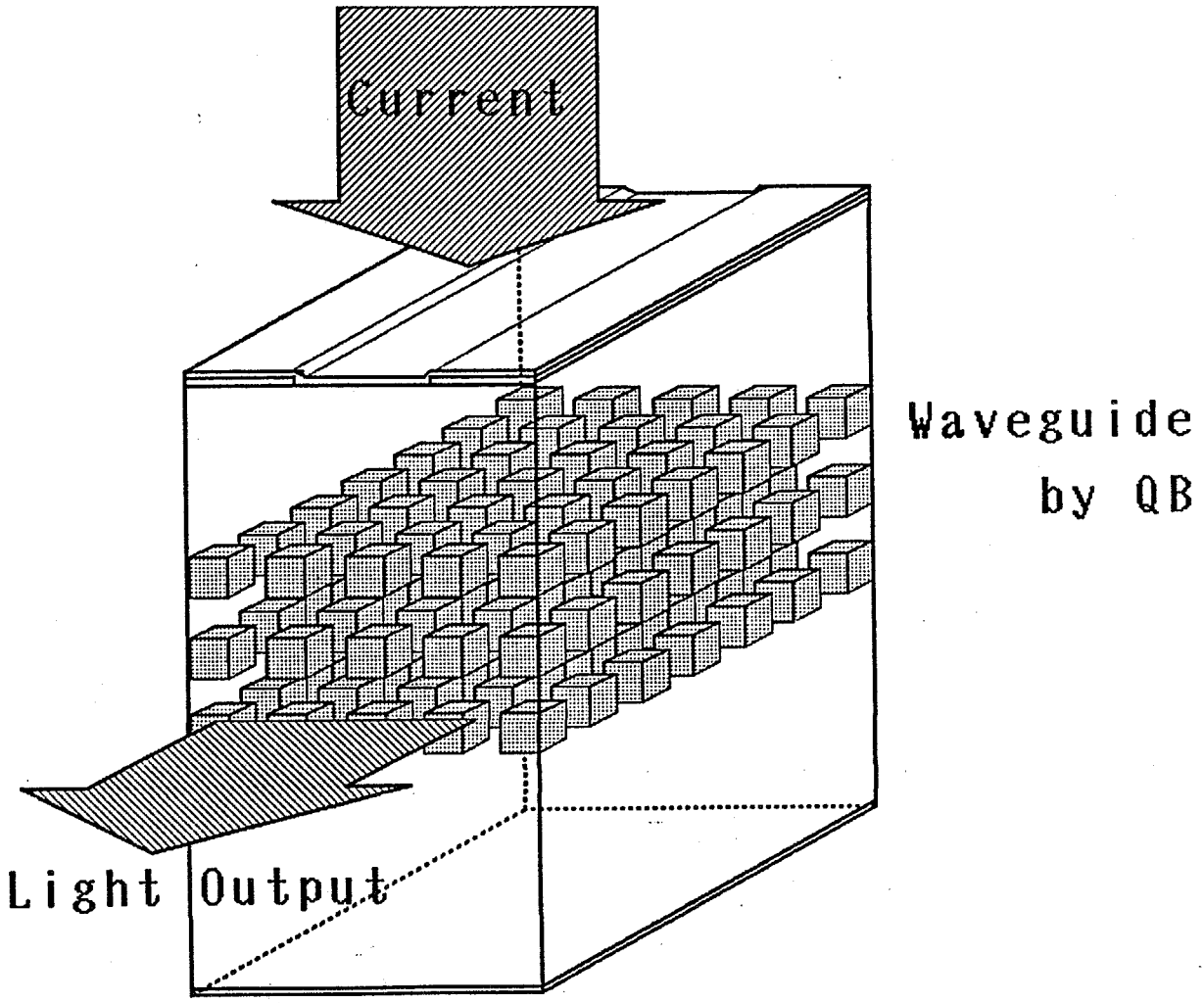

Fig. 5-12 The schematic view of quantum box laser consisting to multi layers of quantum box. In this case, optical confinement effect is introduce by only quantum box region.

sideration and expressed by K_0N with $K_0 \sim 4 \times 10^{-17} cm^2$ (131). Calculated threshold current is shown in Table 5-1. Lowest threshold current is $310A/cm^2$. In this structure, large size of quantum box has advantageous due to large optical confinement factor. The calculation result when the size of quantum box is 12nm is also indicated in Table 5-1. The lowest value is $265A/cm^2$. As a result, this structure is not superior to SCH structure from aspects of threshold current density.

As the next step, fluctuation of size is considered. The spectrum of gain of quantum box have a distribution due to the intraband relaxation time τ_{in} while linewidth of spectrum is about h/τ_{in}, although state density of quantum box is represented by δ-function. If fluctuation of energy levels by fluctuation of size is much smaller than h/τ_{in}, gain is not so changed. For calculation of fluctuation effect, the author assumed fluctuation of size has Lorentz distribution. In this case, fluctuation of size works as decreasing of τ_{in}. Energy shift by change of size is 9meV per 1nm for one direction around 10nm cubic. When 1nm fluctuation is occurred in two directions by patterning fluctuation and remained direction have no fluctuation because abruptness of grown hetero interface can be reduced smaller than one monolayer as described in section 1-4, energy fluctuation is about 18meV and maximum gain is reduced by factor 4 (6meV/(6meV+18meV)). This reduction of gain is severe

Table 5-1 Calculation of optical confinement factor, threshold carrier density and threshold current density. The waveguide consists of multi quantum box layers. The density of quantum box per volume is factor 0.125. (The separation length of each cubic quantum box is equal to a side of quantum box.)

Quantum box size = 100Å

Number of layers	ξ of QB	Jth (A/cm^2)
1	0.0002	-
2	0.0003	-
3	0.0007	-
4	0.0012	-
5	0.0021	-
6	0.0027	-
7	0.0037	1145
8	0.0050	535
9	0.0060	415
10	0.0074	376
11	0.0088	332
12	0.0106	322
13	0.0121	310
14	0.0139	334
15	0.0157	315

Quantum box size = 120Å

Number of layers	ξ of QB	Jth (A/cm^2)
1	0.0002	-
2	0.0003	-
3	0.0012	-
4	0.0017	-
5	0.0027	-
6	0.0037	-
7	0.0051	1976
8	0.0065	892
9	0.0084	498
10	0.0102	363
11	0.0121	277
12	0.0143	265
13	0.0162	287
14	0.0184	310
15	0.0206	332

for lasing. Hence, the author assumes reducing of cavity loss until $20cm^{-1}$ and this value is not so sever to obtain by long cavity length or high reflective mirror. In this case, threshold current density of best SCH structure is increased until $190A/cm^2$, although threshold density can be reduced until $40A/cm^2$ with reduction of cavity loss if gain reduction is not occurred. However, calculated value with fluctuation is sufficient lower than lowest value of conventional quantum well laser[25].

In the present estimation, important parameters are carrier lifetime and intraband relaxation time and those values are determined from bulk value. However, these values have possibility of change by quantization and hence, estimation of change is important.

At first, change of carrier lifetime by quantization was expected. Firstly, the probability of Auger effect may be decreased by eliminating of distributed neighbor levels concerning collision by three dimensional quantized level. Secondly, probability of radiative recombination may be decreased also because probability is decided by integral of state density[25] and state density is decreased by quantization. Consequently, those estimation introduce longer lifetime and lower threshold current density.

As the next, change of intraband relaxation time by quantization is expected. The relaxation time is decided by colli-

sion between carriers mainly. This collision process is similar to Auger process[172] and carrier can transit to other level by transferring of excess energy to other carrier while this carrier transits also another level. Hence, scattering probability is decreased by eliminating of neighbor distributed levels concerning collision by three dimensional quantization and the gain may become larger.

5-4 Ideal structure of quantum box laser

Ideal low threshold current density of quantum box laser is prevented by overflow of optical confinement layer. To eliminate of consumed current in optical confinement layer, new structure must be designed.

Why quantum box require the large injection carrier until large carrier leakage to optical confinement layer is introduced? The problem occur by the number of level. The optical gain is proportional to sum of both occupation as shown in eq. (5-1) and following calculated result indicates that optical gain is determined by occupation ratio of valence band level after almost complete occupation of conduction band level. The author calculated optical gain in 10nm cubic quantum box at $3x10^{18}$ cm^{-3} for carrier density as shown in Fig. 5-2. In this case, numbers of carrier in quantum box in each band is three from volume of quantum box and injected carrier density. Hence, it is enough for occupation of basic level if occupation ratio

of basic level is high. Actually, basic level in conduction band is occupied until 97% and the number of carrier in basic level is about two. Remained one carrier exists in other level. However, basic level in conduction band is occupied until 32% and the number of carrier in basic level is about 0.6. Remained 2.4 hole exists in other levels. This phenomenon is occurred by difference of effective mass and that is indicated in the number of levels. The number of levels in conduction band and valence band are 5 and 106, respectively. If carrier can occupy the both levels completely, optical gain is increased by factor three as shown in Fig. 5-13 because ratio of obtained gain in this calculation to maximum gain is about 30% (97%-(100-32)%).

Hence, if the author increase occupation ratio in valence band, injection carrier density to obtain same optical gain can be reduced and overflow from conduction band level of quantum box can be also reduced. For these improvement, the author propose following two ideas.

The first propose is extending the area for charge neutrality by modulation doping(168). Modulation doping for quantum well laser is proposed by M. Yamada, et al.(169), and K. Uomi, et al.(170), independently. Doping in barrier around quantum box provides carrier to quantum box, while absorption loss and recombination probability by doping are small by wide bandgap. Self-consisted calculation is necessary for estimation of threshold current density of this structure. Hence, the

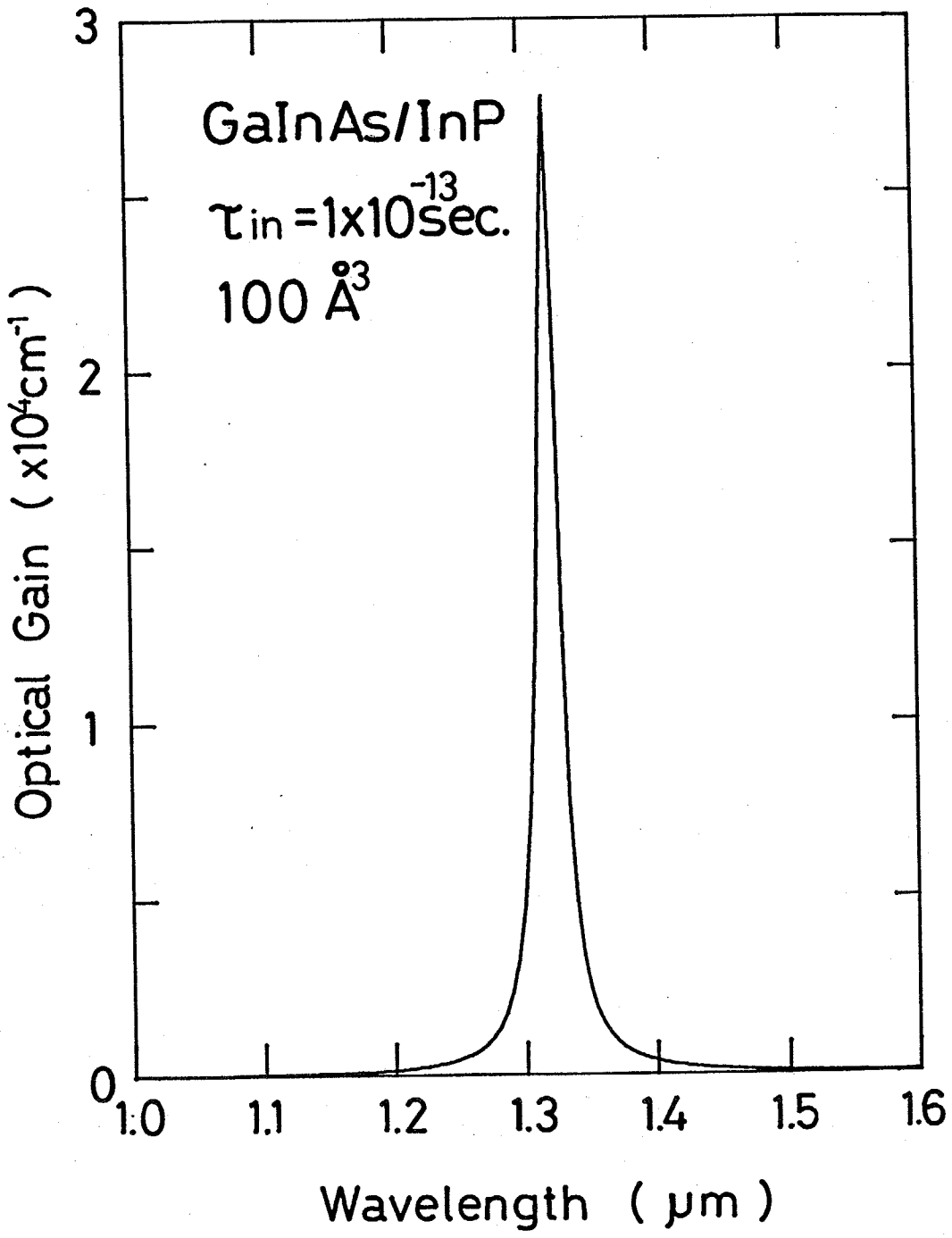

Fig. 5-13 Gain spectra calculated for $Ga_{0.47}In_{0.53}As/InP$ 10nm cubic quantum box with assumption that each basic levels were occupied by carriers completely.

author gives up this calculation. However, calculation by Yamada, et al.[171], was pointed out that threshold current density can be reduced until almost zero by application of this structure to one-dimensional quantum well laser. Hence, drastic reduction of threshold current is also expected in quantum box structure because modulation doping is more effective for fine volume of quantum box.

The other propose is changing of hole mass. The increasing of hole mass introduce large energy separation between each level and decreasing of number of levels.

From design of structure, strained layer super-lattice (SLS)[102, 103] has possibility of change of hole mass. In SLS, degeneration of heavy hole and light hole[173] is solved and top of light hole band is higher than top of heavy hole band by compression. However, quantum well introduce energy shift from base level and that quantity is increased with decreasing of effective mass. Hence, quantized level of light hole is lower than basic level of heavy hole after fabrication of quantum well even if SLS is used.

To achieve change of hole mass, the remained methods is change of materials. It is better that ratio between mass of hole and mass of electron (m_h/m_c)is close to unity. The author assumes GaInAs/InP systems as a materials until now and m_h/m_c of this systems is about 9. The value of III-V compounds materials with direct transition is not so changed from this

value[174]. Hence, the author must find in others materials. Material that have around unity value about this ratio is IV-VI compounds materials[175]. As example, m_h/m_c of PbTe is in the range from 0.92 to 1.3. This range is occurred by anisotropy of band structure. Of course, many subject must be developed for those laser structure.

The change of material can solve another problem of GaInAs/InP quantum box structure, that is offset wavelength from lowest loss region of silica fiber[69-71]. The wavelength of basic level of quantum box fabricated by 10nm cubic GaInAs is 1.32 μ m and lowest region of loss in silica fiber is 1.5 μ m. Hence, longer wavelength materials is required from this point. Most easy method is increasing of In in composition of GaInAs, while strained energy by lattice mismatching can be absorbed by fine structure. However, strained structure has a limit of shift[199] and the peak of gain center cannot shift until 1.5 μ m by strained structure. Hence, material must be changed. From this view point, selection principle of materials is wide bandgap difference by composition change with lattice matching. GaInAlAsSb[176,177] is one of the suitable systems from Fig. 1-1.

5-5 Conclusion remarks

In this chapter, the author analyzes the laser threshold of the three-dimensional quantum-box lasers. At first the author explains that the motive force of reduction of threshold current

density is carrier confinement in basic level by energy separation to neighbor level. Secondly, the threshold current density of quantum box laser is estimated in consideration with effect of fluctuation and carrier leakage. Lowest threshold current density at room temperature is 60 A/cm^2 when the structure is optimized, while that is 190 A/cm^2 with consideration of 10% fluctuation in quantum box size. Those values have advantageous to reported threshold in other structure. Finally, ideal structure of quantum box laser is discussed. Modulation doped structure[169-171] is most attractive for suppression of carrier leakage and material change is necessary for adjusting of wavelength to lowest loss region of optical fiber.

Chapter 6 Fabrication of quantum box laser

6-1. Introduction

It is reported that quantum-box lasers is expected to be greatly enhanced the superior characteristics obtained by conventional quantum well laser by increasing the dimension of the quantization in chapter 5.

Multidimensional quantum well structure was proposed for elimination of electron scattering by the quantum wire structure[178]. Hence, quantum wire structure are studied mainly from a electron properties[179-181]. The first multidimensional quantum well structure for optical properties was fabricated as a quantum wire by Petroff, et al.[182]. The realization of quantum box structure was studied by etching or disordering applied to one dimensional quantum well structure and quantized levels were shown by photoluminescence or cathode-luminescence[183-186]. However, in order to realize the quantum-box laser, a carrier injection mechanism as well as an optical waveguiding mechanism must be incorporated into the structure. As far as the author know, a fabrication of the quantum box laser structure with optical guide structure and p-n junction was not reported before this research.

In this chapter, the author reports the fabrication of GaInAsP/InP quantum-box structure with p-n junction and optical guide structure. Designs of structure and process for less

damaging of quantum box surface are described. It is reported that interference exposure and wet chemical etching can be applied to precise processes for higher dimensional quantum size effect. The wet chemical etching process for quantum box in consideration with anisotropy was developed. The light emission from the quantum-box structure by current injection is observed. Finally, design to reduce the threshold current density is also discussed from experimental result.

6-2. Designs of structure and process

The size of quantum box is requested under electron mean free path (around 30nm). Thus, fabrication process of quantum box has many difficulties. The first difficulty of the fabrication is the patterning of very fine structure. The second difficulty of fabrication is that the quantum box structure would be highly sensitive to the defect around the surface because of small volume of quantum box. Third difficulty is that the size deviation of the structure is limited because each energy levels have distribution by fluctuation of the size. Thus, the author paid special attention to designs of structure and process.

For operation of semiconductor lasers, a carrier injection mechanism as well as an optical waveguiding mechanism must be incorporated into the designed structure. Figure 6-1 shows the structure of fabricated quantum box laser. For optical waveguide, separate confinement heterostructure[154] was applied

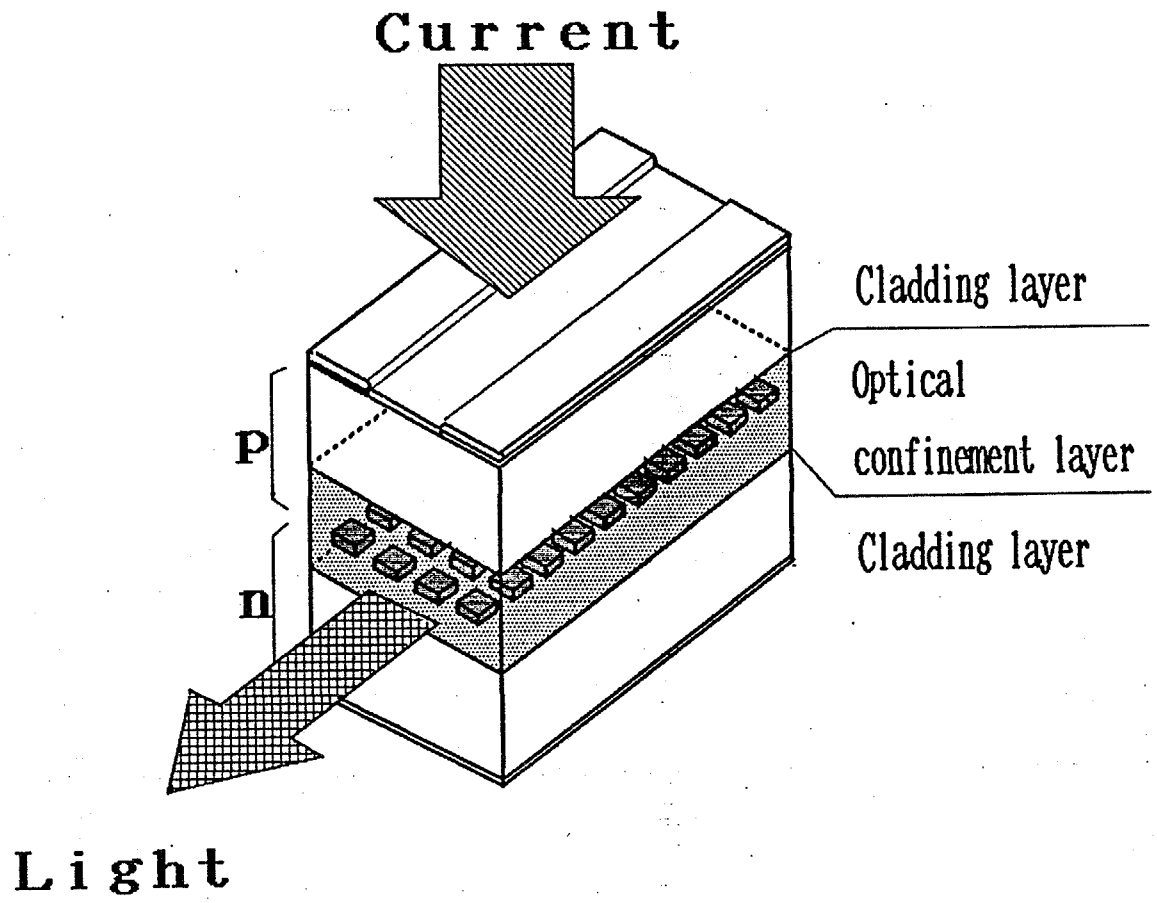

Fig. 6-1 The outlines of fabricated quantum box laser.

and the quantum box array was located in center of the optical confinement layers which were sandwiched by cladding layer. A p-n junction located just above the quantum-box layer provides carrier injection mechanism.

To realize the quantum box structure, the etching process was applied to one dimensional quantum well. To prevent the expose of etching surface, regrowth process was carried out after the etching to form the hetero interface. Moreover, sufficient thickness for optical waveguide was obtained by the regrowth when the thickness of the layers covering the quantum well in the first growth were thin for easiness of patterning.

Single layer was used for based structure of quantum box. If multi quantum well was used, same size patterning on each layers was necessary to prevent large deviation of quantum box size between each layers. Thus, required characteristics of etching are very severe, that is, precisely vertical etching facet with high aspect ratio. Hence, single quantum well would be preferred over than multi quantum well to avoid this difficulty.

GaInAsP/InP system was applied as a material which has good interface property after etching[186] and embedding process. Less damage is expected after the expose of etching surface on the process by this material. The other advantageous of GaInAsP/InP system is that the mass-transport process[137, 138] can be applied to obtain good regrowth inter-

face because binary can be used as cladding layer. Of course GaInAsP/InP has suitable emission wavelength for optical fiber communications.

For patterning of micro structure comparable to size of quantum box, the electron beam (EB) lithography is used conventionally[179, 180, 183-189]. However, EB lithography have a disadvantage of uniform pattern in large area due to fluctuation of beam current in long time exposure. Moreover, fine electron beam lithography technique has difficulties and more research is required. Reported periods of micro-fabrication by EB was about 200nm, usually and this period can be achieved by the interference exposure of laser. This technique have advantageous for uniformity of pattern in large area for laser cavity (around 400 μm) because large area is exposed simultaneously. Hence, interference exposure[190, 191] was used for patterning of the quantum box.

As the etching process, dry etching has also advantageous from problem of anisotropy and ability of pattern copy to sample. However, dry etching has possibility to introduce damage by collision of particle. The author used wet chemical etching as a etching process, because wet chemical etching is easier than dry etching to obtain etched surface without damage. Improvement of etching process to solve the problem of anisotropy is described in next section.

Following experiment was carried out to confirm that patterning by interference exposure and wet chemical etching can be applied to precise process for a fabrication of quantum box. After each etching, photoluminescence measurement at room temperature was done to confirm the crystal quality. Grating with 80nm depth and 204nm period was fabricated along <01$\bar{1}$> on the quantum well wafer as the same manner as mentioned later. The thickness of quantum well layer and InP top layer were 15 and 20nm, respectively. After this process, intensity of photoluminescence was decreased by factor 3-10. As the next process, the width of quantum well was reduced by undercut etching with selective etchant for quaternary described in next section. The quantum size effect of quantum wire was expected by reducing of width. Figure 6-2 shows change of photoluminescence spectra before and after undercut etching. Peak intensity was nearly the same before and after etching. This phenomenon is explained as follows. Number of generated carrier was not so changed by this etching because dominant volume for absorption of excited light was optical confinement layer in this structure. Generated carrier was collected in quantum wire region by energy gap difference. Hence, photoluminescence intensity was not reduced with reduction of volume if non-radiative center was not increased in etching surface.

After 10 second etching, peak of photoluminescence was shifted toward shorter wavelength by about 30nm as shown in

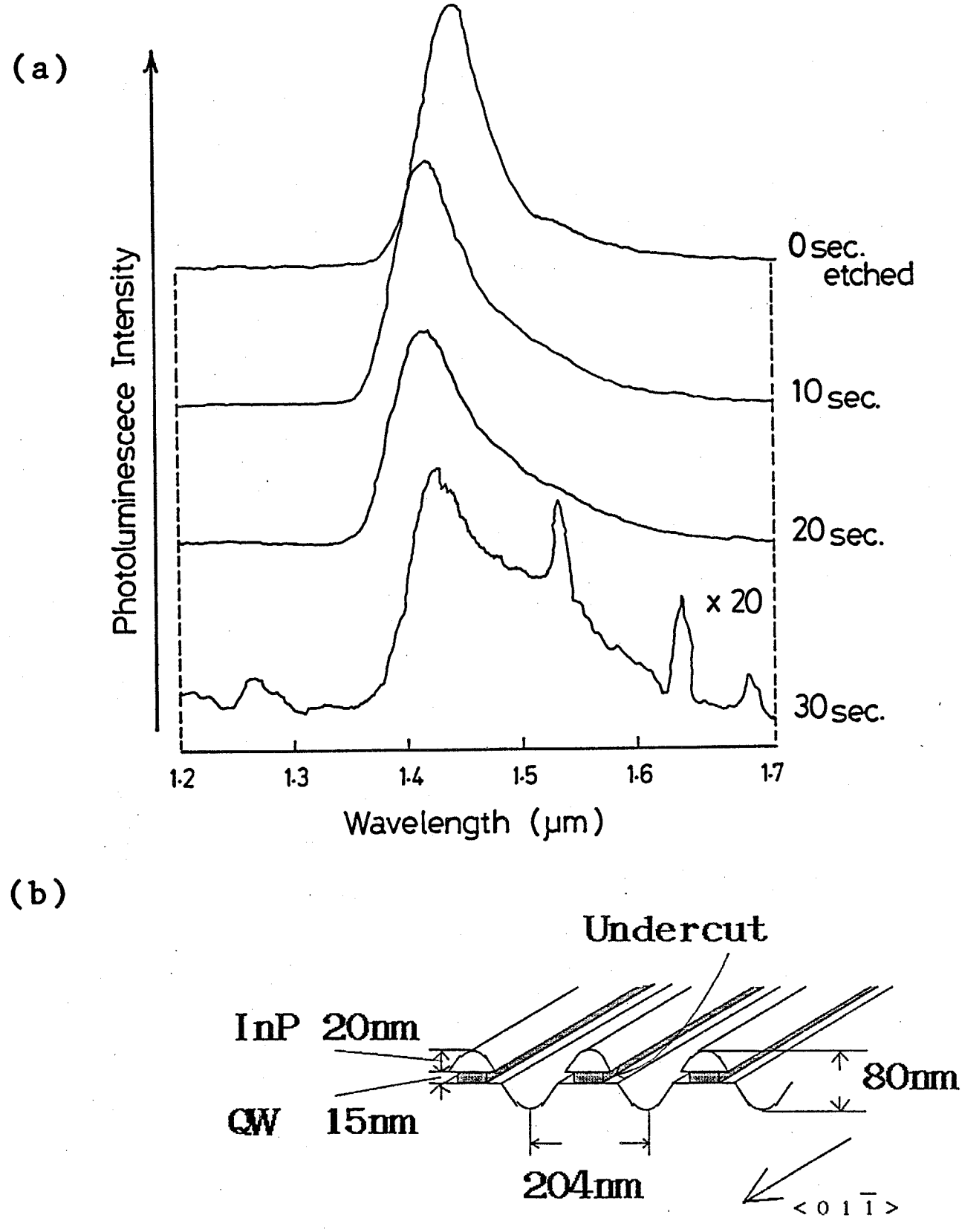

Fig. 6-2 (a) The peak shift in photoluminescence measurement by undercut etching to form the quantum wire structure. The measurement temperature was 77K. (b) Schematic view of etched structure.

Fig. 6-2. The shift of photoluminescence peak would occur by the following two possibilities. One is the quantum size effect and the other is band filling effect(186). To confirm the contribution of band filling effect, intensity of the excitation of photoluminescence was reduced by factor 10 and peak shift after this reduction was still remained over 20nm. Hence, the peak shift occurred by quantum size effect mainly. The diameter of laser beam for sample excitation was about 1mm. Thus, numbers of quantum wire excited simultaneously were of the order of 10^3. As a results, size of quantum wire was almost uniform. The width of quantum wire was estimated to be around 30nm from the peak wavelength shift of 30nm, theoretically. It is difficult that etching accuracy is in this level. Hence, this uniformity indicated some etching stop mechanism and this mechanism was also indicated from additional etching after first shift. As shown in Fig. 6-2, Additional 10-20 second etching was not introduced peak shift and intensity of photoluminescence is decreased drastically after 30 second etching. To explain these phenomenon, the author assumed following model. The etching was stopped after undercutting of quaternary layer by hanging down of upper layer and etching cannot do in very narrow concave. Hence, etching was stopped. After additional etching, carrier supplement from optical confinement layer was stopped and intensity was decreased because remained region of optical confinement layer changed to very narrow and effective carrier injection was stopped by sur-

face defect and depletion layer. Shift quantity had slightly difference in each sample experimentally and those difference would be occurred by width of pattern and thickness of upper layer. Similar experiment in quantum box structure had very strange action. Sometime, peak was returned longer wavelength side again and intensity of peak was not decreased by very long time etching (about 180 sec.) often.

In conclusion of this section, the author believes that the crystal quality of quantum well structure was not degraded by wet chemical etching process and therefore interference exposure and wet chemical etching can be applied as a process to obtain higher dimensional quantum size effect. Recently, application of wet chemical etching of GaAs/GaAlAs for fabrication of quantum wire structure was reported(192) after the author's report.

6-3. Etching Process

To fabricate precise pattern by holographic patterning and wet chemical etching processes, fabrication of fine pattern and improvement of etching technique had to be developed. For fabrication of quantum box, making of the mesa stripes along two directions, <011> and <01$\bar{1}$> were necessary and those etching process had to develop in consideration with problem of anisotropy. Moreover, selective etchant had to develop for undercut etching to reduce the quantum size as described in

fabrication of quantum wire. Etchant must have characteristics of slow etching rate and weak attack of mask for precise etching.

Interference of He-Cd laser beams were used for holographic grating(191) with the period of 204nm. This methods is used for fabrication of grating of brag reflector for distributed feedback laser and distributed brag reflector laser. For patterning of small structure, miss of resist pattern was degraded the fabricated pattern. Particularly miss was observed as small bridges between stripes in fabrication of stripes along <011> direction on InP due to anisotropy as mentioned later. Figure 6-3 is shown pattern after etching between stripes <011>. Many bridges was observed in Fig. 6-3. Hence, plasma ashing was dispensable before etching to eliminate this bridge. Figure 6-4 are shown after plasma ashing of 15, 30, 45 seconds with conditions of 0.5mbar air for atmosphere of chamber and 30W for output power of asher. 30 seconds was selected as ashing time from Fig. 6-4.

For fabrication of stripes, the bromic acid solution, $HBr:HNO_3:10\ H_2O$ (0℃) is one of the suitable etchant for precise process. Because etching rate are not much changed between InP and GaInAsP while attack to resist is weak, although anisotropy was occurred. This etchant is also used for fabrication of brag reflector, conventionally. Thus, the bromic acid solution was applied fabrication of grooves along <01$\bar{1}$> as shown in Fig. 6-5.

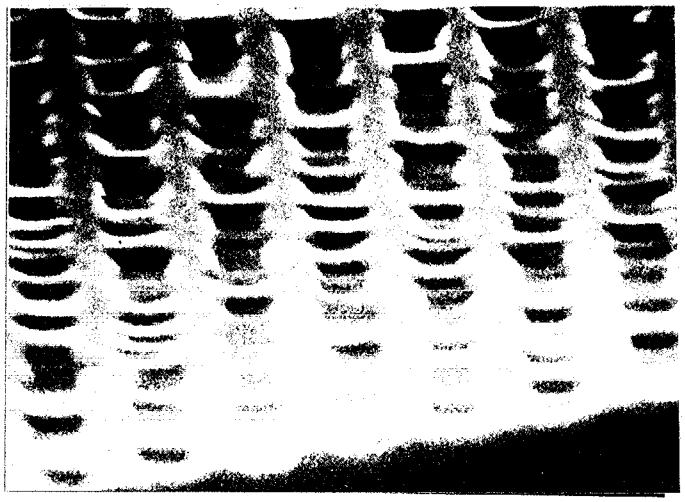

Fig. 6-3 The SEM photograph of many bridges between fabricated stripe patterns along <011>. This patterns was formed without ashing.

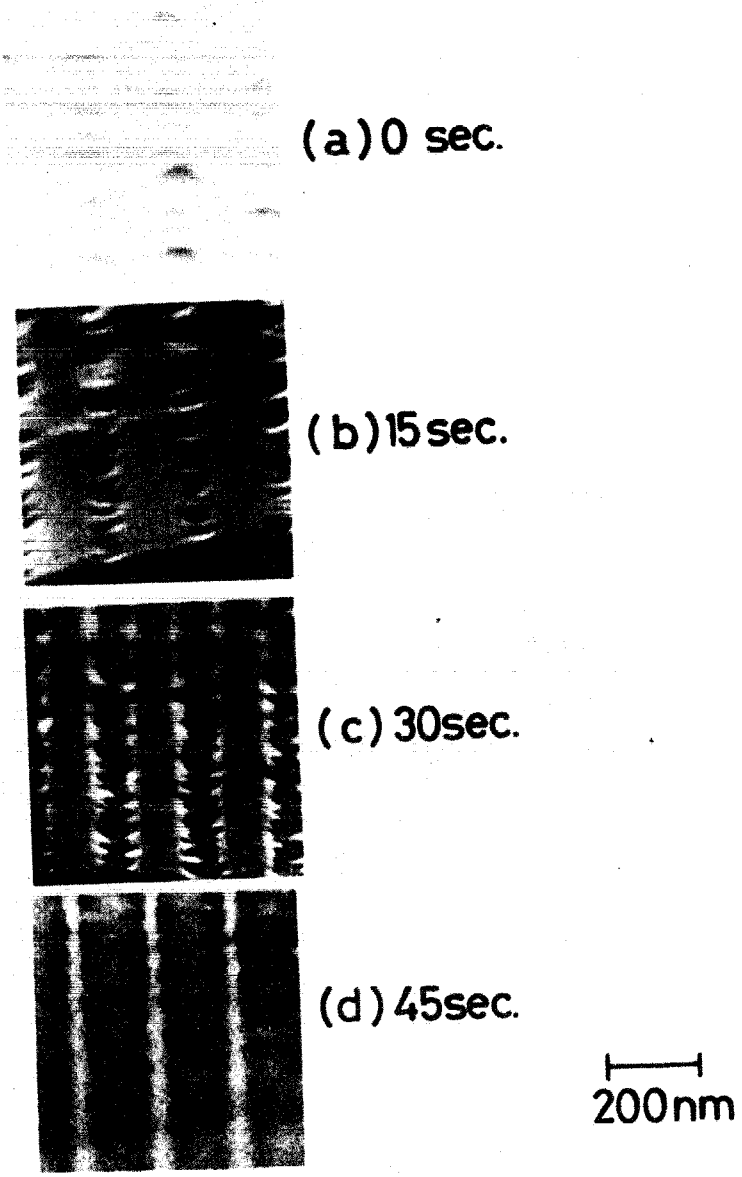

Fig. 6-4 Elimination of an excessive patterns by increasing of ashing time. Ashing times are (a) 0 second, (b) 15 seconds, (c) 30 seconds, and (d) 45 seconds, respectively.

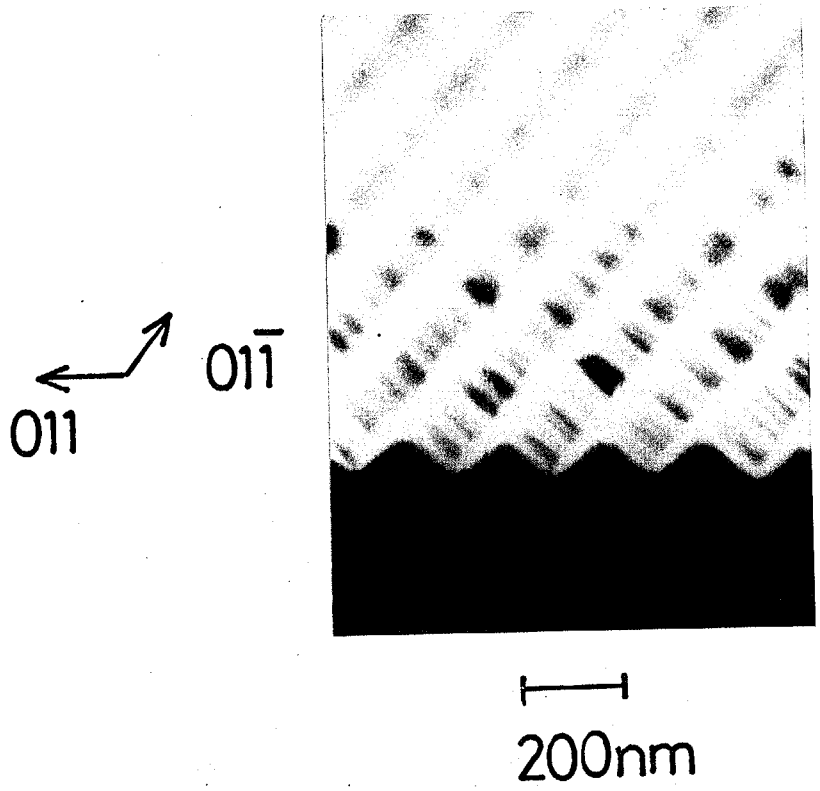

Fig. 6-5 Cross sectional view of fabricated grooves along <01$\bar{1}$>.

However, it was difficult to apply the grooves etching along <011> direction from the problem of anisotropy. Fig. 6-6 shows the etching facet by bromic acid solution with resist pattern along <011> direction on InP substrate. Large penetration of the etching under photo resist mask was occurred and resist mask was removed before etching depth was less than 40nm. This etching depth was not enough for fabrication of quantum box.

To solve the problem of anisotropy, new etching method was developed for fabrication of grooves along <011> direction in consideration with anisotropy. To etch the groove along <011> direction, hydrochloric acid solution is suitable due to vertical etching facet for mesa along this direction. Although, this etchant have tendency to attack AZ1350 and cannot use with thin resist mask. Hence, the author used thin quaternary layer as an etching mask of hydrochloric etchant. At first, mesa stripes of the quaternary layer were formed using AZ1350 resist mask and bromic acid solution as an etchant. This etching was stopped before large penetration of etching under photo resist mask. Then, using the stripes of the quaternary layer as a mask, the InP layer was etched by selectivity of hydrochloric acid. 3 $HCl:HPO_3:H_2O$ at 0℃ was used as this etchant. More dilution of this etchant by water for slower etching speed was lost etching property. HPO_3 was added to eliminate bubble of hydrogen for smooth etching in precise etched structure. Well-shaped rectangular mesa was demonstrated using quaternary mask with InP dummy

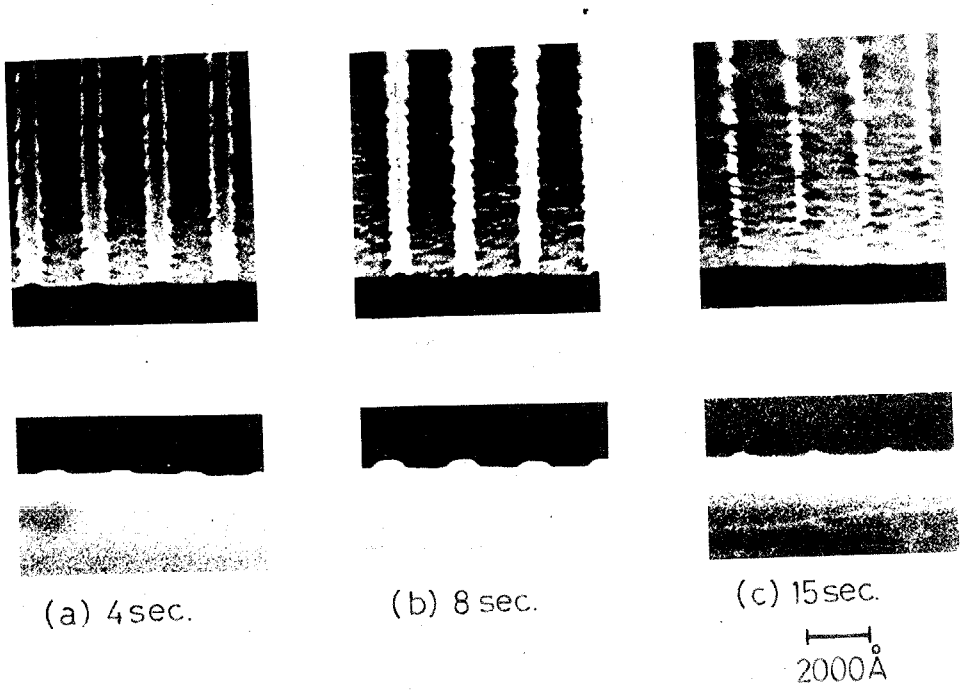

Fig. 6-6 Large penetration under photo-resist mask for fabrication of grooves along <011> by bromic acid solution. The etching times are (a) 4 seconds, (b) 8 seconds and (c) 15 seconds, respectively.

substrate as shown in Fig. 6-7. Penetration under mask was not observed completely. It was pointed out that the mask by epitaxy was the very good characteristics for contact between etched sample and mask from this etching.

As the final etching process, undercut etching was carried out to obtain quantum size. Using the array of the InP squares as a mask, the quaternary quantum-well layer was etched with a selective etchant for quaternary layer. $H_2SO_4:H_2O_2:20\ H_2O$ at 0℃ was used as this selective etchant. The diluted ratio by water of this etchant was selected for slow etching rate and this solution did not lost the etching characteristics by high diluted ratio. The controllability of this etchant was confirmed by experiment of fabrication of quantum wire as mentioned above. Shift of photoluminescence had reproductivity and etching time was in range of suitable time for controllability.

6-4. Fabrication process

To fabricate structure of quantum box laser, processes as shown in Fig. 6-8 were carried out. Each process was decided by discussion in section 6-2 and 6-3.

First, GaInAsP/InP wafers with single quantum well structure were grown by organo-metallic vapor phase epitaxy (OMVPE). Growth condition was same to condition for fabrication of single quantum well laser as described in section 4-4. The following layers were grown on n-InP substrate successively.

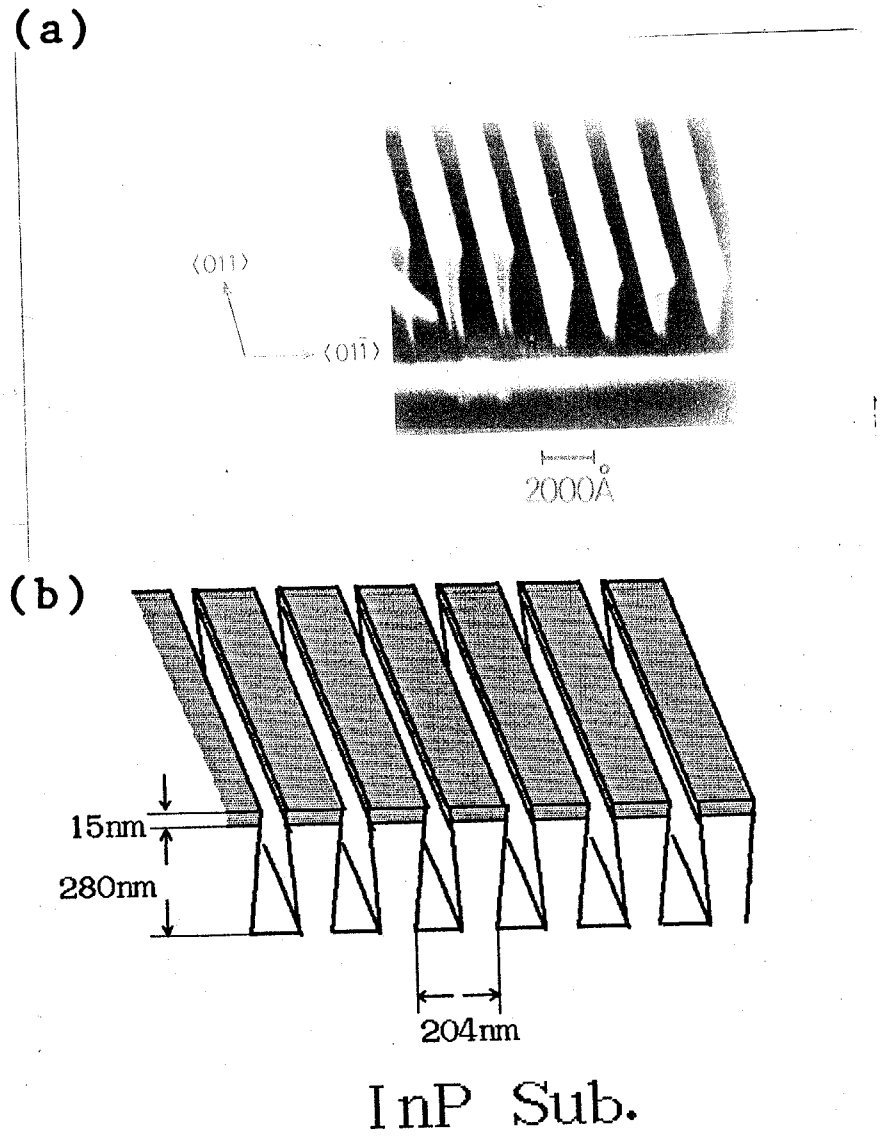

Fig. 6-7 (a) Cross sectional view by SEM of well shaped rectangular mesa fabricated by quaternary mask. (b) Schematic view of etched structure.

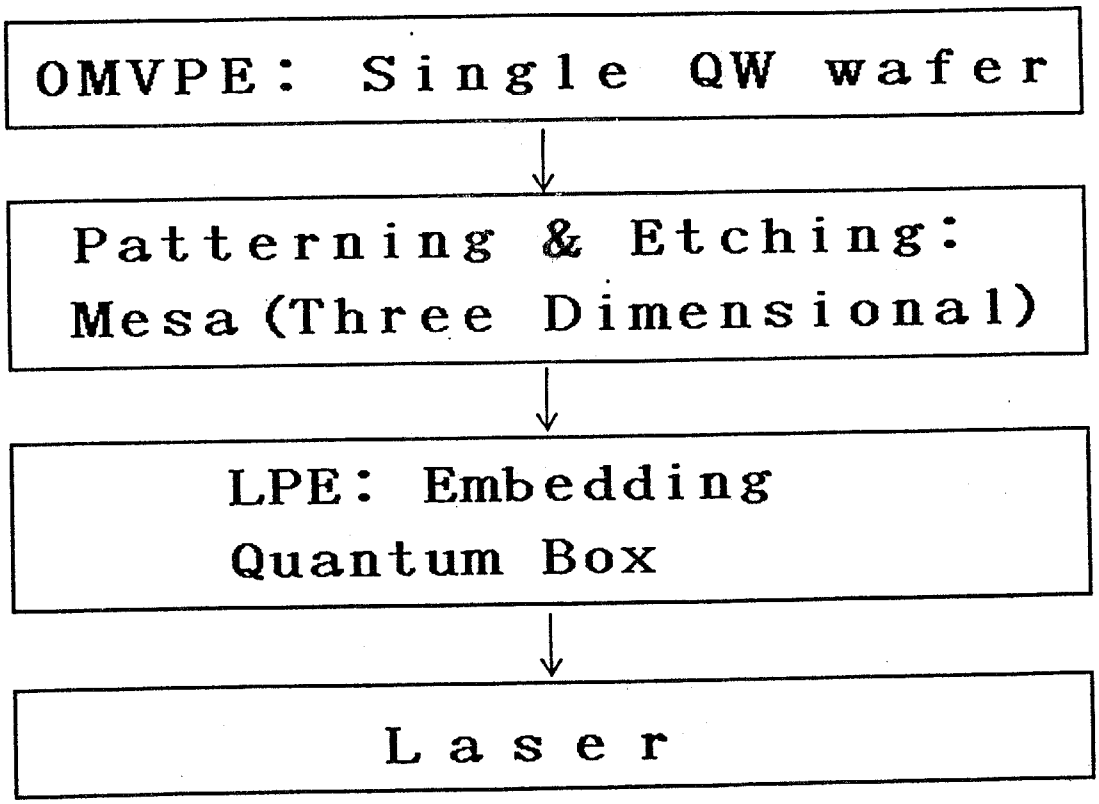

Fig. 6-8 Flow of fabrication process of quantum box.

1) n-InP buffer layer, 200nm thick,

2) n-GaInAsP optical confinement layer with band-gap wavelength λ_g of 1.26 μm and thickness of 150nm,

3) undoped InP barrier layer of 2nm,

4) undoped GaInAsP quantum-well layer with λ_g of 1.66 μm and thickness of 15nm,

5) undoped InP barrier layer 10nm thick,

6) p-InP barrier layer 10nm thick,

7) p-GaInAsP layer with λ_g of 1.66 μm and thickness of 15nm.

Thickness, composition and doping of each layer were determined from experiment of single quantum well laser. Final layer was used as etching mask as mentioned section 6-3.

Secondly, three dimensional structure was fabricated. The etching process is summarized in Fig. 6-9. Fabrication of groove along <011> direction is the first etching. Thin quaternary layer as an etching mask and selective etchant were used as described in section 6-3. Along <011> direction, mesa stripes of the quaternary layers were formed as mentioned above. Then, using the stripes of the quaternary layer as a mask, the InP overlayers above the quantum-well layer were etched by HCl selective etchant. The etching stopped at the surface of the quantum-well layer due to the material selectivity of the etchant as seen in Fig. 6-9 (a).

As the next etching, grooves along <01$\bar{1}$> direction was fabricated. The author used simply the bromic acid solution with

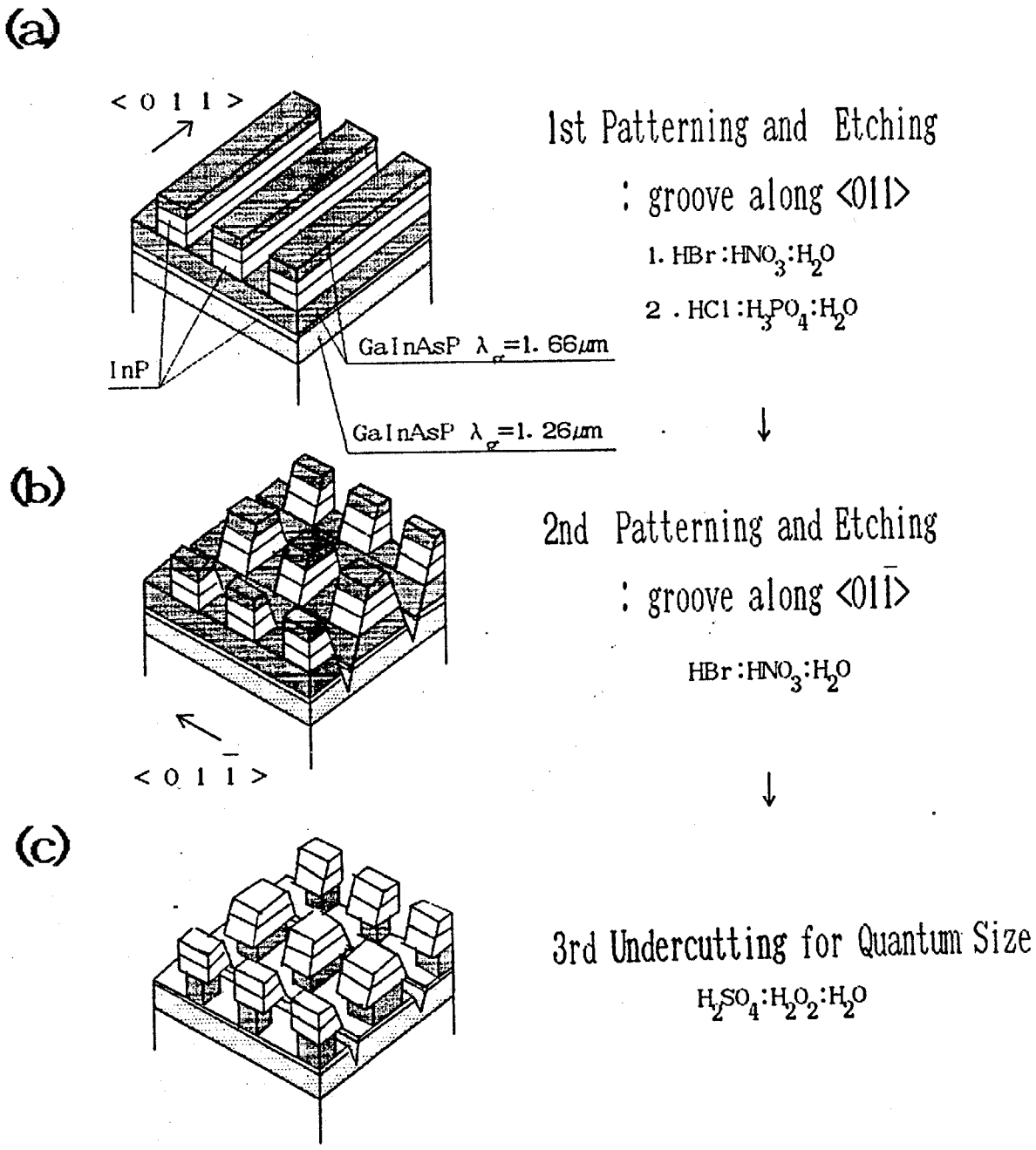

Fig. 6-9 Summary of etching process. (a) 1st patterning and etching for <011> groove. (b) 2nd patterning and etching <01$\bar{1}$> groove. (c) 3rd undercutting for quantum size.

photo resist mask to form the grooves (Fig. 6-9(b)). Figure 6-10 is a SEM picture of the top view of the sample after the fabrication of cross grating. Etching along the two directions was confirmed. Turn of etching from <011> to <01$\bar{1}$> was important for remaining of quantum box region. Signal of photoluminescence was lost by the etching with the reverse of turn from <01$\bar{1}$> to <011>.

As the final etching process, separation of each box and undercut etching were carried out. Using the array of the InP squares as a mask, the quaternary quantum-well layer was etched with a selective etchant. During the etching, undercutting took place, which reduced the width and depth of the box in comparison with those of the InP square mask (Fig. 6-9(c)) to obtain quantum boxes.

As the next step, quantum-box layer was buried by LPE regrowth[193] to form the optical waveguide. Prior to the regrowth, mass-transport process[137, 138, 193] was carried out in the LPE furnace and the surface of quantum box was covered by thin InP layer before the regrowth. Time and temperature for mass transport were 640℃ and 10 minute, respectively. In early stage, the author expected that soak of LPE growth was sufficient for mass transport of this very fine structure. However, peak of photoluminescence was not observed after regrowth without mass transport process. The other hand, sample after regrowth with mass-transport process had a photoluminescence

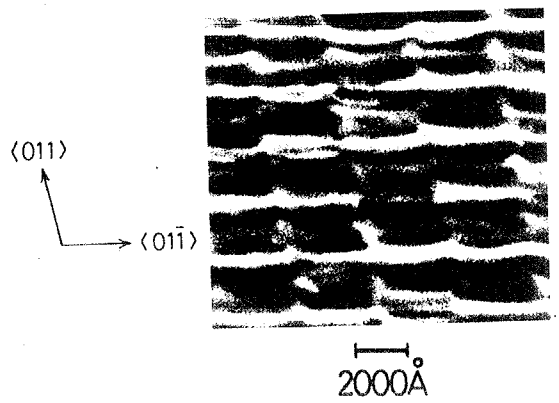

Fig. 6-10 The top view of the sample after fabrication of cross grating.

peak.

After mass transport process, the following layers were regrown by continuous LPE regrowth.

1) p-GaInAsP optical confinement layer with band-gap wavelength λ g of 1.24 μ m and thickness of 150nm,
2) p-InP cladding layer of 1 μ m.
3) p^+-GaInAsP cap layer(λ g = 1.24 μ m).

Finally, wafer was polished and electrodes were formed as the same manner as conventional laser diodes with silicon-dioxide defined stripe geometry. The stripe width was 15 μ m.

6-5, Measurement Results

The processed wafers were cleaved to make a cavity. The length and width of cavity were 380 μ m and 16 μ m, respectively. V-I characteristic has a information of p-n junction. Forward voltage was 0.3-0.5V and this value was too small for voltage of p-n junction in GaInAsP/InP diode characteristics. Reverse voltage was 1.4-4V and larger reverse voltage was observed the sample with larger forward voltage. These results indicated leak point in laser. It was difficult where was the p-n junction in structure from this result. However, possibility that p-n junction was located in quantum box structure was suggested from these low forward voltage.

The fabricated devices were operated by current injection at 77K under pulsed condition with a repetition of 3kHz and a

width on 100ns. Outlines of measurement systems is shown in Fig. 6-11. The sample was sink in the liquid nitrogen dewer. Light output by carrier injection was introduced to optical fiber (200 μ m diameter) faced to cavity facet in liquid nitrogen atmosphere. The spectrum with carrier injection was observed by optical spectrum analyzer, ANRITSU MS96A, as shown in Fig. 6-12. Three different peaks at 1.18, 1.37 and 1.42 μ m, were observed, as shown in Fig. 6-12 (a). The peak at 1.18 μ m corresponds to the luminescence from the optical confinement layer. The other two peaks at 1.37 and 1.42 μ m were to correspond to the quantum-box structure.

Fine structure around 1.37 μ m peak is shown in Fig. 6-12 (b). The spectrum had many peaks like resonant modes. The spacing of those peaks, about 1.1nm, coincided with the calculated mode spacing in the cavity structure when the author assumed effective refractive index is equal 3.5. This phenomenon suggested stimulated emission. Peaks at 1.37 and 1.42 μ m were observed only when cavity length was in the range of 200 μ m-500 μ m. The emission from quantum box may be decreased by gain saturation in short cavity(194) and fluctuations in size of quantum box in long cavity.

I-L characteristics at 1.18 and 1.37 μ m peaks are shown in Fig. 6-13. Light intensity from optical confinement layer was much stronger than that from quantum box by factor 10^3. Lasing of optical confinement layer was occurred at 3.1 kA/cm^2.

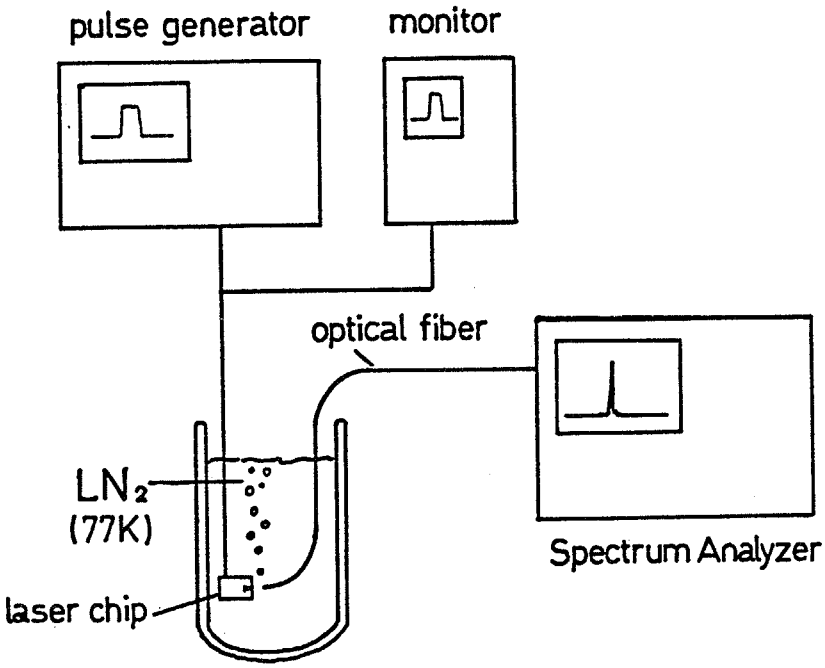

Fig. 6-11 Measurement system for pulsed operation under 77K.

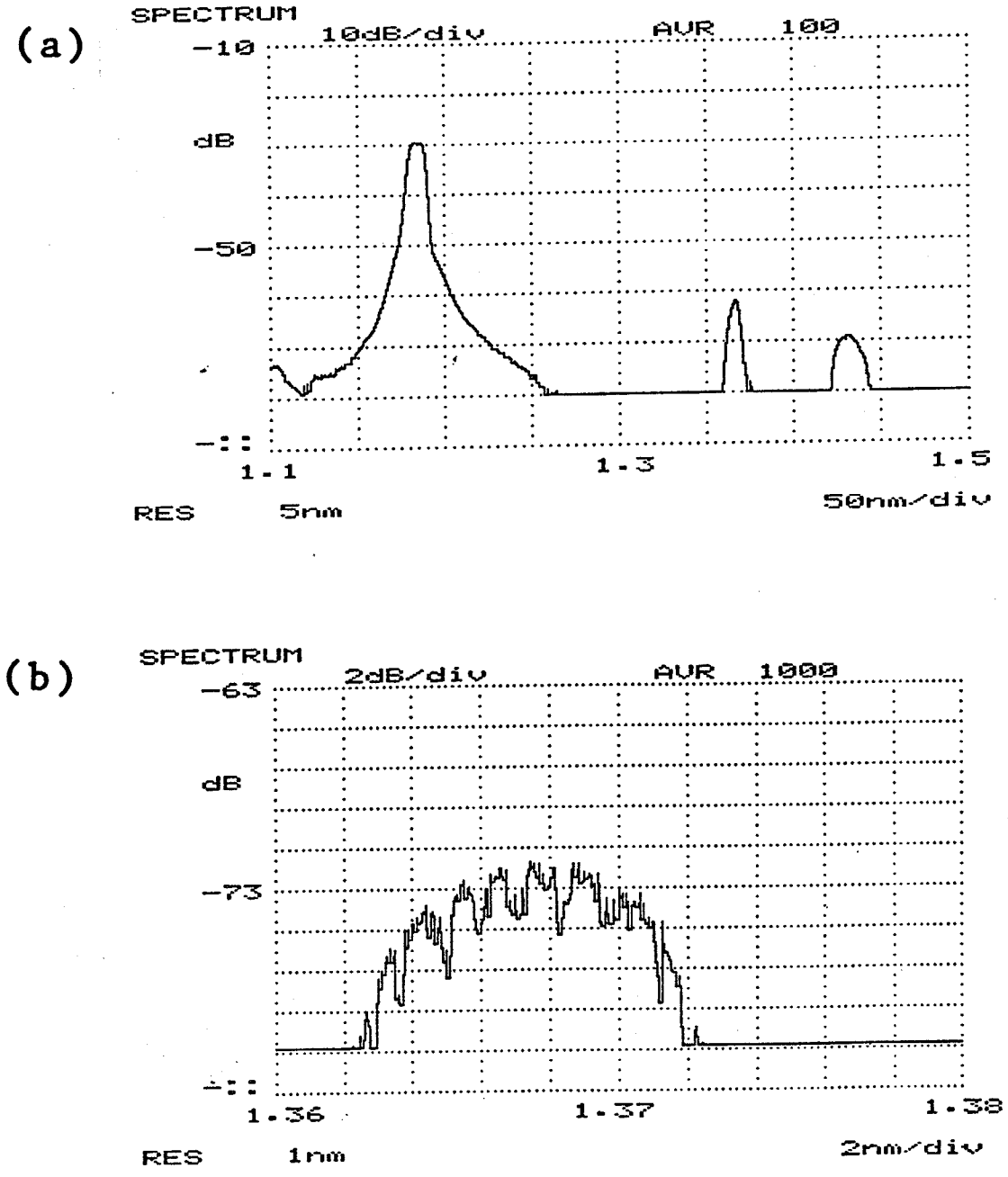

Fig. 6-12 Spectrum from quantum box structure with carrier injection. The measurement condition was pulsed operation at 77K. (a) Spectrum in the wide range. (b) Fine spectrum around 1.37 μ m peak.

Resonant modes around 1.37 μ m peak was observed when carrier injection level was at 22 kA/cm^2. Figure 6-13 suggested that the light emission from quantum box structure was assisted by light emission from the optical confinement layer as optical pumping and it was very difficult to estimate the threshold point of stimulated emission by pure carrier injection of quantum box structure from present results.

CW operation at 77K was tried by same sample. Figure 6-14 shows spectrum by CW operation. The range of injection current is from 100mA to 500mA. Emission from optical confinement layer was observed and emission from quantum box region was not confirmed. This phenomenon suggested the interruption of smooth carrier injection. Spectrum from optical confinement layer had wide half width. Peak of spectrum was shifted to longer wavelength by increasing of injection current. This results was suggested rising of temperature of laser by carrier injection.

For suppression of light emission of optical confinement layer, different structure was tried. Optical confinement layer grown by OMVPE was eliminated and bandgap wavelength of optical confinement layer was changed from 1.26 μ m to 1.1 μ m. Spectrum under pulsed operation at 77K by this sample is shown in Fig. 6-15. Three different peaks at 1.05, 1.23 and 1.31 μ m, were observed. The peak at 1.18 μ m corresponds to the luminescence from the optical confinement layer and intensity of this peak was still strongest. The other two peaks at 1.23 and 1.31 μ m were

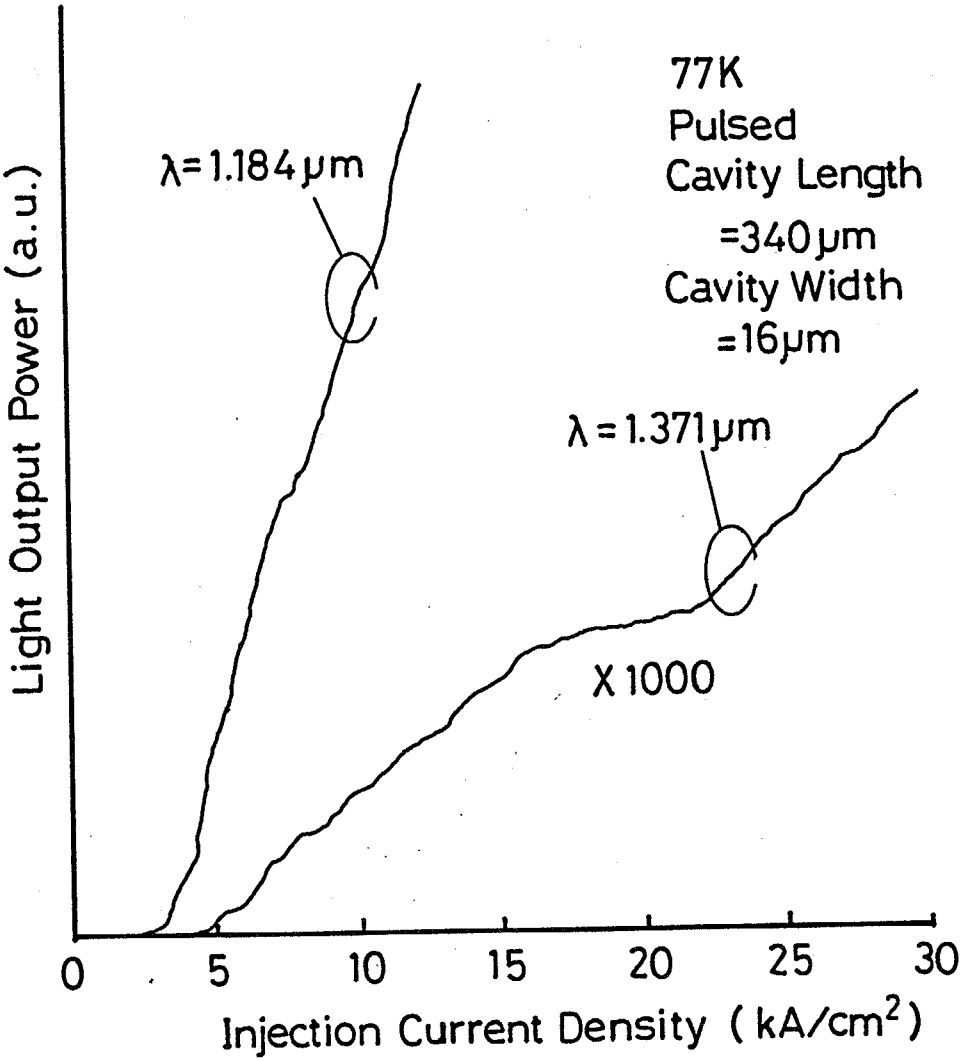

Fig. 6-13 I-L characteristics of 1.18 μ m and 1.37 μ m peaks.

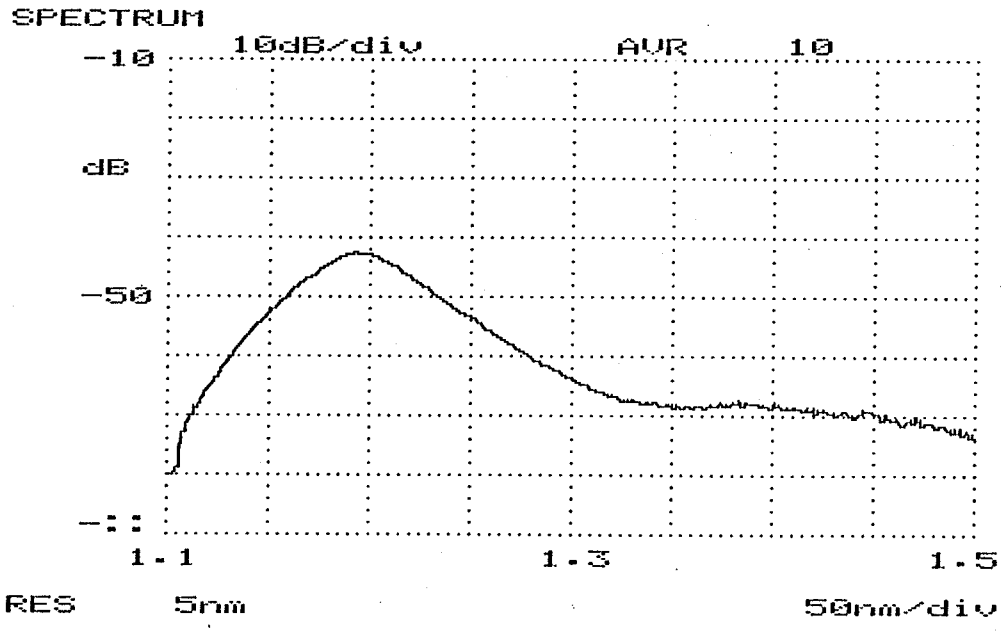

Fig. 6-14 Spectrum under CW operation at 77K. Injection current is 150mA.

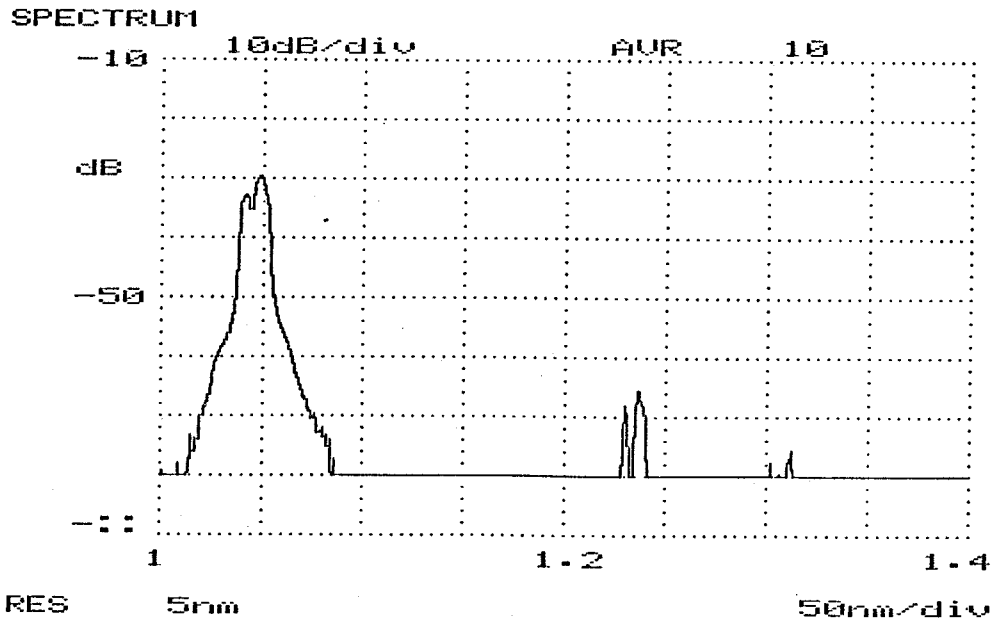

Fig. 6-15 Spectrum under pulsed operation at 77K from sample without lower optical confinement layer.

shifted to shorter wavelength. This shift would be occurred by reduction of size by change of etching condition.

6-6, Discussion of quantum box laser

To characterize each quantum box peak, the size of quantum box was estimated and optical gain by estimated size was calculated. The height of quantum box was 15nm estimated from the growth conditions of OMVPE, and the width along <011> direction was estimated to be about 30nm from the shift of photoluminescence. The width along $<01\bar{1}>$ direction would be almost same as that along <011>, because the lithography techniques were same and undercut etching was done simultaneously. It was also confirmed that widths of two directions were almost same by SEM observation as shown in Fig. 6-10. Assuming the size of quantum box to be 15nm x 30nm x 30nm, spectrum of theoretical optical gain at 77K was calculated, as shown in Fig. 6-16. It was explained that 1.42 μ m and 1.37 μ m peaks were corresponding to the transition between the basic levels and second levels, respectively, and optical gain of 1.37 μ m was higher than that of 1.42 μ m.

From this calculation, the optical gain in cavity can be estimated. The net optical gain of the quantum box is in the order of $10^3 cm^{-1}$. As the next, optical confinement factor in quantum box should be estimated. The occupation ratio of quantum box per plain was only 2% because 30nm x 30nm square was in 200nm x 200nm area. For the direction along perpendicular to plain,

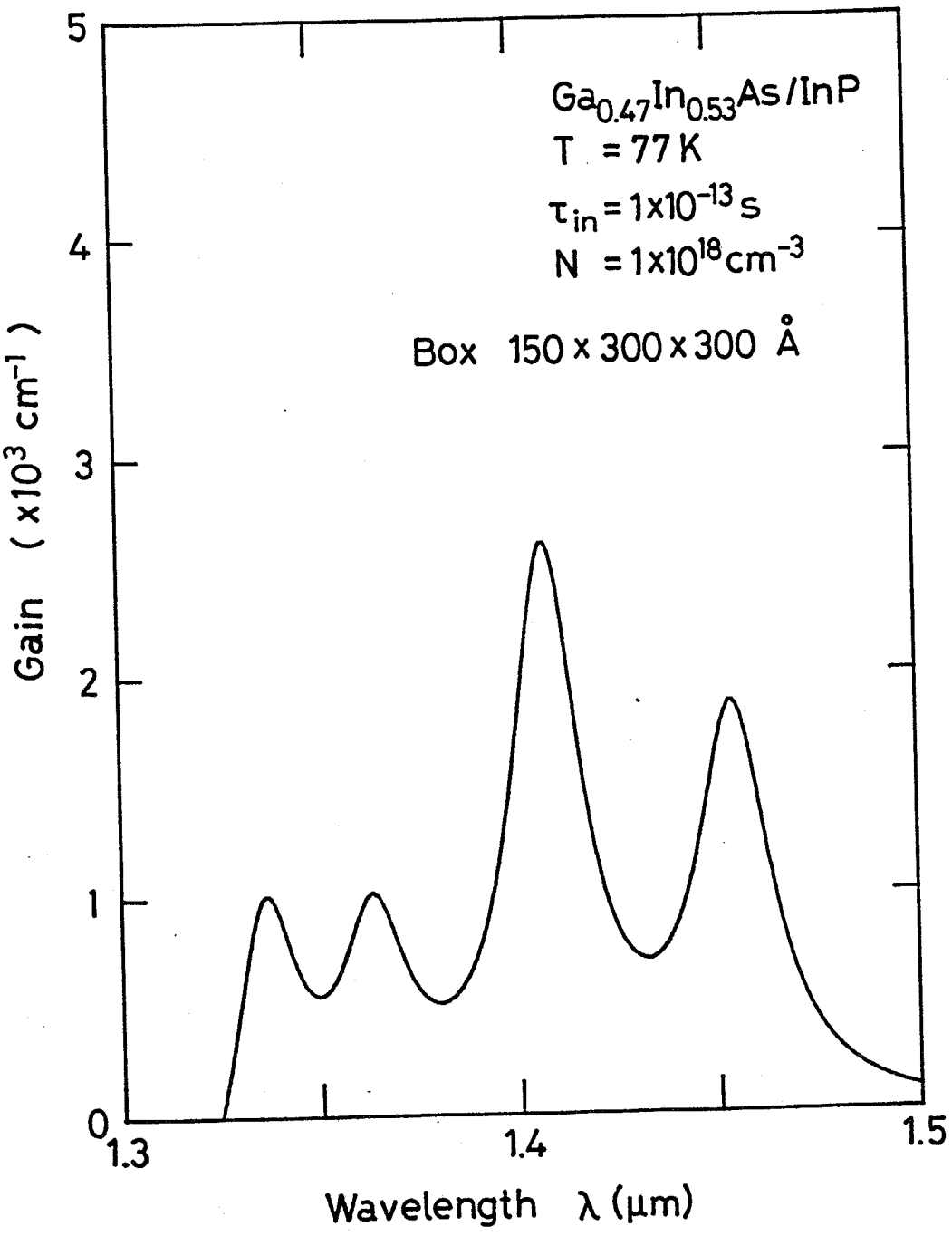

Fig. 6-16 Calculated optical gain from 15nm x 30nm x 30nm size quantum box. Temperature is assumed 77K.

thickness of 15nm was correspond to about 3% of optical confinement factor. As a result, total optical confinement factor of quantum box was small as order of 10^{-4}. Thus, optical gain in cavity was less than $1cm^{-1}$. On the other hand, mirror loss was about $40cm^{-1}$ from the cavity length. Hence, resonant mode should not be observed from this calculation. The possibility to explain stimulated emission was concerning of exiciton for optical gain that were neglected in the calculation described section 5-2.

Fluctuation of size could be estimated from spectrum of quantum box with some assumption. As the first, the author assumed the spectrum of 1.42 μ m peak in Fig. 6-12(a) was formed by spontaneous emission without gain and relaxation time could be neglected because of exiciton effect. If fluctuation was occurred in only patterning of plain and was not occurred in grown thickness, fluctuation of size was estimated from spectrum. Width of 3dB down points was about 16nm. This value was correspond to 9.8meV in energy. Relation between size of plane and energy is 1.2meV/nm when size of quantum box is around 15nm x 30nm x 30nm. Hence, this energy fluctuation corresponds to $\pm$ 4nm as size fluctuation. Of course, this calculation was broken if shape of spectrum changed by stimulated emission.

Expected merits of quantum box, i.e., low threshold current density, were not yet observed at present measurement. To realize the merits of quantum box laser, the following four

points is important. At first, the present size of quantum box was too large and separation between energies of each quantized level was not sufficient. Hence, electron was not confined into one state effectively as shown in Fig. 6-16. For sufficient separation of energies of each level, required volume of quantum box is around 10nm x 10nm x 10nm. Secondly, fluctuation of quantum box size disturbed the effective emission by distribution of energy levels and optical gain was decreased as shown in experiment of long cavity. To prevent the effect of size deviation, distribution of energy levels by size deviation must be less than distribution of emission energy by carrier relaxation time described in section 5-3. Thirdly, optical confinement factor of quantum box was too small in present structure as mentioned above. For increasing of the optical confinement factor, the separation length around 10nm between boxes or multi layer of quantum boxes would be required. As the fourth problem, the majority of injected carrier was consumed in the optical confinement layer in the present experiment and light emission from optical confinement layer was very strong. Moreover, the ratio of consumed carrier in optical confinement layer would increase by rising of temperature to room temperature. This carrier leakage to optical confinement layer must be prevented.

Hence, design of structure and process should be refined in consideration with these problems. To achieve small size and high density of quantum box without size deviation, development

of techniques for fine lithography and etching would be necessary. Multi layer structure of quantum boxes has possibility to get large optical confinement factor and to prevent emission of optical confinement layer, although requirement for etching would be more severe by multi layer. Increasing of carrier confinement in quantum box by the structure, such as MQB[156], has also possibility to improve the characteristics.

To achieve those structure, improvement of process technique is desired. For lithography, 10nm order pattern is required and that is difficult by conventional laser interference lithography. Hence, stable operation of X-ray laser or deep ultra-violet laser is required. EB lithography[187-189, 195] is also attractive from that sharp beam spot and copy with SOR[196, 197] of fabricated pattern with EB can be suppressed by fluctuation of beam spot. As etching, wet chemical etching is difficult for etching of multi-layer structure required for low threshold current density as described in section 5-3 due to the anisotropy. Hence, development of dry-etching without damage is required. For elimination of damage, it is one of the hopeful methods that hybrid methods that rough shape is fabricated by dry-etching and surface is etched by wet-chemical etching slightly for elimination of damage.

Anxiety for operation of quantum box is carrier relaxation mechanism. Although the carrier relaxation time was assumed the same value with bulk in previous calculation, the quantum box

structure has a possibility of increasing of carrier relaxation time introduced interruption of carrier injection. Usual energy relaxation from injected carrier to radiative level is occurred by collision between carrier and carrier. This collision process(172) is similar to Auger process and energy separation between each levels of quantum box introduces decreasing of relaxation probability. In this experiment, separation of energy is not so large (around 30meV) and scattering of polar optical phonon (32-42meV)(143) can be concerned as relaxation from injected carrier to radiative level. However, the possibility of interruption of smooth carrier injection was observed from spectrum. Moreover, energy separation between each level in ideal quantum box laser is larger than energy of phonon. Hence, transition probability will decrease drastically and limitation of carrier supply will be occurred in radiative levels. This situation is very similar to levels of solids state laser(157). Hence, other considerable relaxation mechanism, i.e., Auger effect(135) or recombination between each levels by ultra violet radiation is introduced. Carrier is injected in quantum box levels with competition between transition to quantum box levels and transition of others, as an example, band to band transition of barrier region or non-radiative recombination by defect. Of course, Auger effect introduces other electron jumping to high energy levels and carrier consumes by factor two. From those aspect, this phenomenon is very severe for lasing.

To prevent this low transition probability, hybrid of quantum box and quantum wire structure is desirable. Schematic view of this structure is indicated in Fig. 6-17. By adjustment of width of quantum wire, both basic level can be just fit. Ratio of each structure area would be decided by competition of other transition mechanism in barrier region. When probability of other transition is low, large area of quantum box is better from carrier confinement effect to desirable levels. When probability of other transition is high, large quantum wire area is required because main recombination must be desirable transition and carrier must be introduced to desired state by continuous state of quantum wire.

6-7 Conclusion remarks

In this chapter, the author reports the fabrication[7] of GaInAsP/InP quantum-box structure with p-n junction and optical guide structure. Designs of structure and process for less damage of quantum box surface are described. It is reported that interference exposure and wet chemical etching for precise processes for higher dimensional quantum size effect. The wet chemical etching process for quantum box in consideration with anisotropy was developed. Observation of light emission from the quantum-box structure by current injection are reported. Finally, discussion for design to reduce the threshold current density are also described from experimental result.

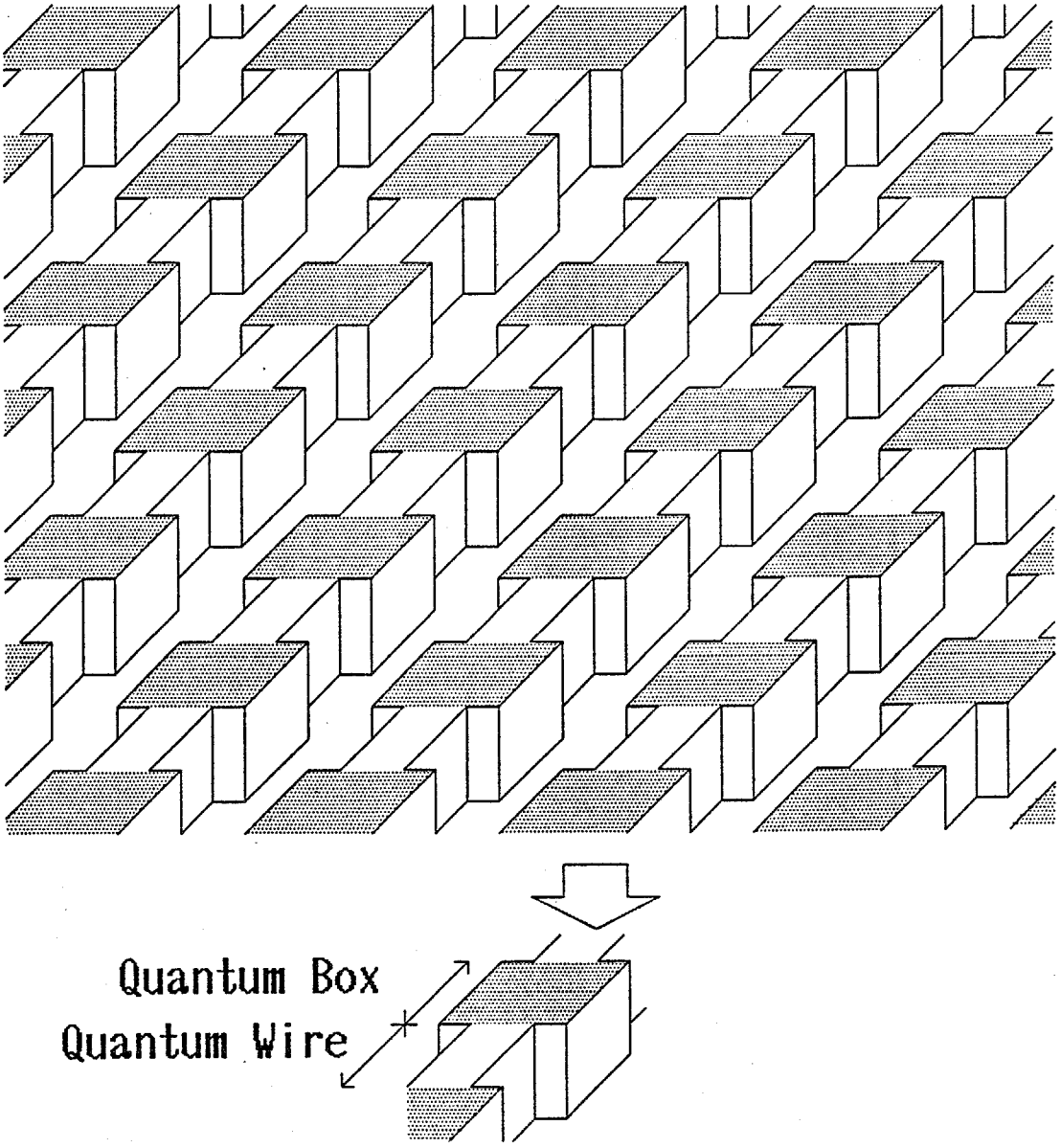

Fig. 6-17 Schematic view of the combination of quantum box and quantum wire for smooth carrier injection to quantum box levels. The state density is continued by adjustment of the each levels by change of width of quantum wire.

Chapter 7. Conclusion

The purpose of this thesis is to improve of GaInAsP/InP crystal quality grown by OMVPE so that those can be applied for the laser devices, especially of three dimensional quantum well (quantum box) structure.

Results obtained by this work are summarized as follows.

1. The author attained good enough crystal quality of GaInAsP/InP by OMVPE by improving apparatus and obtaining growth conditions, The quality was confirmed by laser fabrication as follows.

1-1. The crystal quality was improved by using of nitrogen mixing carrier gas instead pure hydrogen and increasing growth temperature to 640℃.

1-2. The procedure of source gas switching was developed to obtain hetero interface without degradation.

1-3. By using DMZn and H_2Se as p- and n-type doping sources, respectively, p-n junctions for laser devices were formed stable and good enough.

1-4. Lasing threshold current density of $1kA/cm^2$ was attained which was compared with that grown by LPE.

1-5. By fabricating BH laser by hybrid methods, CW operations were attained. Long life time more than 4000 hours

were confirmed for these lasers.

1-6 Buried heterostructure process by OMVPE was developed to also attain CW laser operation. Reliability of laser by this process was confirmed by a several thousands hour's aging test.

2. Good characteristics of multi quantum well structure and single quantum well lasers were obtained.

2-1. By improvement of the apparatus, abrupt interface and narrow linewidth of photoluminescence, step-like shape in absorption characteristics and X-ray satellite peak were observed.

2-2. Single quantum well laser was fabricated to obtain lasing operation of single quantum well laser in GaInAsP/InP crystal system for the first time.

3. The gain and the laser threshold of the three-dimensional quantum-box lasers were analyzed to make clear the following.

3-1. Lowest threshold current density at room temperature is 60 A/cm^2 with estimation of carrier leakage, while that is 190A/cm^2 with consideration of 10% fluctuation in quantum box size.

3-2. Ideal structure of quantum box laser is discussed. It is pointed out that suppression of carrier leakage is

very important for advantageous of quantum box laser. Modulation doped structure is most attractive methods to overcome the problem. It is also pointed out that the material change is necessary for adjusting of wavelength to lowest loss region of optical fiber.

4 GaInAsP/InP quantum-box structure with p-n junction and optical guide structure was fabricated for the first time.

4-1 Structure and process for less damaging of quantum box surface are developed.

4-2. By using interference exposure and wet chemical etching for precise processes for higher dimensional quantum size effect, the quantum box structure were fabricated.

4-3. The wet chemical etching process taking into account anisotropy is applicable for very small size structure.

4-4. Light emission from the quantum-box structure by current injection were observed for the first time. That emission have resonant peak and suggest a stimulated emission.

Acknowledgment

The author is indebted to Professor Yasuharu SUEMATSU for providing such as interesting and frontier theme, and his continuous guidance and encouragement not only academically but also as a person, during his undergraduate and post-graduate courses. The author gratefully acknowledge to Associate Professor Kazuhito FURUYA for that he has been guided the author day and night.

The author would like to express to Prof. K. IGA for his helpful advice and continuous encouragement. The author is grateful to Prof. M. KAWAMURA, M. MATSUMURA, K. TAKAHASHI, H. KUKIMOTO, M. YAMADA (Kanazawa Univ.), Assoc. Prof. M. KONAGAI, the members of the Microwave Research Group of T. I. T. and the members of the Summer Seminar of Optical Communications for their fruitful discussion and hospitality.

The author gratefully appreciate to Assoc. Prof. S. ARAI for his constructive advise and critical comments, Dr. S. SUGOU (NEC) for his encouragement and guidance for OMVPE and Dr. M. ASADA for his guidance and advise for theoretical analysis.

The author is also grateful to Messrs. I. KOMAZAKI (NEC), A. KAMEYAMA (Tohsiba), H. KATSUDA (Fujikura Wiring) for their useful discussion and instruction, Messrs. C. WATANABE (SONY), M. NAGASHIMA (Sumitomo-3M) for their fruitful discussion and experimental cooperation.

The author would like to thank the all members of SUEMATSU-FURUYA-ARAI Lab., especially, Messrs. S. YANG (Jilin. Univ.), M. CAO, K. ISHIHARA (Kawasaki Steel), A. NAKAJIMA, S. KINOSHITA, Y. SHINGAI, K. UESAKA, M. MIYAUCHI, M. TAKADOO (TEL Thermco), K. IBARAKI (TEL Thermco), Dr. P. DASTE, Messrs. K. KURISHIMA, Y. MIYAKE, T. YAMAMOTO, S. KISHITANI, and S. NOGIWA (OMTEC) for their technical assistance of OMVPE and Drs. F. Koyama, Y. Tohmori (NTT), K. G. RAVIKUMAR, Messrs. K. KOMORI, S. TAMURA, K. SHIMOMURA, and T. KIKUGAWA (ANRITSU) for their fruitful discussion and experimental support.

Thanks are extended to the members of TAKAHASHI-KONAGAI Lab., MATSUMURA Lab., NOMURA-ABE Lab., and YAGI-TAKAYANAGHI Lab. especially Drs. Y. UCHIDA (Takushoku Univ.), E. TOKUMITSU, Messrs. M. KOBAYASHI, A. YAMADA, N. MINO (Sumitomo Elec.) for their helpful discussion, encouragement and providing experimental equipment.

The author acknowledge the members of TEL-Thermco Co., especially Messrs. S. SAKAMOTO and H. KITAYAMA for their helpful discussion and financial support for new apparatus.

This work was supported by Scientific Grant-In-Aid from Ministry of Education, Science and Culture, Japan.

Finally, the author would like to express his gratitude to his parents.

Reference

(1) Y. Suematsu and K. Iga, "Introduction to Optical Fiber Communications", John Wiley & Sons, New York, 1982. (Japanese version, OHM-sha, Tokyo, 1976)

(2) S. M. Sze, "Physics of Semiconductor Devices", John WiLey & Sons, New York, 1981.

(3) H. C. Casey, Jr., and M. B. Panish, "Heterostructure lasers", Academic Press, New York, 1978.

(4) P. K. Tien, private communications or Fig. 1 of (T. H. Chiu, and W. T. Tsang, "Reflection high energy electron diffraction studies on the molecular-beam-epitaxial growh of AlSb, GaSb, InAs, InAsSb, and GaInAsSb on GaSb", J. Appl. Phys., vol. 57, No. 10, pp. 4572-4577. May. 1985.).

(5) H. Kroemer, "A proposed class of heterojunction injection lasers", Proc. IEEE, vol. 51, No. 12, pp. 1782-1783, Dec. 1963.

(6) I. Hayashi, M. B. Panish, P. W. Foy, and S. Sumski, "Junction lasers which operate conteniously at room temperature", Appl. Phys. Lett., vol. 17, No. 3, pp. 109-111, Aug. 1970.

(7) Zh. I. Alferov, V. M. Andreev, D. Z. Garbuzov, Yu. V. Zhilyaev, E. P. Morozov, E. L. Portnoi, and V. G. Trofim, "Investigation of the influence of theAlAs-GaAs heterostructure parameter on the laser threshold current and the realization of continuous emission at room temperature", Soviet Phys. Semiconductors, vol. 4, No. 9, pp. 1573-1575, Mar. 1971.

(8) R. Dingle, "Confined Carrier Quantum States in Ultrathin Semiconductor Heterostructure", Festkorperprobleme, XV, pp. 21-48, 1975.

(9) E. A. Rezek, N. Holonyak. Jr., B. A. Vojak, G. E. Stillman, J. A. Rossi, D. L. Keune, and J. D. Fairing, "LPE $In_{1-x}Ga_xP_{1-}$ As_z ($x\sim 0.12$, $z\sim 0.26$) DH laser with multiple thin-layer (<500) active region", Appl. Phys. Lett., vol. 31, No. 4, pp. 288-290, Aug. 1977.

(10) N. Holonyak. Jr., R. M. Kolobas, R. D. Dupuis and P. D. Dapkas, "Quantum-well heterostructure lasers", IEEE J. Quantum Electron., vol. QE16, No. 2, pp. 170-186, Feb. 1980

(11) W. T. Tsang, "A graded-index waveguide separate-confinement laser with very low threshold and a narrow Gaussian beam", Appl. Phys. Lett., vol. 39, No. 2, pp. 134-137, July 1981.

(12) W. T. Tsang, "Extremely low threshold (AlGa)As graded-index waveguide separate-confinemnet heterostructure lasers grown by molecular beam epitaxy", Appl. Phys. Lett., vol. 40, No. 3, pp. 217-219, Feb. 1982.

(13) S. D. Hersee, M. Baldy, P. Assenat, B. de Cremoux, and J. P. Duchemin, 'Very low threshold GRIN-SCH GaAs/GaAlAs laser structure grown by OM-VPE,' Electron. Lett., vol. 18, No. 20, pp. 870-871, Sept. 1982.

(14) R. D. Burnham, W. Streifer, D. R. Scifres, C. Lindstroem, T. L. Paoli, and N. Holonyak, Jr., 'Low-threshold single quantum well (60) GaAlAs lasers grown by MO-CVD with Mg as p-type dopant,' Electron. Lett., vol. 18, No. 25, pp. 1095-1097, Dec. 1982.

(15) P. L. Derry, A. Yariv, K. Y. Lau, N. Bar-Chaim, K. Lee, and J. Rosenberg, "Ultralow-threshold graded-index separate-confinemnet single quantum well buried heterostructure (Al, Ga)As lasers with high reflectivity coating", Appl. Phys. Lett., vol. 50, No. 25, pp. 1773-1775, June 1987.

(16) K. Y. Lau, N. Bar-Chaim, P. L. Derry and A. Yariv, "High-speed digital modulation of ultralow threshold (<1mA) GaAs single quantum well lasers without bias", Appl. Phys. Lett., vol. 51, No. 2, pp. 69-71, July 1987

(17) R. Chin, N. Holonyak. Jr., B. A. Vojak, K. Hess, R. D. Dupuis, and P. D. Dapkus, "Temperature dependence of threshold current for quantum well $Al_xGa_{1-x}As$ heterostructure laser diodes", Appl. Phys. Lett., vol. 36, No. 1, pp. 19-21, Jan. 1980.

(18) H. Iwamura, T. Saku, T. Ishibashi, K. Otsuka, and H. Horikoshi, "Dynamic behaviour of a GaAs-GaAlAs heterostructure lasers", Electron. Lett., vol. 19, No. 5, pp. 180-181, Mar. 1983.

(19) A. Larsson, M. Mittelstein, A. Arakawa, and A. Yariv, "High Efficiency Broad Area Sigle Quantum Well Lasers with Narrow Single-Lobed Far-Field Patterns Prepared by Molecular Beam Epitaxy", Electronics. Lett., vol. 22, No. 2, pp. 79-81, Jan. 1986.

(20) K. Uomi, N. Chinone, T. Ohtoshi, and T. Kajimura, "High relaxation oscillation frequency (beyond 10GHz) of GaAlAs multiquantum well lasers", Jpn. J. Appl. Phys., vol. 24, No. 7, pp. L539-L541, July 1985.

(21) T. H. Wood, C. A. Burrus, D. A. B. Miller, D. S. Chemla, T. C. Damen,

A. C. Gossard and W. Wiegmann, "High-speed optical modulation with GaAs/GaAlAs quantum wells in a p-i-n diode structure", Appl. Phys. Lett., vol. 44, No. 1, pp. 16-18, Jan. 1984.

(22) H. Yamamoto, M. Asada, and Y. Suematsu, "Electric-field-induced refractive index variation in quantum- well structure", Electron. Lett., vol. 21, No. 13, pp. 579-580, June 1985.

(23) H. Yamamoto, M. Asada, and Y. Suematsu, "Intersectional Waveguige Type Optical Switch with Quantum Well Structure", Trans. IECE of Jpn., vol. E68, No. 11, pp. 737-739, Nov. 1985.

(24) Y. Arakawa, and H. Sakaki, "Multidimensional quantum well laser and temperature dependence of its threshold current", Appl. Phys. Lett., vol. 40, No. 11, pp. 939-941, June 1982.

(25) M. Asada, Y. Miyamoto, and Y. Suematsu, "Gain and the threshold of three-dimensional quantum-box lasers", J. Quantum Electron., vol. QE22, No. 9, pp. 1915-1921, Sept. 1986.

(26) J. R. Night, D. Effer, and P. R. Evans, "The preparation of high purity gallium arsenide by vapour phase epitaxial growth", Solid-St. Electron., vol 8, No. 2, pp. 178-180, Feb. 1965.

(27) T. Nozaki, M. Ogawa, H. Terao, and H. Watanabe, "Mutli-layer epitaxial technology for the schottky barrier GaAs field-effect transistor", Inst. Phys. Conf. Ser., No. 24, pp. 46-54, 1974.

(28) J. J. Tietjen, and J. A. Amick, "The preparation and properties of vapor-deposited epitaxial $GaAs_{1-x}P_x$ using arsine and phosphine", J. Electrochem. Soc., vol. 113, No. 7, pp. 724-728, July 1966.

(29) G. H. Olseen, C. J. Nuese, and M. Ettenberg, "Low-threshold 1.25-μm vapor-grown InGaAsP cw lasers", Appl. Phys. Lett., vol. 34, No. 4, pp. 262-264, Feb. 1979.

(30) A. Usui, and H. Sunakawa, "GaAs Atomic Layer Epitaxy by Hydride VPE", Jpn. J. Appl. Phys., vol. 25, No. 3, pp. L212-214, Mar. 1986.

(31) H. M. Manasevit, "Single-crystal gallium arsenide on insulating substrate", Appl. Phys. Lett., vol. 12, No. 4,

pp. 156-159, Feb. 1968.
(32) R. D. Dupius, "AlGaAs-GaAs lasers grown by metalorganic chemical vapor deposition-Review", J. Cryst. Growth, vol. 55, No. 1, pp. 213-222, Oct. 1981.
(33) N. Kobayashi, T. Makimoto, and Y. Horikoshi, "Flow-Rate Modulation Epitaxy of GaAs", Jpn. J. Appl. Phys., vol. 24, No. 12, pp. L962-L964, Dec. 1985.
(34) S. Iwai, A. Doi, Y. Aoyagi, and S. Namba, "Monolayer growth of GaAs by switched laser metalorganic vapor epitaxy", 14th Int. Symp. GaAs and Related Comp., ME(1).7, Heraklion, Crete, Greece, Oct. 1987.
(35) S. Sakai, S. Yamamoto, and M. Umeno, "MOCVD Growth of InP Using Plasma Pre-Cracking", Jpn. J. Appl. Phys., vol. 25, No. 8, pp. 1156-1160, Aug. 1986.
(36) Edited by K. Takahashi, "Molecular Beam Epitaxy Techonology", Kogyo-Chosakai Publishing Co., Ltd., Tokyo, 1984. (in Japanese)
(37) T. Sakamoto, H. Funabashi, K. Ohta, T. Nakagawa, N. J. Kawai, and T. Kojima, "Phase-Locked Epitaxy Using Rheed Intensity Oscillation", Jpn. J. Appl. Phys., vol. 23, No. 9, pp. L657-L659, Sep. 1984.
(38) Y. Horikoshi, M. Kawashima, and H. Yamazaki, "Low-Temperature Growth of GaAs and AlAs-GaAs Quantum-Well layers by Modified Molecular Beam Epitaxy", Jpn. J. Appl. Phys., vol. 25, No. 10, pp. L868-870, Oct. 1986.
(39) G. B. Stringfellow, "OMVPE Growth of $Al_xGa_{1-x}As$", J. Cryst. Growth., vol. 55, No. 1, pp. 42-52, Oct. 1981.
(40) A. Sasaki, "The compounds semiconductor", edited by Kansai-branch of Jpn. Appl. Phys. Soc., p. 86, Nikkan-Kogyo-shinbunsha, Tokyo, 1986.
(41) R. A. Reuhrwein, Japanese-Patent, showa38-7709.
(42) H. M. Manasevit, and W. I. Simpson, "The use of metal-organics in the preparation of semiconductor materials (I. Epitaxial gallium-V compounds)", J. Electrochem. Soc., vol. 116, No. 12, pp. 1725-1732, Dec. 1969.
(43) H. M. Manasevit, and W. I. Simpson, "The use of metal-organics in the preparation of semiconductor materials: II. II-IV compounds" J. Electrochem. Soc., vol. 118, No. 4, pp. 644-647, Apr. 1971.
(44) H. M. Manasevit, and W. I. Simpson, "The use of metal-organics

in the preparation of semiconductor materials: III, Studies of epitaxial III-V alminum compound formation using trimethlalminum", J. Electrochem. Soc., vol. 118, No. 4, pp. 647-651, Apr. 1971.

(45) H. M. Manasevit, F. M. Erdman, and W. I. Simpson, "The use of metal-organics in the preparation of semiconductor materials: IV, the nitrides of aluminum and gallium", J. Electrochem. Soc., vol. 118, No. 11, pp. 1864-1868, Nov. 1971.

(46) H. M. Manasevit, and W. I. Simpson, "The use of metal-organics in the preparation of semiconductor materials: V. The formation of In-group V compounds and alloys", J. Electrochem. Soc., vol. 120, No1. pp. 135-137, Jan. 1973.

(47) R. D. Dupius, and P. D. Dapkus, "Room-temperature operation of $Ga_{(1-x)}As$/GaAs double-heterostructure lasers grown by metalorganic chemical vapor deposition", Appl. Phys. Lett., vol. 31, No. 7, pp. 466-468, Oct. 1977.

(48) R. D. Dupius, and P. D. Dapkus, "$Ga_{(1-x)}As$/$Ga_{(1-y)}As$ double-heterostructure room-temperature lasers grown by metalorganic chemical vapor deposition", Appl. Phys. Lett., vol. 31, No. 12, pp. 839-841, Dec. 1977.

(49) R. D. Dupuis, and P. D. Dapkus, "Continuous room-temperature operation of $Ga_{(1-x)}Al_xAs$-GaAs double-heterostructure lasers grown by metalorganic chemical vapor deposition", Appl. Phys. Lett., vol. 32, No. 7, pp. 406-407, Apr. 1978.

(50) R. D. Dupuis, P. D. Dapkus, N. Holonyak. Jr., E. A. Rezek, and R. Chin, "Room-temperature laser operation of quantum well $Ga_{(1-x)}Al_xAs$ laser diodes grown by metalorganic chemical vapor deposition", Appl. Phys. Lett., vol. 32, No. 5, pp. 295-297, Mar. 1978.

(51) N. Holonyak. Jr., R. M. Kolbas, W. D. Laidig, and B. A. Vojak, "Low-threshold continous laser operation (300-337K) of multilayer MOCVD $Al_xGa_{1-x}As$ quantum-well heterostructures", Appl. Phys. Lett., vol. 33, No. 8, pp. 737-739, Oct. 1978.

(52) T. Nakanishi, T. Udagawa, A. Tanaka, and K. Kamei, "Growth opf high-purity GaAs epilayers by MOCVD and their application to microwave MISFET's", J. Cryst. Growth, vol. 55, No. 1, pp. 255-262, Oct. 1981.

(53) S. D. Hersee, M. Baldy, P. Assenat, "The OMVPE growth of GaAs

and GaAlAs on a large scale", J. de Physique, Colloque-C5, Tome 43, pp. 119-126, Dec. 1982.

(54) J. M. Brown, N. Holonyak. Jr., M. J. Ludowise, W. T. Dietze, and C. R. Lewis, "Monolayer heterointerfaces and thin layers (~ 10) in $Al_xGa_{1-x}As$-GaAs superlattices grown by metalorganic chemical vapor deposition", Electron. Lett., vol. 20, No. 5, PP. 204-205, Mar. 1984.

(55) R. D. Dupius, and P. D. Dapkus, "Very low threshold Ga(1-As/GaAs double-heterostructure lasers grown by metalorganic chemical vapor deposition", Appl. Phys. Lett., vol. 32, No. 8, pp. 473-475, Apr. 1978.

(56) R. D. Burnham, D. R. Scifres, and W. Streifer, "Current threshold uniformity of shallow proton stripe GaAlAs double heterostructure lasers grown by metalorganic-chemical vapor deposition", Appl. Phys. Lett., vol. 40, No. 2, pp. 118-119, Aug. 1982.

(57) J. Vilms and R. W. H. Engelman, "Life test of 30mW GaAlAs TAL laser grown by OMVPE", Jpn. J. Appl. Phys., vol. 22, No. 7, pp. L455-L457, July 1983.

(58) R. D. Buhnham, W. Streifer, T. L. Paoli, and N. Holonyak, Jr., "Growth and characterization of AlGaAs/GaAs quantum well lasers", J. Cryst. Growth., vol. 68, No. 3, pp. 370-382, Sept. 1984.

(59) J. Komeno, "Application to HEMT IC's", Nat. Conv. Rec. of Jpn. Appl. Phys., 19p-B-3, Nagoya, Oct. 1987 (in Japanese).

(60) K. G. Gunter, "Aufdampfschichten aus halbleitenden III-V-Verbindungen", Z. Naturforsch, vol. 13a, pp. 1081-1089, 1958.

(61) J. E. Davey, and T. Pankey, "Epitaxial GaAs filmes deposited by vacuum evaporation", J. Appl. Phys., vol. 39, No. 4, pp. 1941-1948, Mar. 1968.

(62) T. P. Lee, and A. Y. Cho, "Single-transverse-mode injection lasers with embedded stripe layer grown by molecular beam epitaxy", Appl. Phys. Lett., vol. 29, No. 3, pp. 164-166, Aug. 1976.

(63) W. T. Tsang, "Low-current-threshold and high-lasing uniformity GaAs-$Al_xGa_{1-x}As$ double-heterostructure lasers grown by molecular beam epitaxy", Appl. Phys. Lett., vol. 34, No. 7, pp. 473-475, Apr. 1979.

(64) W. T. Tsang, "Extremely low threshold (AlGa)As modified multiquantum well heterostructure lasers grown by molecular

beam epitaxy", Appl. Phys. Lett., vol. 39, No. 10, pp. 786-788, Nov. 1981.

(65) E. Veuhoff, W. Pletschen, P. Balk, and H. Luth, "Metalorganic CVD of GaAs in a molecular beam system", J. Cryst. Growth., vol. 55, No. 1, pp. 30-34, Oct. 1981.

(66) E. Tokumitsu, Y. Kudoh, M. Konagai, and K. Takahashi, "Molecular beam epitaxial growth of GaAs using trimethyl-gallium as a Ga source", J. Appl. Phys., vol. 55, No. 8, pp. 3163-3165, Apr. 1984.

(67) W. T. Tsang, "GaInAsP/InP double heterostructure lasers emitting at 1.5 μ m grown by chemical beam epitaxy", Appl. Phys. Lett., vol. 50, No. 2, pp. 63-65, Jan. 1987.

(68) W. T. Tsang, "Chemical beam epitaxy of $Ga_{0.47}In_{0.53}As$/InP quantum wells and heterostructure devices", J. Cryst. Growth, vol. 81, Nos. 1-4, pp. 261-269, Feb. 1987.

(69) Y. Suematsu, "Long-wavelength optical fiber communication", Proc. IEEE, vol. 71, No. 6, pp. 692-721, June 1983.

(70) T. Moriyama, O. Fukuda, H. Sanada, K. Inada, T. Edahiro and K. Chida, "Ultimately low OH content V. A. D. optical mode fibres", Electron. Lett., vol. 16, No. 18, pp. 698-699, Aug. 1980.

(71) Y. Suematsu, S. Arai, and K. Kishino, "Dynamic single-mode lasers with a distributed reflector", IEEE J. Lightwave Tech., vol. LT1, No. 1, p. 161-176, Mar. 1986.

(72) W. T. Tsang, "1.3 μ m wavelength GaInAsP/InP double heterostructure lasers grown by molecular beam epitaxy", Appl. Phys. Lett., vol. 41, No. 11, pp. 1094-1096, Dec. 1982.

(73) J. P. Duchemin, J. P. Hirtz, M. Razeghi, M. Bonnet, and S. D. Hersee, "GaInAs and GaInAsP materials grown by low pressure MOCVD for microwave and optoelectronic applications", J. Cryst. Growth., vol. 55, No. 1, pp. 64-73, Oct. 1981.

(74) R. Didchenko, J. E. Alix, and R. H. Toenickoetter, "Reactions of phosphine with trimethyindium", J. Inorg. Nucl. Chem., vol. 14, Nos. 1/2, pp. 35-37, 1960.

(75) T. Fukui, and Y. Horikoshi, "Properties of InP films grown by organometallic VPE mrthod", Jpn. J. Appl. Phys., vol. 19, No. 7, pp. L395-L397, July 1980.

(76) J. P. Duchemin, M. Bonnet, G. Beuchet, and F. Koelsch, "Organometallic growth of device-quality InP by cracking

of $In(C_2H_5)_3$ and PH_3 at low pressure", Inst. Phys. Conf. Ser., No. 45, pp. 10-18, 1978.

(77) J. P. Hirtz, M. Razeghi, M. Bonnet, and J. P. Duchemin;'GaInAsP alloy Semiconductor' edited by T. P. Pearsall, Chap. 3, pp. 61-86, John Wiley and Sons Ltd. 1982.

(78) J. P. Hirtz, J. P. Duchemin, P. Hirtz, B. De. Cremoux, T. P. Pearsall, and M. Bonnet, "$Ga_xIn_{1-x}As_yP_{1-y}$/InP D. H. laser emitting at 1.15 μ m grown by low pressure metalorganic C. V. D.", Electron. Lett., vol. 16, No. 8, pp. 275-277, Apr. 1980.

(79) S. Sugou, A. Kameyama, H. Katsuda, Y. Miyamoto, K. Furuya, and Y. Suematsu, "Alloy composition and flow rates in Ga_xIn_{1-} As_yP_{1-y} lattice matched to InP grown by MOCVD", Electron, Lett., vol. 19, No. 24, pp. 1036-1037, Nov. 1983.

(80) M. Razeghi, and J. P. Duchemin, "Growth and characterization of InP using metalorganic chemical vapor deposition at reduced pressure", J. Cryst. Growth, vol. 64, No. 1, pp. 76-82, Nov. 1983.

(81) Y. Guldner, J. P. Vieren, P. Voisin, M. Voos, M. Razeghi, and M. A. Poisson, "Two-dimnesional electron gas in a $In_{0.53}Ga_{0.47}As$-InP heterojunction grown by metalorganic chemical vapor deposition", Appl. Phys. Lett., vol. 40, No. 10, pp. 877-879, May 1982.

(82) M. Razeghi, J. P. Hirtz, U. O. Ziemelis, C. Delalande, B. Etienne, and M. Voos, "Growth of $Ga_{0.47}In_{0.53}As$-InP quantum wells by low pressure metalorganic chemical vapor deposition", Appl. Phys. Lett., vol. 43, No. 6, pp. 585-587, Sept. 1983.

(83) M. Razeghi, J. Nagle, P. Maurel, F. Omnes, and J. P. Pocholle, "Room-temperature excitons in $Ga_{0.47}In_{0.53}As$-InP superlattices grown by low-pressure metalorganic chemical vapor deposition ", Appl. Phys. Lett., vol. 49, No. 17, pp. 1110-1111, Oct. 1986.

(84) M. Razeghi, A. Tardella, R. A. Davies, A. P. Long, M. J. Kelly, E. Britton, C. Boothroyd, and W. M. Stobbs, "Negative difference resistance at room temperature from resonant tunnelling in GaInAs/InP double-barrier heterostructure", Electron. Lett., vol. 23, No. 3, pp. 116-117, Jan. 1987.

(85) H. Renz, J. Weidlein, K. W. Benz, and M. H. Pikuhn, "InP epitaxy with a new metalorganic compounds", Electron. Lett.,

vol. 16, No. 6, p. 228, Mar. 1980.

(86) R. H. Moss, and J. S. Evans, "A new approach to MOCVD of indium phophide and gallium-indium arsenide", J. Cryst. Growth, vol. 55, No. 1, pp. 129-134, Oct. 1981.

(87) S. J. Bass, C. Pickering, and M. L. Young, "Metal organic vapor phase epitaxy of indium phosphide", J. Cryst. Growth, vol. 64, No. 1, pp. 68-75, Nov. 1983.

(88) C. C. Hsu, R. M. Cohen , and G. B. Stringfellow, "OMVPE growth of InP using TMI", J. Cryst. Growth, vol. 63, No. 1, pp. 8-12, Sept. 1983.

(89) A. Mircea, R. Azoulay, L. Dugrand, R. Mellet, K. Rao, and M. Sacilotti ;'Metalorganic InP and $In_{1-x}Ga_xAs_yP_{1-y}$ on InP epitaxy at atmospheric pressure' J. Electron. Mater., vol. 13, No. 3, pp. 603-620, May 1984.

(90) A. Mircea, R. Mellet, B. Rose, D. Robein, H. Thibierge, G. Leroux, P. Daste, S. Godefroy, P. Ossart, and A. M. Pougnet, "The growth and characterization of devices quality InP $Ga_{1-x}In_xAs_yP_{1-y}$ double heterostructures by atmospheric-pressure MOVPE using trimethylindium", J. Electron. Matter., vol. 15, No. 4, pp. 205-213, July 1986.

(91) R. D. Dupuis, H. Temkin, and C. Hopkins: "InGaAsP/InP double heterostructure lasers grown by atmospheric-pressure MOCVD", Electron. Lett., vol. 21, No. 2, pp. 60-62, Jan. 1985.

(92) A. W. Nelson, R. H. Moss, J. C. Regnault, P. C. Spurdens, and S. Wong:' Double heterostructure and multi-quantumwell lasers at 1.5-1.7 μ m grown by atmospheric pressure MOVPE', Electron. Lett., vol. 21, No. 12, pp. 329-331, Apr. 1985.

(93) B. I. Miller, U. Koren, and R. J. Capik, "Planer buried heterostructure InP/GaInAs lasers grown entirely by OMVPE", Electron. Lett., vol. 22, No. 18, pp. 947-949, Aug. 1986.

(94) M. Ohishi, M. Nakao, Y. Itaya, K. Sato, and Y. Imamura, "MOVPE-grown 1.5 μ m distributed feedback lasers on corrugated InP substrates", IEEE J. Quantum Electron., vol. QE-23, No. 6, pp. 822-827, June 1987.

(95) T. Sasaki, Y. Kuwamura, M. Kitamura, and I. Mito, "Doping condition of MOVPE grown 1.5-1.6 μ m InGaAsP DH lasers", Nat. Conv. Rec. of Jpn. Appl. Phys. Soc., 30p-ZH-7, Tokyo, Mar. 1987 (in Japanese).

(96) H. Ishiguro, K. Kawabata, and S. Koike, "Very low threshold

planer buried heterostructure InGaAsP/InP laser diodes prepared by three-stage metalorganic chemical vapor deposition", Appl. Phys. Lett., vol. 51, No. 12, pp. 874-876, Sept. 1987.

(97) T. Sanada, K. Nakai, K. Wakao, M. Kuno, and S. Yamakoshi, "Planer-embedded InGaAsP/InP heterostructure laser with semi-insulating InP current-blocking layer grown by metalorganic chemical vapor deposition", Appl. Phys. Lett., vol. 51, No. 14, pp. 1054-1056, Oct. 1987.

(98) K. Kobayashi, S. Kawata, A. Gomyo, I. Hino, and T. Suzuki, "Room-temperature cw operation of an AlGaInP double-heterostructure visible laser", Electron. Lett., vol. 21, No. 20, pp. 931-932, Sept. 1985.

(99) M. Ikeda, K. Nakano, Y. Mori, K. Kaneko, and N. Watanabe, "Room-temperature continuous-wave operation of an AlGaInP mesa stripe laser", Appl. Phys. Lett., vol. 48, No. 2, pp. 89-91, Jan. 1986.

(100) M. Ishikawa, Y. Ohba, H. Sugawara, M. Yamamoto, and T. Nakanishi, "Room temperature cw operation of InGaP/InGaAlP visible laser diodes on GaAs substrates grown by metalorganic chemical vapor deposition", Appl. Phys. Lett., vol. 48, No. 3, pp. 207-208, Jan. 1986.

(101) M. Razeghi, J. P. Duchemin, J. C. Portal, L. Dmowski, G. Remeni, R. J. Nicholas, and A. Briggs, Appl. Phys. Lett., vol. 48, No. 11, pp. 712-714, Mar. 1986.

(102) G. C. Osbourn, "$In_xGa_{1-x}As$-$In_yGa_{1-y}As$ strained-layer superlattices: A proposal for useful, new electronic mateials", Physical Review B, vol. 27, No. 8, pp. 5126-5128, Apr. 1983.

(103) M. Kobayashi, and K. Takahashi, "Review of strained-layer superlattices", Oyo-Buturi, vol. 55, No. 6, pp. 595-600, June 1986 (in Japanese).

(104) F. C. Eversteyn, P. J. W. Severin, C. H. J. v. d. Brekel, and H. L. Peek, "A Stagnant layer model for the epitaxial growth of silicon from silane in a horizontal reactor", J. Electrochem. Soc., vol. 117, No. 7, pp. 925-931, July 1970.

(105) S. Ito, T. Shinohara, and Y. Seki, "Properties of epitaxial gallium arsenide from trimethylgallium and arsine", J. Electrochem., Soc., vol. 120, No. 10, pp. 1419-1428, Oct. 1973.

(106) M. R. Leys, and H. Veenvliet, "A study of the growth mechanism of epitaxial GaAs as grown by the technique of metal organic vapour phase epitaxy", J. Cryst. Growth, vol. 55, No. 1, pp. 145-153, Oct. 1981.
(107) J. Nishizawa, and T. Kurabayashi, "On the reaction mechanism of GaAs MOCVD", J. Electrochem. Soc., vol. 130, No. 2, pp. 413-417, Feb. 1983.
(108) D. H. Reep, and S. K. Ghandhi, "Deposition of GaAs epitaxial layers bt organometallic CVD -temperature and orientation dependence- ", J. Electrochem. Soc., vol. 130, No. 3, pp. 675-680, Mar. 1983.
(109) D. J. Schlyer, and M. A. Ring, "An examination of the product-catalyzed reaction of trimethygallium", J. Organometallic chem., vol. 114, No. 1, pp. 9-14, July 1976.
(110) Y. Mori, "MOCVD: Hetero growth and ultra thin film growth", The second crystal engeneering symposium of Jpn. Appl. Phys. Soc., No. 6, July 1985 (in Japanese).
(111) A. Mircea, B. Couchaux, Y. Gao, B. Rose, and C. Carrier, "OMCVD growth of high quality InP/GaInAsP heterostructures without hydrogen", 14th Int. Symp. GaAs and Related Comp., ME(2).3, Heraklion, Crete, Greece, Oct. 1987.
(112) J. P. Duchemin, M. Bonnet, F. Koelsch, and D. Huyghe, "A new methods for growing GaAs epilayers by low pressure organometallic", J. Electrochem. Soc., vol. 126, No. 7, pp. 1134-1142, July 1979.
(113) Y. Mori, "Collection of practical data of epitaxial growth technique -1-1, MOCVD - ", edited by Y. Mori, pp. 40-45, Science Forum, Tokyo, 1986 (in Japanese).
(114) S. Sugou, A. Kameyama, Y. Miyamoto, K. Furuya and Y. Suematsu, "Conditions for OMVPE growth of GaInAsP/InP crystal", Jpn. J. Appl. Phys., vol. 23, No. 9, pp. 1182-1189, Sept. 1984.
(115) L. J. Giling, "Gas flow patterns in horizontal epitaxial reactor cells observed by interference holography", J. Electrochem. Soc., vol. 129, No. 3, pp. 634-644, Mar. 1982.
(116) C. P. Kuo, J. S. Yuan, R. M. Cohen, J. Dunn, and G. B. Stringfellow, "Organometallic vapor phase epitaxial growth of high purity GaInAs using trimethylindium", Appl. Phys. Lett., vol. 44, No. 5, pp. 550-552, Mar. 1984.
(117) M. A. DiForte-Poisson, C. Brylinski, and J. P. Duchemin, "Growth of ultrapure and Si-doped InP by low pressure

metalorganic chemical vapor deposition", Appl. Phys. Lett., Vol. 46, No. 5,, pp. 476-478, Mar. 1985.

(118) S. J. Bass, S. J. Barnett, G. T. Brown, N. G. Chew, A. G. Cullis A. D. Pitt and M. S. Skolnick, "Effect of groth temperature in the optical, electrical and crystallographic properties of epitaxial indium gallium arsenide grown by MOCVD in an atmospheric pressure reactor", J. Cryst. Growth, vol. 76, Nos. 1-3, pp. 678-685, Dec. 1986.

(119) W. Walukiewicz, J. Lagowski, L. Jastrzebski, P. Rava, M. Lichtensteiger, C. H. Gatos, and H. C. Gatos, "Electron mobility and free-carrier absorption in InP; determination of the compensation ratio", J. Appl. Phys., vol. 51, pp. 2659-2668, May 1980.

(120) A. Rosental, Y. Itaya, and Y. Suematsu, "Measurement of Zn doping level in InGaAsP/InP DH lasers", Jpn. J. Appl. Phys. vol. 18, No. 8, pp. 1655-1656, Aug. 1979.

(121) H. A. Skinner "Advances in organometallic chemistry", edited by F. G. A. Stone, and R. West, vol. 2, p. 98, Academic Press, New York, 1964.

(122) H. Asai and H. Sugiura, "Se doping mechanisms in MOCVD GaAs layers", Jpn. J. Appl. Phys., vol. 24, No. 10, pp. L815-817, Oct. 1985.

(123) M. Razeghi, B. De Cremoux, and J. P. Duchemin, "1.2-1.6 μ m $Ga_xIn_{1-x}As_yP_{1-y}$-InP DH lasers grown by LPMOCVD", J. Cryst. Growth, vol. 68, No. 1, pp. 389-397, Sept. 1984.

(124) W. J. Devlin, J. Sidhu, S. Cole, M. Harlow, L. D. Westbrook, A. W. Nelson and J. C. Regnault, "Very low threshold current (0.8kA/cm^2) InGaAsP/InP DH 1.5 μ m lasers grown by atmospheric MOVPE", Electron. lett., vol. 22, No. 11, pp. 584-585, May 1986.

(125) Y. Itaya, S. Arai, K. Kishino, M. Asada and Y. Suematsu, "1.6 μ m wavelength GaInAsP/InP lasers prepared by two phase solution technique", IEEE. J. Quantum. Electron., vol. QE17, pp No. 5, pp. 635-640, May 1981.

(126) M. Asada, K. Itoh, Y. Suematsu and S. Arai, "Cavity length dependence of differential quantum efficiency of GaInAsP/InP lasers", Electron. Lett., vol. 17, No. 14, pp. 486-487, July 1981.

(127) Y. Nakano, K. Takahei, Y. Noguchi, Y. Suzuki, H. Nagai, and K. Nawata, "High power output InGaAsP/InP

buried heterostructure lasers", Electron. Lett., vol. 17, No. 21, pp. 782-783, Oct. 1981.

(128) A. W. Nelson, W. J. Devlin, R. E. Hobbs, C. G. D. Lenton, and S. Wong, "High-power, low-threshold BH lasers operating at 1.52 μ m grown entirely by OMVPE", Electron. Lett., vol. 21, No. 20, pp. 888-889, Sep. 1985.

(129) Y. Itaya, M. Ohoishi, M. Nakao, K. Sato, Y. Kondo, and Y. Imamura, "Lasing characteristics of 1.5 μ m BH-DFB lasers grown entirely by MOVPE", Nat. Conv. Rec. of IEICE of Jpn., No. 865, Yokohama, Mar. 1987 (in Japanese).

(130) Y. Hirayama, H. Furuyama, M. Morinaga, M. Nakamura, M. Kushibe, M. Funamizu, K. Eguchi, and T. Nakanishi, "Long wavelength BH lasers grown by MOCVD", Nat. Conv. Rec. of Jpn. Appl. Phys. Soc., 20p-ZR-4, Nagoya, Oct. 1987 (in Japanese).

(131) M. Asada, A. R. Adams, K. E. Stubkjear, Y. Suematsu, Y. Itaya and S. Arai, "The temperature dependence of the threshold current of GaInAsP/InP DH lasers", IEEE J. Quantum Electron., vol. QE17, No. 5, pp. 611-619, May 1981.

(132) M. Yamada and Y. Suematsu, "Analysis of gain suppression in undoped injection lasers", J. Appl. Phys., vol. 52, No. 4, pp. 2653-2664, Apr. 1981.

(133) Y. Itaya, Y. Suematsu, S. Katayama, K. Kishino and S. Arai, "Low threshold current density (100) GaInAsP/InP double-heterostructure lasers for wavelength 1.3 μ m", Jpn. J. Appl. Phys., vol. 18, No. 9. pp. 1795-1805, Sept. 1979.

(134) T. Ikegami, "Reflectivity of mode at facet and oscillation mode in double-heterostructure injection lasers", IEEE J. Quantum Electron., QE-8, No. 6, pp. 470-476, June 1972.

(135) A. Sugimura, "Band-to-band Auger effect in longwavelength multinary III-V alloy semiconductor lasers", IEEE J. Quantum Electron., vol. QE18, No. 3, pp. 352-363, Mar. 1982.

(136) A. Yamaguchi, S. Komiya, I. Umebu, O. Wada, and K. Akita, "Photoluminescence Intensity in InGaAsP/InP double-heterostructure", Jpn. J. Appl. Phys., vol. 21, No. 5, pp. L297-L299, May 1982.

(137) Z. L. Liau, and J. N. Walpole, "A novel technique for GaInAsP/InP buried heterostructure laser fabrication", Appl. Phys. Lett., Vol. 40, No. 7, pp. 568-570, Apr. 1982.

(138) T. R. Chen, L. C. Chiu, A. Hasson, K. L. Yu, U. Koren, S. Margalit, and A. Yariv, "Study and application of the mass transport phenomenon in InP", J. Appl. Phys., vol. 54, No. 5, pp. 2407-2412, May 1983.

(139) M. Oishi and K. Kuroiwa, "Low pressure metalorganic vapor phase epitaxy of InP in a vertical reactor", J. Electrochem. Soc., vol. 132, No. 5, pp. 1209-1214, May 1985.

(140) R. Plastow, M. Harding, I. Griffith, A. C. Carter, and R. C. Goodfellow, "Low-threshold current cw operation of multiple infil buried heterostructure 1.3 μ m GaInAsP lasers", Electron. Lett., Vol. 18, No. 6, pp. 262-263, Mar. 1982.

(141) R. J. Betsch, "Parametric anarysis of control parameters in MOCVD", J. Cryst. Growth, vol. 77, Nos. 1-3, pp. 210-218, Sept. 1986.

(142) John F. O' Hanlon, "A user's guide to vacuum technology", John Wiley and Sons, Inc., New york, 1980.

(143) T. P. Pearsall, R. Caeles, and J. C. Portal, " Single longitudinal-mode optical phonon scattering in $Ga_{0.47}In_{0.53}As$", Appl. Phys. Lett., vol. 42, No. 5, pp. 436-438, Mar. 1983.

(144) P. M. Petroff, A. C. Gossard, A. Savage, and W. Wiegmann, "Molecular beam epitaxy of Ge and $Ga_{1-x}Al_xAs$ ultra thin film superlattices", J. Cryst. Growth, vol. 46, No. 2, pp. 172-178, Feb. 1979.

(145) T. S. Kuan, and C. A. Chang, "Electron microscope studies of a Ge-GaAs superlattice grown by molecular beam epitaxy", J. Appl. Phys., No. 8, vol. 54, pp. 4408-4413, Aug. 1983.

(146) K. Yagi, K. Takayanagi, and G. Honjo, "In-situ UHV electron microscope of surfaces", Crystals, Growth, Properties and Application, vol. 7, pp. 47-74, Springer-Verlag, Berlin, Heidelberg, 1982.

(147) N. Yamamoto, and S. Muto, "Direct observation of Al_xGa_{1-} As/GaAs superlattices by REM", Jpn. J. Appl. Phys., vol. 23, No. 10, pp. L806-808, Oct. 1984.

(148) G. A. Lincoln, M. W. Geis, and S. Pang, and N. N. Efremow, "Large area ion beam assisted etching of GaAs with high etch rates and controlled anisotropy", J, Vac. Sci. Technol. B, vol. 1, No. 4, pp. 1043-1046, Oct-Dec. 1983.

(149) M. Asada, A. Kameyama, and Y. Suematsu ;' Gain and inter-

valence band absorption in quantum well lasers', J. Quantum. Electron. vol. QE20, No. 7, pp. 745-753, July 1984.
(150) C. M. Garner, C. Y. Su, Y. D. Shen, C. S. Lee, G. P. Pearson, W. E. Spicer, D. D. Edwall, D. Miller, J. S. Harris, Jr., "Interface studies of $Al_xGa_{1-x}As$-GaAs heterojunctipons", J. Appl. Phys., vol. 50, No. 5, pp. 3383-3389, May 1979.
(151) R. D. Dupuis, L. A. Moudy, P. D. Dapkas, "Preparation and properties of $Ga_{1-x}Al_xAs$-GaAs heterojunctions grown by metalorganic chemical vapour deposition", Inst. Phys. Conf. Ser., No. 45, pp. 1-9, 1978.
(152) N. Bouadma, J. F. Hogrel, J. Charil and M. Carre, "Fabrication and characteristics of ion beam etched cavity InP/GaInAsP BH lasers", IEEE J. Quantum. Electron., vol. QE23, vol. 6, pp. 909-914, June 1987.
(153) R. Bisaro, G. Laurencin, A. Friederich, and M. Razeghi, "An accurate methods to check chemical interfaces of epitaxial III-V compounds", Appl. Phys. Lett., vol. 40, No. 11, pp. 978-980, June 1982.
(154) M. B. Panish, H. C. Casey, JR., S. Sumski, and P. W. Foy, "Reduction of threshold current density in GaAs-Al_xGa_{1-x} heterostructure lasers by separate optical and carrier confinement", Appl. Phys. Lett., vol. 22, No. 11, pp. 590-591, June 1973
(155) J. Nagle, S. Hersee, M. Razeghi, M. Krakowski, B. De Cremoux, and C. Weisbuch, "Properties of 2D quantum well lasers", Surface Science, vol. 174, Nos. 1-3, pp. 148-154, Aug. 1986.
(156) K. Iga, H. Uenohara, and F. Koyama, "Electron reflectance of multiquantum barrier (MQB)", Electron. Lett., vol. 22, No. 19, pp. 1008-1010, Sept. 1986.
(157) H. Takuma, "Introduction of quantum electronics", Baihu-kan, Tokyo, 1972 (in Japanese).
(158) M. Asada and Y. Suematsu, "Density-matrix theory of semiconductor lasers with relaxation broadening model -- Gain and gain-suppression in semiconductor lasers", IEEE J. Quantum Electron., vol. QE-21, No. 5, pp. 434-442, May 1985.
(159) R. J. Nicholas, S. J. Sessions and J. C. Prtal, "Cyclotron resonance and magnetrophonon effect in $Ga_xIn_{1-x}As_yP_{1-y}$", Appl. Phys. Lett., vol. 37, No. 2, pp. 178-180, July 1980
(160) M. Yamanishi and I. Suemune, "Comment on polarization dependent momentum matrix elements in quantum well lasers",

Jpn. J. Appl. Phys., vol. 23, No. 1, pp. L35-L36, Jan. 1984.
(161) M. Asada, Y. Miyamoto, and Y. Suematsu, "Theoretical gain of quantum-well wire lasers", Jpn. J. Appl. Phys., vol. 24, No. 2, pp. L95-L97, Feb. 1985.
(162) N. K. Dutta, "Calculated absorption, emission, and gain in $In_{0.72}Ga_{0.28}As_{0.6}P_{0.4}$", J. Appl. Phys., vol. 51, No. 12, pp. 6095-6100, Dec. 1980.
(163) W. A. Harrison, "Electronic structure and the properties of solids", W. H. Freeman and Company, San Francisco, 1980.
(164) A. R. Adams, M. Asada, Y. Suematsu, and S. Arai, "The temperature dependence of the efficiency and threshold current of $In_{1-x}Ga_xAs_yP_{1-y}$ lasers related to intervalence band absorption", Jpn. J. Appl. Phys., vol. 19, No. 10, pp. L621-L624, Oct. 1980.
(165) K. Stubkjaer, M. Asada, S. Arai, and Y. Suematsu, "Spontaneous recombination, gain, and refractive index variation for 1.6 μ m wavelength InGaAsP/InP lasers", Jpn. J. Appl. Phys., vol. 20, No. 8, pp. 1499-1505, Aug. 1981.
(166) M. Asada, and Y. Suematsu, "Measurement spontaneous emission effciency and non-radiative recombinations in 1.58-μ m wavelength GaInAsP/InP crystals", Appl. Phys. Lett., vol. 41, No. 4, pp. 353-355, Aug. 1982.
(167) M. Yamada, S. Ogita, T. Miyabo, and Y. Nashida, "A theoretical analysis of lasing gain and threshold current in GaAs/GaAlAss SCH lasers", Trans. IECE of Jpn., vol. E69, No. 9, pp. 948-955, Sept. 1986.
(168) R. Dingle, H. L. Stormer, A. C. Gossard, and W. Wiegmann, "Electron mobilities in modulation doped semiconductor injection superlattices", Appl. Phys. Lett., vol. 33, No. 7, pp. 665-667, Oct. 1978.
(169) M. Yamada, and X. Feng, "Gain of semiconductor laser under non-neutral condition", Nat. Conv. Rec. of Jpn. Appl. Phys., 1a-K-1, Chiba, Apr. 1986 (in Japanese).
(170) K. Uomi, N. Chinone, T. Ohotoshi, and S. Katajima, "Theoretical analysis of relaxation oscillation frequency of impurity doped MQW lasers - Polarity of modulation doped impurity and high speed characteristics", Nat. Conv. Rec. of Jpn. Appl. Phys., 2a-K-3, Chiba, Apr. 1986 (in Japanese).
(171) M. Yamada, K. Omi, Y. Nashida, and M. Gamo, "Proposal of a

potential controlled low threshold laser", Trans. IEICE of Jpn., vol. E70, No. 3, pp. 178-180, Mar. 1987.
(172) M. Asada and Y. Suematsu, "Intraband relaxation time in quantum well lasers due to electron-electron scattering", to be presented in Nat. Conv. Rec. of Jpn. Appl. Phys., Mar. 1988. (in Japanese)
(173) Y. C. Chang, "Enhancement of optical nonlinearity in p-type semiconductor quantum wells due to confinement ans stress", Appl. Phys. Lett., vol. 46, No. 8, pp. 710-712, Apr. 1985.
(174) H. Ohno, "Ultra-high speed compounds semiconductor devices", edited by M. Ohomori, chap. 2, p. 23, Bihu-kan, Tokyo, 1986 (in Japanese).
(175) Yu. I. Ravich, B. A. Efimova, and I. A. Smirnov, "Semiconducting lead chalcogenides", p. 352, Plenum press, New York-London, 1970.
(176) N. Kobayashi, Y. Horikoshi, and C. Uemura, "Room temperature operation of the InGaAsSb/AlGaAsSb DH laser at 1.8 μ m wavelength", Jpn. J. Appl. Phys., vol. 19, No. 1, pp. L30-L32, Jan. 1980.
(177) T. H. Chiu, W. T. Tsang, J. P. Ditzenberger, and J. P. van der Ziel, "Room-temperature operation of InGaAsSb/AlGaSb double heterostructure lasers near 2.2 μ m prepared by molecular beam epitaxy", Appl. Phys. Lett., vol. 49, No. 17, pp. 1051-1052, Oct. 1986.
(178) H. Sakaki, "Scattering suppression and high-mobility effect of size quantized electrons in ultrafine semiconductor wire structure", Jpn. J. Appl. Phys. Lett., vol. 19, No. 12, pp. L735-738, Dec. 1980.
(179) W. J. Skocpol, L. D. Jackel, E. L. Hu, R. E. Howard, and L. A. Fetter, "Dimensional localization and interaction effects in narrow (0.1 μ m) silicon inversion layers", Phys. Rev. Lett., vol. 49, No. 13, pp. 951-955, Sep. 1982.
(180) M. Laviron, P. Averbuch, H. Godfrin, and R. E. Rapp, "One and two-dimensional quantum localization in GaAs wires of rectangular cross-sections", J. Physique, vol. 44, No. 24, pp. L1021-L1026, Dec. 1983.
(181) T. Hiramoto, K. Hirakawa, and T. Ikoma, "Quasi-one-dimensional, planer GaAs wires fabricated by focused ion beam implantation", 14th Int. Symp. GaAs and Related

Comp., PT. 1, Heraklion, Crete, Greece, Sept. 1987.
(182) P. M. Petroff, A. C. Gossard, R. A. Logan, and W. Wiegmann, "Toward quantum well wires: Fabrication and optical properties", Appl. Phys. Lett., vol. 41, No. 7, pp. 635-638, Oct. 1982.
(183) M. A. Reed, R. T. Bate, K. Bradshaw, W. M. Duncan, W. R. Frensley, J. W. Lee and H. D. Shih, "Spatial quantization in GaAs-AlGaAs multiple quantum dots", J. Vac. Sci. Technol. B, vol. 4, No. 1, pp. 358-360, Jan./Feb. 1986.
(184) J. Cibert, P. M. Petroff, G. J. Dolan, S. J. Pearton, A. C. Gossard and J. H. English, "Optically detected carrier confinement to one and zero dimension in GaAs quantum well wires and boxes", Appl. Phys. Lett., vol. 49, No. 19, pp. 1275-1277, Nov. 1986.
(185) K. Kash, A. Scherer, J. M. Worlock, H. G. Craighead and M. C. Tamargo, "Optical spectroscopy of ultrasmall structures etched from quantum wells", Appl. Phys. Lett., vol. 49, No. 16, pp. 1043-1045, Oct. 1987.
(186) H. Temkin, G. J. Dolan, M. B. Panish and S. N. G. Chu, "Low temperature photoluminescence from InGaAs/InP quantum wires and boxes", Appl. Phys. Lett., vol. 50, No. 7, pp. 413-415, Feb. 1987.
(187) G. Mollenstedt, Proc. Third Symp. on EB Technology, p. 340, edited by R. Bakish, Mar. 1961.
(188) F. Emoto, K. Gamo, S. Namba, N. Samoto, and R. Shimizu, "8nm wide line fabrication in PMMA on Si wafers by electron beam exposure", Jpn. J. Appl. Phys., vol. 24, No. 10, pp. L809-L811, Oct. 1985.
(189) A. Scherer, and H. G. Draighkeah, "Fabrication of small laterally patterned multiple quantum wells", Appl. Phys. Lett., vol. 49, No. 19, pp. 1284-1286, Nov. 1986.
(190) L. F. Johnson, G. W. Kammlott, and K. A. Ingersoll, "Generation of periodic surface corrugations", Appl. Opt., vol. 17, No. 8, pp. 1165-1181, Apr. 1978.
(191) H. Kawanishi, Y. Suematsu. Y. Itaya, and S. Arai, "Ga_xIn_{1-} As_yP_{1-y}-InP Injection laser partially loaded with distributed bragg reflector", Jpn. J. Appl. Phys., vol. 17, No. 8, pp. 1439-1440, Aug. 1978.
(192) T. Ichiguchi, M. Hundhausen, and Y. Shiraki, "Multiple quantum wire in GaAs/GaAlAs", Nat. Conv. Rec. of Jpn. Appl.

Phys. Soc., 18p-ZD-14, Nagoya, Oct. 1987 (in Japanese).
(193) S. Koentjoro, K. G. Ravikumar, K. Shimomura, K. Komori, S. Arai and Y. Suematsu, "Mass Transport Buried Heterostructure Laser Using p-InP Substrate", Trans. IECE of Japan., vol. E69, No. 9, pp. 920-922, Sept. 1986.
(194) Y. Tokuda, K. Fujiwara, N. Tsukada, K. Hamanaka and T. Nakayama, "Lasing-Wavelength Switching and Multi-Wavelength Emitting of GaAs Single-Quantum-Well Laser Diode," First Optoelectronics Conference (OEC-86), Post-deadline papers, A11-2, Tokyo, July 1986.
(195) A. Muray, M. Scheinfein, and M. Isaacon, "Radioysis and resolution limits of inorganic halaide resists", J. Vac. Sci. Technol. B, vol. 3, No. 1, pp. 367-372, Jan./Feb. 1985.
(196) E. Spiller, D. E. Eastman, R. Feder, W. D. Grobman, W. Gudat, and J. Topalian, "Application of synchrotron raddiation to x-ray lithography", J. Appl. Phys., vol. 47, No. 12, pp. 5450-5459, Dec. 1976.
(197) T. Nishimura, H. Kotani, S. Matsui, O. Nakagawa, H. Aritome, and S. Namba, "X-ray replication of masks by synchrotron radiation of INS-ES", Jpn. J. Appl. Phys. vol. 17, Suppl. 17-1, pp. 13-17, 1978.
(198) R. S. Wiliams, R. J. Nelson, and A. R. Schlier, "Depth resolution degradation of sputter-profiled InP/$In_xGa_{1-x}As_yP_{1-y}$ interfaces caused by cone formation", Appl. Phys. Lett., vol. 36, No. 10, pp. 827-829, May 1980.
(199) I. J. Fritz, S. T. Picraux, L. R. Dawson, T. J. Drummond, W. D. Laidig amd N. G. Anderson, "Dependence of critical layer thickness on strain for $In_xGa_{1-x}As$/GaAs strained-layer superlattices", Appl. Phys. Lett., vol. 46, No. 10, pp. 967-969, May 1985.

List of the publications

Papers and letters

(1) S. Sugou, A. Kameyama, H. Katsuda, Y. Miyamoto, K. Furuya, and Y. Suematsu, "Alloy composition and flow rates in Ga_xIn_{1-} As_yP_{1-y} lattice-matched to InP grown by MOCVD", Electron. Lett., vol. 19, No. 24, pp. 1036-1037, Nov. 1983.

(2) S. Sugou, A. Kameyama, Y. Miyamoto, K. Furuya, and Y. Suematsu, "Conditions for OMVPE growth of GaInAsP/InP crystal", Japan. J. Appl. Phys., vol. 23, No. 9, pp. 1182-1189, Sept. 1984.

(3) M. Asada, Y. Miyamoto, and Y. Suematsu, "Theoretical gain of quantum-well wire lasers", Japan. J. Appl. Phys., vol. 24, No. 2, pp. L95-L97, Feb. 1985.

(4) S. Yang, Y. miyamoto, C. Watanabe, M. Nagashima, K, Furuya, and Y. Suematsu, "Gain and loss of GaInAsP (λ g=1.5 μ m) grown by OMVPE estimated from lasing characteristics", Trans. IECE of Japan, vol. E-68, No. 8, pp. 521-523, Aug. 1985.

(5) M. Nagashima, Y. Miyamoto, K. Furuya, Y. Suematsu, C. Watanabe, and S. Yang, "Mass transported 1.55 μ m GaInAsP/InP BH laser grown by OMVPE", Trans. IECE of Japan, vol. E-68, No. 9, pp. 563-565, Sept. 1985.

(6) Y. Miyamoto, C. Watanabe, M. Nagashima, K. Furuya, Y. Suematsu, Y. Tohmori, and S. Arai, "OMVPE grown GaInAsP/InP BH laser on p-type substrate", Trans. IECE of Japan, vol. E-68, No. 12, pp. 796-797, Dec. 1985.

(7) M. Nagashima, Y. Miyamoto, C. Watanabe, Y. Suematsu, and K. Furuya, "1.55 μ m GaInAsP/InP buried heterostructure lasers with multiple p-n current blocking layer entirely grown by low-pressure OMVPE", Trans. IECE of Japan, vol. E-69, No. 2, pp. 92-94, Feb. 1986.

(8) C. Watanabe, S. Kinoshita, K. Furuya, and Y. Miyamoto, "GaInAs/InP MOSFETs by Organometallic Vapor Phase Epitaxy", Trans. IECE of Japan, vol. E-69, No. 7, pp. 779-781, July 1986.

(9) M. Asada, Y. Miyamoto, and Y. Suematsu, "Gain and the threshold of three-dimensional quantum-box lasers", IEEE J. Quantum Electron., vol. QE-22, No. 9, pp. 1915-1921, Sept. 1986.

(10) Y. Miyamoto, C. Watanabe, M. Nagashima, K. Furuya, and Y. Suematsu, "Fabrication of GaInAsP/InP Heterostructure for 1.5 μ m lasers by OMVPE", Trans. IEICE of Japan, vol. E-70, No. 2, pp. 121-129, Feb. 1987.

(11) Y. Miyamoto, M. Cao, K. Furuya, and Y. Suematsu, "GaInAsP/InP single quantum-well lasers by OMVPE", Japan. J. Appl. Phys., vol. 26, No. 3, pp. L176-L178, Mar. 1987.

(12) Y. Miyamoto, M. Cao, Y. Shingai, K. Furuya, Y. Suematsu, K. G. Ravikumar and S. Arai, "Light emission from quantum box structure by current injection", Japan. J. Appl. Phys., vol. 26, No. 4, p. L225-L227, Apr. 1987.

(13) K. Ishihara, S. Kinoshita, K. Furuya, Y. Miyamoto, K. Uesaka, and M. Miyauchi, "GaInAs/InP Hot Electron transistors grown by OMVPE", Japan. J. Appl. Phys., vol. 26, No. 6, pp. L911-L913, June 1987.

International Conference

(1) S. Sugou, A. Kameyama, Y. Miyamoto, C. Watanabe, K. Furuya, and Y. Suematsu, "OMVPE GaInAsP/InP crystal growth for integrated optics", Top. Meeting on Integrated and Guided-wave Optics, ThB-1, Kissmmee, Florida/USA, Apr. 1984.

(2) S. Sugou, A. Kameyama, Y. Miyamoto, C. Watanabe, K. Furuya, and Y. Suematsu, "Growth conditions and doping control in GaInAsP/InP OMVPE", The 16th Int. Conf. Solid. State Devices and Materials, D-11-5, Kobe, Sept. 1984.

(3) Y. Miyamoto, M. Nagashima, C. Watanabe, K. Furuya, and Y. Suematsu, "Devices techniques for GaInAsP/InP OMVPE", Second Biennal OMVPE Workshop, Session IV, Itaca, NY/USA, Aug. 1985.

(4) Y. Miyamoto, M. Cao, Y. Shingai, K. Furuya, Y. Suematsu, K. G. Ravikumar, and S. Arai, "Fabrication of quantum-box structure with p-n junction and optical guide structure", 13th European Conference on Optical Communication, p. 35, Helsinki/Finland, Sept. 1987.

Domestic Conference

(1) Y. Miyamoto, M. Nagashima, C. Watanabe, K. Furuya, and Y. Suematsu, "GaInAsP/InP OMVPE selective regrowth for 1.5

μ m buried heterostructure laser", First Optoelectronics Conference, P2-8, Tokyo, July 1986.

National conventional records

(1) S. Sugou, I. Komazaki, A. Kameyama, Y. Miyamoto, H. Katsuda, K. Furuya, and Y. Suematsu, "GaInAsP/InP crystal growth by MOCVD method and its photoluminescence", Nat. Conv. Rec. of Japan Soc. Appl. Phys., 4p-S-12, Chiba, Apr. 1987.

(2) S. Sugou, A. Kameyama, Y. Miyamoto, H. Katsuda, K. Furuya, and Y. Suematsu, "1.30-1.52 μ m GaInAsP/InP crystal growth by MOCVD method", Nat. Conv. Rec. of Japan Soc. Appl. Phys., 28a-F-7, Sendai, Sept. 1983.

(3) S. Sugou, A. Kameyama, Y. Miyamoto, C. Watanabe, K. Furuya, and Y. Suematsu, "1.5 μ m GaInAsP/InP crystal growth and semiconductor lasers by LP-MOCVD", Nat. Conv. Rec. of IECE of Japan, No. 1019, Tokyo, Mar. 1984.

(4) S, Sugou, A. Kameyama, Y. Miyamoto, C. Watanabe, K. Furuya, and Y. Suematsu, "GaInAsP/InP grown by LP-MOCVD and its lasing", Nat. Conv. Rec. of Japan Soc. Appl. Phys., 31a-D-7, Tokyo, Mar. 1984.

(5) C. Watanabe, Y. Miyamoto, K. Furuya, and Y. Suematsu, "Growth on structured surface and in-situ etching by InP systems OMVPE", Nat. Conv. Rec. of Japan Soc. Appl. Phys., 14a-S-8, Okayama, Oct. 1984.

(6) M. Asada, Y. Miyamoto, and Y. Suematsu, "Gain in quantum-well wire lasers", Nat. Conv. Rec. of Japan Soc. Appl. Phys., 14p-R-7, Okayama, Oct. 1984.

(7) M. Nagashima, Y. Miyamoto, C. Watanabe, S. Yang, K. Furuya, and Y. Suematsu, "OMVPE GaInAsP/InP laser by mass transport technique", Nat. Conv. Rec. of IECE of Japan, No. 895, Kanagawa, Apr. 1985.

(8) Y. Miyamoto, C. Watanabe, M. Nagashima, S. Yang, K. Furuya and Y. Suematsu, "Low threshold current of GaInAsP/InP semiconductor lasers by OMVPE", Nat. Conv. Rec. of Japan Soc. Appl. Phys., 30a-Z-6, Tokyo, Mar. 1985.

(9) M. Asada, Y. Miyamoto, and Y. Suematsu, "Gain increase in multidimensional quantum-well lasers", Nat. Conv. Rec. of Japan Soc. Appl. Phys., 30p-ZB-5, Tokyo, Mar. 1985.

(10) Y. Miyamoto, C. Watanabe, M. Nagashima, K. Furuya, and

Y. Suematsu, "1.5 μ m GaInAsP/InP semiconductor laser grown by OMVPE on p-type substrate", Nat. Conv. Rec. of Japan Soc. Appl. Phys., 2p-N-17, Kyoto, Oct. 1985.

(11) Y. Miyamoto, C. Watanabe, M. Nagashima, A. Nakajima, K. Furuya, and Y. Suematsu, "GaInAsP/InP SCH quantum-well laser by OMVPE", Nat. Conv. Rec. of IECE of Japan, No. S12-4, Niigata, Mar. 1986.

(12) C. Watanabe, S. Kinoshita, K. Furuya, and Y. Miyamoto, "GaInAs/InP MOSFETs by organimetallic vapor phase epitaxy", Nat. Conv. Rec. of IECE of Japan, No. 308, Niigata, Mar. 1986.

(13) M. Nagashima, Y. Miyamoto, C. Watanabe, M. Cao, K. Furuya, and Y. Suematsu, "GaInAsP/InP BH laser by OMVPE technique", Nat. Conv. Rec. of Japan Soc. Appl. Phys., 3a-K-8, Chiba, Apr. 1986.

(14) M. Cao, Y. Miyamoto, K. Furuya, and Y. Suematsu, "GaInAsP/InP SCH quantum-well laser by OMVPE (II)", Nat. Conv. Rec. of IECE of Japan, No. 207, Tokyo, Sept. 1986.

(15) Y. Miyamoto, M. Cao, Y. Shingai, K. Furuya, and Y. Suematsu, "GaInAsP/InP multi-dimensional quantum-well by interference exposure and wet-etching", Nat. Conv. Rec. of Japan Soc. Appl. Phys., 30p-V-11, Tokyo, Mar. 1986.

(16) K. Ishihara, S. Kinoshita, K. Furuya, Y. Miyamoto, K. Uesaka, and M. Miyauchi, "Hot electron transport in GaInAs/InP grown by OMVPE", Nat. Conv. Rec. of IEICE of Japan, No. 209, Kumamoto, Nov. 1987.

Technical Group Meetings

(1) S. Sugou, A. Kameyama, Y. Miyamoto, H. Katsuda, K. Furuya, and Y. Suematsu, "GaInAsP/InP lasers grown by LP-MOCVD and its lasing characteristics", Appl. Solid State Phys., Division of Japan Soc. Appl. Phys., Technical group meeting, No. 4D2, pp. 13-18, Tokyo, Jan. 1984.

(2) S. Yang, Y. Miyamoto, C. Watanabe, M. Nagashima, K. Furuya, and Y. Suematsu, "Lasing characteristics of 1.5 μ m-GaInAsP/InP grown by OMVPE", Tech. Group Meeting, Opto and Quantum Electron., IECE of Japan, OQE85-6, Tokyo, Apr. 1985.

(3) M. Asada, Y. Miyamoto, and Y. Suematsu, "Gain and the threshold of three-dimensional quantum-box laser", Tech.

Group Meeting, Opto and Quantum Electron., IECE of Japan, OQE85-74, Tokyo, Sept. 1985.

Review paper

(1) Y. Miyamoto, and K. Furuya, "Organometallic vapor phase epitaxy of quaternary alloy semiconductor for diode laser", Oyo Buturi, vol. 56, No. 3, pp. 357-360, Mar. 1987.